12-2013

Synthesis and Characterization of Multi-Component Enrichment Polymer Layers for Chemical Sensor Applications

James Giammarco
Clemson University, jmgiamm@clemson.edu

Recommended Citation

Giammarco, James, "Synthesis and Characterization of Multi-Component Enrichment Polymer Layers for Chemical Sensor Applications" (2013). *All Dissertations*. 1205.
https://tigerprints.clemson.edu/all_dissertations/1205

SYNTHESIS AND CHARATERIZATION OF MULTI-COMPONENT ENRICHMENT POLYMER LAYERS FOR CHEMICAL SENSOR APPLICATIONS

A Dissertation
Presented to
the Graduate School of
Clemson University

In Partial Fulfillment
of the Requirements for the Degree
Doctor of Philosophy
Materials Science & Engineering

---

by
James Matthew Giammarco
December 2013

Accepted by
Dr. Igor Luzinov, Committee Chair
Dr. O. Thompson Mefford
Dr. Scott Husson
Dr. Gary Lickfield

ABSTRACT

This dissertation presents the building and study of a “universal” enrichment polymer layer system (EPLS). Thin polymer films have been utilized as enrichment layers for evanescent waveguide chemical sensors. The chemical nature of the polymer provides affinity which promotes the analyte to be absorbed. Having one highly sensitive polymer layer is suitable for a single target volatile organic compound (VOC). Here, the development of multi-layered and multi-component thin polymer films has been done to allow for more diverse affinity.

Several parameters were identified to make the EPLSs suitable as enrichment layers for chemical sensor devices. The evanescent sensor devices used chalcogenide (ChG) glass, which is an infrared (IR) transparent material, and the principle of attenuated total reflection (ATR). This allowed the use of mid-IR spectroscopy to identify the absorbance of the absorbed VOCs in the polymer films. Changes of the absorbance due to influences of the EPLS were observed. These changes have not been reported before by researchers but can potentially be used to aid in fast and accurate identification of chemical compounds. The thicknesses of the total EPLS were kept to ≤ 30 nm so the evanescent wave would not be completely absorbed by the EPLS and absorbed VOC. Poly(glycidyl methacrylate) (PGMA) was a binding polymer for all EPLSs. As such, a single component PGMA film was tested to understand how the polymer influences the EPLS. Sensitivity to VOC concentration was conducted by mixture analysis and dilution by nitrogen gas in dynamic flow conditions. Comparison of each EPLS is done as well as to determine wavelengths of interest. Polymers were applied to ChG microdisk and amorphous silicon microring resonators and were found to increase sensitivity versus no polymer film at all.

Two distinct layered enrichment nanoscale systems were synthesized and characterized – a six layer system and a five layer system. The polymer layered systems were characterized by atomic force microscopy, ellipsometry, and IR spectroscopy. Polymers utilized were PGMA, poly(acrylic acid), 60% epoxidized poly(butadiene), and poly(4-vinyl pyridine). *In-situ* ellipsometry was done to determine the swelling fraction of the film. *In-situ* attenuated total reflection (ATR) FT-IR spectroscopy was used to identify absorbance differences. Each EPLS proved to promote unique interactions which brought about differences in VOC absorbance in the mid-IR region.

DEDICATION

This dissertation is dedicated to my first teachers, my parents. To my dad, Richard, who taught me the importance of endurance, the value of knowledge, and to always challenge what I know and to think critically. To my mom, Linda, who taught me to always be prepared, and that the strength of mind, and character are invaluable. I also dedicate this to all of my family for their constant support over the years.

ACKNOWLEDGMENTS

I want to thank my advisor, Dr. Igor Luzinov, for his guidance during my research, for his patience, and for his never yielding optimistic attitude toward my work even when days seemed to be bad. For all the time speaking with me and helping me along my PhD career, I want to thank my committee members: Dr. O. Thompson Mefford, Dr. Scott Husson, and Dr. Gary Lickfield.

I am thankful to the Department of Energy for funding this research which has brought about new understanding and methods in Materials Science & Engineering and for giving me the privilege to strive towards my PhD.

A special thanks to Dr. Kathleen Richardson, whose support and praise of my project is much appreciated. Additionally, I want to thank Dr. Anu Agarwal and Vivek Singh at MIT, whose questions kept me focused on long term goals of my project. I think we all taught each other.

I also owe a special debt of gratitude to Dr. Bogdan Zdyrko and Dr. Ruslan Burtovvy for their patience and guidance to help me think about my research in new ways.

I also owe a large debt of gratitude to Dr. Deborah Lickfield for all the help and fruitful discussions throughout my 5 years of work. All of the Lickfields, Mounces, and Kimmitts took me in like I was family and I will forever be in their debt and grateful to them.

I would like to acknowledge Mrs. Kimberly Ivey, who was always there for a great conversation, a laugh, and to teach me that hard work is its own reward. Her strength in the most difficult of situations is something I hope to one day possess. I will never forget her.

I am extremely grateful to Mr. Bob Bowen, a.k.a. Uncle Bob (The Grill Master). His willingness to host events and grill on Sunday nights even after long trips on the road demonstrates his never ending commitment to keeping the MS&E department a family.

Many thanks go to Dr. Darya Monaenkova, Dr. Taras Andrukh, Dr. Olha Hoy, and Dr. Sasha Tokarev. We had great times together which I will never forget. Sorry I couldn't learn Russian!

I would like to acknowledge my entire research group both past and present for their help and friendship for the last 5 years. Specifically I want to acknowledge Dr. Marius Chyasnavichyus for his helpful scientific discussions, Dr. Michael Seeber who was always able to ask questions, Yuriy Galabura who was always a model worker and a true friend, Fehime Vatansever who has never stopped being kind and her help when I first came to Clemson will always be remembered, AnnaPaola Soliani whose cooking and friendship I will never forget (we got so many people to watch the Big Bang Theory, CBS should pay us!!), Tugba Demir whose hospitality in her home country of Turkiye and from her family are so strong that I will never forget it, and to Jake Townsend who is always ready to laugh and to take science to its limits. Thank you for all the encouragement, support, and helpful suggestions that you provided me throughout my graduate studies. It has been an experience I will never forget. Thanks to Misha Savchak and Nikolay Borodinov! Good luck to you both! You are in good hands!

I am grateful to Dr. Gulya Korneva for helping me find my way to Clemson University and to meet Dr. Luzinov. If she hadn't believed and pushed me, I may have stopped with my Bachelors from Drexel University.

I am indebted to the Department of Materials Science and Engineering at Clemson University for the opportunity to work towards my PhD degree. I came here with the intent to challenge myself and with the help of many people, both scientifically and emotionally; I was able to make it through. I have made so many good friends at Clemson from so many parts of the country as well as different parts of the world (and quite a lot from Bordeaux!!) that there are too many to name, but to all of them, I say Thank You!!

There is something special about Clemson University and
the Department of MS&E which has made me feel at home.

TABLE OF CONTENTS

LIST OF TABLES

LIST OF FIGURES

Chapter 1. Introduction

1.1 Motivation

Detection technologies are needed in a world where threats of technological disasters and chemical and radiological attacks are constantly present. In this context, remote sensing is an area of specific interest because it allows one to safely identify hazardous chemicals or radiation levels. Remote sensing provides the capability of a synoptic view of an area, and for collecting continuous datasets.[1]

The detection of hazardous gases and vapors in any environment has been plagued by issues of capturing the target chemical(s). The application of polymers, in the form of enrichment polymer layers (EPL), to absorb gases for detection was developed in the late 1980s. The viability of polymers as chemical absorbents comes from the tunability of their properties through modification of the chemical structure. Specifically, the properties of polymers stem from the monomer selection, and any substituent functional groups they possess, and the degree of polymerization of the final polymer molecule.[2-6] Customization of polymer structures yields macromolecules with the capability to interact and swell with various volatile organic compounds (VOCs).

Typical EPLs researched to date have been polymer films, deposited in a 1 to 5 μm layer onto a sensor surface. The layers are intended to extend the qualitative and quantitative limits of detection by attracting analytes to the sensor surface via chemical and physical interactions. EPLs were studied to determine the strongest interaction with a particular analyte. Previous work in this area utilized many integrated sensor platforms which were coated with a single layer of polymer; however, there is no polymer that can universally attract every VOC.[7-9] The use of multiple polymers of a different chemical nature in an EPL increases the chances of capturing the molecules for detection and analysis. There has been a void in researching the use of different polymers to form a quasi-universal enrichment polymer layer system (EPLS) that can be deposited onto the one sensor element.

Infrared (IR) spectroscopy is an important analytical method that can be used for the “universal” sensor element, where a waveguide is covered with the “universal” EPLS. In fact, it has already been demonstrated that Fourier Transform Infrared Spectroscopy (FT-IR) can be used effectively for remote sensor applications.[10-13] Furthermore, detection by IR analysis can be applied to multiple areas, including chemical warfare agents, hazardous chemicals in industry, volatile biological agents, continuous monitoring of an environment and in laboratories.

One of the major limitations for IR remote sensing has been the bulky size of detectors and sources. Developing highly efficient, optical sensing devices that can be handheld has been in development over the last several decades, such as optical IR resonators.[14-17] These optical resonators, or microcavities, are capable of trapping photons and electrons for a significant period of time.[18-19] Classically, these are confocal and concentric mirrors which allow very low loss of light energy (Q-factor). Through constructive interference, these devices can increase the intensity of an optical signal, and have classically been used in laser technology, frequency modulation, and Fabrey-Parot interferometers.[19] The geometry of microresonators directly affects their Q-factor and performance.[20] As such, many shapes have been researched, including microspheres, microrings, microdisks, micropillars, and microhexagons.[21] The development of resonator devices has incorporated the use of attenuated total reflection to trap IR light. The surfaces of the devices become rich with evanescent waves that are produced from multiple bounces of the light at the waveguide-ambient interface. If a sample comes into contact with the resonator surface, it can either shift the wavelength of light—due to a difference in its refractive index compared to the ambient environment—or absorb the IR energy due to its own fundamental IR resonance. In an extension of this technology, the use of IR resonator devices combined with EPLS may lead to the development of miniature IR-based sensing devices.

1.2 Goal and objectives

The main goal for this dissertation was to design and characterize a multi-layered, quasi-universal EPLS capable of attracting various chemicals to the surface of IR waveguides to ensure their spectroscopic identification. The multi-layered design was selected in order to effectively modify an array of microdisk resonators with an EPLS possessing the same parameters over the whole array. The resonator array offers detection at multiple wavelengths and can provide detailed information on the absorbed VOC to be identified. A representation of the multi-layer system on a waveguide and how each layer can target different VOCs is provided in **Figure 1.1**.

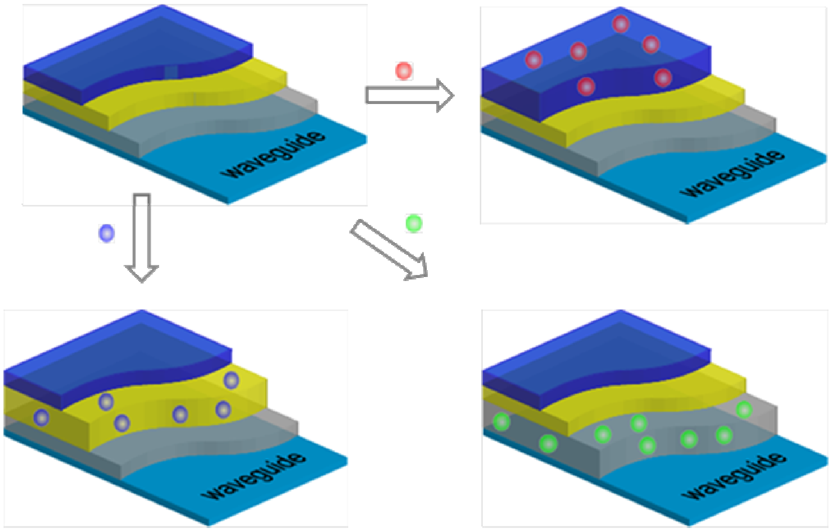

Figure 1.1. Scheme of layered polymers on waveguides where each layer has an affinity to a particular VOC.

It is more challenging and more expensive to fabricate, reproducibly, an array of resonators with each microdisk resonator having a unique polymer coating than the multi-layered concept proposed above. In addition, the device based on this array will be significantly larger. For example, for an array of 10 resonators working at 10 different wavelengths to have the efficacy of a 5-layered EPLS, five separately coated 10 resonator arrays would need to be connected in a single sensor device. This not only increases the size of the device but also the cost of having 50 resonators in one sensor device.

As an alternative to the multi-layered design, a phase-segregated, polymer blend grafted/cross-linked system was also considered to reach the goal for a quasi-universal EPLS. However, the phase separation in the systems is on the level of hundreds of nanometers that is comparable with dimensions of optical elements of the resonators.

To achieve the main goal, the following specific objectives were identified:

(1) To synthesize anchored (by covalent bonds), enrichment polymer, multi-layered systems (EPLSs), and to characterize them;

(2) To identify the extent of interaction of the EPLSs with various VOC vapors and to identify trends;

(3) To discern changes in the fundamental IR absorbance of VOCs absorbed in the enrichment layers;

(4) To evaluate the potential for the employment of EPLSs for solvent mixtures;

(5) To assess the possibility of EPLSs to be coated on, and grafted to, IR microdisk resonators.

1.2.1 Design and Function of the EPLS

The multi-layered EPLS was designed to incorporate several polymers of different functionality onto one waveguide surface. Building the layered enrichment system required the polymers to have reactive groups capable of covalently bonding with the silicon waveguides. The proposed layer design of the EPLS can house multiple polymers onto one substrate, provided that compatible functional groups are present to form covalent bond linkages between the layers. The step method designed to obtain the layered ELPS in this work are illustrated in **Figure 1.2**.

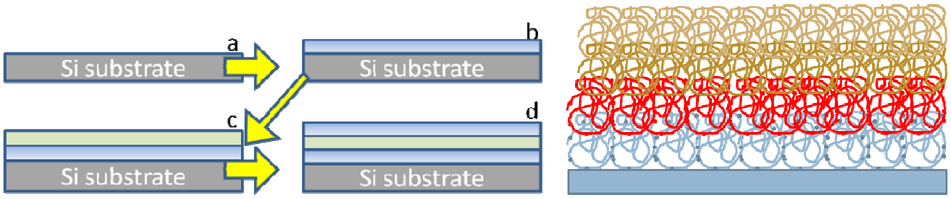

Figure 1.2. A schematic representation of the procedure to build the EPLS by consecutive grafting (left) starts with a) a silicon wafer or crystal; which is then dip coated to obtain b) a one-polymer layer on the surface; which is then grafted by annealing, allowing to dip coat another polymer onto the first polymer layer to obtain c). Continuing this process gives polymer system d). The resulting EPLS (right) can have as many layers as needed.

The macromolecules constituting the layers were selected based on the following properties: (a) *immiscibility*, to ensure the individuality of each layer; (b) *chemical structure*, to ensure that each layer is capable of attracting substances of different natures; and (c) *complementary chemical reactivity*, to ensure that each consecutive top layer is chemically anchored to the bottom layer. The latter condition is especially important for proper functioning of the coating, since the ultrathin polymer film has to retain its structure after multiple swelling/deswelling cycles. Without the strong connection between the layers delamination and dewetting may occur.[22-23]

The operation of the EPLS is based on several parameters. First, the polymer and organic molecule will have significant interactions; energy would be released from the absorption of the organic vapor into the EPLS. These interactions will promote conformational changes in the polymer chain, resulting in the film swelling. Second, the chemical functionality in each layer will target specific VOCs. When combined into a system, each layer will still maintain its inherent attractive nature without repelling other organic molecules. Third, each layer will be only tens of nanometers or less to allow rapid diffusion of organic molecules. The operation of an EPLS deposited on top of a silicon ATR crystal is displayed in **Figure 1.3**.

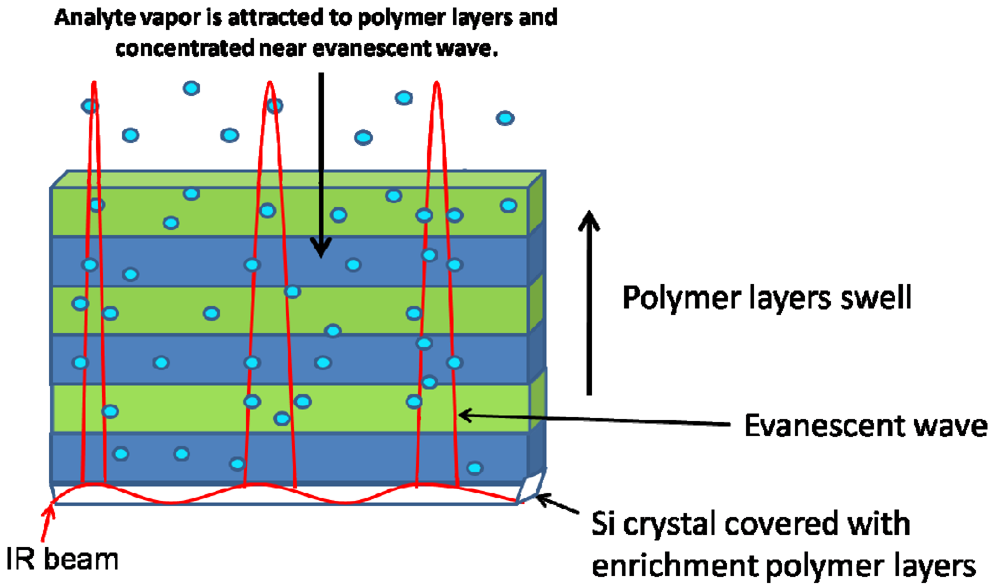

Figure 1.3. Operation of an EPLS in the presence of volatile organic vapor.

1.3 Synthesis of EPLS structures

The synthesis of the EPLS starts with a covalently grafted anchoring layer on the substrate.[24-29] Poly(glycidyl methacrylate) (PGMA) was used as anchoring layer in this work because it can be chemically bonded to many surfaces including silicon oxide.[30] The anchoring of the system to a substrate as well as bonding each layer by covalent bond linkages ensures that the enrichment system can withstand a significant number of swelling and deswelling cycles.[31] Silicon wafers were used for swelling experiments, and silicon ATR crystals were used for *in-situ* FT-IR experiments. Since each repeating unit of PGMA has an epoxy group which can crosslink; the polymer provides a robust foundation for the EPLS. Moreover, because of the “loop and tail” conformation that polymers form when anchored by multiple points to a surface, not every epoxy group participates in the reaction. Therefore, polymers with complimentary groups can be chemically grafted to PGMA.

All polymers in this work were applied by dip coating. They were bonded by grafting. This procedure, the “grafting to” approach, has been shown to produce uniform polymer layers with high stability and low roughness.[24, 32] **Figure 1.4** presents the scheme of PGMA bonding to the surface followed by free groups bonding with poly(acrylic acid) (PAA) as an example.

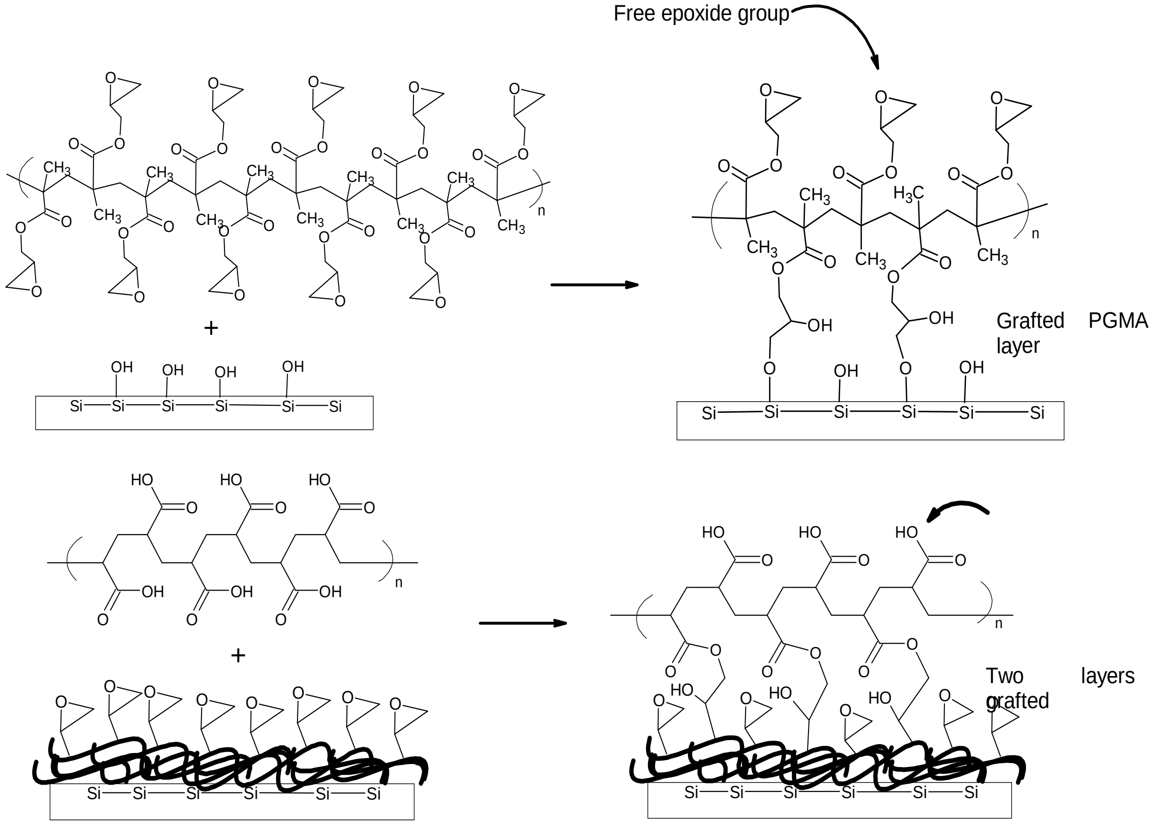

Figure 1.4. Scheme of PGMA bonding with Si surface and PAA.

1.3.1 The Layered design

The layered design of the EPLS, which incorporates polymers on top of each other, is naturally well suited for dip coating procedures where layer parameters can be controlled. With this design, an EPLS with many polymer layers with differing chemical natures was synthesized. The EPLS thickness was kept below 100 nm to assure that the swollen EPLS was within the evanescent wave field region of the ATR FT-IR. Polymers used for this design included the following: PGMA; poly(acrylic acid) (PAA); 60% epoxidized poly(butadiene) (EPB60); and poly 2-vinylpyridine (P2VP). The chain ends of P2VP are terminated with carboxylic acid groups. With these polymers two distinct systems were synthesized. In Chapter 4, a single-enrichment layer of PGMA was studied, as it is a major component in a multi-stack EPLS. A six-layer system of PGMA and PAA was obtained and the experimental results are presented in Chapter 5 starting at page 116. A multi-polymer EPLS was studied and is presented in Chapter 6 starting at page 139**.**

1.4 Scientific Contribution

This research provides an understanding of the synthesis of multi-layered EPLSs as well as the interactions between an analyte and an EPLS. Polymer films and EPLSs were 100 nm or below and demonstrated fast signal generation for VOC detection. This work demonstrates that new specific IR absorbance peaks arise when the VOC is absorbed into the polymer film. The wavelengths of these new absorbance peaks can be used to generate new fingerprints for VOCs to make detection faster. This work demonstrates that EPLSs do not interrupt the IR coupling of microdisk resonator sensor devices, and are a viable and realistic aid for analyte absorption.

1.5 References

1. Obade, V. d. P.; Lal, R., Assessing land cover and soil quality by remote sensing and geographical information systems (GIS). *Catena* **2013,** *104*, 77-92.

2. Burtovyy, O. Synthesis and Characterization of Macromolecular Layers Grafted to Polymer Surfaces. PhD Dissertation, Clemson University, Clemson, 2008.

3. Burtovyy, O.; Klep, V.; Chen, H. C.; Hu, R. K.; Lin, C. C.; Luzinov, I., Hydrophobic modification of polymer surfaces via "grafting to" approach. *Journal of Macromolecular Science Part B-Physics* **2007,** *46* (1), 137-154.

4. Dias, D. T.; Medina, A. N.; Baesso, M. L.; Bento, A. C., Statistical design of experiments: Study of cross-linking process through the phase-resolved photoacoustic method as a multivariable response. *Applied Spectroscopy* **2005,** *59* (2), 173-180.

5. Draper, J.; Luzinov, I.; Minko, S.; Tokarev, I.; Stamm, M., Mixed polymer brushes by sequential polymer addition: Anchoring layer effect. *Langmuir* **2004,** *20* (10), 4064-4075.

6. Iyer, K. S.; Luzinov, I., Stimuli sensitive grafted layers for switchable surface properties. *Abstracts of Papers of the American Chemical Society* **2004,** *227*, U884-U884.

7. LeMieux, M. C.; McConney, M. E.; Lin, Y. H.; Singamaneni, S.; Jiang, H.; Bunning, T. J.; Tsukruk, V. V., Polymeric nanolayers as actuators for ultrasensitive thermal bimorphs. *Nano Letters* **2006,** *6* (4), 730-734.

8. Li, X. X.; Lee, D. W., Integrated microcantilevers for high-resolution sensing and probing. *Measurement Science & Technology* **2012,** *23* (2), 1-40.

9. Maute, M.; Raible, S.; Prins, F. E.; Kern, D. P.; Ulmer, H.; Weimar, U.; Gopel, W., Detection of volatile organic compounds (VOCs) with polymer-coated cantilevers. *Sensors and Actuators B-Chemical* **1999,** *58* (1-3), 505-511.

10. Dobbs, G. T.; Balu, B.; Young, C.; Kranz, C.; Hess, D. W.; Mizaikoff, B., Mid-infrared chemical sensors utilizing plasma-deposited fluorocarbon membranes. *Analytical Chemistry* **2007,** *79* (24).

11. Flavin, K.; Hughes, H.; Dobbyn, V.; Kirwan, P.; Murphy, K.; Steiner, H.; Mizaikoff, B.; McLoughlin, P., A comparison of polymeric materials as pre-concentrating media for use with ATR/FTIR sensing. *International Journal of Environmental Analytical Chemistry* **2006,** *86* (6), 401-415.

12. Mizaikoff, B., Infrared optical sensors for water quality monitoring. *Water Science and Technology* **2003,** *47* (2), 35-42.

13. Harrick, N. J., Total Internal Reflection and Its Application to Surface Studies. *Annals of the New York Academy of Sciences* **1963,** *101*, 928-959.

14. Siegman, A. E., Laser beams and resonators: The 1960s. *Ieee Journal of Selected Topics in Quantum Electronics* **2000,** *6* (6), 1380-1388.

15. Janata, J.; Bezegh, A., Chemical Sensors. *Analytical Chemistry* **1988,** *60* (12), R62-R74.

16. Janata, J.; Josowicz, M.; Vanysek, P.; DeVaney, D. M., Chemical sensors. *Analytical Chemistry* **1998,** *70* (12), 179R-208R.

17. Downs, C.; Vandervelde, T. E., Progress in Infrared Photodetectors Since 2000. *Sensors* **2013,** *13* (4), 5054-5098.

18. Dowling, J.; Gea-Banacloche, J., Evanescent Light -Wave Atom Mirrors, Resonators, Waveguides, and Traps. *Advances in Atomic, Molecular, and Optical Physics* **1996,** *36*, 1-127.

19. Silfvast, *Laser Fundamentals*. Cambridge University Press: New York, NY, **2004**; p 625.

20. Siegman, A. E., Laser beams and resonators: Beyond the 1960s. *Ieee Journal of Selected Topics in Quantum Electronics* **2000,** *6* (6), 1389-1399.

21. Benson, T. M.; Boriskina, S. V.; Sewell, P.; Vukovic, A.; Greedy, S. C.; Nosich, A. I., Micro-optical resonators for microlasers and integrated optoelectronics - Recent advances and future challenges. In *Frontiers in Planar Lightwave Circuit Technology Design, Simulation, and Fabrication*, Janz, S.; Ctyroky, J.; Tanev, S., Eds. **2006**; Vol. 216, pp 39-70.

22. Carroll, G. T.; Turro, N. J.; Koberstein, J. T., Patterning dewetting in thin polymer films by spatially directed photocrosslinking. *Journal of Colloid and Interface Science* **2010,** *351* (2), 556-560.

23. Raegen, A.; Chowdhury, M.; Calers, C.; Schmatulla, A.; Steiner, U.; Reiter, G., Aging of Thin Polymer Films Cast from a Near-Theta Solvent. *Phys. Rev. Lett.* **2010,** *105* (22), 1-4.

24. Zdyrko, B.; Iyer, K. S.; Luzinov, I., Macromolecular anchoring layers for polymer grafting: comparative study. *Polymer* **2006,** *47* (1), 272-279.

25. Pukanszky, B., Interfaces and interphases in multicomponent materials: past, present, future. *European Polymer Journal* **2005,** *41* (4), 645-662.

26. Klep, V.; Luzinov, I., Surface modification via sequential ATRP grafting. *Abstracts of Papers of the American Chemical Society* **2004,** *228*, U467-U467.

27. Liu, Y.; Klep, V.; Luzinov, I., Surface modification with segregated grafted polymer layers. *Abstracts of Papers of the American Chemical Society* **2004,** *228*, U467-U467.

28. Luzinov, I.; Minko, S.; Tsukruk, V. V., Adaptive and responsive surfaces through controlled reorganization of interfacial polymer layers. *Prog. Polym. Sci.* **2004,** *29* (7), 635-698.

29. Zdyrko, B.; Hoy, O.; Luzinov, I.; Tokarev, I.; Minko, S.; Varshney, S. K., Gradient polymer brushes for combinatorial surface modification studies. *Abstracts of Papers of the American Chemical Society* **2005,** *230*, U3751-U3752.

30. Burtkovyy, O.; Klep, V.; Chen, H. C.; Hu, R. K.; Lin, C. C.; Luzinov, I., Hydrophobic modification of polymer surfaces via "grafting to" approach. *Journal of Macromolecular Science Part B-Physics* **2007,** *46* (1), 137-154.

31. Minko, S., Grafting on Solid Surfaces: “Grafting to” and “Grafting from” Methods. In *Polymer Surfaces and Interfaces,* Stamm, M., Ed. Springer: **2008**.

32. Liu, Y.; Klep, V.; Zdyrko, B.; Luzinov, I., Synthesis of high-density grafted polymer layers with thickness and grafting density gradients. *Langmuir* **2005,** *21* (25), 11806-11813.

Chapter 2. Literature Review

2.1. Introduction

Research in the area of enrichment polymer layers for sensor waveguides has focused on determining one suitable polymer to target a specific analyte (liquid or vapor). This review focuses on key aspects of consideration that researchers have studied over the last several decades when identifying polymers for selectivity, separation, ease of synthesis, and characterization methods as well as quantitative analysis of targeted analytes. The main goal of this review is to give the reader the fundamental basis of key areas that are important for building enrichment polymer layers and some characterization techniques.

2.2. Materials used for enrichment layers

2.2.1. Polymers

Polymers began to be integrated into analytical devices to aid in detection capabilities in the 1980's.[1-2] The use of polymers to provide an enrichment layers on sensor surfaces has rapidly increased since then. When applied to chemical sensors, polymer enrichment layers serve to capture analytes, and/or protect the sensor platform from harmful environments, thereby enhance detection capabilities. Absorption of low molecular weight molecules can alter certain properties of the polymers that can be detected. For example, monitoring mechanical properties, glass transition temperature, crystallinity, ionic charge, and volume can be done with high sensitivity and attributed to low molecular weight molecules. Polymer film thicknesses for this application have ranged from approximately 1 to 5 μm.

Polymers are commonly chosen for enrichment layers because they can be modified to interact with their environment through physical and chemical changes. The chemical structure of the polymer chain can be designed through meticulous consideration of the starting monomers or a polymer chain can be modified through performing a post polymerization alteration.[3] By adding different chemical functionality to the polymer chain in either of these fashions, a chemical gradient can also be made to yield unique characteristics. It is, therefore, possible to synthesize a complex macromolecule that has unique properties and affinities that allow for either broad or specific chemical targeting.

The chemistry along the backbone or branched structural fragments of the polymer chain are capable of dispersive, polar, and/or hydrogen bonding.[4] These interactions will determine what solvents are most apt for dissolving/swelling the polymer. When the chain is attached to a surface and in the presence of a solvent for which it has high affinity, the chain becomes fully extended. Conversely, the polymer will contract when in the presence of a solvent with which it has low affinity and is known as a collapsed coil. By undergoing these conformational changes, the polymer can be in a different state where its height (single layer thickness) is greater than, equal to, or less than its radius of gyration. These states of the polymer are defined as a fully extended, mushroom, and fully collapsed state (**Figure 2.1**).

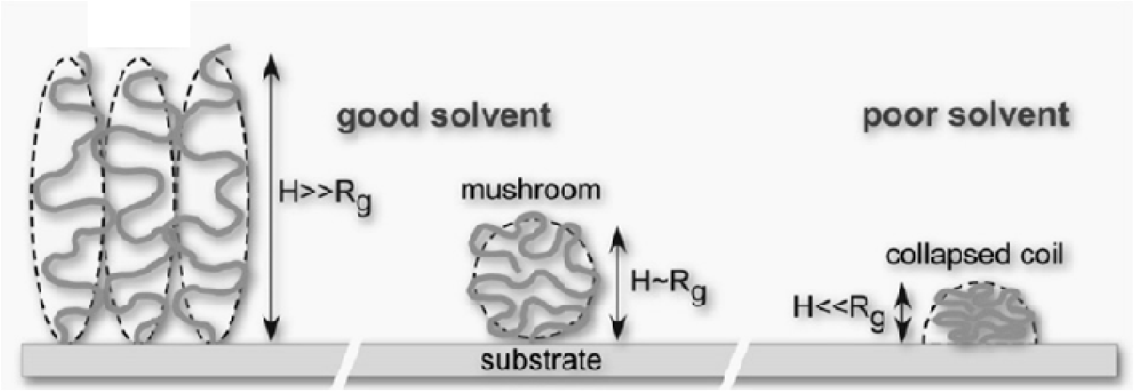

Figure 2.1. Polymer extension based on exposure to solvents of varying degrees of affinity. Reprinted with permission from Elsevier.[3]

The interactions of polymers with solvents are quantified by use of the solubility parameters.[5] The solubility parameter; related to cohesive energy, (which is the energy needed to cause the phase transition from the liquid state to the gas state) can be used to predict how well an analyte will be absorbed by a polymer film. By this, one can gauge a polymer's targeting strength for an analyte by determining if the polymer and analyte have very close solubility parameters.

$$\delta = (\frac{\Delta E}{V})^{1/2} = \sqrt{\delta_d + \delta_p + \delta_h} \quad (2.1)$$

The energy of vaporization, ΔE, and the molar volume, V define the solubility parameter. The term $\boldsymbol{\delta_d}$refers to the dispersive energy associated with an analyte, while the terms $\boldsymbol{\delta_p}$and $\boldsymbol{\delta_h}$ refer to the polar and hydrogen bonding energies, respectively. Solubility parameters can be combined as

$$\delta_v = \sqrt{\delta_d + \delta_p} \quad (2.2)$$

Figure 2.2 shows that solubility parameters between polymers and solvents can be used to form, in this case, a 2D radius which defines an estimate of good solubility.

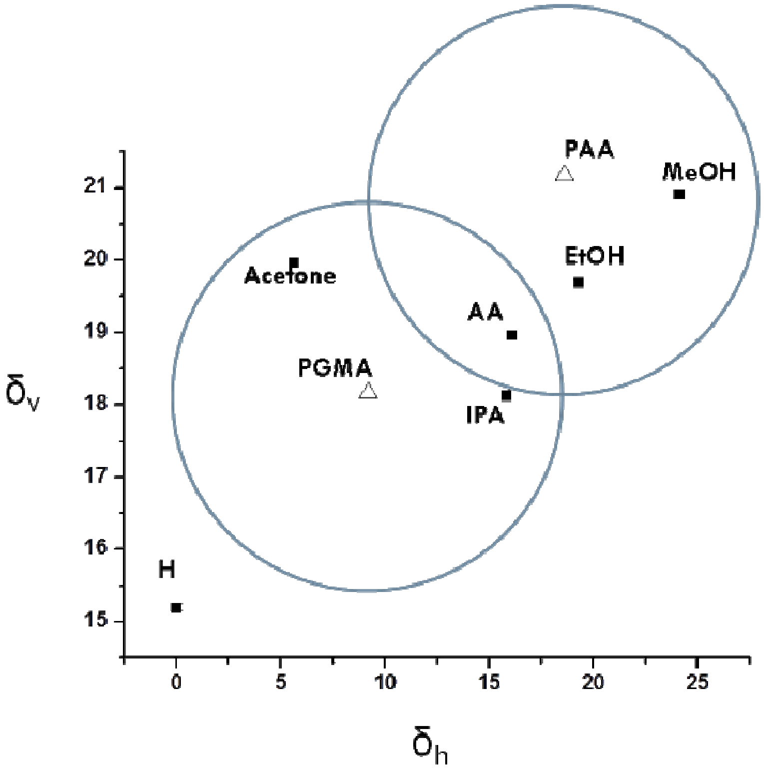

Figure 2.2. Relative solubility radii of PGMA and PAA using the van Krevelin method. Further away from the radius, solvents are less likely to be soluble with the polymer. The radius is defined by a solvent that will dissolve the polymer in question.

The Flory-Huggins interaction parameter is the specific parameter to quantify interactions

$$\chi_{12} = \frac{\Delta H_m}{kTN_1v_2} \approx \frac{V_1}{RT}(\delta_1 - \delta_2)^2 \tag{2.3}$$

In equation 2.2 above, enthalpy, ΔH, Boltzmann constant, k, temperature, T, the number of solvent molecules per a given volume, n_1, the volume fraction of polymer, v_2, the gas constant R, the molar volume of the analyte, V_1, and, finally, the solubility parameters corresponding to the polymer and solvent are used to define the interaction parameter. (For the reader's knowledge, research into modeling solvent interactions has been made with the linear salvation energy relationships (LSERs) which have been in development for the last few decades.[6-10])

Considerations one should use when choosing a polymer to act as an enrichment layer, were developed back in the early 1990s.[11] First, absorption bands should not be present or weak in the region of interest. Second, the substances to be analyzed should not be irreversibly dissolved into the film. Third, the time to detect enrichment should not exceed a specified amount. Lastly, the polymer should have simple preparation. Heinrich et al. analyzed the partitioning of several different chlorinated compounds dissolved in water into PDMS, trichloroctadecylsilane, polyethylene, and poly(ether-esteramide). While most of the results centered on diffusion and error analysis, they found that di-chloroethane diffused into PDMS with a greater concentration then in any other polymer. A notable observation they made was that the diffusion coefficient for most of the analytes was lower than previous reports and they attributed this to chains being linked to the surface and, therefore, have minimal space to allow for absorbed analytes, especially bulky ones.

Many different polymer materials have been compared to determine the most effective enrichment layer for specific analytes. Eastman et al.[12] studied carbon loaded poly(isobutylene), poly(butadiene, 1,2-syndiotactic), poly(vinyl alcohol), poly(ethylene-vinyl acetate), polyethylene-co-vinylacetate copolymer, and poly(diphenoxyphosphazene) on ionic conducting platforms and measured the electrical change when organic vapors were introduced using nitrogen carrier gas. Utilizing solubility parameters, they were able to characterize the polymer materials with the strength of the resistance change to each analyte. They tested and reported on 26 analyte vapors whose solubility parameters range from 14 - 48 MPa$^{1/2}$. In **Figure 2.3** below, the polymers that have close solubility parameters with the analyte vapor were noted to increase the response of the sensor, unless there was a strong ionic or chemical reaction (as with the case of PVA to a couple of analytes).

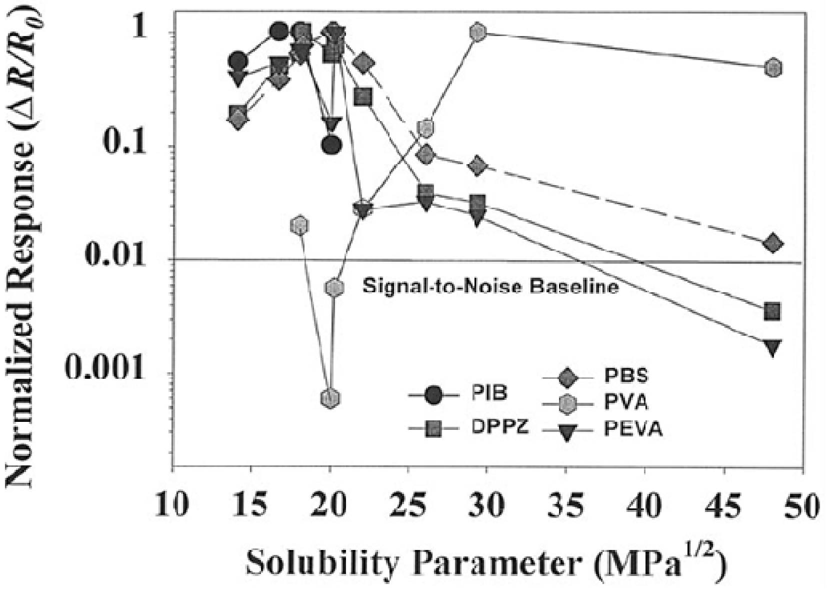

Figure 2.3. Sensor response as a function of solubility parameters. Reprinted with permission from The Electro Chemical Society.[12]

Selecting appropriate polymers for vapors sensing was analyzed for conductive sensors. Patel et al.[13] developed parallel plate micro chemicompacitive sensors where polyethylene-co-vinylacetate (PEVA), poly(epichlorohydrin) (PECH), polycarbonate urethane (PCUT), poly(isobutylene) (PIB), and poly(dimethyl siloxane) (PDMS) were added to aid absorption of VOCs. Toluene, acetone, water and dimethyl-methyl-phosphonate were selected for targeting. The signal strength was measured as a function of analyte vapor concentration, and the relative permittivity change. It was determined that the strongest signals generated in the PIB and PDMS films was due to strong polar-polar interactions with analytes. Analytes that have dielectric constants (above 4 up to 20) were noted to affect the permittivity within the polymer film even though they may not swell the polymer film to a large extent. Similarly, analytes that have low dielectric constant (below 3), or a high dielectric constant (above 22), will not swell the polymer film and only a weak signal was produced. In addition, if a chemical reaction can occur between the analyte and polymer film, are likely to be much stronger with low concentration analytes; however a slow recovery will result, if recovery is possible at all.

Over the past few decades, Peter McLoughlin has been one of the pioneers of Mid-IR sensing with polymer coating enrichment layers. Flavin & McLoughlin[14] compared Teflon AF2400, poly(dimethylsiloxane) (PDMS), and poly(styrene-co-butadiene) (PSB), and poly (acrylonitrile-co-butadiene) (PAB) with analytes of toluene, tetrahydrofuran (THF), ethanol and acetonitrile. It was found that because PAB, has hydrophobic and hydrophilic groups, it allows the greatest diffusion constant per micron of thickness for all four analytes allowing speedier detection while the Teflon had significant affinity to toluene only. In addition they observed that bulky compounds, such as toluene, diffused more slowly and THF diffused more quickly. Their later work focused on chlorinated compounds diffusing into polymer films and observing shifting of mid-IR peaks of the polymer film.[15] These studies demonstrate that particular polymers are more suited for targeting specific analytes. From here, a hypothesis can be drawn that using multiple polymers with different characteristics would help to extend the targeting capabilities of a sensor.

Dobbs and Mizaikoff worked with plasma deposited fluorocarbon polymer layers (membranes) for liquid phase chemical sensing of tetrachloroethylene.[16] The choice of fluoropolymers was based on their thermal and chemical stability, low absorption in the IR region, but most importantly their hydrophobic nature which could be used to probe for very low concentrations of organic compounds in aqueous matrices. The analyte, flowing over the film in water, partitioned into the film and reached equilibrium after approximately 35 minutes. They reported that the signals are nearly twice the reported values for comparable IR-ATR measurements with various types of Teflon membranes due to the fact that plasma-polymerized fluoropolymer membranes are typically highly crosslinked, which is in contrast to solution deposited fluoropolymer films. Complete depletion of the analyte in the enrichment membrane was achieved after approximately 95 min by flushing with deionized water. Despite comparatively slower analyte transport into membranes, limits of detection below 300 ppb were obtained from two separate batches of plasma deposited films by integration of the peak of the C-Cl stretch at 913 cm^{-1}.

2.2.2. Selective separation

2.2.2.1. Molecularly imprinted polymers

It is, however, a different situation when biological elements such as antibodies, enzymes and nucleic acids are needed to be recognized with high accuracy. The traditional sensitivity that characterizes polymers becomes less pronounced due partly to their tendency to be bulky in size, which led scientists to molecular imprinting polymer (MIP) techniques. “Molecular imprinting is a template-directed technique that allows the design and synthesis of materials with well-defined artificial receptor sites for a wide range of chemical and biochemical compounds”.[17] **Figure 2.4** shows the process of making a film that is molecularly imprinted. In step one, a molecule of interest has specific binding molecules attached by physical interactions or chemical bonds that can be removed later. In step two, initiator or monomer molecules are chemically and permanently attached to the binding molecules. In step three, a polymerization occurs. In step four, the initial molecule of interest is removed from the binding leaving the binding molecules. For sensor technology, MIPs have been the object of focus for their improved discrimination between different biological analytes.[17-19]

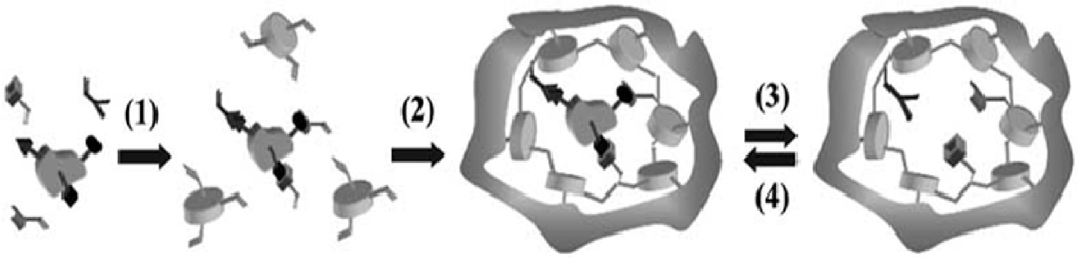

Figure 2.4. Molecularly imprinting scheme. Reprinted with permission from Bentham Science Publisherrs.[17]

Boris Mizaikoff et al. performed extensive research into MIP with organic molecules.[20-22] They have found that application with IR sensors have produced highly selective analysis.[20] The specific target analytes they used was an herbicide 2,4-dichlorophenoxyacetic acid (2,4-D) and phenoxyacetic acid (POAc). They used three different MIPs, at different ratios. Specifically, 4-Vinylpyridine (4-VP), methyl methacrylate (MMA), and ethylene glycol dimethacrylate (EGDMA) with a low amount of a cross linking agent were used. To quantify the sorption properties of the MIP, they fit the experimental data to a theoretical model obtained by combining a Langmuir isotherm with a linear term. From this model fit, they were able to extract dissociation constants for 2,4-D and POAc and determined that high cross linking affected the absorption of analytes. IR spectroscopic sensing, they noted, was a sensitive method to analyze binding of analyte into the MIP and that the selectivity and robust nature of MIPs can mimic biological receptor binding in addition to be able to tolerate extreme environmental conditions without losing sensitivity.

2.2.2.2. Polymer membranes

Membranes play a crucial role in selective separation of separating desired substances from a mixture. Polymer brushes are particularly attractive because they can have binding capacities with proteins. Bruening et al.[23] performed layer by layer depositions of alternating ionic polymer films on porous alumina membranes, and porous polymer membranes for different applications. Some of their preparation methods included: a) deposition of a multilayer polyelectrolyte film on a support with 20-nm-diameter surface pores; (b) growing polymer brushes inside a support with 0.2- to 5-μm-diameter pores; and (c) layer-by-layer deposition of polyelectrolytes and charged metal nanoparticles (**Figure 2.5**). Their goal was not in detection but nanofiltration of gases and purification of proteins by polyelectrolytes and polymer brushes; however, it was understood that attachment of different polymers deposited layer by layer on a single substrate gave more durability and could be utilized to separate various mixtures.

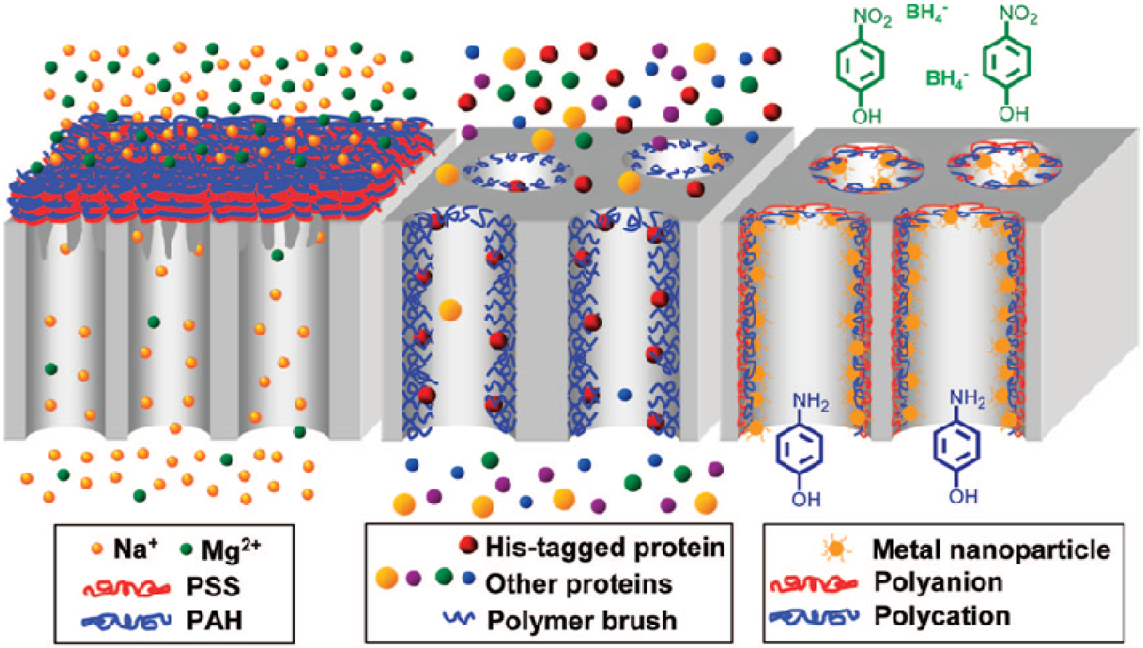

Figure 2.5. Multi-layer polymers held together by ionic complex interactions and primarily used for filtration of ionic compounds. Reprinted with permission from the American Chemical Society.[23]

2.2.3. Stimuli responsive polymers

It has been established that a polymer chain will undergo conformational changes in the presence of solvents. These changes can also be triggered with specific stimuli depending on the polymer. Common stimulants are pH, temperature, light and chemical potential which can influence specific chemistry along a polymer backbone. In **Figure 2.6,** certain regions of the polymer chain have been modified to be selectively responsive to stimuli. [24-26] By alternating any of these, one can tune the properties of a polymer chain or film to a desired stimulus. Poly(N-isopropylacrylamide) (PNIPAM) and poly(N-vinylcaprolactam) (PVCL) have been intensely researched due to their natural lower critical solution temperature (LCST) being around body temperature (37°C).[27-28] Much of the focus for these types of polymers has been in biomedical, biomimetics, drug delivery, and textiles however these polymers are also finding their way in sensor technology as well.[27, 29]

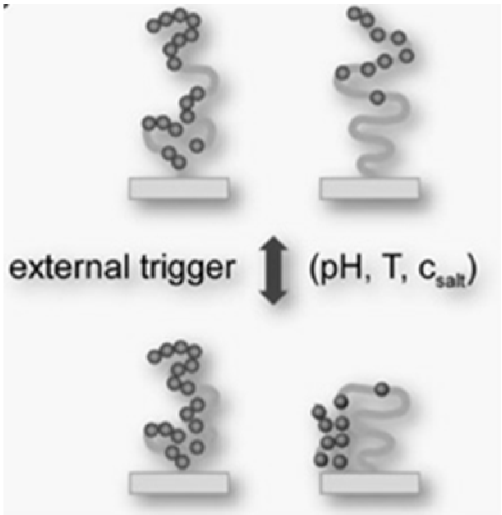

Figure 2.6. Depiction of external stimuli trigger on environmentally sensitive polymer. Reprinted with permission from Elsevier.[3]

2.2.4. Shape memory polymer systems

Kunzelman et al.[30] has initiated using shape memory polymers (SMPs) for sensor applications. SMPs are polymetric materials that have the ability to ‘‘memorize’’ a particular shape. They can be deformed to a temporary shape under specific conditions of temperature and stress but will relax to the original, stress-free state upon release of the external stimulus. This relaxation is associated with elastic deformation stored during fixation. There are one-way shape memory (1 W-SM) and two-way (reversible) shape memory (2 W-SM) phenomena that have been reported. The SMP that the researchers employed in this study was poly(cyclooctene) (PCO) that was subsequently cross-linked through a free-radical process using dicumyl peroxide. In order to determine the sensitivity the polymer has to various temperatures, the polymer was blended with a cyano-OPV fluorescent dye. This allowed identification of conformational changes that the polymer undergoes with the intensity of the fluorescent emission spectrum. The ratio of the excitation/emission intensity as a function of temperature is presented in **Figure 2.7**. They demonstrate that when the PCO is in its relaxed state, at room temperature, the dye is not available to fluoresce. When the "programmed" temperature is reached, the dye becomes available and an intense green color can be seen under UV excitation, when cooled, the dye emission is in the red region (the heating cycle is the circles and the cooling cycle is the squares). The process was demonstrated to be reversible.

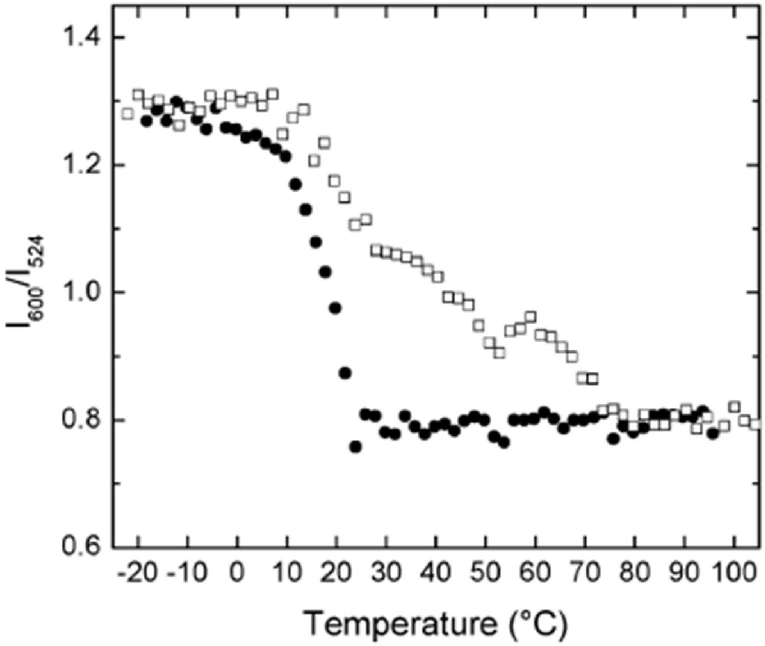

Figure 2.7. Ratio of excitation/emission intensity as a function of temperature that occurs with polymer shape changes. Reprinted with permission from the Royal Society of Chemistry.[30]

Another area of stimuli responsive polymers known as electroactive polymers (EP) has been research by Bar-Cohen et al[31]. Several different types of EPs have been classified including ferroelectric, dielectric, ionic gels, and conducting polymers. EPs are attracting attention because recently it was found that certain EP can change their shape with various stimuli. Applications for this are biomimetics as well as actuators and sensors.[32-33]

2.2.5. Additives improving detection

There are further methods to modify a polymer film to increase its sensitivity for detection. Namely, additives are incorporated into the films that are activated by a specific molecule. Carey et al.[34] added an acid indicator, chromazurol-S, to a blend of polybenzimidazole and polyimide that was coated onto a sapphire waveguide. Vapors of hydrochloric and nitric acid solutions were pumped into a cell that housed the waveguide. They were able to study light absorption from the dye as acid was picked up by the polymer film. By knowing the concentration of the analyte, the intensity of absorption was used to build a calibration curve. In addition to the sensitivity that was observed with the dye in the film, they conducted longevity study for the coating. When strong chemical reactions occur they can lead to degradation of the integrity of the film structure and then can lead to decreased sensitivity. In these studies, the films were found to remain intact without losing sensitivity for approximately 8 weeks. A last aspect of this reported research focused on the optical properties of polymer film swelling versus film thickness. It was observed that large offsets of the non-absorbing wavelengths are due to the refractive index changes of the nitric acid solutions by concentration. This indicated that the waveguide is evanescently coupled to the sensing medium even if there is no absorption. To reduce the refractive index changes that result from the incorporation of analyte, it is suggested that a thin polymer film (<0.5um) is enough to avoid interferences from swelling in the acid solution by reducing the concentration of analyte that can concentrate in the polymer film.

2.2.6. Other materials and uses of polymer films

It is important to mention that polymers are not the only materials that can be used to enrich a sensor and achieve significantly greater sensitivity and targeting capabilities. Magnetic materials have been used for detection of hazardous heavy metals. Polymers have significantly less affinity to metallic ions. Magnetic materials, such as iron oxide nanoparticles, were incorporated onto sensor platforms by Karatapanis et al.[35] Briefly, the enrichment made possible the determination of sub-parts per billion concentrations of Cd(II), Pb(II), Ni(II), Cr(VI) and As(V) from water samples.

In addition, metals have been previously shown to aid IR spectroscopic detection by electron promotion when it is engaged with an analyte. Sudo et al. deposited gold and silver nanoparticles to the surface of an attenuated total reflectance crystal and performed experiments to identify impurities in paint.[36] The specific technique they performed is known as surface enhanced IR absorption (SEIRA). The technique is still being heavily research and optimized as the ATR crystal material can influence sensitivity and the morphology of the metal used can affect the refractive index of the area above the surface of the ATR crystal.

2.3. Diffusion of penetrants in polymer films

Considerations for choosing polymers have been obtained largely from diffusion experiments. For detection purposes, fast diffusion of analytes to the sensing surface is preferable. Diffusion also offers insight to specific mechanisms of sorption and desorption of penetrants into polymer films. The microstructure and arrangement of polymer chains, as stated by Vesely, have a strong influence on diffusion.[37] The penetrant transport through the polymer film is critically dependent on the spacial and conformational arrangement of the macromolecules. Polymers can be amorphous or semi-crystalline and both phases behave differently. The amorphous and crystalline regions have their own sensitivity to processing methods, and rate of cooling and annealing. Most penetrants will plasticize or soften the film with only little quantities but will substantially reduce its glass transition temperature.[4]

Briefly, to understand why amorphous and semi-crystalline polymers behave differently, one must understand that the structure of crystalline regions of polymers is usually in the form of a spherulite. This phase has ‘fibrils’ a few hundred nanometers in diameter which grow from a nucleus in all directions. Polymer chains are closely packed and closely follow the crystalline order. Amorphous material fills the space in between the fibrils and thus is less dense and disordered. The chains can be entangled and intermolecular forces give rise to the material’s mechanical strength and can be a very significant factor, not only for strength, and melt viscosity, but also for diffusion.[4, 38-40]

The presence of the crystalline phase can complicate diffusion studies due to lower free volume available.[41-44] The random amorphous regions are thus the most likely the carrier phase during the diffusion process. The absorption of the penetrant requires a change in the chain configuration to accommodate the penetrants molecules and also the neighboring chains. This means that the polymer can only swell in the direction opposite to the direction of diffusion. Sizes of these openings can be on the order of hundreds of nanometers, and can cause light scattering effects and dramatic changes in refractive index if the polymer film is several hundred microns or thicker (less likely for ultrathin polymer films).[45-46]

Diffusion properties of polymers can be further influenced by chemical reactions, thermal history, homogeneity, additives, contaminants, solvents (plasticizers), and also by branching and cross linking.[47-48] It can, therefore, be concluded that, in experimentation, direct comparison can only be done using polymer from the same batch and of the same formulation and thermal history. Subsequently, the literature data can only be compared for trends and not in their absolute values.

Penetrant considerations have also been examined by many researchers. Specifically, Murphy and McLoughlin[49-50] studied the diffusion of 1,2-dichloroethylene (*cis*-DCE), dichlorobenzene (DCB), trichloroethylene (TCE), trichlorobenzene (TCB), and tetrachloroethylene (TeCE) in aqueous solutions through Teflon membranes. Their purpose was to compare the diffusion of molecules with similar polarity but of varying size of the penetrant. By monitoring the IR absorbance peak of the absorbing molecule, they were able to assess the diffusion. Results showed that as the number of chlorine atoms increased, the diffusion coefficient was reduced. In addition, by increasing the number of carbon atoms, the diffusion of the penetrants was slowed significantly. Similarly, compounds that are bulky by nature, such as dichlorobenzene, had limited diffusion into the Teflon membrane and varying the positions of chlorine atoms along the chain had little effect. For isomers of dichloroethylene, results suggest that the position of the chlorine atoms do affect the molecule's diffusion. It was hypothesized that this was the result of the molecule's molar volume.

2.4. Fabricating Polymer films

2.4.1. Synthesis and chemical modification

By applying polymers to surfaces, one can transform a surface with limited functionality to one with greater application potential and alter properties such as colloid stabilization, lubrication, rheology, immobilization of catalysts, generation of multiphase materials, adhesion, friction, wettability, and biocompatibility.[51-54] Understanding how to synthesize and build polymer films and multiple layers is essential to create an anchored enrichment layer that is effective. The method of synthesis of a polymer relies on the starting monomers but polymerizations can fall into a few categories such as radical, condensation, ionic, photoinitiated, and radiation initiated.[55] **Figure 2.8** shows different possible polymer layers that can be synthesized. The versatility to control the functionality, density and forming gradients with post reaction techniques as well as the adaptability to any surface (flat or spherical) are trademarks that make using and building polymer brushes so appealing. **Figure 2.9** illustrates that post polymerization modification can be versatile and done in various stages or amounts.

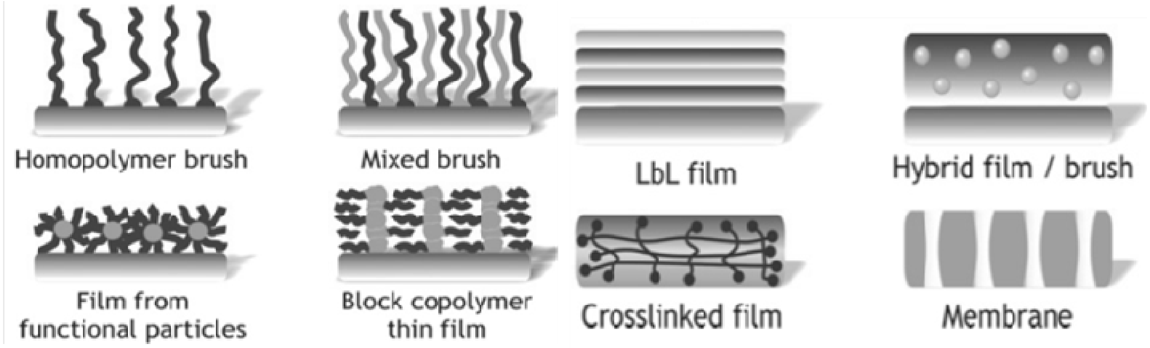

Figure 2.8. Functionalized surfaces achieved by use of polymer brushes, layers, thin films, modified particles and membranes. Reprinted with permission from the Royal Society of Chemistry.[54]

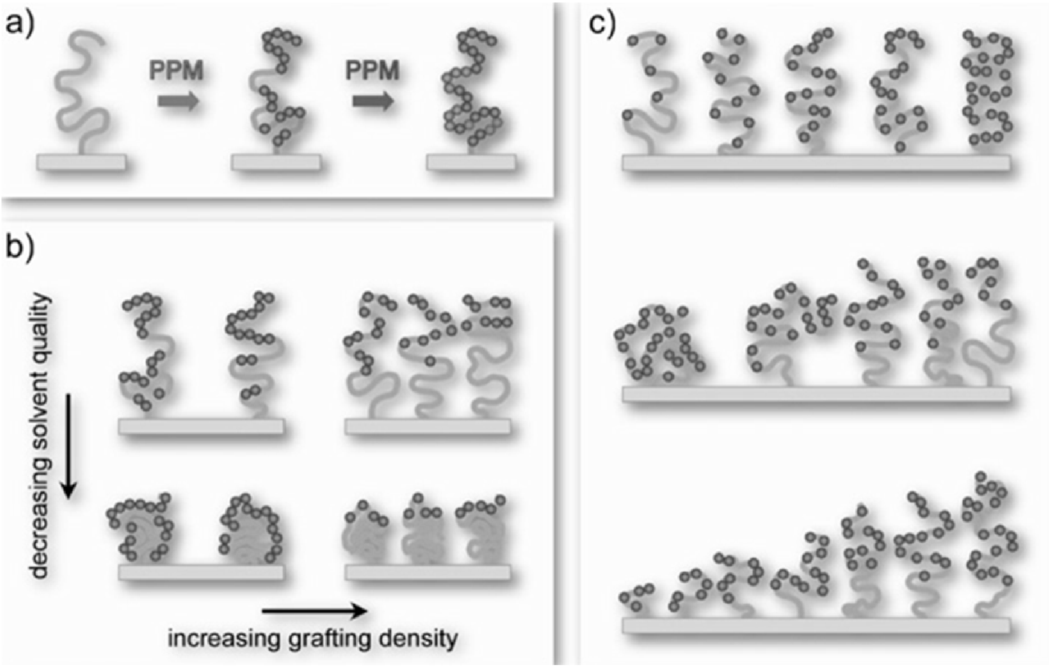

Figure 2.9. Modification of surface chemistry through post-polymerization methods a) multi-step with different functionality, b) strategic modification for environment sensitivity, c) gradient modification. Reprinted with permission from Elsevier.[3]

2.4.2. Coating methods

Fabrication of polymer films relies on reproducibility. Polymer films made from pre-synthesized polymers can be time saving but there are potential hazards of which one must be cautious. Large wrinkles, incorporation of unwanted particles, and slow evaporating solvents can have consequences that will influence the polymer film's stability, wettability, and uniformity. There are well known techniques available that provide high reproducibility of polymer films that can be used.

2.4.2.1. Dip coating

Dip coating is a straightforward method to deposit polymer films and build layers. Dip coating, and a similar technique known as curtain coating, have been used for specific applications in industry.[56-57] The dip coating process can be accomplished on any substrate. If wetting of the surface is not favorable for the solvent, reducing the speed can allow the polymer coat the surface by kinetic diffusion. The concentration and subsequently the viscosity of polymer solutions is the primary controlling mechanism for the thickness of polymer films that can be made. Much research has been done on the rheology fluid dynamics of polymer solutions.[58-59] The substrate is submerged into the polymer solution of choice at a constant velocity, V_{sub}, and retracted at a constant velocity, V_{ret}, however, V_{sub} and V_{ret} do not have to be equal (**Figure 2.10**). For non-volatile solvents, v_{ret} is often much lower in mm/min so to allow diffusion of the molecules through the coated polymer film.

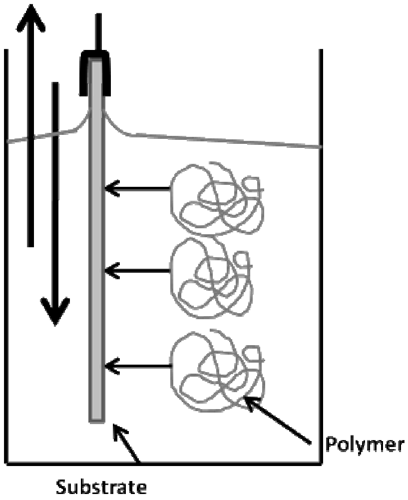

Figure 2.10. Dip coating scheme. The polymer will adsorb onto the substrate with high affinity or given enough time, kinetically adsorb.

2.4.2.2. Spin Coating

Spin coating is another method to deposit polymers as films. Spin coating is used in numerous applications such as coating of photoresist, protective coatings, paint coatings, optical coatings and membranes. Rate of the sample rotation is a primary factor that influences polymer film thickness (**Figure 2.11**). Spin-coating is widely employed for the highly reproducible fabrication of thin film coatings over large areas with high structural uniformity. Research in recent years has extended the scope of spin-coating by chemically engineering the interface of support and solution to obtain specific structural order in the resulting supported thin films.[60] The rate of solvent evaporation, however, can be crucial for obtaining a smooth and uniform surface.[61] The equation in **Figure 2.11,** η_0 Initial viscosity, and ω angular velocity are known, while k and α (~0.5) are empirically determined and β is the initial solution viscosity which is observed to be in the range 0.29–0.39 for polymer solutions.[60, 62-63]

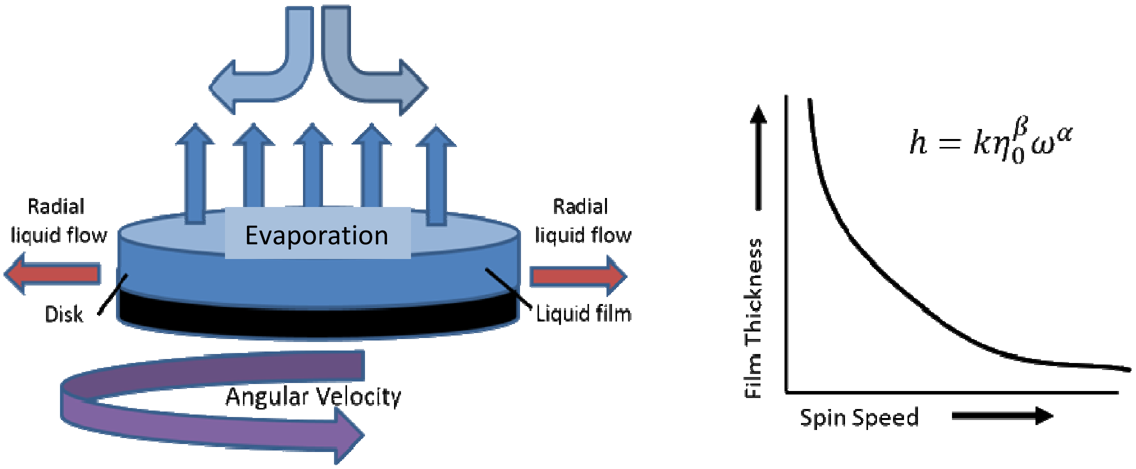

Figure 2.11. Operation of spin coating thin films with relationship of thickness to viscosity and angular momentum. Re-drawn from Reference #60.

2.5. Grafting Polymers to surfaces

2.5.1. “Grafting to”

Anchoring polymers by the “grafting to” method, where a polymer chain is tethered with a chemical bond to a surface by either one end group or multiple along the backbone, is relatively straight forward (**Figure 2.12**). Modification of inorganic surfaces is often based on reaction with surface hydroxyl groups.[48-50] The ϖ-functional alkoxy- or chloro-silanes are covalently grafted to these surfaces, most notably silicon substrates. For gold substrates ϖ-functional thiols are commonly used. Modification of polymer surfaces depends on reactivity of functional groups in polymer chains. The polymer surface can be activated using plasma treatment, UV- or γ-irradiation, or chemical oxidation that can be controlled so as to not destroy the polymer sample but to introduce reactive functional groups (–OH, –NH2, –COOH) onto the polymeric substrate if reactive groups are not present or not compatible.[53, 64-66]

For inorganic surfaces that do not have an oxide layer, specifically silicon, thermal radiation, UV radiation or radical initiation is used to activate the surface and attach an alkene through hydrosilylation.[67] The alkene attaches via a Si-C bond and usually carries with it a short or long hydrocarbon chain with an end group that can be used for grafting the desired macromolecule.[64, 67-72] Any limitation that “grafting to” techniques have lie in the diffusion of reactive groups to the surface of the substrate causing only a limited number of chains to be grafted. This essentially reduces the possible thickness of grafted layers.

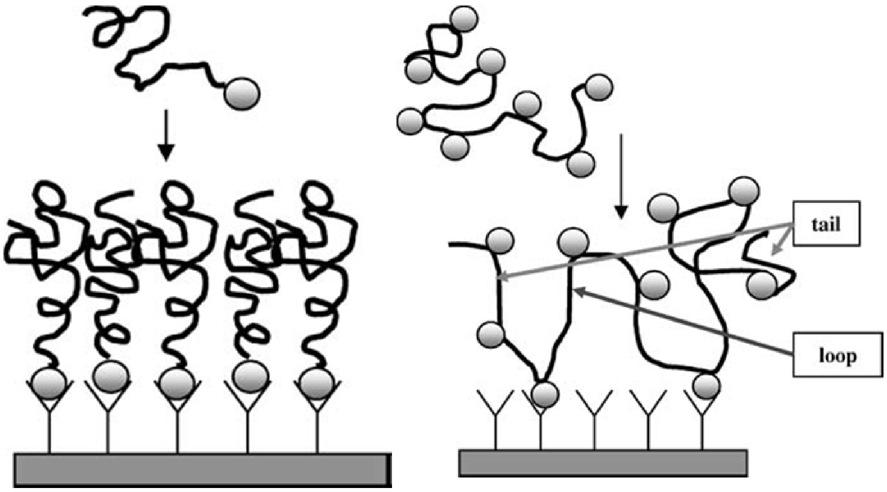

Figure 2.12. Grafting to represented with end group attachment (left) and backbone group attachment (right). Reprinted with permission from Springer.[53]

2.5.2. “Grafting from”

Another form of polymer anchoring includes “grafting from”[65], where a polymer is synthesized from a solution of monomer having the initiator already chemically bonded to the substrate surface which can be any shape (**Figure 2.13**).[73] Polymerization reactions that are utilized in this methodology encompass nearly all radical, living, plasma, ionic and ATRP type reactions.[70, 73-75] This grafting method is often found to be the one most commonly used because one can grow a polymer brush with a much higher molecular weight and thickness than in the “grafting to” technique because there is a higher probability of monomers diffusing through the film to find the reactive end of the brush. Similarly, one can form a block film by synthesizing a block copolymer and controlling the molecular weight of each block. This tends to reduce the need to find one solvent for different monomers which can affect the outcome of the polymerization.

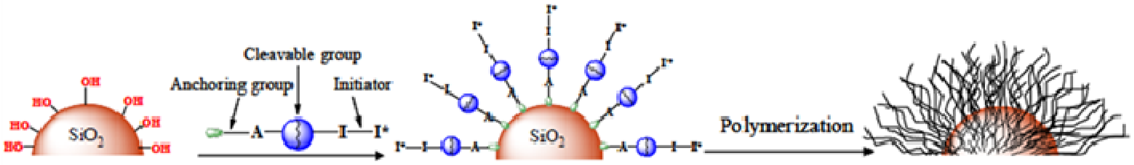

Figure 2.13. Scheme of silica particles undergoing a "grafting from" polymerization. Reprinted with permission from Materials.[71]

2.5.3. Crosslinking

A challenge for EPLs is that the polymer films need to be durable through multiple swelling cycles and be sustainable in harsh environments. Cross linking in a polymer film restricts the chains from moving past each and restricts the viscous flow, creating a more stable film. It also causes a reduction in crystallinity, and impedes chain orientation. This can lead to the polymer becoming more elastic, and gaining a lower melting point. A slightly cross linked polymer film will also have changes in its local molecular packing which can lead to a decrease in free volume. This often leads to a reduced ability to swell with penetrating analytes, however, in harsh environmental conditions it is essential for the enrichment layer to not delaminate. In addition, cross linking has been found to improve mechanical properties of films.[76]

Sakai et al.[77] in 1991 performed experiments to develop an electrode sensor to measure relative humidity. Polytetrafluoroethylene (PTFE) and poly-4-vinylpyridine (P4VP) were deposited on a gold electrode, and then grafted and slightly cross linked as a film. While this was a long way from being a foolproof way to measure relative humidity, it gained ground developing environmentally resistant EPLs. Cross linking of polymers can be done by annealing the polymer with complimentary functional groups at high temperatures or by adding a cross linking agent. UV curing has also become a well known technique in industrial coatings as it is fast and has no need of solvents.[76, 78] Resulting cross link density can be determined by swelling ratios of the polymer film.[79]

2.6. Characterization of polymer enrichment layers

Polymer film mechanical, physical and chemical properties require an in depth examination to identify what mechanisms or characteristics have yielded specific properties. Characterization techniques that can be used to characterize EPLs are Fourier transform IR spectroscopy (FT-IR), ellipsometry, scanning probe microscopy (SPM), and x-ray diffraction (XRD) analysis. These techniques yield information on chemical functionality, surface morphology, atomic percentages over long and short ranges and optical properties such as refractive index as well as thickness.

2.6.1. Fourier-Transform IR Spectroscopy (FT-IR)

Fundamental vibrations of organic functional groups present in the polymer chain are readily identified with FT-IR.[80-82] This technique operates on the principle that atomic bonds vibrate with certain frequencies based on their mass and bond strength and that resonance frequencies can be absorbed when samples are irradiated.[83] The equation for determining these frequencies is given

$$\upsilon = \frac{1}{2\pi c}\sqrt{\frac{f}{(\frac{M_x M_y}{M_x + M_y})}} \qquad (2.4)$$

where ν is frequency, c is the speed of light, *f* is a force constant representing the bond strength, and M_x M_y are the masses of the atoms in this particular diatomic model. Calculated wavenumbers for some common diatomic functional groups are given in **Table 2.1**.

Table 2.1. Calculation of diatomic functional groups by equation 2.3

Element	Atom mass [g]	Bond	Bond force constant [dyne/cm^{-1}]	Functional group	Theoretical Wavenumber [cm^{-1}]
Carbon	1.99236E-23	Single	500000	C=O	1578
Hydrogen	1.6603E-24	Double	1000000	C-C	1193
Oxygen	2.65648E-23	Triple	1500000	C-H	3042
Nitrogen	2.32442E-23			O-H	3012
Deuterium	3.3206E-24			N-H	3025
				O-D	2192
				C-D	2232
				N-D	2209

Neighboring functional groups will draw electron density or donate electron density which will shift fundamental resonance frequencies of simple two atom systems. Overtones of these natural vibrations are known to absorb in the near IR region and are integer multiples of the fundamental frequencies.[84] When identifying compounds, these neighboring groups can help to set the absorption spectrum apart from similar compounds, however, one must be careful when preparing a sample so no contaminate is present that would artificially offset absorption peaks. FT-IR is such a profoundly powerful technique to identify specific chemical functionality that it is cited as a standard analytical tool for any synthetic research.[20, 49, 81, 85-91]

Acquisition of FT-IR spectra can be successfully conducted in static and dynamic conditions. This is due to the rapid development of software that can collect multiple spectra is short amounts of time. This allows scientists to perform time resolved analysis of shifting frequencies due to active stimuli that is applied.[92] Many methods of preparing samples exist and with them different methods have been developed to characterize polymers by FT-IR and should be applied to the appropriate sample form (**Table 2.2**). Sample recovery is easy as no damage to samples is necessary. One of the most widely used techniques due to its speed and lack of need for much sample preparation is the attenuated total reflection (ATR) FT-IR methods. The two most popular ATR crystal materials used for polymer analysis are zinc selenide (ZnSe) and diamond. The differentiation for use of ZnSe or diamond is the form and hardness of the polymer sample.[94] Both of these crystals have a refractive index of 2.4 and with a typical polymer

Table 2.2. Sampling techniques for FT-IR spectroscopy of polymers. Reprinted from Perkin Elmer[93]

Sample Form	Suitable Techniques
Thin films (<25um)	Transmission
Fine powders (<2um)	Transmission (KBr), ATR, DRIFT
Large items	DRIFT (abrasive sampling)
Irregular shapes, pellets	ATR, DRIFT (abrasive sampling)
Polymers soluble in volatiles solvents	Transmission (cast film)
Flat, reflective surfaces	Specular reflectance, ATR, DRIFT (abrasive sampling)
Single fibers	Diamond ATR or IR microscope

having a refractive index of 1.5, the depth of penetration into the sample is the greatest for these two crystal materials. As the refractive index increase with the crystal material, the depth of penetration decreases.

FT-IR can show molecular interactions and changes after some event by comparing the before and after spectrum to visualize drifts in waveband, especially when changes occur due to temperature or in polymerblends or via diffusion.[91, 95-98] The technique is also able to detect structural alteration upon surface treatments.[99] Polarization of the IR light is a useful way to gauge the percentage of chain orientation of a polymer sample. When polymer chains are put under an oriented strain, they arrange to that direction. By polarizing the IR radiation, the ratio of chain orientation can be determined as IR energy will not be absorbed by chains that are arranged perpendicularly. New IR microspectroscopy mapping techniques have been developed to determine the composition of polymer blend gradients.[100]

In attenuated total reflection (ATR), optical effects of materials are used to manipulate IR light to probe a sample’s chemical identity. The main mechanism is the evanescent wave (EW). The EW is formed above the surface of the waveguide material when the IR light hits the interface between the waveguide crystal and the sample at a critical angle. The critical angle allows most of the energy to be reflected to advance to the detector. Energy that is lost is absorbed by the sample. The EW has a depth of penetration into the sample and when other conditions are held constant, the depth is dependent on the wavelength of light. This means that shorter wavelengths tend to not penetrate far into the sample compared to longer wavelength. As the EW leaves the waveguide material, it has an exponential decay of intensity from the surface. The depth of penetration into the sample material is determined by

$$d_p = \frac{\lambda}{2\pi n_1\sqrt{\sin^2\theta-(n_2/n_1)^2}} \tag{2.5}$$

Where d_p , λ, θ, n_1, and n_2 are the penetration depth, wavelength, incident angle, ATR crystal refractive index and sample refractive index, respectively. With this equation it is possible to gage the maximum depth that the radiation wavelength can penetrate into the material assuming that there is no absorption for that wavelength. **Figure 2.174** depicts the evanescent decay away from the surface of the waveguide crystal with a sample that is non-absorbing and the d_p is the maximum height of the wave.

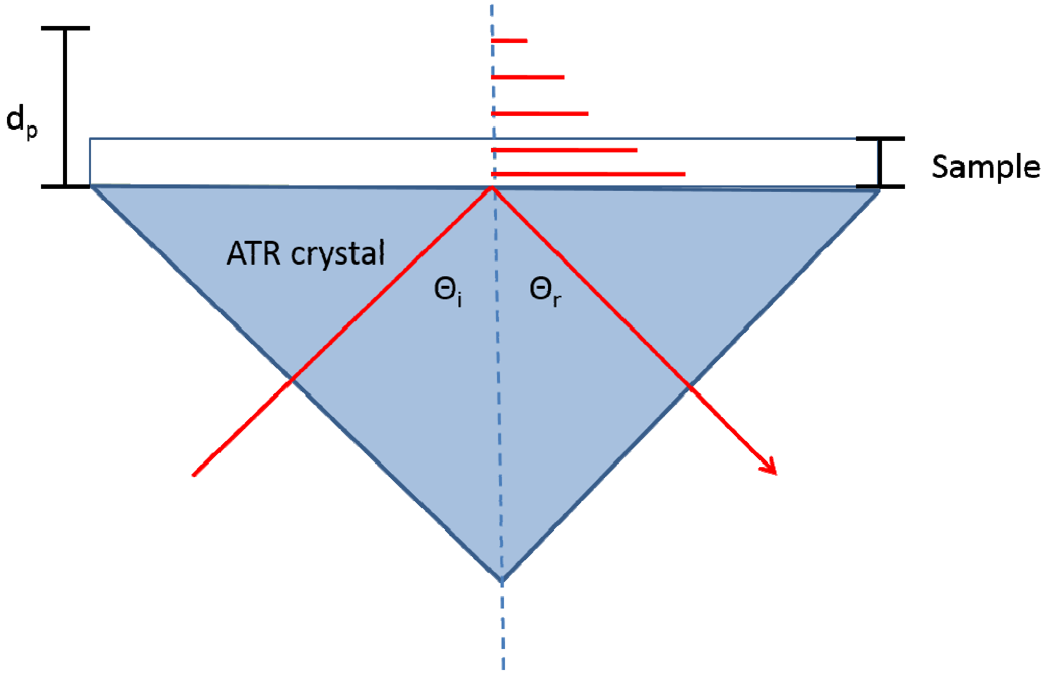

Figure 2.14. Diagram of ATR crystal with IR light bouncing off the surface at a critical angle to produce an evanescent wave. The d_p is dependent on the refractive index of the material.

Because there are several bounces in the waveguide crystal, this increases the distance the radiation travels in the sample despite the film being nanometers thick. Consequently, the sensitivity of the technique is increased. FT-IR spectroscopy follows the Beer-Lambert law, which means there is a relationship between the intensity of the absorption and the concentration of the species absorbing the radiation. In fact, there is absorption by the polymer films and because of this, the thickness of the films is kept well below the depth of penetration of the evanescent wave. For example, the depth of penetration for 1700 cm^{-1} is approximately 0.5um. What this means is that as the VOC is absorbed by the polymer film, it is close to the most intense portion of the evanescent wave.

2.6.2. **Atomic force microscopy (AFM)**

Atomic force microscopy (AFM) is a primary method to gain topological and morphological information of a surface at the micron and sub-micron scale. Morphology of polymer surfaces reveals chain behavior after processing and is highly adept at providing structure–property relationships. It is been used when studying polymer blends, crystallization, and lamellae. Moreover, mechanical properties, electrostatic, adhesive, and magnetic properties of a polymer film can also be determined.[101-109] The powerful functionality of SPM comes from its use of ultasharp probes that allow nanoscale resolution as well as the manipulation of matter on the surface. A voltage is applied to the piezo cantilever which oscillates the probe tip. The voltage can control the level of oscillations which allows the tip to probe the surface of the sample either by direct contact or non-direct contact. Imaging under a wide variety of environments, including ambient conditions, fluidic conditions, gases, and under different temperatures can be accomplished without much special sample preparation.[110]

There are three common modes that are employed for different types of materials or experimental conditions (**Figure 2.15**). The first being contact or static mode which involves relatively large shear forces by having the probe actually drag along the surface. This frequently causes damage and distortion of soft surfaces. A second mode of operation is a noncontact mode. This has the probe operating about 5–40 nm above the sample surface, perturbed by the attractive van der Waals forces between the tip and the sample. In order to extend the ability of non-contact mode due to the limitation of the relatively weak tip–sample interaction forces observed, the cantilever is set to oscillate at or slightly off of the resonance frequency. This reduces the typical operational forces by at least one order of magnitude and eliminates the shear force compared to contact mode. For studying soft materials such as polymers, most often the third mode, known as tapping mode is employed so as to not create mechanical deformations on the sample.[103] To date, tapping mode has been extensively employed for imaging a wide variety of polymer surfaces that are glassy, crystalline, rubber, gels, fibers, blends, block copolymers, and composites. This mode operates by oscillating the probing cantilever so it does make contact with the surface but in such a way so the interacting van Der Waals forces are minimal. Nonetheless, it can result in surface modification as well as affect the phase shift angle.

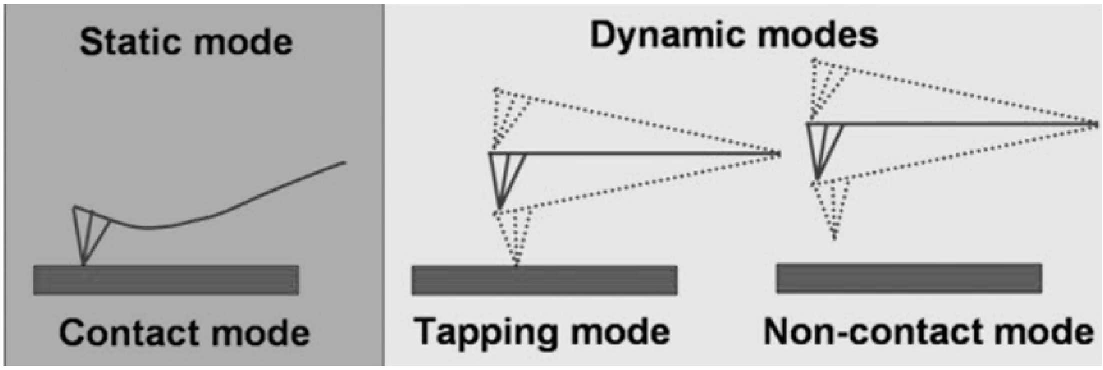

Figure 2.15. Representation of AFM modes of operations. Reprinted with permission from Taylor and Francis Publications.[123]

Mechanical properties of a polymer surface can be done by studying the force-distance curves while moving the probe toward the surface and back (**Figure 2.16**). From the slope of the force–distance curve when tip is pushed against surface (point B) compliance or elastic modulus can be determined while the pull-off forces correspond to the adhesive forces. Sensitivity to amplitude damping and phase shift can provide information about the viscoelastic surface properties including the storage and loss modulus and the adhesion properties. Phase images provide the best contrast of discrete morphological and nanostructural features due to their high sensitivity to surface imperfections. On surfaces with local variations of mechanical properties, the phase changes are even more informative. The images emphasize surface nanostructure of the microlayer, where the force leads to frequency and phase shifts, both measured with respect to the frequency and phase of the freely oscillating cantilever. Although the usefulness of SFM to examine adhesion and mechanical behavior of polymers at submicron scales is well established, quantitative studies have only recently been undertaken.[110-112]

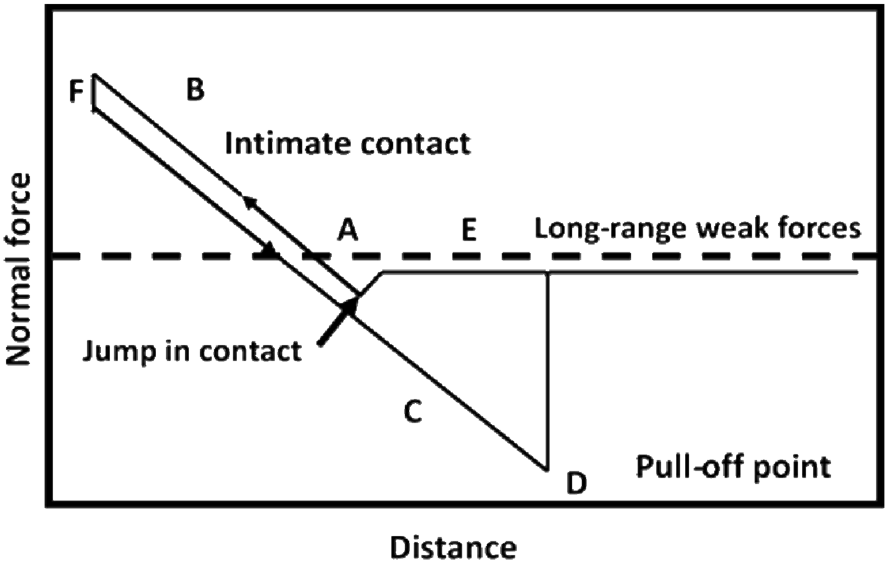

Figure 2.16. Representative force vs distance curve for determining mechanical properties of a polymer film. Re-drawn from #125.

2.6.3. Ellipsometry for polymer films

Ellipsometry is a sensitive optical technique that is used to gain information about the structure of the surface, film interface, refractive index, and film thickness. In addition, this technique has been developed to probe other topics such as phase transitions in monolayers, wetting transitions, molecular conformation, interfacial broadening, Marangoni effects, and critical phenomena.[113]

Figure 2.17 demonstrates how the incident light, E, forms a plane of interest through the sample. E_{ip} and E_{is} represent the two polarizations of the incident light. E_{rp} and E_{rs} are the reflected light that enters the detector. The technique measures the change in the state of the polarization of light at a known angle-of-incidence with a known wavelength upon specular reflection from a planar interface.

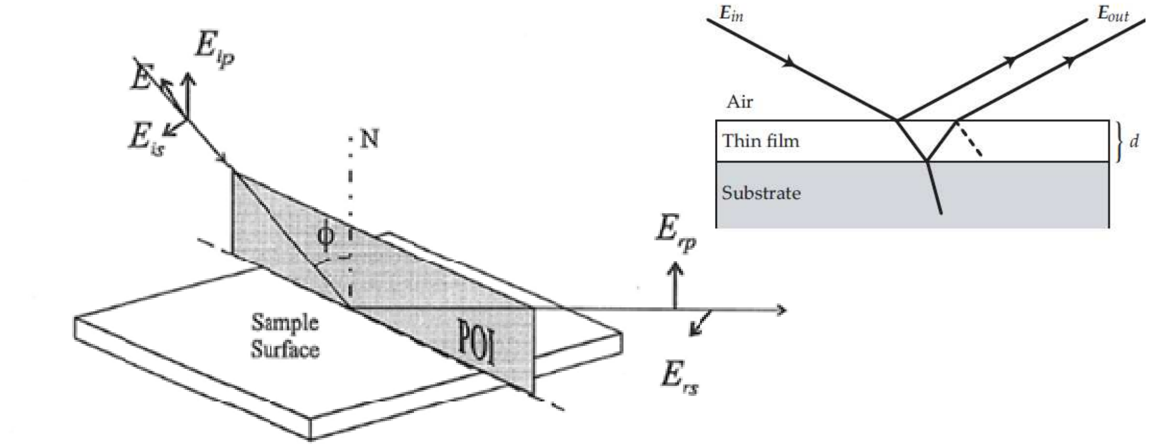

Figure 2.17. Depiction of incident light (left) as it bounces off the sample surface and (right) as it penetrates through the sample layer.

To measure the changes of the incident light, a ratio of intensities for two orthogonally polarized light beams are needed. A polarizer filter is used to polarize the incident light, E, at a known angle, E_{ip}. At the same time, a filter for the detector is used to allow light at the same angle of the incident polarized light that has been reflected from the surface of the substrate, E_{rp}, to enter the detector. In the same measurement time period, the detector filter switches to allow any amount of the complimentary orthogonal component of the incident light that is produced from the physical properties of the sample as it reflects off the substrate surface, E_{rs}, to enter the detector. At a separate time, the incident angle plus 90 degrees, E_{is}, is produced for the orthogonal component. The detector measures both angles once again. When the polarizer filter closes; the detector measures background intensity. **Figure 2.18** shows the arrangement of the filters versus the intensity readings over time.

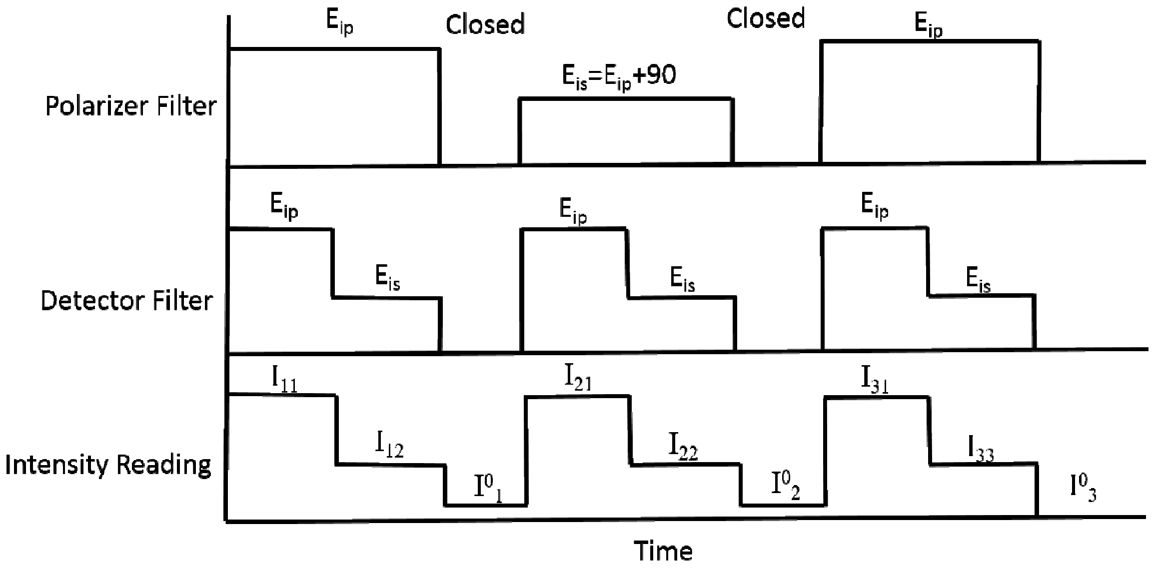

Figure 2.18. Filter positions and intensity readings in time for ellipsometry operations.

Derived from Snell's law, the relative changes in the amplitude of the polarized light, expressed as tanΨ, and the relative change in the phase difference between the s- and p-components of the light, expressed as cosΔ, are determined through ratios of intensities of the light at polarized angles.[114-116]

$$\Delta \approx \frac{I_{11}}{I_{22}}, \Psi \approx \frac{I_{12}}{I_{21}} \tag{2.6}$$

Changes of phase and amplitude are modeled to calculate a thickness or refractive index as long as one variable is known.[117] This variable is usually thickness which can be determined from direct measurements such as AFM. By modeling the Δ and Ψ components of the light, it is possible to determine many physical attributes of the sample.

An ongoing concern with the technique of ellipsometry is identifying the best way to process information from a data set for the system being studied. Ellipsometry is not a direct measurement of film thickness and optical constants. To find the sample structure whose optical response best matches experimental measurements, regression analysis is used. Through regression analysis, unknown sample properties ("fit" parameters) whose response best matches the experimental data, are found — this process is also referred to as "fitting" the experimental data. "Ellipsometric accuracy is defined as the residual error between the experimentally measured and ideal values of ellipsometric data, where the experimental data are acquired/averaged over a long enough time period to reduce the random errors (noise) to negligible levels".[118] Due to the extremely high precision and sensitivity obtainable by modern ellipsometer systems, it is essentially impossible to fabricate a reference sample in which the ideal ellipsometric values are known to a level comparable to the ellipsometric precision. Most of the pitfalls lie in the fact that Ψ, and Δ rely on each other but in depth coverage on this topic is beyond the scope of this chapter.

The technique has gained strong usage with "in situ" to studies of film growth by physical and chemical vapor deposition techniques.[113, 119-120] The development of variable-angle spectroscopic ellipsometry (VASE) can provide much more detailed information. It has offered additional means for the examination of multilayer samples, using a fit over the entire wavelength and angular range. VASE is also sensitive to gradients in material properties vs. depth in the film, optical anisotropy, and any physical parameter that depends on the material optical constants (such as crystallinity, alloy composition, and temperature).[121-123]

IR spectroscopic ellipsometry (IRSE) has become increasingly useful for thin film characterization. IRSE measures both the amplitude ratio Ψ and phase difference Δ of *p*-

and *s*-polarized light while additionally studying molecular bond absorption strengths in-plane and out-of-plane which provides information about average molecular orientations.[124-127] Additional information present in IRSE data allows simultaneous determination of accurate dielectric function, IR absorption, and thin film thickness. Furthermore, IRSE is capable of characterizing anisotropic materials, for example, the polymers polyethylene terephthalate (PET) and polyethylene naphthalate (PEN). The optical properties of these polymers become direction dependent when prepared as thick sheets. Characterization with their direction-dependent anisotropy (e.g. the refractive index is not the same in the x, y, z planes) thus is more complicated.[125]

2.6.4. **X-Ray scattering analysis**

In long range dimensions, semi-crystalline polymers have a structural hierarchy. This is usually taken in the form of lamellae or small crystallites. Further organization of these crystals into the next level of hierarchy depends on the external constraints, but they can have significant effects on the bulk properties. X-ray diffraction (XRD) has been successfully used to study these structures in semi-crystalline polymers. XRD utilizes the diffraction pattern of x-ray waves out of the sample which will have a pattern unique to the morphology and crystallinity in the sample. Small-angle X-ray scattering (SAXS) can gauge structures at length scales larger than a unit cell to study electron density and identify inhomogeneities.[128-129] Conversely, wide angle X-ray diffraction (WAXD) is used to study the orientation of the crystals, and the packing of the polymer chains within these crystals.[130-132] SAXS can also provide information about the fibrillar morphology.

Interfaces between immiscible polymers, and at interfaces with solid substances is critical for understanding and improving the performance of polymer multi-component systems and the X-ray techniques available are arguably the most widely used quantitative technique for this analysis (other techniques include scanning electron microscopy (SEM), transmission electron microscopy (TEM), and neutron reflectivity).[129, 133-136] X-ray reflectivity techniques have a penetration depth of several hundred nanometers with a spatial resolution of 1 nm, but the information obtained is the optical transform of the concentration profile in the specimen which requires model calculations to interpret the data.[136]

In addition, X-ray photoelectron spectroscopy (XPS) has become a standard quantitative method for characterizing polymer surfaces and interfaces. The surface sensitivity of XPS stems from the extremely short mean free path of the electrons ($\lambda \sim 2.3$ nm) and their strong dependence on kinetic energy. For atoms of carbon, nitrogen, and oxygen, compositions of 0.2 atom% is possible, however, it is not possible to obtain an absolute number of atoms in this range. One must rely on the ratios of the signals coupled with known photoionization cross sections to determine concentrations. Additionally, it can be used to determine hybridization of carbon at different depth in a sample.[137-139]

Near Edge X-ray Absorption Fine Structure (NEXAFS) spectroscopy is a strong technique to determine compositional analysis in soft matter.[140] Polymers in particular are sensitive to radiation damage caused by X-ray and electron irradiation and there is a risk that the sample and its spectrum might degrade faster than any meaningful analysis can be performed.[141] In general, the radiation chemistry and damage of polymers can take several forms, such as loss of crystallinity, loss of mass, or chemical modification. With a quantitative understanding of the radiation damage kinetics, it can be possible to design experiments that work within a tolerable damage limit. Currently, the level of radiation damage for X-ray microscopy of polymers is not so severe as to prohibit the analysis of most polymer materials, however, the push to higher spatial resolution and the elucidation of more subtle spectroscopic differences will make radiation damage a growing concern.[142]

2.7. References

1. Janata, J.; Bezegh, A., Chemical Sensors. *Analytical Chemistry* **1988,** *60*, 62R-74R.

2. Semancik, S.; Cavicchi, R. E., The use of surface and thin film science in the development of advanced gas sensors. *Applied Surface Science* **1993,** *70* (71), 337-346.

3. Galvin, C. J.; Genzer, J., Applications of surface-grafted macromolecules derived from post-polymerization modification reactions. *Prog. Polym. Sci.* **2012,** *37*, 871-906.

4. Sperling, L. H., *Physical Polymer Science*. 4th ed.; John Wiley & Sons Inc.: Hoboken, 2006.

5. Hansen, C. M.; Abbott, S.; Yamamoto, H.; Valpey III, R. S. *HSPiP*, 2; **2009**.

6. Panayiotou, C., Partial solvation parameters and LSER molecular descriptors. *Journal of Chemical Thermodynamics* **2012,** *51*, 172-189.

7. Vitha, M.; Carr, P. W., The chemical interpretation and practice of linear solvation energy relationships in chromatography. *Journal of Chromatography A* **2006,** *1126*, 143-194.

8. Difilippo, E. L.; Eganhouse, R. P., Assessment of PDMS-Water Partition Coefficients: Implications for Passive Environmental Sampling of Hydrophobic Organic Compounds. *Environmental Science & Technology* **2010,** *44*, 6917-6925.

9. Robak, W.; Apostoluk, W.; Ochromowicz, K., Linear Solvation Energy Relationship (LSER) Analysis of Liquid-Liquid Distribution Constants of 8-Hydroxyquinoline and Its Derivatives. *Journal of Chemical & Engineering Data* **2011,** *56*, 3971-3983.

10. Shih, Y.-h.; Chou, S.-m.; Peng, Y.-H.; Shih, M., Linear Solvation Energy Relationships Used To Evaluate Sorption Mechanisms of Volatile Organic Compounds with One Organomontmorillonite under Different Humidities. *Journal of Chemical & Engineering Data* **2011,** *56*, 4950-4955.

11. Heinrich, P.; Wyzgol, R.; Schrader, B.; Hatzilazaru, A.; Lubbers, D. W., Determination of Organic Compounds by IR/ATR Spectroscopy with Polymer-Coated Internal-Reflection Elements. *Applied Spectroscopy* **1990,** *44* (10), 1641-1646.

12. Eastman, M. P.; Hughes, R. C.; Yelton, G.; Ricco, A. J.; Patel, S. V.; Jenkins, M. W., Application of the solubility parameter concept to the design of chemiresistor arrays. *Journal of the Electrochemical Society* **1999,** *146* (10), 3907-3913.

13. Patel, S. V., Chemicapacitive microsensors for volatile organic compound detection. *Sensors and Actuators B: Chemical* **2003,** *96* (3), 541-553.

14. Flavin, K.; Hughes, H.; Dobbyn, V.; Kirwan, P.; Murphy, K.; Steiner, H.; Mizaikoff, B.; McLoughlin, P., A comparison of polymeric materials as pre-concentrating media for use with ATR/FTIR sensing. *International Journal of Environmental Analytical Chemistry* **2006,** *86* (6), 401-415.

15. Flavin, K.; Hughes, H.; McLoughlin, P., The development of a novel smart mid-infrared sensing methodology for residual solvents. *International Journal of Environmental Analytical Chemistry* **2007,** *87* (1), 29-42.

16. Dobbs, G. T.; Balu, B.; Young, C.; Kranz, C.; Hess, D. W.; Mizaikoff, B., Mid-infrared chemical sensors utilizing plasma-deposited fluorocarbon membranes. *Analytical Chemistry* **2007,** *79* (24).

17. Moreno-Bondi, M. C.; Navarro-Villoslada, F.; Benito-Pena, E.; Urraca, J. L., Molecularly Imprinted Polymers as Selective Recognition Elements in Optical Sensing. *Current Analytical Chemistry* **2008,** *4* (4), 316-340.

18. Sharma, P. S.; Pietrzyk-Le, A.; D'Souza, F.; Kutner, W., Electrochemically synthesized polymers in molecular imprinting for chemical sensing. *Analytical and Bioanalytical Chemistry* **2012,** *402* (10), 3177-3204.

19. Henry, O. Y. F.; Piletsky, S. A.; Cullen, D. C., Fabrication of molecularly imprinted polymer microarray on a chip by mid-infrared laser pulse initiated polymerisation. *Biosensors & Bioelectronics* **2008,** *23* (12), 1769-1775.

20. Jakusch, M.; Janotta, M.; Mizaikoff, B.; Mosbach, K.; Haupt, K., Molecularly imprinted polymers and infrared evanescent wave spectroscopy. A chemical sensors approach. *Analytical Chemistry* **1999,** *71* (20), 4786-4791.

21. Mahony, J. O.; Nolan, K.; Smyth, M. R.; Mizaikoff, B., Molecularly imprinted polymers-potential and challenges in analytical chemistry. *Analytica Chimica Acta* **2005,** *534* (1), 31-39.

22. Wei, S. T.; Jakusch, M.; Mizaikoff, B., Capturing molecules with templated materials - Analysis and rational design of molecularly imprinted polymers. *Analytica Chimica Acta* **2006,** *578* (1), 50-58.

23. Bruening, M. L.; Dotzauer, D. M.; Jain, P.; Ouyang, L.; Baker, G. L., Creation of functional membranes using polyelectrolyte multilayers and polymer brushes. *Langmuir* **2008,** *24* (15), 7663-7673.

24. Janata, J.; Josowicz, M.; DeVaney, D. M., Chemical Sensors. *Analytical Chemistry* **1994,** *66*, 207R-228R.

25. Hu, J. L.; Meng, H. P.; Li, G. Q.; Ibekwe, S. I., A review of stimuli-responsive polymers for smart textile applications. *Smart Materials and Structures* **2012,** *21* (5), 1-23.

26. Ramireddy, R. R.; Raghupathi, K. R.; Torres, D. A.; Thayumanavan, S., Stimuli sensitive amphiphilic dendrimers. *New Journal of Chemistry* **2012,** *36* (2), 340-349.

27. Weber, C.; Hoogenboom, R.; Schubert, U. S., Temperature responsive bio-compatible polymers based on poly(ethylene oxide) and poly(2-oxazoline)s. *Prog. Polym. Sci.* **2012,** *37* (5), 686-714.

28. Shim, M. S.; Kwon, Y. J., Stimuli-responsive polymers and nanomaterials for gene delivery and imaging applications. *Advanced Drug Delivery Reviews* **2012,** *64* (11), 1046-1058.

29. Delcea, M.; Mohwald, H.; Skirtach, A. G., Stimuli-responsive LbL capsules and nanoshells for drug delivery. *Advanced Drug Delivery Reviews* **2011,** *63* (9), 730-747.

30. Kunzelman, J.; Chung, T.; Mather, P. T.; Weder, C., Shape memory polymers with built-in threshold temperature sensors. *Journal of Materials Chemistry* **2008,** *18* (10), 1082-1086.

31. Bar-Cohen, Y.; Zhang, Q. M., Electroactive polymer actuators and sensors. *Mrs Bulletin* **2008,** *33* (3), 173-181.

32. Huang, T. C.; Lin, S. T.; Yeh, L. C.; Chen, C. A.; Huang, H. Y.; Nian, Z. Y.; Chen, H. H.; Yeh, J. M., Aniline pentamer-based electroactive polyimide prepared from oxidation coupling polymerization for electrochemical sensing application. *Polymer* **2012,** *53* (20), 4373-4379.

33. Nguyen, C. H.; Alici, G.; Wallace, G. G., Modelling trilayer conjugated polymer actuators for their sensorless position control. *Sensors and Actuators a-Physical* **2012,** *185*, 82-91.

34. Carey, W. P.; DeGrandpre, M. D., Polymer-Coated Cylindrical Waveguide Absorption Sensor for High Acidities. *Analytical Chemistry* **1989,** *61*, 1674-1678.

35. Karatapanis, A. E.; Petrakis, D. E.; Stalikas, C. D., A layered magnetic iron/iron oxide nanoscavenger for the analytical enrichment of ng-L-1 concentration levels of heavy metals from water. *Analytica Chimica Acta* **2012,** *726*, 22-27.

36. Sudo, E.; Esaki, Y.; Sugiura, M.; Murase, A., Attenuated total reflection surface-enhanced infrared absorption microspectroscopy for identification of small thin layers on material surfaces. *Applied Spectroscopy* **2007,** *61* (3), 269-275.

37. Vesely, D., Diffusion of liquids in polymers. *International Materials Reviews* **2008,** *53* (5), 299-315.

38. Low, A.; Vesely, D.; Allan, P.; Bevis, M. J., Investigation of Microstructure and Mechanical Properties of High Density Polyethylene Spherulites. *Journal of Materials Science* **1978,** *13*, 711-721.

39. Vesely, D., The development of spherulite morphology in polymers. *Journal of Macromolecular Science-Physics* **1996,** *35* (3-4), 411.

40. Rabek, J. F., *Experimental methods in polymer chemistry: physical principles and applications*. John Wiley & Sons: New York, **1980**.

41. Szocs, F.; Sausa, O.; Kristiakova, K.; Kristiak, J.; Klimova, M., Influence of high pressure annealing on free volume in polycarbonate studied by positron annihilation. *European Polymer Journal* **1994,** *31* (10), 1019-1020.

42. Ramesh, N.; Davis, P. K.; Zielinski, J. M.; Danner, R. P.; Duda, J. L., Application of Free-Volume Theory to Self Diffusion of Solvents in Polymers Below the Glass Transition Temperature: A Review. *Polymer Physics* **2011,** *49*, 1629-1644.

43. Nealy, P. F. Diffusion of Diluents in Glassy Polymers. PhD Dissertation, Massachusetts Institute of Technology, Cambridge, **1994**.

44. Frisch, H. L., Mechanisms for Fickian Diffusion of Penetrants in Polymers. *Polymer Letters* **1965,** *3*, 13-16.

45. Meares, P., The Diffusion of Gases Through Polyvinyl Acetate. *Journal of the American Chemical Society* **1954,** *76* (13), 3415-3422.

46. Koros, W. J.; Smith, G. N.; Stannett, V., High-pressure sorption of carbon dioxide in solvent-cast poly(methyl methacrylate) and poly(ethyl methacrylate) films. *Journal of Applied Polymer Science* **2003,** *26* (1), 159-170.

47. Zhu, M.; Vesely, D., The effect of polymer swelling and resistance to flow on solvent diffusion and permeability. *Euroopean Polymer Journal* **2007,** *43* (10), 4503-4515.

48. Madkour, T. M., Development of the molecular design rules of ultra-permeable poly[1-(trimethylsilyl)-1-propyne] membranes. *Polymer* **2000,** *41* (20), 7489-7497.

49. Murphy, B.; Kirwan, P.; McLoughlin, P., Study of the impact of penetrant characteristics upon diffusion into Teflon membranes to further assess the performance of an ATR/FTIR sensor. *Analytical and Bioanalytical Chemistry* **2003,** *377* (1), 195-202.

50. McLoughlin, P.; Flavin, K.; Kirwan, P.; Murphy, B.; Murphy, K., Modelling of Fickian diffusion to enhance polymer-modified sensor performance. *Sensors and Actuators B-Chemical* **2005,** *107* (1), 170-177.

51. Klep, V.; Minko, S.; Luzinov, I., Mixed polymer layers by "grafting to"/"grafting from" combination. *Abstracts of Papers of the American Chemical Society* **2003,** *226*, U483-U483.

52. Tokarev, I.; Motornov, M.; Minko, S., Molecular-engineered stimuli-responsive thin polymer film: a platform for the development of integrated multifunctional intelligent materials. *Journal of Materials Chemistry* **2009,** *19* (38), 6932-6948.

53. Minko, S., Grafting on Solid Surfaces: “Grafting to” and “Grafting from” Methods. In *Polymer Surfaces and Interfaces*, Stamm, M., Ed. Springer: **2008**.

54. Zdyrko, B.; Luzinov, I., AFM studies of the high density poly (ethylene glycol) grafted layers. *Abstracts of Papers of the American Chemical Society* **2004,** *228*, U465-U465.

55. Odian, G. G. Principles of polymerization. http://public.eblib.com/EBLPublic/PublicView.do?ptiID=469767.

56. Chang, H.-K.; Shih, C.-J.; Liu, T.-J.; Tiu, C., Curtain Coating of Dilute Suspensions. *Polymer Engineering and Science* **2012**, 1-11.

57. Siau, S.; Vervaet, A.; Degrande, S.; Schacht, E.; Van Calster, A., Dip coating of dielectric and solder mask epoxy polymer layers for build-up purposes. *Applied Surface Science* **2005,** *245*, 353-368.

58. Oron, A.; Davis, S. H.; Bankoff, S. G., Long-scale evolution of thin liquid films. *Reviews of Modern Physics* **1997,** *69* (3), 931-980.

59. Ruschak, K. J., Coating Flows. *Annual Review of Fluid Mechanics* **1985,** *17*, 65-89.

60. Norrman, K.; Ghanbari-Siahkali, A.; Larsen, N. B., Studies of spin coated polymer films. *Annu. Rep. Prog. Chem., Sect C* **2005,** *101*, 174-201.

61. Postech Research - Polymer Insulator. http://www.postech.ac.kr/ce/lamp/research3-3.html.

62. Weill, A.; Dechenaux, E., The spin-coating process mechanism related to polymer solution properties. *Polymer Engineering and Science* **1988,** *28* (15), 945-1011.

63. Spangler, L. L.; Torkelson, J. M.; Royal, J. S., Influence of solvent and molecular weight on thickness and surface topography of spin-coated polymer films. *Polymer Engineering and Science* **1990,** *30* (11), 644-653.

64. Iyer, K. S.; Zdyrko, B.; Malz, H.; Pionteck, J.; Luzinov, I., Polystyrene layers grafted to macromolecular anchoring layer. *Macromolecules* **2003,** *36* (17), 6519-6526.

65. Liu, Y.; Klep, V.; Zdyrko, B.; Luzinov, I., Synthesis of high-density grafted polymer layers with thickness and grafting density gradients. *Langmuir* **2005,** *21* (25), 11806-11813.

66. Burtovyy, O.; Klep, V.; Chen, H. C.; Hu, R. K.; Lin, C. C.; Luzinov, I., Hydrophobic modification of polymer surfaces via "grafting to" approach. *Journal of Macromolecular Science Part B-Physics* **2007,** *46* (1), 137-154.

67. Li, Y.; Cai, C. Z., Click Chemistry-Based Functionalization on Non-Oxidized Silicon Substrates. *Chemistry-an Asian Journal*, **2011**, *6* (10), 2592-2605.

68. Burtovyy, O. Synthesis and Characterization of Macromolecular Layers Grafted to Polymer Surfaces. PhD Dissertation, Clemson University, Clemson, 2008.

69. Luzinov, I.; Minko, S.; Senkovsky, V.; Voronov, A.; Hild, S.; Marti, O.; Wilke, W., Synthesis and behavior of the polymer covering on a solid surface. 3. Morphology and mechanism of formation of grafted polystyrene layers on the glass surface. *Macromolecules* **1998,** *31* (12), 3945-3952.

70. Minko, S.; Ionov, L.; Sydorenko, A.; Houbenov, N.; Stamm, M.; Zdyrko, B.; Klep, V.; Luzinov, I., Gradient stimuli-responsive polymer grafted layers. In *Stimuli-Responsive Polymeric Films and Coatings*, **2005**; Vol. 912, pp 68-83.

71. Tsukruk, V. V.; Luzinov, I.; Julthongpiput, D.; Malz, H.; Piontek, J., Grafting polymer brushes from melt: Polystyrene layers tethered to epoxysilane self-assembling monolayers. *Abstracts of Papers of the American Chemical Society* **1999,** *218*, U558-U558.

72. Zdyrko, B.; Iyer, K. S.; Luzinov, I., Macromolecular anchoring layers for polymer grafting: comparative study. *Polymer* **2006,** *47* (1), 272-279.

73. Liu, Y.; Klep, V.; Zdyrko, B.; Luzinov, I., Polymer grafting via ATRP initiated from macroinitiator synthesized on surface. *Langmuir* **2004,** *20* (16), 6710-6718.

74. Ranjan, R.; Brittain, W. J., Tandem RAFT Polymerization and Click Chemistry: An Efficient Approach to Surface Modification. *Macromolecular Rapid Communications* **2007,** *28*, 2084-2089.

75. Friedrich, J., Mechanisms of Plasma Polymerization - Reviewed from a Chemical Point of View. *Plasma Processes and Polymers*, **2011**, *8* (9), 783-802.

76. Junk, M. J. N.; Berger, R.; Jonas, U., Atomic Force Spectroscopy of Thermoresponsive Photo-Cross-Linked Hydrogel Films. *Langmuir* **2010,** *26* (10), 7262-7269.

77. Sakai, Y.; Sadaoka, Y.; Matsuguchi, M.; Kanakura, Y.; Tamura, M., A Humidity Sensor Using Polytetrafluorethylene-graft-Quaternized-Polyvinylpiridine. *J. Electrochem. Soc.* **1991,** *138* (8), 2474-2478.

78. Zhang, Y.; Miao, H.; Shi, W., Photopolymerization behavior and properties of highly branched polyester acrylate containing thioether linkage used for UV curing coatings. *Progress in Organic Coatings* **2011,** *71*, 48-55.

79. Berikanl, M.; Hepburn, C., Determination of Crosslink Density by Swelling in the Castable Polyurethane Elastomer Based on 1/4 - Cyclohexane Diisocyanate and para-Phenylene Diisocyanate. *Iranian Journal of Polymer Science & Technology* **1992,** *1* (1), 1-5.

80. Ishida, H., *Fourier Transform Infrared Characterization of Polymers*. Plenum Press: New York **1987**; Vol. 36.

81. Shi, F. F., Recent advances in polymer thin films prepared by plasma polymerization Synthesis, structural characterization, properties and applications. *Surface & Coatings Technology* **1996,** *82* (1-2), 1-15.

82. Yue, Y.-M.; Xu, K.; Liu, X.-G.; Chen, Q.; Sheng, X.; Wang, P.-X., Preparation and Characterization of Interpenetration Polymer Network Films Based on Poly(vinyl alcohol) and Poly(acrylic acid) for Drug Delivery. *Journal of Applied Polymer Science* **2008,** *108*, 3836-3842.

83. Silverstein, R. M.; Webster, F. X.; Kiemle, D. J., *Spectrometric Identification of Organic Compounds*. Seventh ed.; John Wiley & Sons, Inc.: New York, 2005.

84. Burns, D. A.; Ciurczak, E. W., *Handbook of Near Infrared analysis*. Marcel Dekker, Inc.: New York, **1992**.

85. Aizpurua, J.; Taubner, T.; de Abajo, F. J.; Brehm, M.; Hillenbrand, R., Substrate-enhanced infrared near-field spectroscopy. *Optics Express* **2008,** *16* (3), 1529-1545.

86. Gregoriou, V. G.; Kandilioti, G.; Bollas, S. T., Chain conformational transformations in syndiotactic polypropylene/layered silicate nanocomposites during mechanical elongation and thermal treatment. *Polymer* **2005,** *46* (25), 11340-11350.

87. Ku, B. C.; Froio, D.; Steeves, D.; Kim, D. W.; Ahn, H.; Ratto, J. A.; Blumstein, A.; Kumar, J.; Samuelson, L. A., Cross-linked multilayer polymer-clay nanocomposites and permeability properties. *Journal of Macromolecular Science-Pure and Applied Chemistry* **2004,** *A41* (12), 1401-1410.

88. Pattanayak, A.; Jana, S. C., Properties of bulk-polymerized thermoplastic polyurethane nanocomposites. *Polymer* **2005,** *46* (10), 3394-3406.

89. Qu, X. W.; Guan, T. J.; Liu, G. D.; She, Q. Y.; Zhang, L. C., Preparation, structural characterization, and properties of poly(methyl methacrylate)/montmorillonite nanocomposites by bulk polymerization. *Journal of Applied Polymer Science* **2005,** *97* (1), 348-357.

90. Xie, S. B.; Zhang, S. M.; Wang, F. S.; Liu, H. J.; Yang, M. S., Influence of annealing treatment on the heat distortion temperature of nylon-6/montmorillonite nanocomposites. *Polymer Engineering and Science* **2005,** *45* (9), 1247-1253.

91. Zagar, E.; Grdadolnik, J., An infrared spectroscopic study of H-bond network in hyperbranched polyester polyol. *Journal of Molecular Structure* **2003,** *658,* 143-152.

92. Elabd, Y. A.; Baschetti, M. G.; Barbari, T. A., Time-resolved Fourier transform infrared/attenuated total reflection spectroscopy for the measurement of molecular diffusion in polymers. *Journal of Polymer Science Part B-Polymer Physics* **2003,** *41* (22), 2794-2807.

93. Infrared Spectroscopy. Perkin Elmer: **2011**.

94. PikeTechnologies, Analysis of Polymers by ATR/FT-IR. **2006**.

95. HAMEED, N.; GUO, Q., Self-Assembled Complexes of Poly(acrylic acid) and Poly(styrene)-block-Poly(4-vinyl pyridine). *Journal of Polymer Science Part B-Polymer Physics* **2009,** *47,* 1192-1202.

96. Hong, J.-L.; Lin, H.-J., Hydrogen-bond interactions between poly[(ethyl acrylate)-*co*-(acrylic acid)] and polycyanate derived from bisphenol A dicyanate. *Macromolecular Chemistry and Physics* **1999,** *200,* 845-851.

97. Gao, B.; Wu, Y. C.; Zhang, Z. G.; Hua, J. J.; Yao, K. D.; Hou, X., Poly(acrylamide-co-acrylic acid)/Poly(vinyl pyrrolidone) Polymer Blends Prepared by Dispersion Polymerization. *Journal of Macromolecular Science-Physics* **2008,** *47*, 544-554.

98. Eklind, H.; Hjertberg, T., Determination of Interdiffusion in Thin Polymer Films Using FTIR Reflection Absorption Spectroscopy. *Macromolecules* **1993,** *26*, 5844-5851.

99. Geyter, N. D.; Morent, R.; Leys, C., Surface characterization of plasma-modified polyethylene by contact angle experiments and ATR-FTIR spectroscopy. *Surface and Interface Analysis* **2007,** *40*, 608-611.

100. Eidelman, N.; Simon, C. G., Characterization of Combinatorial Polymer Blend Composition Gradients by FTIR Microspectroscopy. *Journal of Research of the National Institute of Standards and Technology* **2004,** *109* (2), 219-231.

101. Burtovyy, R.; Liu, Y.; Luzinov, I.; Zdyrko, B.; Tregub, A.; Moinpour, M.; Buehler, M., Polymer anchoring layer for atomic force microscopy studies of nanoparticle-substrate interactions. *Journal of Macromolecular Science Part B-Physics* **2007,** *46* (1), 231-244.

102. Hildebrand, M.; Doktycz, M. J.; Allison, D. P., Application of AFM in understanding biomineral formation in diatoms. *Pflugers Archiv-European Journal of Physiology* **2008,** *456* (1), 127-137.

103. Magonov, S. N.; Reneker, D. H., Characterization of polymer surfaces with atomic force microscopy. *Annual Review of Materials Science* **1997,** *27*.

104. Meza, L. I.; Anderson, M. W.; Slater, B.; Agger, J. R., In situ atomic force microscopy of zeolite A dissolution. *Physical Chemistry Chemical Physics* **2008,** *10* (33), 5066-5076.

105. Papp, S.; Dekany, I., Colloid chemical characterisation of layered titanates, their hydrophobic derivatives and self-assembled films. *Colloid and Polymer Science* **2005,** *283* (10), 1116-1122.

106. Ray, C.; Brown, J. R.; Kirkpatrick, A.; Akhremitchev, B. B., Pairwise interactions between linear alkanes in water measured by AFM force spectroscopy. *Journal of the American Chemical Society* **2008,** *130* (30), 10008-10018.

107. Shulha, H.; Lin, Y. H.; Tsukruk, V. V., Multilayered nanoscale systems and atomic force microscopy mechanical measurements. *Applications of Scanned Probe Microscopy to Polymers* **2005,** *897*, 133-146.

108. Sokolov, I.; Ong, Q. K.; Shodiev, H.; Chechik, N.; James, D.; Oliver, M., AFM study of forces between silica, silicon nitride and polyurethane pads. *Journal of Colloid and Interface Science* **2006,** *300* (2), 475-481.

109. Steffens, C.; Leite, F. L.; Bueno, C. C.; Manzoli, A.; Herrmann, P. S. D., Atomic Force Microscopy as a Tool Applied to Nano/Biosensors. *Sensors*, **2012**, *12* (6), 8278-8300.

110. McConney, M. E.; Singamaneni, S.; Tsukruk, V. V., Probing Soft Matter with the Atomic Force Microscopies: Imaging and Force Spectroscopy. *Polymer Reviews 50* (3), 235-286.

111. LeMieux, M. C.; Peleshanko, S.; Anderson, K. D.; Tsukruk, V. V., Adaptive nanomechanical response of stratified polymer brush structures. *Langmuir* **2007,** *23* (1), 265-273.

112. Tsukruk, V. V., Scanning probe microscopy of polymer surfaces. *Rubber Chemistry and Technology* **1997,** *70* (3), 430-467.

113. Langereis, E.; Heil, S. B. S.; Knoops, H. C. M.; Keuning, W.; van de Sanden, M. C. M.; Kessels, W. M. M., *In situ* spectroscopic ellipsometry as a versatile tool for studying atomic layer deposition. *Journal of Physics D: Applied Physics* **2009,** *42*, 1-19.

114. Morton, D. E.; Johs, B.; Hale, J.; Woollam, J. A. In *Recent Developments in Spectroscopic Ellipsometry for Materials and Process Control*, 45th Annual Technical Conference Proceedings, Lincoln, NE, Society of Vacuum Coaters: Lincoln, NE, **2002**; pp 365-370.

115. Hilfiker, J. N.; Synowicki, R. A.; Tompkins, H. G. In *Spectroscopic Ellipsometry Methods for Thin Absorbing Coatings*, 51st Annual Technical Conference Proceedings, Chicago, IL, Society of Vacuum Coaters: Chicago, IL, **2008**; pp 365-370.

116. Woollam, J. A., Emerging applications of Spectroscopic Ellipsometry. J. A. Woodllam Co., I., Ed. Glass Coatings: Lincoln, NE, **2007**; Vol. 1.

117. Buijs, K.; Maurice, M. J., Some Considerations on Apparent Deviations from Lambert-Beers Law. *Analytica Chimica Acta* **1969,** *47* (3), 469-&.

118. Johs, B.; Herzinger, C. M., Quantifying the accuracy of ellipsometer systems. *Physical Status Solidi C* **2008,** *5* (5), 1031-1035.

119. Urayama, K.; Takigawa, T.; Masuda, T., Poisson Ratio of Poly(vinyl alcohol) Gels. *Macromolecules* **1993,** *26* (12), 3092-3096.

120. Yamazaki, H.; Takeda, M.; Kohno, Y.; Ando, H.; Urayama, K.; Takigawa, T., Dynamic Viscoelasticity of Poly(butyl acrylate) Elastomers Containing Dangling Chains with Controlled Lengths. *Macromolecules*, **2011**, *44* (22), 8829-8834.

121. Woollam, J. A.; Johs, B.; Herzinger, C. M.; Hilfiker, J.; Synowicki, R.; Bungay, C. L. In *Overview of Variable Angle Spectroscopic Ellipsometry (VASE), Part I: Basic Theory and Typical Applications*, Critical Reviews of Optical Science and Technology, Denver, Colorado, Critical Reviews: Denver, Colorado, **1999**; p 28.

122. Johs, B.; Woollam, J. A.; Herzinger, C. M.; Hilfiker, J.; Synowicki, R.; Bungay, C. L. In *Overview of Variable Angle Spectroscopic Ellipsometry (VASE), Part II: Advanced Applications,* Critical Reviews of Optical Science and Technology, Denver, Colorado, Critical Reviews: Denver, Colorado, **1999**; p 28.

123. Hilfiker, J. N.; Johs, B.; Hale, J.; Herzinger, C. M.; Tiwald, T. E.; Bungay, C. L.; Synowicki, R.; Pribil, G. K.; Woollam, J. A. In *Recent Developments in Spectroscopic Ellipsometry for Materials and Process Control*, 46th Annual Technical Conference Proceedings, Lincoln, NE, Society of Vacuum Coaters: Lincoln, NE, **2003**; pp 365-370.

124. Tompkins, H. G.; Tiwald, T.; Bungay, C., Use of Molecular Vibrations to Analyze Very Think Films with Infrared Ellipsometry. *Journal of Physical Chemistry B* **2004,** *108*, 3777-3780.

125. Bungay, C.; Tiwald, T. E., Infrared spectroscopic ellipsometry study of molecular orientation induced anisotropy in polymer substrates. *Thin Solid Films* **2004,** *455-456*, 272-277.

126. Woollam, J. A.; Bungay, C.; Hilfiker, J.; Tiwald, T., VUV and IR spectroellipsometric studies of polymer surfaces. *Nuclear Instruments and Methods in Physics Research B* **2003,** *208,* 35-39.

127. Hilfiker, J. N.; Singh, N.; Tiwald, T.; Convey, D.; Smith, S. M.; Baker, J. H.; Tompkins, H. G., Survey of methods to characterize thin absorbing films with Spectroscopic Ellipsometry. *Thin Solid Films* **2008,** *516*, 7979-7989.

128. Murthy, N. S., Recent Developments in Polymer Characterization Using X-Ray Diffraction. *The Rigaku Journal* **2004,** *21* (1), 15-24.

129. Smilgies, D.-M.; Busch, P.; Posselt, D.; Papadakis, C. M., Characterization of Polymer Thin Films with Small-Angle X-ray Scattering under Grazing Incidence (GISAXS) *Synchrotron Radiation New* **2002,** (15.5).

130. Benetti, E. M.; Causin, V.; Marega, C.; Marigo, A.; Ferrara, G.; Ferraro, A.; Consalvi, M.; Fantinel, F., Morphological and structural characterization of polypropylene based nanocomposites. *Polymer* **2005,** *46* (19), 8275-8285.

131. Chavarria, F.; Paul, D. R., Comparison of nanocomposites based on nylon 6 and nylon 66. *Polymer* **2004,** *45* (25), 8501-8515.

132. Xu, Y. Z.; Xu, Y. B., Structuring & rheology of molten polymer/clay nanocomposites. *Chinese Journal of Polymer Science* **2005,** *23* (2), 147-153.

133. Causin, V.; Marega, C.; Marigo, A.; Ferrara, G., Assessing organo-clay dispersion in polymer layered silicate nanocomposites: A SAXS approach. *Polymer* **2005,** *46* (23), 9533-9537.

134. Gelfer, M. Y.; Burger, C.; Chu, B.; Hsiao, B. S.; Drozdov, A. D.; Si, M.; Rafailovich, M.; Sauer, B. B.; Gilman, J. R. W., Relationships between structure and rheology in model nanocomposites of ethylene-vinyl-based copolymers and organoclays. *Macromolecules* **2005,** *38* (9), 3765-3775.

135. Pomper, T.; Lode, U.; Karl, A.; Von Krosigk, G.; Minko, S.; Luzinov, I.; Senkovsky, V.; Voronov, A.; Wilke, W., Investigation of craze development using small-angle X-ray scattering of synchrotron radiation. *Journal of Macromolecular Science-Physics* **1999,** *B38* (5-6), 869-883.

136. Russell, T. P., The Characterization of Polymer Interfaces. *Annual Review of Materials Science* **1991,** *21*, 249-268.

137. Jackson, S. T.; Nuzzo, R. G., Determining Hybridization differences for amorphous carbon from the XPS C 1s envelope. *Applied Surface Science* **1995,** *90* (2), 195-203.

138. Beshkov, G.; Dimitrov, D. B.; Georgiev, S.; Juan-Cheng, D.; Petrov, P.; Velchev, N.; Krastev, V., XPS spectra of thin CNx films prepared by chemical vapor deposition. *Diamond and Related Materials* **1999,** *8* (2-5), 591-594.

139. Gouzman, I.; Brener, R.; Hoffman, A., Electron spectroscopic study of C-N bond formation by low-energy nitrogen ion implantation of graphite and diamond surfaces. *Journal of Vacuum Science & Technology a-Vacuum Surfaces and Films* **1999,** *17* (2), 411-420.

140. Coffey, T.; Urquhart, S. G.; Ade, H., Characterization of the effects of soft X-ray irradiation on polymers. *Journal of Electron Spectroscopy and Related Phenomena* **2002,** *122,* 65-78.

141. Rightor, E. G.; Hitchcock, A. P.; Ade, H.; Leapman, R. D.; Urquhart, S. G.; Smith, A. P.; Mitchell, G.; Fischer, D.; Shin, H. J.; Warwick, T., Spectromicroscopy of Poly(ethylene terephthalate):□ Comparison of Spectra and Radiation Damage Rates in X-ray Absorption and Electron Energy Loss. *Journal of Physical Chemistry B* **1997,** *101* (11), 1950–1960.

142. Beamson, G.; Briggs, D., *High Resolution XPS of Organic Polymers: The Scienta ESCA300 Database*. Wiley: **1992**; p 295.

Chapter 3. Experimental

3.1. Introduction

Included in this chapter are the experimental details for the techniques used in this work along with all materials.

3.2. Chemical Reagents and Polymers Used

3.2.1. Chloroform [$CHCl_3$]:

MSDS name: Trichloromethane; 99.8% environmental grade (stabilized with ethanol)

Purchased from: Alpha Aesar

CAS number: 67-66-3

3.2.2. Methanol [CH_3OH]:

MSDS name: Methyl alcohol; ACS grade

Company Identification: BDH

CAS number: 67-56-1

3.2.3. Toluene [$C_6H_5CH_3$]:

MSDS name: Methylbenzene, Phenylmethane; ACS grade

Company Identification: BDH

CAS number: 108-88-3

3.2.4. Ethanol [CH_3CH_2OH]:

MSDS name: Ethyl alcohol; 99.5% ACS 200 Proof

Company Identification: Acros Organics

CAS number: 64-17-5

3.2.5. Isopropanol [$(CH_3)_2CHOH$]:

MSDS name: 2-Propanol, 2-hydroxy propane; OMNISolv for HPLC

Company Identification: EMD

CAS number: 67-63-0

3.2.6. Hexane [$CH_3(CH_2)_4CH_3$]:

MSDS name: Hexane; CHROMASOLV®, for HPLC, ≥95% linear

Company Identification: Sigma-Aldrich

CAS number: 110-54-3

3.2.7. Ammonium Hydroxide[NH_4OH]:

MSDS name: Ammonia; 28% w/w, Density at 20°C: 0.91

Company Identification: Alpha Aesar

CAS number: 1336-21-6

3.2.8. Acetone [$(CH_3)_2CO$]:

MSDS name: 2-Propanone, Dimethyl ketone DMK, Propanone

Company Identification: Alpha Aesar; ACS grade

CAS number: 67-64-1

3.2.9. Methyl ethyl ketone [$CH_3CH_2COCH_3$]:

MSDS name: 2-Butanone, Ethyl methyl ketone MEK, Butanone

Company Identification: BDH, ACS grade (EK 500 Additive)

CAS number: 78-93-3

3.2.10. Deuterated Acetone [$(CD_3)_2CO$]:

MSDS name: Acetone-d6, 99.8% deuterated

Company Identification: Acros Organics

CAS number: 666-52-4

3.2.11. Glacial Acetic Acid [CH_3COOH]:

MSDS name: Acetic Acid, 99%

Company Identification: Alpha Aesar

CAS number: 64-19-7

3.2.12. Methanol –^{13}C [$^{13}CH_3OH$]:

MSDS name: Methyl-^{13}C alcohol; 99%

Company Identification: Sigma-Aldrich

CAS number: 14742-26-8

3.2.13. Deuterated solution of Ammonium (deuterium monoxide)[ND_4OD]:

MSDS name: Ammonium-d_4 deuteroxide solution, 25%wt deuterated ammonia; 99% deuterated

Company Identification: Sigma-Aldrich

CAS number: 12168-30-8

3.2.14. Dodecane [$CH_3(CH_2)_{10}CH_3$]:

MSDS name: n-Dodecane; 99%

Company Identification: Acros Organics

CAS number: 112-40-3

3.2.15. Tri-n-octylamine [$(C_8H_{17})_3N$]:

MSDS name: tri-n-octylamine; 95%

Company Identification: Alpha Aesar

CAS number: 1116-76-3

3.2.16. Sulfuric Acid [H_2SO_4]:

MSDS name: Sulfuric acid; 93%

Company Identification: Alpha Aesar

CAS number: 7664-93-9

3.2.17. Hydrogen peroxide [H_2O_2]:

MSDS name: Hydrogen peroxide aqueous solution; 35%

Company Identification: BDH

CAS number: 7722-84-1

3.2.18. Poly(glycidyl methacrylate) (PGMA)

Synthesized by Dr. B. Zdyrko according to a previously published procedure[1], M_n = 135k Da, PDI= 2.97 measured by GPC (Waters Breeze). Glycidyl methacrylate was purchased from Sigma-Aldrich.

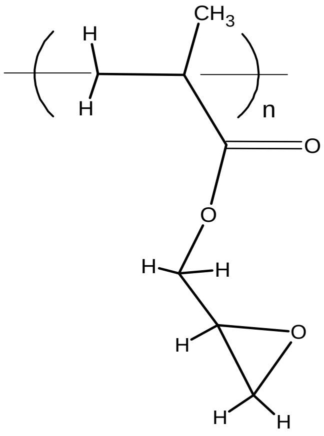

(S.1)

3.2.19. Poly(acrylic acid) (PAA)

Mn = 100k Da, dried from a 35% water solution, purchased from Sigma-Aldrich.

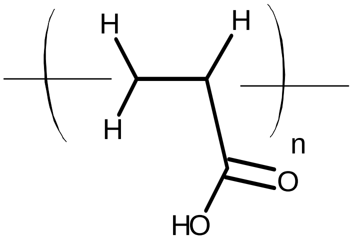

(S.2)

3.2.20. Poly(2-vinyl pyridine) (P2VP) Carboxy terminated

Mn = 53k Da, PDI = 1.06, purchased from Polymer Source, Inc.

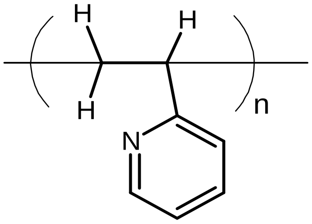

(S.3)

3.2.21. Poly(butadiene) epoxidized ~60% (EPB60)

Polybutadiene was purchased from Sigma Aldrich (Mn= 471k Da) and epoxidized 60% by Dr. B. Zdyrko as described elsewhere.[1] Presented below is the 1,2 and 1,4 structures.

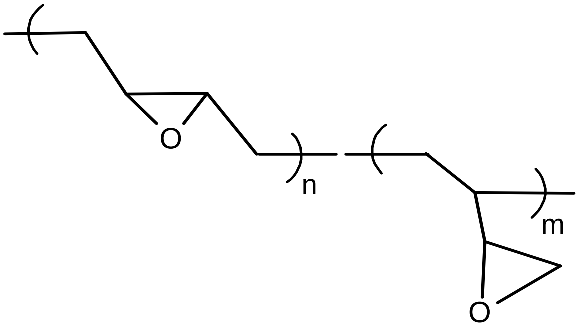

(S.4)

3.3. Surface cleaning of substrates

3.3.1. Piranha solution treatment

Surface cleaning of silicon wafers (purchased from Universitywafer.com) and silicon crystals (purchased from Pike Technologies) was done by chemical treatment with a piranha solution (3:1 v/v sulfuric acid and hydrogen peroxide 35% w/w). Silicon samples were individually cleaned in the solution in glass test tubes for a minimum period of 2 hours at 80°C. The solution was drained into a glass waste container (piranha solution is extremely corrosive to organics and can build pressure when the container is tightly capped). All silicon samples were rinsed by filling the test tube with the deionized (DI) water and then drained five times. The silicon samples were dried with an ultra high purity nitrogen stream in a clean room.

3.3.2. Plasma treatment

Plasma cleaning was performed using a Harrick Plasma Cleaner/Sterilizer model PDC-32G. This cleaning was done primarily to silicon crystals to remove polymers coated on the surface. Pirhana treatment followed to reuse silicon waveguide crystals. Power was set to 18 watts for 10-15 minutes.

3.4. Synthesis of polymer coatings

3.4.1. Deposition

Dip coating[1] was accomplished using a Mayer Feintechnik D-3400 dip-coater. Rates were kept the same for each polymer at 240 mm/min for submersion and withdrawing.

3.4.2. Grafting

Grafting was accomplished by placing polymer films that had been coated onto the substrate into a VWR vacuum oven preheated to a desired temperature. Temperatures that were used were above the polymer's glass transition temperature (T_g). Polymer glass transition temperatures were confirmed separately using a TA Instruments differential scanning calorimeter (DSC) Q1000 model. The glass transition temperatures and the corresponding grafting temperatures for the polymers used in this work is provided in **Table 3.1**.

Table 3.1. Glass transition temperatures and grafting temperatures for major polymers used in this work.

Polymer	Tg [°C]	Grafting Temp. [°C]
PAA	106	120
PGMA	70	120
PVP	147	150
EPB60	95	120

The atmosphere in the oven was reduced by vacuum elimination. The resulting internal pressure in the oven was approximately 50mmHg. The time for grafting each layer is given in individual chapters.

3.5. Characterization

3.5.1. Surface grafting density

The polymer surface coverage, $\Gamma(\mathrm{mg/m^2})$, was determined from the film height, h(nm), obtained from ellipsometry and density, ρ, of the polymer[2-3]:

$$\Gamma = h\rho \tag{3.1}$$

The density for PGMA is approximately $1.08(\mathrm{g/cm^3})$.[2] The chain density, σ (chains/nm^2), on the surface (taking into account unit conversions) was calculated from[2-3]:

$$\sigma = \frac{\Gamma * \mathrm{N_A} * 10^{-21}}{\mathrm{M}} = \frac{6023 * \Gamma}{\mathrm{M_n}} \tag{3.2}$$

where N_A is Avagadro's number, M (g/mol) is the molar mass of the attached macro molecule. $\sigma^{-1}$is the average area occupied by the polymer chain on the surface.

3.5.2. Ellipsometry

An InOm Tech Products Inc. model COMPEL ELC-11 ellipsometer and accompanying ELLIPS software were used to measure the dry polymer film thickness which was verified by a scratch test performed by AFM. In this experiment, the brush was scratched with an ultra-sharp needle to delaminate the layer down to the Si-wafer. The sample was then scanned over the area with the scratched line. Thickness of the film was determined using cross-section of the height image. Standard error of the measurements is approximately 5%. The wavelength of light used in this setup was 651 nm which is known not to be absorbed by any of the films, and the incident angle of the light was always set to 70°. The refractive index of each polymer is given in **Table 3.2.** The refractive index of PGMA was estimated from PMMA.[4]

Table 3.2. Refractive indices for major polymers used in this work.

Polymer	Refract Index
PGMA	**1.49**
PAA	**1.52**
EPB60	**1.5**
P2VP	**1.53**

For each sample, one spot was measured by collecting a measurment per second over a 10 second period for a single thickness. Five different spots were analyzed on each sample film to determine an average film thickness.

3.5.2.1. *In-situ* Ellipsometry

In-situ ellipsometry was conducted to identify trends of polymer film swelling with various VOC vapors using the same ellipsometer mentioned in the previous section. A wafer covered with one of the polymer coatings was placed in an enclosed cell with a reservoir of analyte under ambient conditions (**Figure 3.1**). Fluorinated grease was used to seal the cell. Psi and delta parameters were monitored and recorded for 2,500 seconds (approximately 40 minutes). For each experiment, there remained some amount of liquid analyte in the reservoir indicating that vapor was saturated in the cell. Conversion of raw ellipsometry data to thickness was done using software which modeled the change of psi and delta with the refractive index held constant. The data was modeled with the ELLIPS software using a refractive index of 1.5.(Justification in the Appendix, Section 1)

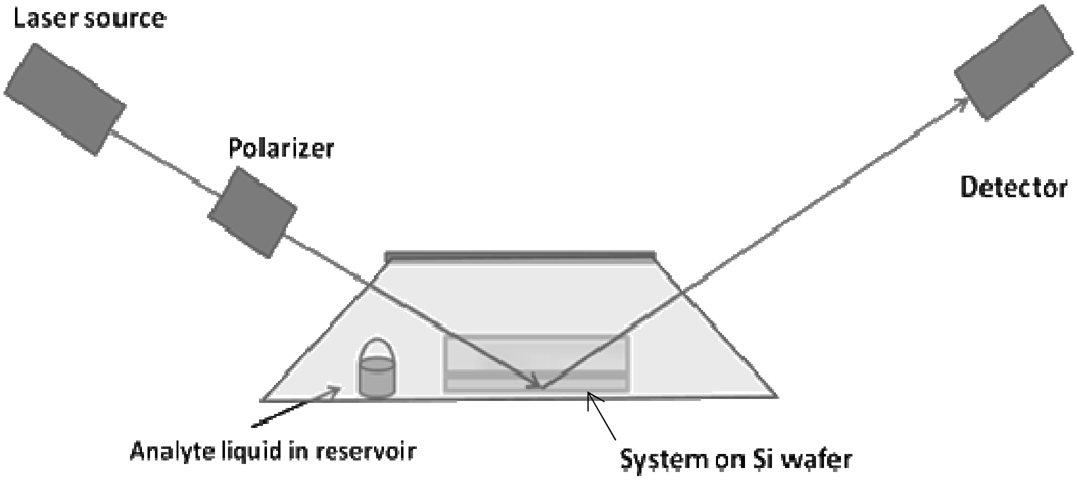

Figure 3.1. Schematic representation of experimental set-up used for ellipsometric absorption measurments.

3.5.3. Atomic force microscopy (AFM)

AFM was performed using a VEECO Dimension 3100 to determine layer morphology, uniformity, thickness, and roughness. The images of the sample surface were always taken under ambient conditions using n-type silicon tips (NSC16/AlBS) purchased from μMasch. Data collection was done with VEECO Nanoscope software (Version 5.03r3.sr3) and image sizes were 256 lines. Data was obtained from an area of 1x1um. AFM was used to confirm ellipsometry thickness values by analyzing a scratch in the polymer film. Standard deviation of the thickness was calculated using the Gwyddion 2.32 1D mean statistical fitting function. RMS roughness of the surface was calculated by using VEECO Nanoscope software.

3.5.4. Attenuated Total Reflectance Mid-IR Spectroscopy

The IR spectrophotometer used was a Thermo Nicolet Nexus 870 e.s.p. FT-IR. All spectra were analyzed using OMNIC software. Spectroscopic measurements were conducted using PIKE Technologies Variable Angle Multi-Reflection ATR accessory. A single spectrum was an average of 32 scans. CO_2 absorbance has been removed from the spectra.

3.5.4.1. Static absorption measurements

To conduct static vapor absorption measurements, a custom made cell was placed on top of the Si crystal waveguide. Silicon crystal waveguides used in the IR experiments were purchased from Harrick and were 45^o trapezoids. Kalrez o-rings, used to seal the perimeter of the IR cell, were purchased from McMaster-Carr. The ATR FT-IR spectrum of the EPL layered coating was taken as a background. The liquid analyte of interest was placed in a small reservoir and was allowed to vaporize in the closed cell to replicate static conditions used in ellipsometry (**Figure 3.2**). Measurements were collected in ambient at room temperature. Each spectrum was taken as an average of 32 scans over 19 seconds with a resolution of 4 cm^{-1}. Spectra were collected after 20 minutes of exposure, unless otherwise stated. The average deviations of the absolute value of the absorbance are given in spectra of specific analytes. Spectra of the analyte in the vapor phase using a non-coated silicon crystal were obtained as well. Spectra of the analytes in the liquid phase were obtained by applying one to three drops of an analyte on a non-coated silicon crystal.

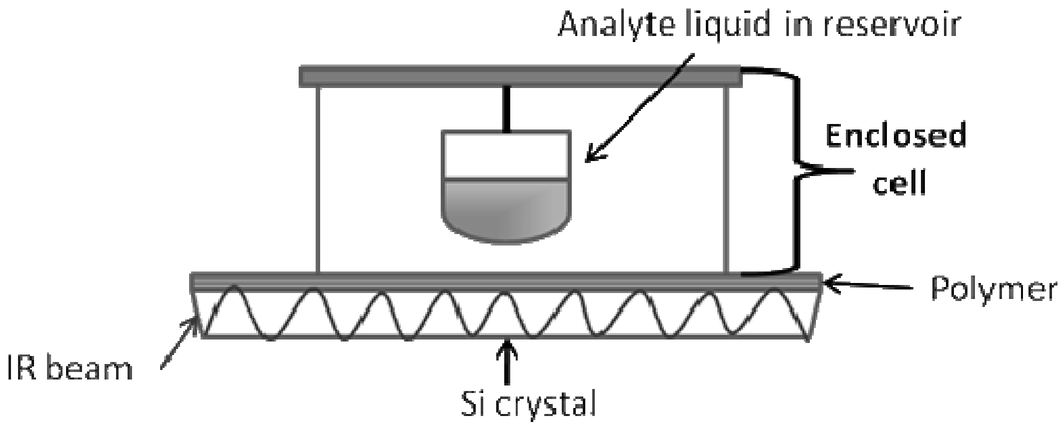

Figure 3.2. Schematic representation of set-up used for mid-IR detection in static loading conditions.

3.5.4.2. Efficiency of absorption as a function of IR absorbance

It is beneficial to evaluate the efficiency of the enrichment system toward detecting VOCs by FT-IR in order to compare different enrichment systems and thicknesses. The absorbance of mid-IR energy in ATR FT-IR is subject to the Beer-Lambert law. This law has a saturation point where the change in absorption goes to zero due primarily to scattering of the light before it reaches the detector.[5-6] The maximum IR signal for analytes for this experimental ATR setup was determined by calculating the maximum absorbance per square centimeter of the top surface of the silicon crystal. For this purpose, a silicon crystal was specially modified. This was done by first applying a protective coating of polystyrene (PS) to three areas of a silicon crystal. The crystal surface was then coated with silver by plasma vapor deposition (PVD) to a thickness of approximately 1um. The PS was then removed with toluene leaving the three areas free of silver (**Figure 3.3**). The remaining silver reflects the IR light so the uncovered spots are only areas where the energy can be absorbed. The area of these spots, which was 0.779 cm^2 and the total crystal surface was 5.341 cm^2, was measured from a digital photograph using the software imageJ (Version 1.45). The total absorbance of liquid analyte on the spots was used to calculate the total absorbance per area of the silicon waveguide crystal. It is therefore possible to obtain a maximum absorbance for an analyte absorbed in an EPLS on this specific IR instrument.

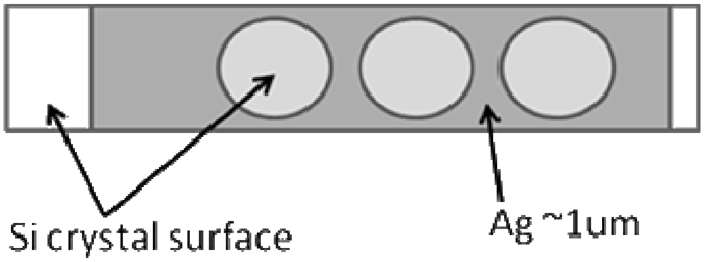

Figure 3.3. Schematic representation of silver deposited onto a silicon crystal surface.

3.5.4.3. Dynamic Absorption Measurements

Spectroscopic measurements were conducted using PIKE Technologies Variable Angle Multi-Reflection ATR accessory. To conduct measurements, a custom made stainless steel cell was placed on top of the enrichment polymer layered system coated onto a Si crystal. An o-ring purchased form McMaster-Carr was used as a gasket. Stainless steel tubing was used in the delivery system. The cell was stablized by applying a locking press. Dry nitrogen was allowed to pass through the cell at 30 mL/min for 30-40 minutes to purge it. The polymer layer with the cell and o-ring was taken as a background. A scheme of the setup used to deliver analyte vapor to the enrichment polymer layers under dynamic conditions is provided in **Figure 3.4**. Spectra were an average of 32 scans with resolution set at 4 cm^{-1}. Spectra were taken over a period of time until it was apparent that the intensity was not changing. All dynamic experiments were done at room temperature. The average deviations for absolute absorbance values decrease when purged with nitrogen before collection. All spectra were analyzed using OMNIC software.

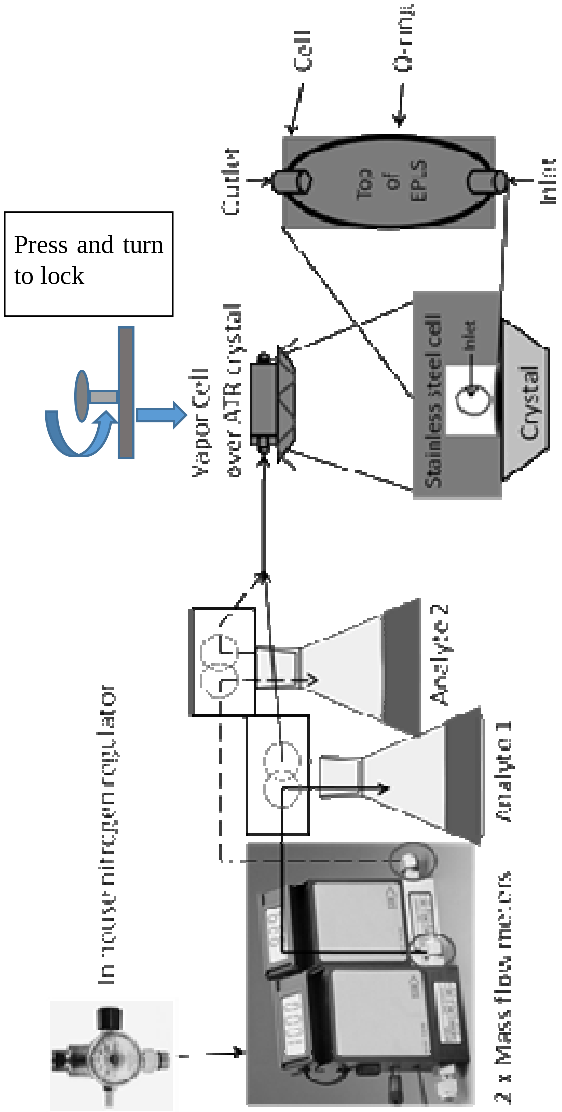

Figure 3.4. The scheme of the set-up for dynamic flow and mixing of analyte vapors using nitrogen as a carrier gas.

3.5.4.4. Processing FT-IR spectra from VOC exposure experiments

Spectra collected for all FT-IR experiments were processed in the following manner using OMNIC 5.1b Nicolet Instrument Corp 1992-1999 software. The steps of processing a sample spectrum are given below.

(1) A background spectrum of the EPL or EPLS unexposed to VOC vapor was collected as a single beam spectrum.

(2) A single beam spectrum of the sample is taken at a later time, which is the EPL or EPLS with the absorbed VOC vapor (polymer + absorbed VOC). In **Figure 3.5**, the single beam spectra are provided.

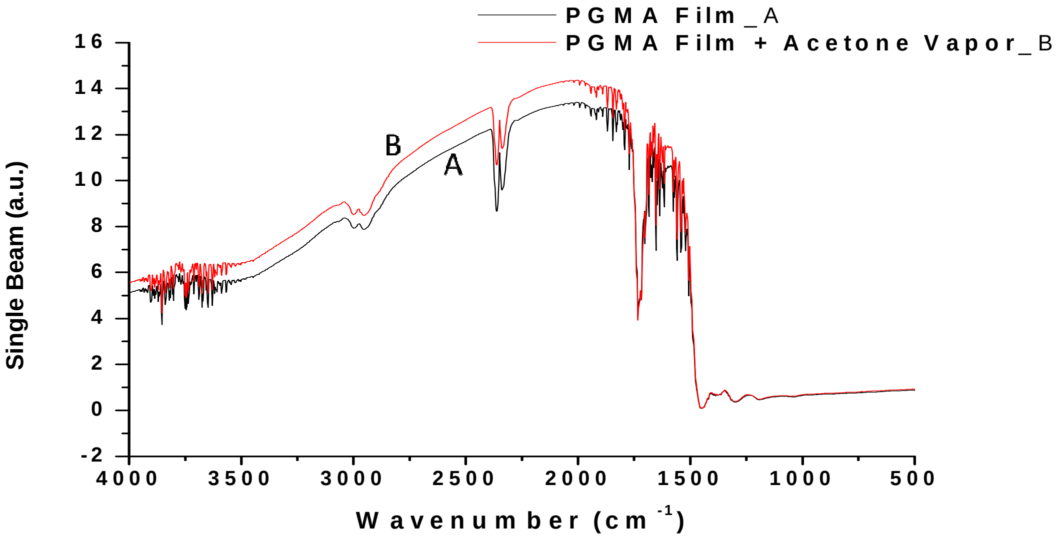

Figure 3.5. Single beam IR spectra of a PGMA coated silicon waveguide crystal before (A) and after acetone exposure (B).

(3) The intensity of the single beam spectrum of the sample, *I*, is divided by the intensity of the background, I_o, which gives the transmittance, T (**Figure 3.6**).

$$T = \frac{I}{I_0} \tag{3.3}$$

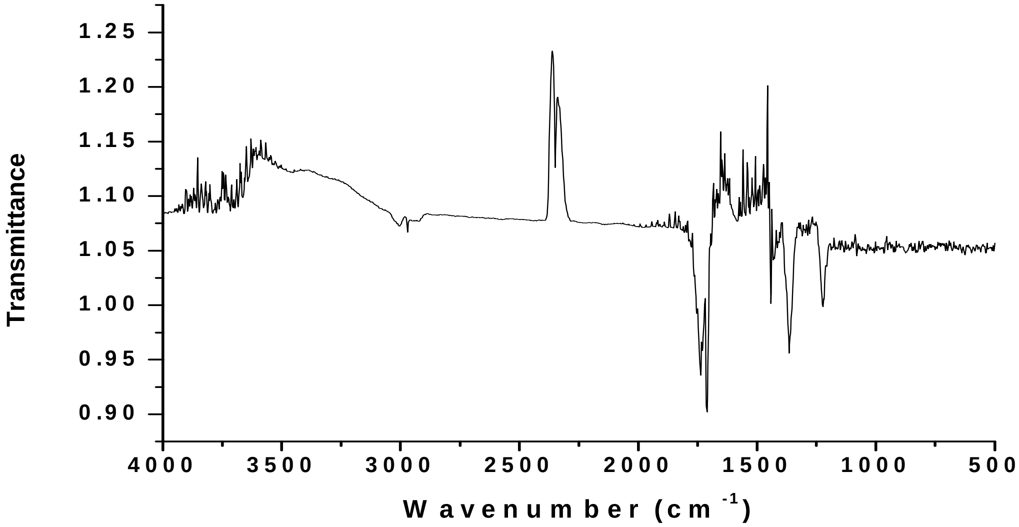

Figure 3.6. The transmittance IR spectrum of acetone absorbed into a PGMA single component film.

(4) The raw absorbance spectrum is generated from the relationship between transmission and absorbance, which is[7]

$$A = -\log(T) \tag{3.4}$$

The Nicolet software allows one to do these conversions automatically.

(5) The absorbance spectrum requires an ATR correction due to the fundamental aspect of the evanescent wave having a depth of penetration that is a function of wavelength. “This correction applies a linear ramp [function] to the ATR spectrum in order to approximate the relative band intensities that would be found in a transmission experiment.”[8]

(6) Spectra are shifted from zero due to the inherent noise that comes from the instrument. This shift is treated in common practice by a base line correction which

sets a zero point for the spectrum. Automatic baselines cannot always give a good zero line for the spectrum and are prone to give either higher or lower corrected absorbance values. For all of the spectra presented in this dissertation, a baseline was created manually by careful analysis of the spectrum. Spectra to illustrate parts (4) through (6) are presented in **Figure 3.7**

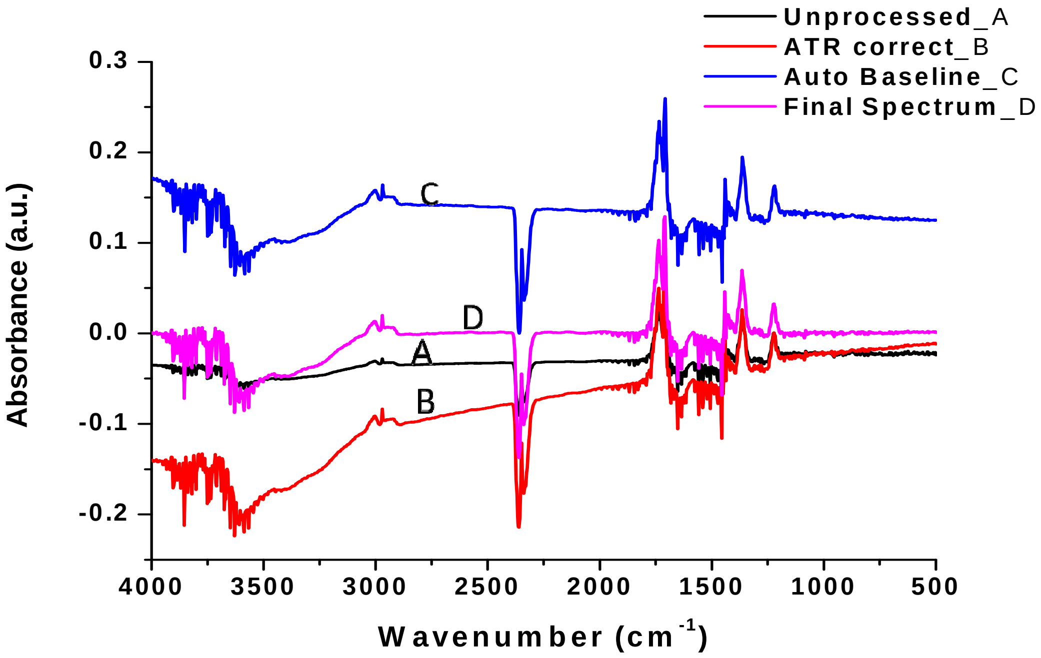

Figure 3.7. Absorbance spectrum of acetone absorbed into a PGMA film illustrating the procedure.

Spectra were smoothed in Origin Ver 6.1 by use of the FFT filtering operation using a 3rd order polynomial and averaging five points (**Figure 3.8**). The CO_2 peaks that are present from approximately 2300 to 2400 cm^{-1}, are removed from spectra for better clarity.

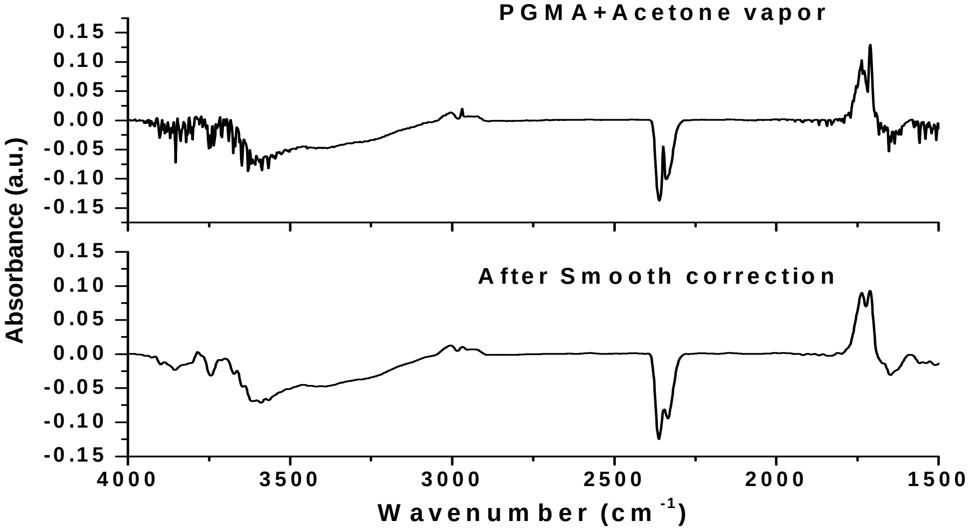

Figure 3.8. Final absorbance spectrum of acetone vapor absorbed into a PGMA film before (top) and after (bottom) smoothing.

3.6. References

1. Zdyrko, B.; Iyer, K. S.; Luzinov, I., Macromolecular anchoring layers for polymer grafting: comparative study. *Polymer* **2006,** *47* (1), 272-279.

2. Zdyrko, B.; Klep, V.; Luzinov, I., Grafting of high-density poly(ethylene glycol) brush to poly(glycidyl methacrylate) monolayers. *Abstracts of Papers of the American Chemical Society* **2002,** *223*, D6-D7.

3. Zdyrko, B.; Klep, V.; Luzinov, I., Synthesis and surface morphology of high-density poly(ethylene glycol) grafted layers. *Langmuir* **2003,** *19* (24), 10179-10187.

4. Polyanskiy, M. Refractive Index Database. http://refractiveindex.info/?group=PLASTICS&material=PMMA (accessed June **2010**).

5. Buijs, K.; Maurice, M. J., Some Considerations on Apparent Deviations from Lambert-Beers Law. *Analytica Chimica Acta* **1969,** *47* (3), 469-&.

6. Zaccanti, G.; Bruscaglioni, P., Deviation from the Lambert-Beer Law in the Transmittance of a Light-Beam through Diffusing Media - Experimental Results. *Journal of Modern Optics* **1988,** *35* (2), 229-242.

7. Silverstein, R. M.; Webster, F. X.; Kiemle, D. J., *Spectrometric Identification of Organic Compounds*. Seventh ed.; John Wiley & Sons, Inc.: New York, **2005**.

8. Nunn, S.; Nishikida, K., Advanced ATR Correction Algorithm. Thermo Fisher Scientific, I., Ed. **2009**.

Chapter 4. Poly(glycidyl methacrylate) as an EPL

4.1. Introduction

This chapter explores the use of poly(glycidyl methacrylate) (PGMA) as a one-component enrichment polymer layer (EPL). PGMA was studied as a single EPL for two reasons: 1) it is a primary component of more complex EPLS and 2) it has its own unique chemistry, which can be utilized for targeting multiple VOCs. The VOCs used in the experiments represent a range of chemical species possessing different chemical natures. Specifically, the VOCs tested were acetone, methanol, ethanol, isopropyl alcohol (IPA), acetic acid, hexane, and ammonium hydroxide.

PGMA films were produced with a well-known technique reported previously.[1] PGMA film thickness was measured by ellipsometry. The surface was examined by AFM to analyze the morphology and uniformity of the film. Finally, the chemical functionality of the deposited film was characterized by FT-IR analysis.

The applicability of PGMA to serve as an EPL for VOCs was evaluated by *in-situ* ellipsometry. The IR absorbance signature of the VOCs absorbed by the PGMA layer, were monitored by *in-situ* ATR FT-IR.

4.2. Experimental Details

4.2.1. Polymer film and grafting details

PGMA films of varying thickness were prepared by dip coating a substrate in polymer solutions of various concentrations in chloroform. Thicknesses, solution concentration, annealing time, and substrate type are given in **Table 4.1**. For one sample, a silicon wafer surface was modified with PGMA using a 0.07% w/v solution, which was then rinsed in pure chloroform by dip coating. This produced a 8 nm layer. Rinsing was done to remove ungrafted polymer. For the rest of the samples, rinsing was done by submerging the grafted sample in pure chloroform. The chloroform was removed and a fresh portion was added. This was repeated three times after time intervals of 10 mins, 10 mins, and 2 hrs minimum (in some instances overnight).

Table 4.1. Experimental parameters used to build PGMA layers

PGMA grafted Thickness [nm]	Annealing Time [min]	Silicon substrate	Solution concentration [w/v%]
8	20	Wafer	0.07
15	60	ATR Crystal	1
60	720	ATR crystal	1
90	900	Wafer	2
130	900	ATR crystal	2

The polymer surface coverage, Γ (mg/m^2), was calculated from Equation 3.1. [2-3] The density of the PGMA is approximately 1.08 g/cm^3.[2] The chain density on the surface was calculated from Equation 3.2.[2-3] **Table 4.2** presents the surface coverage of the PGMA films used in this investigation, with their respective chain densities.

Table 4.2 Grafted layer characteristics of PGMA films.

PGMA Thickness (nm)	Surface Coverage, Γ [mg/m^2]	Chain density, σ[chains/nm^2]
8	8.64	0.04
15	16.2	0.07
60	64.8	0.29
90	97.2	0.43
130	140.4	0.63

Standard deviation of the thickness was calculated using the Gwyddion 2.32 1D mean statistical fitting function. Deviation was within ±1-2 nm. RMS roughness of the surface was calculated from the VEECO Nanoscope software.

4.3. Results and Discussion

4.3.1. Characterization

The AFM morphologies of the 8 nm and 90 nm PGMA films are presented in **Figure 4.1**. The thin PGMA film is susceptible to slight dewetting, which presents as pits or holes in the film. This can be due to instability in the thin film, which is most prominently linked to stress in the film. The stress can come from a number of factors, including solvent evaporation from the film during dip coating. These stresses are a function of the polymer's relaxation time; if the solvent evaporates at a fast rate, stresses in the film can occur.[4-6] In fact, for thicker films, diffusion of the solvent takes longer,[7] thereby allowing more time for the polymer chains to be plasticized and rearranged. In addition, phase separation caused by water condensing on the surface as the solvent evaporates can cause surface deformations.

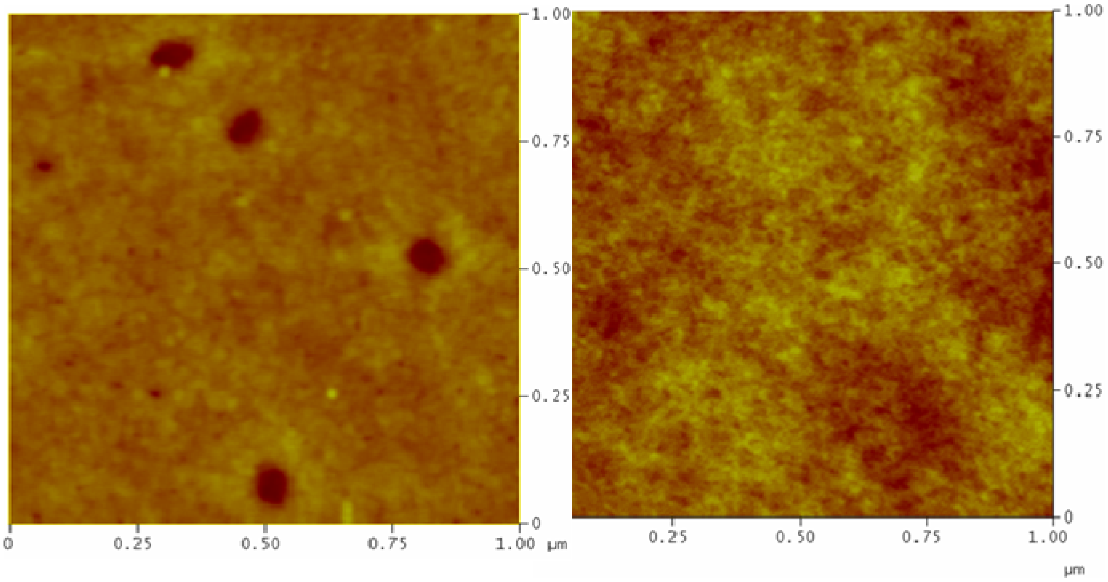

Figure 4.1. AFM topographical images of (left) an 8 nm PGMA film and (right) a 90 nm PGMA film. For both, the vertical scale is 10 nm, and dimensions of the image are 1x1um. RMS roughness values are = 0.4, and 0.3 nm, respectively.

4.3.2. Swelling of PGMA films with various VOCs

The swelling extent was measured for an 8 nm film exposed to: acetone, methanol, and hexane. At least three measurements were conducted for the each solvent. The values are presented in **Figure 4.2**. The swelling fraction is determined as

$$\text{Swelling fraction} = \Delta d/d_o \tag{4.1}$$

where Δd is the change in thickness of the swollen film from the dry state and d_o is the film's dry state thickness. From an evaluation with a Student's T-test, using a single tail, 95% confidence interval, it was determined that the swelling of the layer with hexane was statistically different from that of acetone and methanol (t values of 9.89 and 8.49, respectively). However, the data shows that there was not a statistically significant difference between the swelling fractions for acetone and methanol absorption (t value of 2.23).

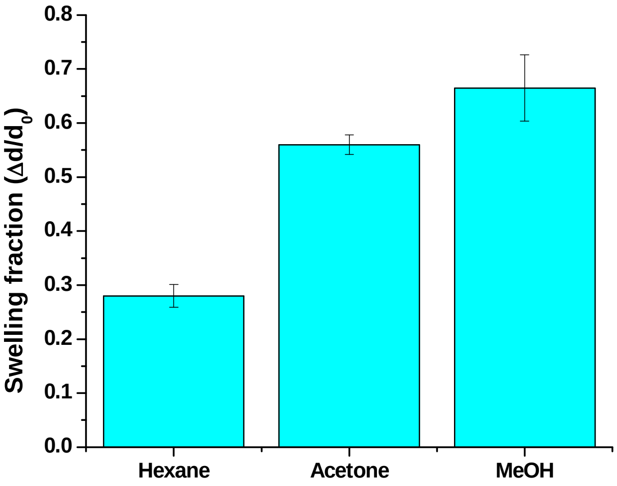

Figure 4.2. Single 8nm PGMA layer swelling fractions in the presence of various analyte vapors.

The swelling extent of the 90 nm PGMA film by organic vapors is presented in **Figure 4.3**. For each analyte, the PGMA layer produced a different maximum swelling thickness. All three alcohols reached approximately 14% swelling within a standard deviation. Acetone, known to be a good solvent for PGMA, swelled the film to nearly 40%. Hexane, a poor solvent, swelled the film to 4%. These results demonstrate that the PGMA layer has significant swelling capabilities.

A Student's T-test was performed for the swelling data with a 95% confidence interval to determine statistical significance. The evaluation found that the swelling of the layer caused by the alcohols was not statistically different; the swelling fractions of acetic acid, acetone, and hexane were statistically significant. T values with accompanying p values are given in the appendix, section 3.

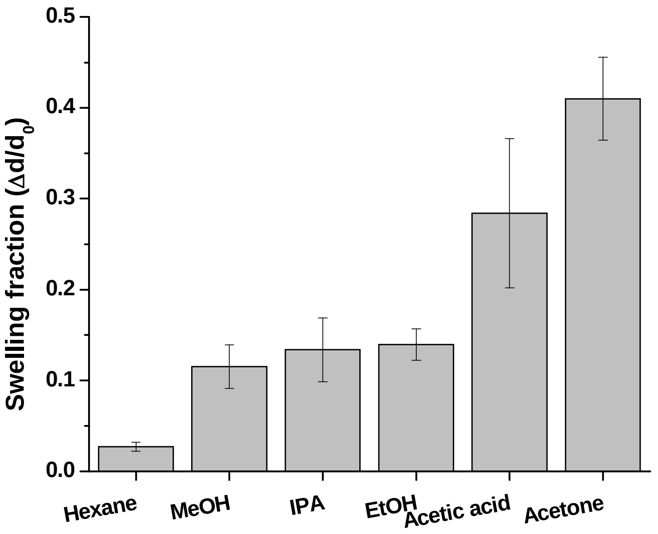

Figure 4.3. Swelling fraction of 90 nm PGMA film in the presence of various analyte vapors.

The swelling kinetics for VOC sorption in the 90 nm PGMA film is presented in **Figure 4.4**. Each curve is an average of 2–3 swelling experiments. From this plot, it can be seen that each analyte except AA reaches a saturation region after about 1,200 seconds. Acetic acid is the only VOC that takes longer than 40 minutes to reach equilibrium. It is suggested that at least two phenomena might be responsible for the slower kinetics. First, acetic acid can dimerize. The dimerization can keep acetic acid from diffusing fast into the PGMA film.[7-8] Second, acetic acid can trigger the opening of the epoxide ring causing additional cross-linking, thereby slowing down the diffusion of the analyte into the film. In fact, in a model experiment (conducted by Dr. Zdyrko) we treated PGMA film with acetic acid (in liquid form) at room temperature and, using ellipsometric measurements, observed attachment of the acid to the PGMA layer.

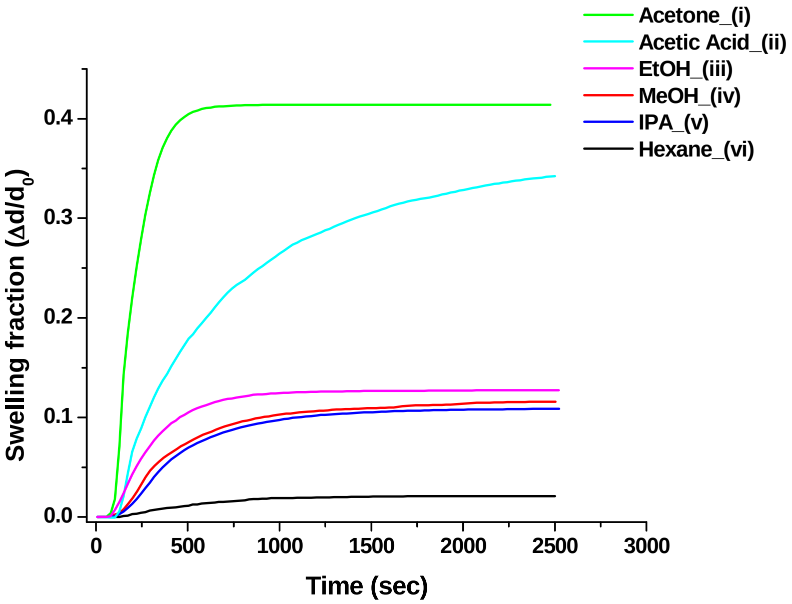

Figure 4.4. Kinetics of VOC vapor sorption into 90 nm PGMA film.

As the *in-situ* ellipsometry studies were conducted with a saturated VOC vapor, the question of how the swelling of the polymer film is affected by vapor pressure came into play. The vapor pressures of each of the VOCs are listed in **Table 4.3** were calculated with the Antoine equation[9] (below) using parameters A, B, and C taken from the NIST website.[10]

$$\log(\mathrm{p}) = \mathrm{A} - \frac{\mathrm{B}}{\mathrm{C}+\mathrm{T}} \tag{4.2}$$

In bold, the respective rank in swelling fraction with the PGMA film (from highest to lowest) is indicated next to each VOC vapor pressure. It can be seen that the swelling fractions do not follow the vapor pressures of the VOCs. This indicates that the swelling of the system depends on other factors as well. One such factor is the thermodynamic affinity of the polymer film toward the VOC which can be assessed using the Flory–Huggins approach.

Table 4.3. Vapor pressure values of examined VOCs calculated from Antoine parameters at 25°C.

VOC	Vapor Pressure [mmHg]
Acetone	228.04 **(1)** *
Hexane	150.27 **(6)**
Methanol	126.06 **(5)**
Ethanol	58.51 **(3)**
Isopropanol	42.33 **(4)**
Acetic acid	15.72 **(2)**

*Numbers in bold rank the VOCs by their volume swelling fraction in **Figure 4.3**

4.3.3. Interaction Parameter, χ

Using the swelling data of the polymer film, it is possible to determine polymer–solvent interaction parameters to describe polymer-solvent pairs based on known thermodynamic relationships.[11] As the cross-linked and anchored PGMA film swells, the total free energy can be expressed as

$$\Delta G_T = \Delta G_m + \Delta G_e \tag{4.3}$$

ΔG_m represents the free energy of mixing of the polymer in the uncross-linked state and ΔG_e represents the free energy change upon expanding the polymer network. The first term in the equation is the Flory-Huggins total free energy of dilution. The second term is related to parameters that can be known or measured. Assuming that there is isotropic expansion of the network under isothermal conditions, the term ΔG_e can be expressed as reversible work per unit volume, *w*, where

$$w = \frac{3\rho RT}{2M_c}\left(\phi_2^{-2/3} - 1\right) \tag{4.4}$$

Equation 4.4 is derived from a treatment of the change of entropy of an elastomer system. R and T are the gas constant and temperature respectively, ρ is the density of the polymer and φ_2 is the volume fraction of the polymer in the swollen state. M_c is the number average molar mass of the active chain lengths between crosslinks. The volume fraction of the polymer can be expressed in terms of the number of moles of liquid expanding the elastomer, n_1, the number of moles of the polymer, n_2, and the molar volume of the solvent, V_1, and polymer,V_2, as

$$\phi_2 = \frac{n_2V_2}{n_1V_1+n_2V_2} \tag{4.5}$$

After a substitution to equation 4.4 and taking the differential with respect to n_1, the final equation for the free energy change of the elastomer swelling is

$$\Delta G_e = \frac{\rho RT}{M_c} V_1 \phi_2^{1/3} \tag{4.6}$$

Substituting the full equation for the change of free energy in 4.3, the Flory-Rehner equation is obtained:

$$\Delta G_T = RT\left[\ln(1-\phi_2) + \left(1-\frac{1}{N}\right)\phi_2 + \chi\phi_2^2 + \frac{\rho V_1}{M_c}\phi_2^{1/3}\right] \tag{4.7}$$

N is the degree of polymerization and if it is high, the term (1-1/N)ϕ_2 can be reduced to ϕ_2. When dealing with the vapor and liquid phases of a component in a mixture, in this case the VOC and polymer, it is proper to use the fugacity of the VOC.[12]

$$\Delta G_T = RT\ln\frac{f_i}{f_i^o} \tag{4.8}$$

This can be set equal to equation 4.7 for real vapor-liquid mixtures

$$RT\ln\frac{f_i}{f_i^o} = RT\left[\ln(1-\phi_2) + \phi_2 + \chi\phi_2^2 + \frac{\rho V_1}{M_c}\phi_2^{1/3}\right] \tag{4.9}$$

The ratio of the fugacity of the VOC component in the polymer film,f_i, to a standard fugacity of the component,f_i^o, is known as the VOC activity, *a*

$$a_i = \frac{f_i}{f_i^o} \tag{4.10}$$

Taking the polymer-VOC system as an ideal, the activity of the component is directly proportional to the ratio of the partial pressure of the component to its vapor pressure at equilibrium.

$$a_i = \frac{p_i}{p_i^o} \tag{4.11}$$

Under conditions that are not ideal, the activity can be calculated using the second virial coefficient, which can be determined from separate experiments (not presented in this dissertation)[13]

$$a_i = \frac{p_i}{p_i^o} e^{-\frac{B}{RT}(p_i^o - p_i)} \tag{4.12}$$

As a first approximation, the system presented is considered to behave as ideal:[14]

$$\ln\frac{p_i}{p_i^o} = \left[\ln(1-\phi_2) + \phi_2 + \chi\phi_2^2 + \frac{\rho V_1}{M_c}\phi_2^{1/3}\right] \quad (4.13)$$

The standard temperature of this equation is taken to be at 25°C which is the approximate temperature at which these experiments were conducted. It is assumed that the internal pressure of the cell at which the swelling experiments were performed is very close to the saturation pressure of the vapor bringing the ratio of partial pressure to vapor pressure close to 1.[15] Therefore, the swelling equation for our system is

$$0 = \left[ln(1-\phi_2) + \phi_2 + \chi\phi_2^2 + \frac{\rho V_1}{M_c}\phi_2^{1/3}\right] \quad (4.14)$$

The equation below states that at equilibrium swelling, using a polymer of high molecular weight, M_c can be determined from the following equation:

$$M_c = \left[\frac{-(\ln(1-\phi_2))-\phi_2-\chi\phi_2^2}{\rho V_1\phi_2^{1/3}}\right]^{-1} \quad (4.15)$$

Likewise, the interaction χ parameter was found for VOC-PGMA pairs used in this work by the following rearrangement of equation 4.15:

$$\chi = \frac{-(\ln(1-\phi_2))-\phi_2-(\frac{\rho V_1}{M_c}\phi_2^{1/3})}{\phi_2^2} \quad (4.16)$$

This approximation provides a good qualitative comparison for polymer-solvent pairs with regard to the affinity of the solvent to the system and the cross linked/grafted sites.

Poly(methyl methacrylate) (PMMA) has a chemistry close to that of PGMA which can be seen from known solubility parameters based on chemical functional groups and determined from Hansen parameters (**Table 4.4**). PMMA dissolution in solvents has also been studied extensively.

Table 4.4. Solubility parameters for PGMA and PMMA

	δ_d [(MPa)$^{1/2}$]	δ_p [(MPa)$^{1/2}$]	δ_H [(MPa)$^{1/2}$]	Total δ [(MPa)$^{1/2}$]
PMMA	18.6	10.5	5.1	22.0
PGMA	16.5	7.6	9.2	19.6

The interaction parameter, χ_{12}, for PMMA and acetone of 0.479 has been reported in literature.[16] Using this known χ value, and estimating that PGMA and acetone have an interaction parameter close to 0.5, the number average molar mass of the chain lengths between crosslinks and grafting points can be estimated with the measured swelling of PGMA with acetone. That estimation for the 8 nm PGMA film is 1195 g/mol and for the 90 nm PGMA film it is 465 g/mol. It is noted that while the cross linking density of the 90nm film should be more than the 8nm, this appears to be an over estimation. Future experiments would need to accurately determine the exact cross linking density. Next, the interaction parameter was estimated for the remaining PGMA-VOC pairs for both the 8 nm film and the 90 nm film and are presented in **Table 4.5** and **Table 4.6** respectively.

Table 4.5. χ parameters calculated for 8 nm PGMA film

VOC	φ_{poly}	$\varphi_{solvent}$	χ
Acetone	0.45	0.55	0.479
MeOH	0.35	0.65	0.36
Hexane	0.72	0.28	0.84

Table 4.6. χ parameters calculated for 90 nm PGMA film

VOC	φ_{poly}	$\Phi_{solvent}$	χ
Acetone	0.6	0.4	0.479
MeOH	0.87	0.13	1.42
Hexane	0.98	0.02	2.73
IPA	0.86	0.14	1.26
EtOH	0.85	0.15	1.26
AA	0.72	0.28	0.81

It can be clearly observed that the values for the parameter are significantly different for 8 nm and 90 nm films. For the thicker film the parameters are corresponding to the solubility of the PGMA in the solvents. In fact, PGMA is soluble only in acetone ($\chi<0.5$). It can be suggested that the lower values for the thinner film are associated with significant influence of the silicon surface on the solvent sorption.

4.3.4. Partition coefficient for VOCs in PGMA

In order to understand the absorption behavior of the polymer films on the quantitative level, the partition coefficient, K, was calculated for the PGMA films (8 nm and 90 nm)[17-18]

$$K_{calc} = \frac{RT\rho}{Mp\exp\frac{V(\delta_1-\delta_2)^2}{RT}} \tag{4.17}$$

where ρ is the density of polymer film, p is the vapor pressure of the solvent, M is the molecular weight of monomeric unit of polymer, δ_1 is the solubility parameter of the solvent vapor, and δ_2 is the solubility parameter of the polymer. The term in the exponential can be substituted directly with the χ parameter determined in the previous section. The equation then becomes

$$\mathrm{K_{calc}} = \frac{\mathrm{RT\rho}}{\mathrm{Mpe^{\chi}}} \tag{4.18}$$

The experimental data obtained from swelling experiments was used to calculate an experimentally observed partition coefficient. The equation for the experimental partition coefficient is[17-18]

$$\mathrm{K_{exp}} = \frac{\rho\upsilon}{\mathrm{pM_s}/_{\mathrm{RT}}} \tag{4.19}$$

The ratio of the mass of solvent vapor per cm^3 of polymer coating to the mass of solvent vapor per cm^3 of vapor volume defines the partition coefficient. Here, M_s is the molecular weight of solvent, ρ is the density of the solvent, ν is the volume fraction of the solvent in a polymer determined from ellipsometry, R is the gas constant, T is the temperature of the system and p is the vapor pressure of the solvent at the system temperature. K can be defined as the ratio of the mass of solvent vapor per cm^3 of polymer coating to the mass of solvent vapor per cm^3 of vapor volume.

Equations 4.18 and 4.19 were used to calculate the partitioning of VOCs into the PGMA films. The results of the partition coefficient calculations for the 8 nm PGMA film and the 90 nm PGMA film are presented in **Table 4.7** and **Table 4.8** respectively. The thicker 90 nm PGMA film, which has a higher level of cross linking, has reduced partitioning of three analytes compared to the 8 nm film. The response of both PGMA films to most solvent vapors is in good agreement with the predicted value within an order of magnitude. However, the response of the thinner PGMA film to methanol is significantly higher. In this case, it is suggested that there are strong interactions between the surface of the silicon wafer and methanol, which cause increased swelling of the thin PGMA film with methanol. Acetic acid is also in good agreement despite the fact that it can dimerize in the vapor phase and in the film. From the data obtained it can be concluded that the Flory-Rehner equation can be used to estimate interaction parameters for thin films anchored to the surface.

Table 4.7 Calculated partition coefficients and experimental partition coefficients for 8 nm PGMA film

	K_{Calc}	K_{exp}
Acetone	383	622
Hexane	406	263
Methanol	780	2420

Table 4.8. Calculated partition coefficients and experimental partition coefficients for 90 nm PGMA film

	K_{calc}	K_{exp}
Acetone	383	444
Hexane	61	19
MeOH	270	474
IPA	805	804
EtOH	683	816
AA	3993	5787

4.3.5. FT-IR ATR spectra obtained in static conditions

FT-IR spectra were obtained for PGMA films deposited on a silicon crystal waveguide and exposed to various VOCs. A non-modified crystal was exposed to the same VOCs to demonstrate that a polymer coating is indeed necessary to pick up vapor to produce substantial IR signals. The IR spectrum of the VOC absorbed into the PGMA film is compared to an IR spectrum of the liquid VOC analyte taken on the same FT-IR instrument on a non-coated silicon waveguide ATR crystal.

4.3.5.1. Methanol

Figure 4.5 contains the FT-IR spectra for PGMA film swollen with methanol, alongside the spectrum of liquid methanol and the spectrum of a non-coated silicon waveguide crystal exposed to methanol vapor. All spectra were recorded on the same instrument. The spectrum of a non-coated silicon waveguide crystal exposed to methanol vapor shows a small absorbance band in the 2900 cm^{-1} region. Beyond this there are no identifiable peaks to distinguish methanol. Methanol as a liquid has a broad and intense band between 3100 and 3600 cm^{-1} corresponding to the hydrogen oxygen stretching (O-H). Obtained spectroscopic data clearly demonstrates that methanol was "picked-up" by the PGMA enrichment polymer coating and produced unique spectroscopic signature.

There is a difference in the carbon-hydrogen (C-H) stretching of the methanol absorbed into the PGMA film compared to its original liquid. PGMA has its own C-H stretching along its backbone, which can contribute to this difference. In fact, the repeat unit for PGMA has three CH_2 groups to one CH_3 group while there is only one CH_3 group in methanol. Therefore, there is likelihood that CH_3 from both methanol and the PGMA layer overlap, which makes accurate interpretation of the C-H spectra rather challenging.

The carbonyl group from the PGMA ester in the background interacts with the methanol resulting in a negative IR absorbance region between 1560 cm^{-1} and 1725 cm^{-1}; however, a "new" vibrational frequency is seen as a sharp peak at 1733 cm^{-1}. This type of peak is not associated with any fundamental frequencies in either the polymer film or the VOC in question. Rather, it represents interactions between the two substances. The interaction produces resonance frequencies distinguishably different from the background spectrum. This will be referred to as a secondary peak for the enrichment of the layer-solvent system. The absorbance value for the peak is 0.019 and the negative region associated with the interaction is 1.69. Peaks such as this are highly desirable as they can provide unique characteristics for quick identification. The PGMA layer is thus capable of incorporating methanol, which can be identified by its absorbance bands and secondary absorbance peaks.

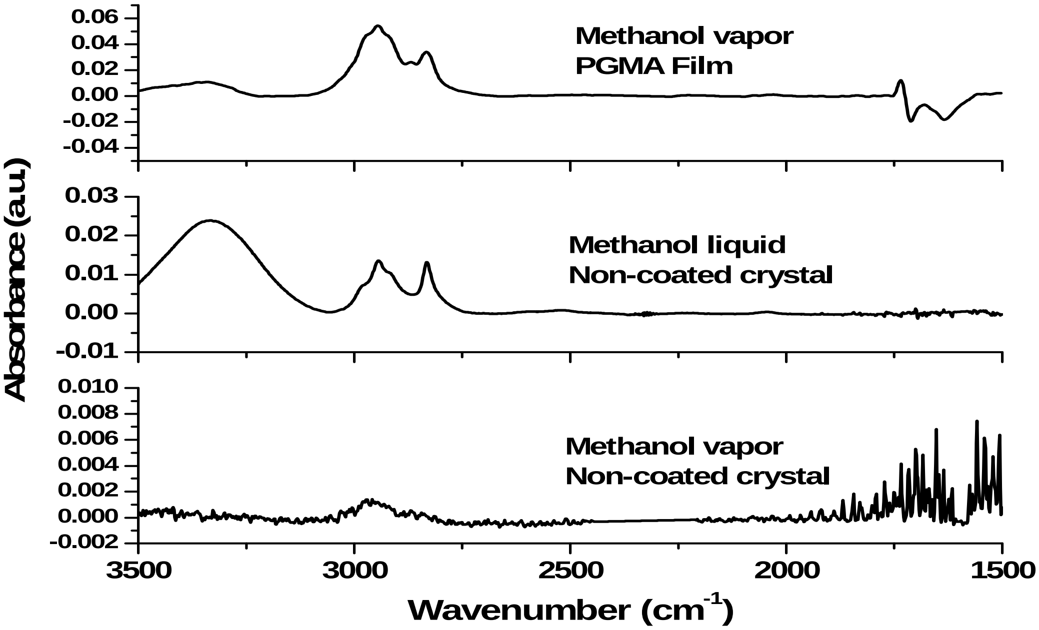

Figure 4.5. The IR spectra of methanol absorbed by a 130 nm PGMA film. The IR spectrum of liquid methanol and vapor exposed to a non-modified ATR crystal are added for comparison.

4.3.5.2. Ethanol

In **Figure 4.6**, the FT-IR spectra for PGMA film swollen with ethanol, the spectrum of liquid ethanol, and the spectrum of a non-coated silicon waveguide crystal exposed to ethanol vapor are presented. For the non-coated silicon waveguide crystal, there is only noise in the spectrum and no identifiable peaks of ethanol. Conversely, spectroscopic signature of ethanol can be clearly observed for the PGMA layer swollen with the solvent. In general, absorbed ethanol has spectral regions and characteristics similar to methanol, but it has significantly different peak appearance. The differences between ethanol and methanol lie primarily in the strength of their polar and hydrogen bonding. It is a general characteristic that the polarities of functional groups such as hydroxyl groups to be less prominent as the length of the hydrocarbon chain increases. The secondary carbonyl peak has an absorbance value of 0.017 and the negative region has an area of 1.4. These values are slightly less than those of methanol.

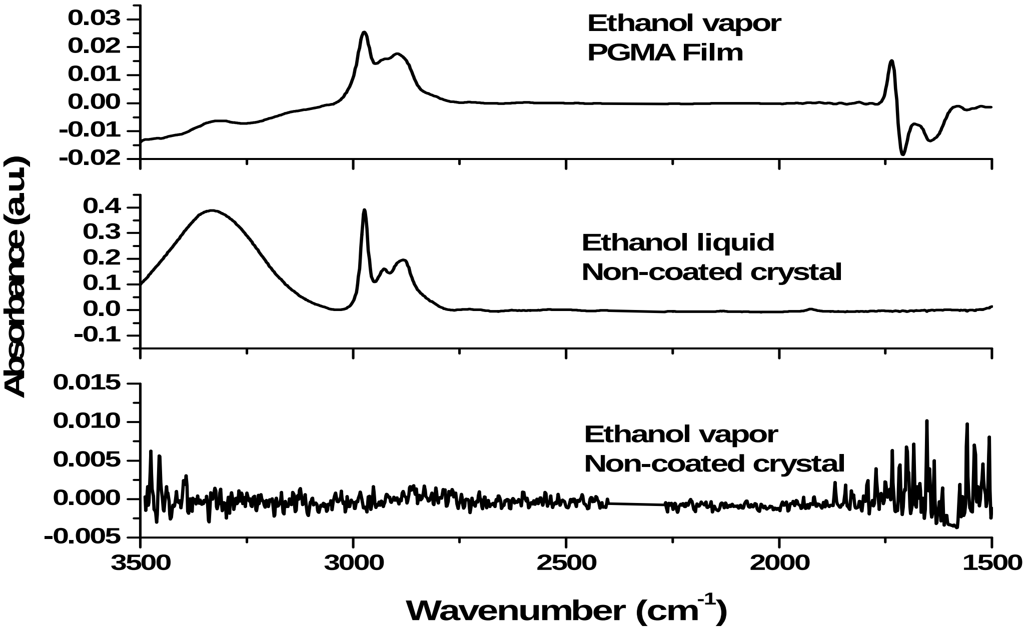

Figure 4.6. The IR spectra of ethanol absorbed by a 130 nm PGMA film. The IR spectrum of liquid ethanol and vapor exposed to a non-modified ATR crystal are added for comparison.

4.3.5.3. Isopropyl alcohol (IPA)

In **Figure 4.7**, the FT-IR spectrum of the IPA swollen PGMA film, the spectrum of liquid IPA, and the spectrum of a non-coated silicon waveguide crystal exposed to IPA vapor are presented. Once again there is not a signal above the noise when a non-coated crystal is exposed to the vapor. The spectrum for the PGMA film produced spectroscopic signature of IPA. The secondary carbonyl peak has an absorbance value of 0.02 and the negative region has an area of 1.85. These values are slightly greater than those of methanol and ethanol.

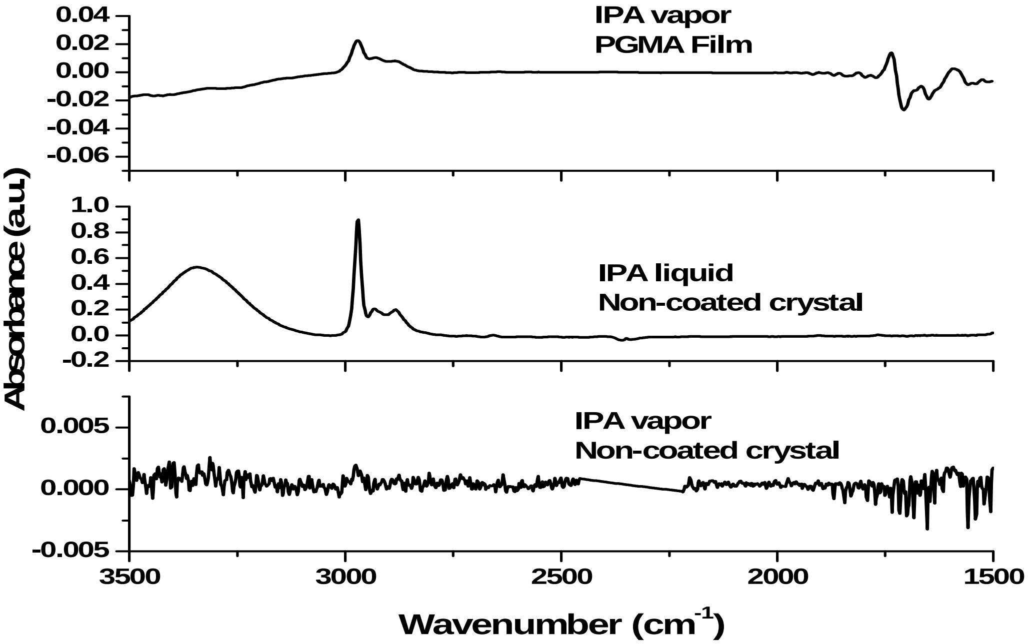

Figure 4.7. The IR spectra of IPA absorbed by a 130 nm PGMA film. The IR spectrum of liquid IPA and vapor exposed to a non-modified ATR crystal are added for comparison.

4.3.5.4. Acetone

Figure 4.8 contains the FT-IR spectrum of acetone vapor absorbed into a 130 nm PGMA film, the liquid acetone spectrum, and the spectrum of a non-coated silicon waveguide crystal exposed to acetone vapor. The spectrum of acetone vapor with the non-coated crystal shows no discernible acetone signature. However, the baseline is distorted which can suggest some slight interactions with the surface. Broadening of the fundamental carbonyl (C=O) peak of acetone at 1710 cm^{-1} can be observed in the spectrum of acetone vapor absorbed into the PGMA film. In the acetone swollen film, there is splitting of the carbonyl region showing an additional peak at higher wavenumbers. There is little C-H stretching observed as acetone is absorbed into the film. The absorbance present in the 2800-2980 cm^{-1} region is minimal.

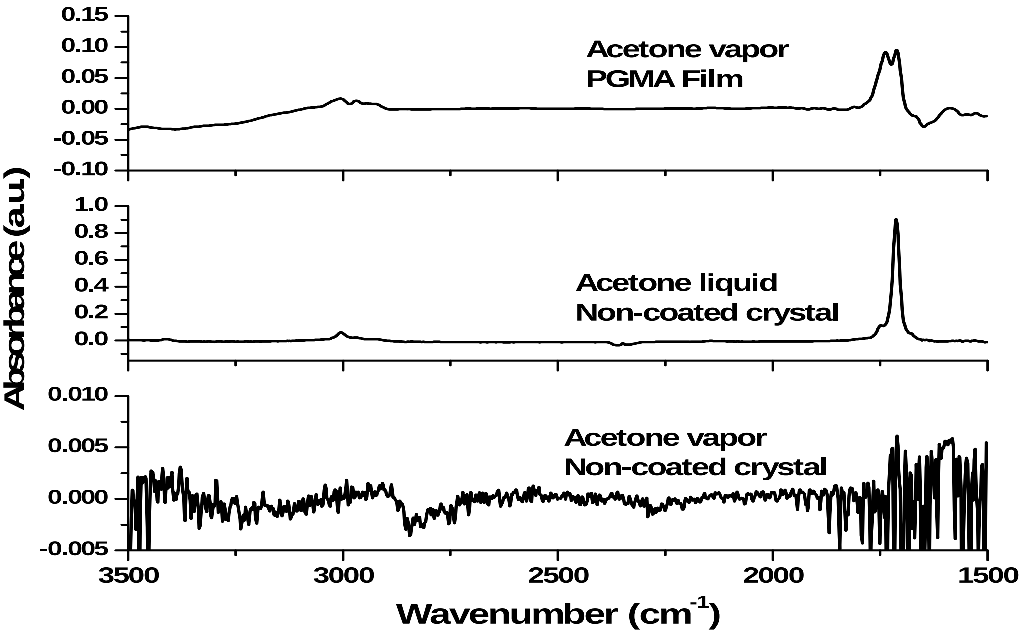

Figure 4.8. The IR spectra of acetone absorbed by a 130 nm PGMA film. The IR spectrum of liquid acetone and vapor exposed to a non-modified ATR crystal are added for comparison.

4.3.5.5. Acetic Acid

In **Figure 4.9**, the FT-IR spectra of the 130 nm PGMA film loaded with acetic acid vapor, the liquid acetic acid absorbance spectrum, and the spectrum of the non-coated crystal are provided. The spectrum of vapor exposed to a silicon crystal with no polymer film has no discernable peaks. The carbonyl peaks broadens for the acetic acid absorbed into the PGMA film. The O-H region appears positive and broad from the acetic acid hydroxyl group absorbed in the layer. In addition, there is virtually no observable C-H stretching as it is overshadowed by the intensity of the carbonyl and O-H region both in the liquid state and as a vapor absorbed into the PGMA film.

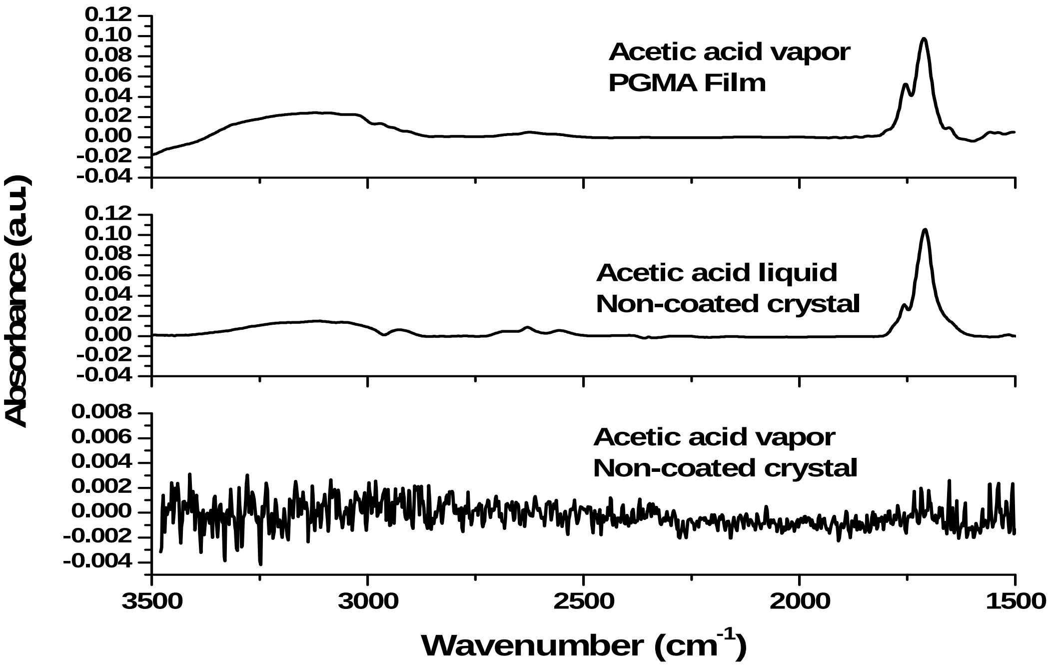

Figure 4.9. The IR spectra of acetic acid absorbed by a 130 nm PGMA film. The IR spectrum of liquid acetic acid and vapor exposed to a non-modified ATR crystal are added for comparison.

4.3.5.6. Hexane

By now, it is evident that PGMA has good absorption capabilities towards VOCs that have a polar functional group. **Figure 4.10** shows the spectra for the 130 nm PGMA film exposed to hexane vapor and to the non-coated silicon waveguide crystal which are both compared to the spectrum of liquid hexane. Surprisingly, there is a weak but identifiable hydrocarbon signal from the non-coated crystal after exposure to hexane vapor. With the PGMA layer the signal is increased 20 times. Here the strong C-H stretching characteristic of hexane indicates that while the polymer systems primarily have polar groups, non-polar VOCs can still penetrate into the film. The C-H stretching region is broadened. Specifically, two peaks are present in the hexane liquid spectrum, at

2924 cm^{-1} and 2958 cm^{-1} have merged in the absorbed vapor spectrum. In addition, peaks at 2860 cm^{-1} and 2873 cm^{-1} in the hexane liquid spectrum seemingly merge to make a peak at 2879 cm^{-1}. This could also be a secondary peak, as it is not a fundamental absorbance peak of in the hexane liquid. Interestingly, secondary peak in carbonyl area is also observed in the spectrum. To conclude, PGMA allows for a strong enrichment of non-polar types of VOCs.

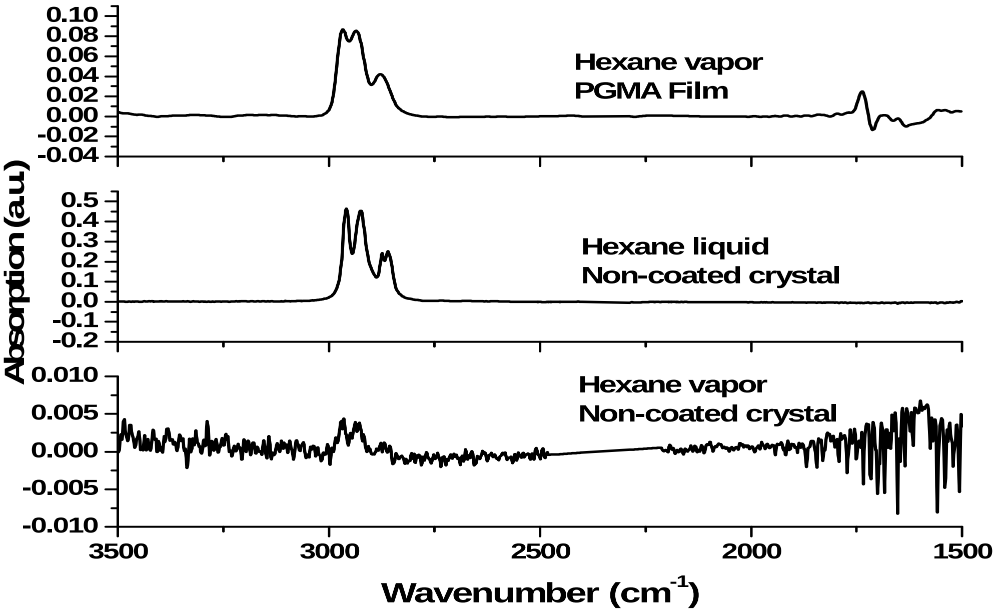

Figure 4.10. The IR spectra of hexane absorbed by a 130 nm PGMA film. The IR spectra of liquid hexane and vapor exposed to a non-modified ATR crystal are added for comparison.

4.3.5.7. Ammonium hydroxide

The FT-IR spectrum of the 130 nm PGMA film exposed to the vapor of a 0.5% ammonium hydroxide solution is presented in **Figure 4.11**. For comparison, the liquid spectrum of the ammonium solution, and the non-coated crystal exposed to the vapor are also provided in **Figure 4.11**. PGMA will absorb ammonia to a certain extent. A decrease in IR absorbance intensity around 1740 cm^{-1} was observed. The O-H region shows a positive absorbance which can be an additive result of both the water vapor and ammonia.

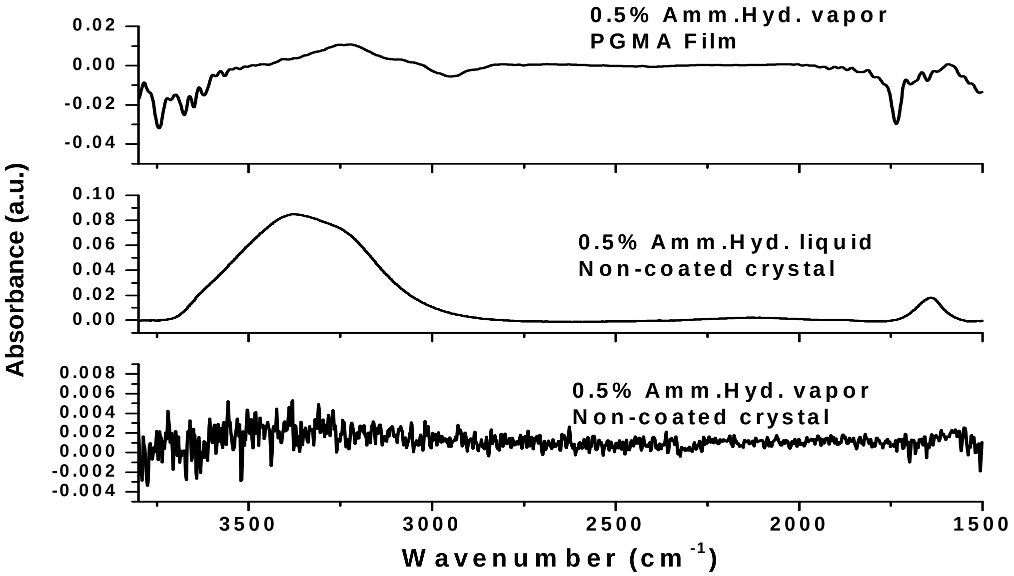

Figure 4.11. The IR spectra of ammonium hydroxide absorbed by a 130 nm PGMA film. The IR spectrum of the liquid solution and vapor exposed to a non-modified ATR crystal are added for comparison.

4.3.6. IR absorbance as a function of film thickness

A large signal to noise ratio is crucial when developing a chemical sensor. One aspect of the enrichment layers that can affect signal intensity is the thickness of the film. In theory, as the film increases in thickness, it can load more analyte. **Figure 4.12a** shows how the IR absorbance of the acetone signal increases with different thicknesses of PGMA. **Figure 4.12b** is a plot of the intensity of the 1710 cm^{-1} carbonyl IR absorbance as a function of the film thickness. Polymer chains in the thinner film are not as cross-linked. This allows more conformational freedom and allows additional loading of the analyte. In addition, the IR absorbance intensity is calculated per nanometer thickness of polymer film (right axis). A decrease in the capability of the film to load with VOC molecules per nanometer is observed. This is most probably due to the increased cross linking of the thicker films which restricts chain conformational changes.

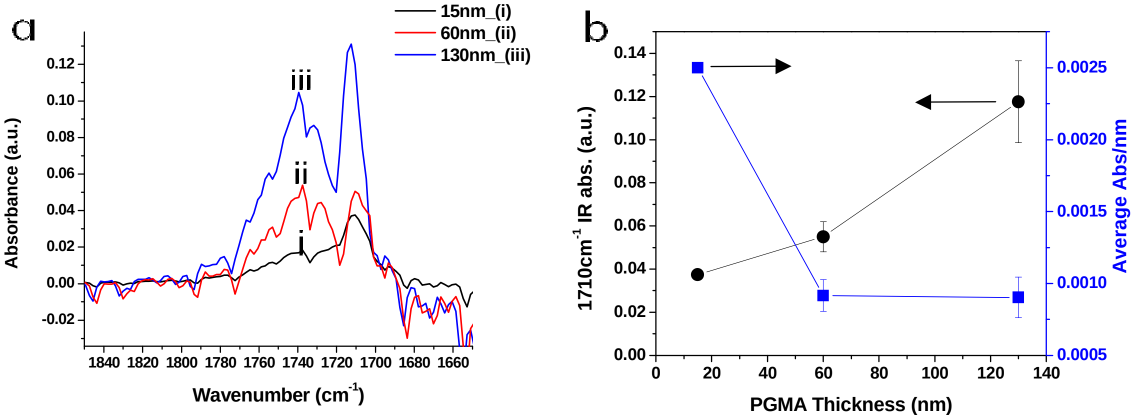

Figure 4.12. a) IR spectra of acetone vapor absorbed into three films of different thickness PGMA; b)(●) average absorbance of the 1710 cm^{-1} carbonyl peak for each PGMA thickness and (■) absorbance per nanometer ratio.

In order to demonstrate that absorbance intensity does not increase just for acetone, two more VOCs were used—hexane and methanol. For hexane absorbance (**Figure 4.13**), the characteristic peaks in the 15 nm layer are broader and less defined. As the PGMA film thickness increases, more hexane is able to load and each peak becomes more defined. In addition, the 2879 cm^{-1} C-H stretch exhibits concentration dependence. As the film becomes thicker, it can absorb more analyte and signal intensity increases. However, nanometer per nanometer, the absorbance decreases and is most likely due to the increased crosslinking present in the film.

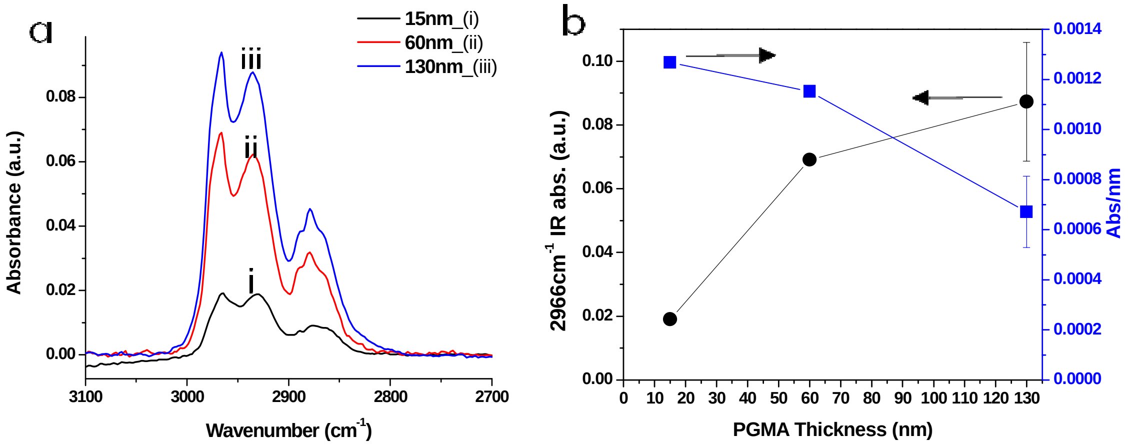

Figure 4.13. a) IR spectra of hexane vapor absorbed into three different thicknesses of PGMA; b) (●) average absorbance of the 2966 cm^{-1} carbonyl peak for each PGMA thickness and (■) absorbance per nanometer ratio.

The IR absorbance of methanol with different PGMA film thicknesses is given in **Figure 4.14**. There was only a small increase in the intensity of the C-H stretching peaks between the 60 nm and 130 nm films for absorbed methanol. The O-H stretching intensity shows more variability. Conclusively, the IR absorbance intensity per nanometer of the film decreases with methanol as it did with acetone and hexane. The cross linking of the PGMA causes this diminished loading of VOC vapor. The increase in signal intensity enables the use of thicker films to produce robust IR signatures and still be within the realm of the evanescent wave penetration for the ChG resonators.

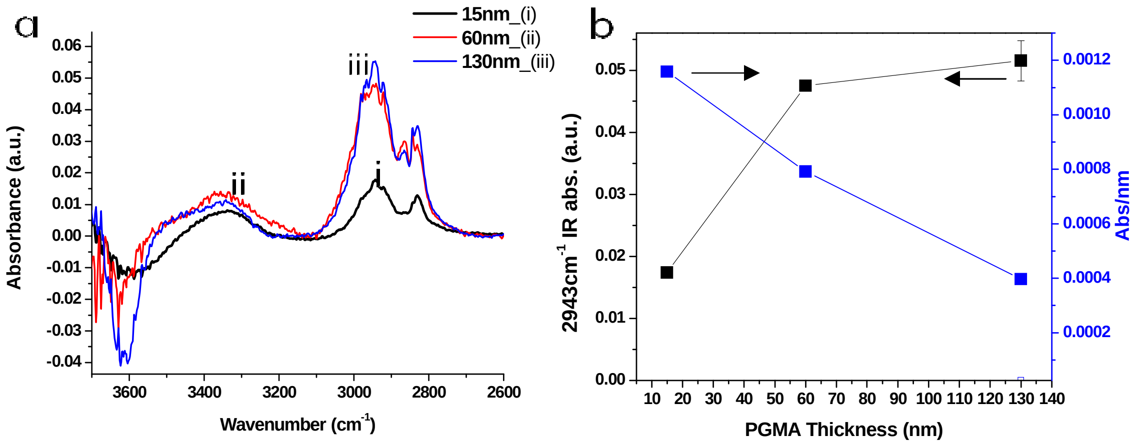

Figure 4.14. a) IR spectra of methanol vapor absorbed into three different thicknesses of PGMA; b) (●) average absorbance of the 1710 cm^{-1} carbonyl peak for each PGMA thickness and (■) absorbance per nanometer ratio.

4.3.7. Efficiency of PGMA enrichment layer

The EPLs were designed to attract and concentrate VOCs in the evanescent wave region to produce a substantial signal. In order to quantify the ability of the PGMA layer to attract VOCs, the efficiency of the system was determined. The efficiency is defined as the ratio of the IR absorbance due to vapor exposure per cm^2 (at a specific wavelength) and the IR absorbance of the liquid VOC (same wavelength) per cm^2 of the given ATR crystal. The equation is as follows:

$$E = \left(\frac{A_f}{A_c} \right) * 100\% \qquad (4.20)$$

where A_f is the IR absorbance of vapor per cm^2 (at a specific wavelength) and A_c is the IR absorbance of the liquid VOC (same wavelength) per cm^2 of the given ATR crystal, using our IR spectrometer. The parameter A_c was determined from experimental results described in Chapter 3 Section 6.2.1.

The absolute values of the efficiency of the enrichment layers used in this work apply strictly to the Nexus IR instrument, and the silicon waveguide crystals which were used. This is because different IR spectrometers have different detectors and different power levels are used in the IR source. These two factors affect the initial intensity of light that can go through the layer and be detected by the instrument. If the power is too weak, it makes the EPL seem as though it is close to 100% efficiency all the time.

The maximum C-H absorbance of the absorbed vapor in the polymer film is provided in **Table 4.9** with the "main" peak absorbance (if C-H stretching is not the dominant peak). Because the efficiency is a ratio of the absorbance of the liquid VOC, it is expected to be low as the EPL is not exposed to liquid.

Table 4.9. IR peak absorbances of liquid VOCs taken from silver modified silicon waveguide crystal.

	From liquid spectra			
VOC	**C-H peak***	**abs/cm^2**	**Main peak****	**abs/cm^2**
Acetone	0.19	0.04	0.38	0.07
MeOH	0.39	0.07	0.98	0.18
Hexane	0.30	0.04		
EtOH	0.22	0.04	0.76	0.14
IPA	0.27	0.04	0.35	0.06
Acetic acid	0.07	0.01	0.84	0.16

*Asymmetrical C-H stretching peak for the respective VOC.
**Main peaks refer to other strong absorbing peaks in the VOC besides the asymmetrical C-H stretch. For acetone and acetic acid, this is the carbonyl, and for the alcohols it is the O-H stretch.

It was found, in agreement with expectations, that the thicker layer was more efficient. As shown in **Table 4.10**, the C-H stretching was used to normalize the efficiency, as all of the VOCs have C-H stretching. The specific wavenumber for each compound was different but all were the highest absorbance in the C-H stretching region.

The greatest efficiency was observed for hexane when wavelengths in the C-H stretching region were used. The efficiency for each VOC decreases with decreasing thickness of the polymer film. In **Table 4.11**, the efficiencies toward the pure VOCs used in this work are given. The efficiency toward acetone is lower when using C-H peak versus the "main" peak carbonyl absorbance at 1710 cm^{-1}. Increased efficiency could be due more interactions within the PGMA layer. Hydroxyl absorbance was not used for the alcohols as "main" peaks due to the influence of humidity.

Table 4.10 Percentage efficiency for PGMA films (three thicknesses): C-H stretching.

	PGMA -130 nm C-H (a.u.)	**PGMA -130 nm C-H [abs/cm^2]**	**% Efficiency***
Acetone	0.023	0.0043	12
MeOH	0.0552	0.0103	14
Hexane	0.094	0.0176	41
EtOH	0.0271	0.0051	12
IPA	0.0247	0.0046	12
Acetic acid	0.005	0.0009	8.8
	PGMA 60 nm C-H abs	**PGMA -60 nm CH [abs/cm^2]**	**% Efficiency**
Acetone	0.01285	0.0024	6.8
MeOH	0.048	0.0090	12
Hexane	0.0685	0.0128	30
	PGMA -15 nm CH abs	**PGMA -15 nm CH [abs/cm^2]**	**% Efficiency**
Acetone	0.0027	0.0005	1.4
MeOH	0.0178	0.0033	4.5
Hexane	0.0191	0.0036	8.3
EtOH	0.0147	0.0028	6.6
IPA	0.0137	0.0026	6.4

*Based on **Equation 4.20**

Table 4.11. Percentage efficiency for PGMA films (three thicknesses): acetone carbonyl stretching .

PGMA 130 nm	**Vapor [abs]**	**[abs/cm^2]**	**% Efficiency**
Acetone	0.131	0.025	34.2
PGMA 60 nm	**Vapor [abs]**	**[abs/cm^2]**	**% Efficiency**
Acetone	0.056	0.010	14.5
PGMA 15 nm	**Vapor [abs]**	**[abs/cm^2]**	**% Efficiency**
Acetone	0.037	0.007	9.7

4.3.8. Concentration dependence using a PGMA EPL in dynamic flow

The next step was to determine a) whether the 130 nm PGMA film would still pick up acetone vapor after multiple dilutions with nitrogen and b) whether it would be possible to discern a VOC signal from absorbance intensity alone. To do this, acetone was delivered using the dynamic delivery setup, depicted in Chapter 3, **Figure 3.4,** with nitrogen carrier gas. Starting from a total flow of 20 mL/min, the 130 nm PGMA film was exposed to nitrogen saturated with acetone. Keeping the total flow to 20 mL/min, the acetone was diluted stepwise with nitrogen from a second line. This caused the acetone signal to drop. The change of the acetone carbonyl absorbance at 1710 cm^{-1} is given in **Figure 4.15**. The absorbance diminishes as more nitrogen is introduced. All points on the curve are the maximum of a separate run and each are after 20 minutes of exposure; however, the last point was taken after 40 minutes to reach a signal above the noise. The trend, however, has a positive deviation from a linear dependence. This could be due to a high affinity between the VOC analyte and the polymer film.

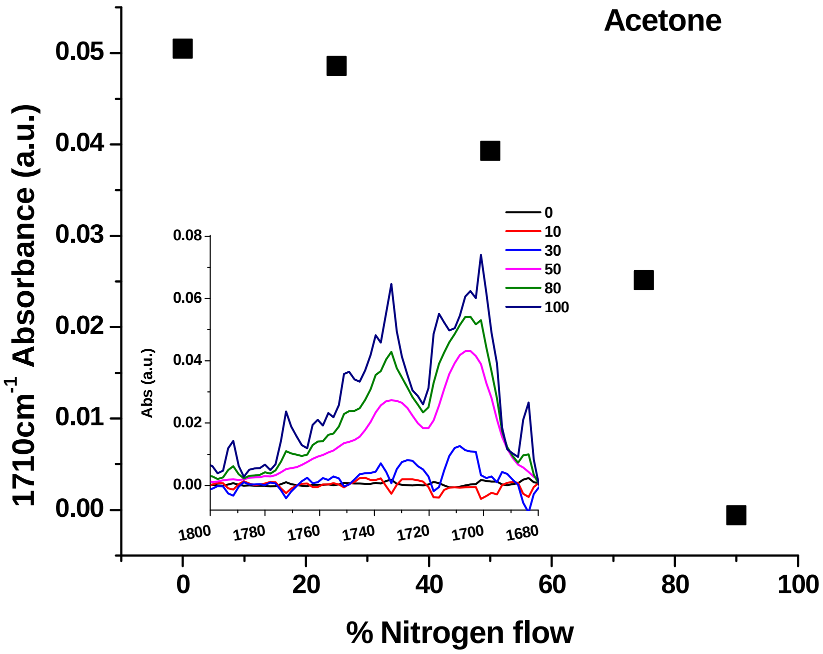

Figure 4.15. The IR absorbance intensity of the 1710 cm^{-1} peak of acetone loading into a 130 nm PGMA film. The acetone was running at 20mL/min flow, which decreased with increasing amounts of nitrogen. The inset depicts the spectra of 1710 cm^{-1} peak with increasing nitrogen content.

4.4. Conclusions

PGMA can be utilized as a single component EPL. Exposure to VOCs with *in-situ* ellipsometry showed a swelling trend for PGMA. *In-situ* FT-IR showed new peak formations that were not present in the VOC. This may provide better identification of VOCs. The strongest IR signals for VOCs were obtained with the thicker 130 nm film, however, even 15 nm PGMA film is sufficient to trap VOC molecules and obtain spectra. The time that is needed to confirm VOC absorption is less than 30 seconds under static conditions and identification can be accomplished in less than a minute. Equilibrium time can be up to 20 minutes for high vapor pressure VOCs. A minimum of 40 minutes is required for low vapor pressure VOCs to reach equilibrium in static conditions. Dynamic conditions decrease these times.

4.5. References

1. Minko, S., Grafting on Solid Surfaces: “Grafting to” and “Grafting from” Methods. In *Polymer Surfaces and Interfaces*, Stamm, M., Ed. Springer: **2008**.

2. Zdyrko, B.; Klep, V.; Luzinov, I., Grafting of high-density poly(ethylene glycol) brush to poly(glycidyl methacrylate) monolayers. *Abstracts of Papers of the American Chemical Society* **2002,** *223*, D6-D7.

3. Zdyrko, B.; Klep, V.; Luzinov, I., Synthesis and surface morphology of high-density poly(ethylene glycol) grafted layers. *Langmuir* **2003,** *19* (24), 10179-10187.

4. Eastman, M. P.; Hughes, R. C.; Yelton, G.; Ricco, A. J.; Patel, S. V.; Jenkins, M. W., Application of the solubility parameter concept to the design of chemiresistor arrays. *Journal of the Electrochemical Society* **1999,** *146* (10), 3907-3913.

5. Bruening, M. L.; Dotzauer, D. M.; Jain, P.; Ouyang, L.; Baker, G. L., Creation of functional membranes using polyelectrolyte multilayers and polymer brushes. *Langmuir* **2008,** *24* (15), 7663-7673.

6. Patel, S. V., Chemicapacitive microsensors for volatile organic compound detection. *Sensors and Actuators B: Chemical* **2003,** *96* (3), 541-553.

7. Flavin, K.; Hughes, H.; Dobbyn, V.; Kirwan, P.; Murphy, K.; Steiner, H.; Mizaikoff, B.; McLoughlin, P., A comparison of polymeric materials as pre-concentrating media for use with ATR/FTIR sensing. *International Journal of Environmental Analytical Chemistry* **2006,** *86* (6), 401-415.

8. Friess, K.; Jansen, J. C.; Vopicka, O.; Randova, A.; Hynek, V.; Sipek, M.; Bartovska, L.; Izak, P.; Dingemans, M.; Dewulf, J.; Van Langenhove, H.; Drioli, E., Comparative study of sorption and permeation techniques for the determination of heptane and toluene transport in polyethylene membranes. *Journal of Membrane Science* **2009,** *338*, 161-174.

9. Gutmann, F.; Simmons, L. M., A Theoretical Basis for the Antoine Vapor Pressure Equation. *The Journal of Chemical Physics* **1949,** *18* (5), 696-697.

10. NIST NIST Standard Reference Data. http://webbook.nist.gov/chemistry/name-ser.html.

11. Young, R. J. L. P. A., *Introduction to polymers*. CRC Press/Taylor & Francis Group: Boca Raton [etc.],**2011**, 688 Pages.

12. Fried, J. R., *Polymer science and technology*. Prentice Hall Professional Technical Reference: Upper Saddle River, NJ, **2003**.

13. Booth, C.; Devoy, C. J., . *Polymer* **1971,** *12*, 320.

14. Elbs, H.; Krausch, G., Ellipsometric determination of Flory-Huggins interaction parameters in solution. *Polymer* **2004,** *45*, 7935-7942.

15. Chyasnavichyus, M. Synthesis and Characterization of Nanoscale Fluorescent Polymer Films PhD Dissertation, Clemson University, Clemson, **2012**.

16. Barton, A. F. M., *CRC handbook of polymer-liquid interaction parameters and solubility parameters*. CRC Press: Boca Raton, **1990**.

17. Snow, A.; Wohltjen, H., Poly(ethylene maleate) Cyclopentadiene - A model Reactive Polymer Vapor System for Evaluation of a Saw Microsensor. *Analytical Chemistry* **1984,** *56* (8), 1411-1416.

18. Burtovyy, O. Synthesis and Characterization of Macromolecular Layers Grafted to Polymer Surfaces. PhD Dissertation, Clemson University, Clemson, **2008**.

Chapter 5. PGMA-PAA Enrichment Polymer Layer System

5.1. Introduction

After thorough studies of PGMA-based enrichment layers, the next step was the addition of other polymers that can be grafted to PGMA and enhance targeting sensitivity for a specific VOC. To this end, this chapter presents the synthesis, characterization, and behavior of a multi-layered (six layers) two-component PGMA-poly(acrylic acid) system acting as an enrichment polymer layer system. Each repeat unit of PAA has a carboxylic acid making it highly sensitive to VOCs that are proton accepting and are capable of hydrogen bonding. After the grafting of PAA to a PGMA layer, free carboxyl groups remain present along the backbone of the grafted polymer to add an additional layer of PGMA. This allows for a highly feasible layer-by-layer design of enrichment polymer layer systems.

The swelling fractions, interaction parameters, and partitioning coefficients for VOC/six-layer PGMA-PAA EPLS were determined. IR absorbance signatures of the VOCs plus polymer system were obtained using *in-situ* FT-IR Attenuated Total Reflectance (ATR). *In-situ* FT-IR ATR studies were performed in both a static environment and a dynamic flow environment. Conditions were the same as with the PGMA films described in Chapter 4 unless otherwise noted.

5.2. Experimental

The six layer PGMA-PAA EPLS was prepared by dip coating. All PGMA layers were prepared using a 0.07% w/v chloroform solutions All PAA layers were prepared using a 1% w/v solution in methanol. The annealing temperature for the grafting was

$120^{o}C$ for all layers. The grafting time period was 20 minutes. An 8 nm layer of PAA was deposited by dip coating onto a 1 nm anchoring layer of PGMA.

5.3. Results and Discussion

5.3.1. Swelling of a single anchored layer of PAA

In-situ ellipsometry swelling experiments were performed on a PAA layer, with the same VOCs as used on PGMA films reported in Chapter 4. In **Figure 5.1**, the average swelling fraction of the grafted 8 nm PAA film with methanol, acetone, and hexane is presented. A Student's T-test was conducted for statistical analysis using a confidence interval of 95%. The average swelling with methanol and acetone was found to be statistically the same. The average swelling for hexane was significantly lower than for methanol and acetone. A student's T-test was performed, using the same parameters, on the VOC swelling fractions between the 8nm PGMA (Chapter 4, **Figure 4.2**) and 8nm PAA films. Analysis of the results show that the swelling fraction of hexane is statistically different (t value calculated is 3.7). It is also statistically significant compared to acetone and methanol (t values are 20.5 and 5.49, respectively).

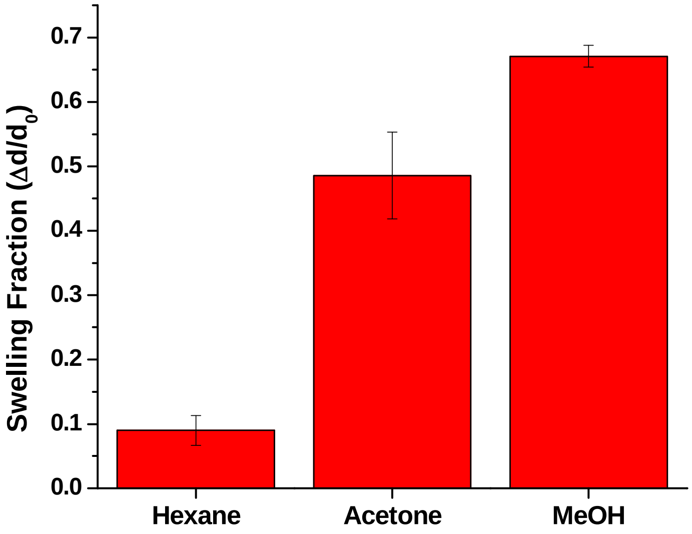

Figure 5.1. Swelling extent of an 8 nm PAA film to VOC analytes: methanol, acetone, and hexane.

The enthalpy of mixing (heats of dissolution) and corresponding interaction parameter, χ, for PAA-ethanol solutions can be found in literature.[1] Because the enthalpy of mixing was found to be exothermic, the literature experiments yielded an interaction parameter that is negative. χ for PAA-ethanol was used with the swelling fraction of PAA-methanol to determine M_c. The result was is 378 g/mol. Using M_c, it is possible to estimate χ parameters for acetone and hexane from the swelling fractions with the film. The parameters are presented in **Table 5.1** below. The parameters determined

Table 5.1. χ parameters calculated for 8 nm PAA film

VOC	φ_{poly}	$\varphi_{solvent}$	χ
MeOH	0.3	0.7	-0.34 (Ref. [1])
Acetone	0.67	0.35	0.45
Hexane	0.79	0.21	0.55

for acetone and hexane are somewhat lower that can be expected from the known non-solubility of PAA in the solvents. The same phenomenon was found for the 8 nm PGMA film (Chapter 4) indicating that the presence of silicon (high surface energy) surface changes the swelling pattern for the ultrathin films.

Equation 4.18 was used for the prediction of the partition coefficient for these three VOCs and the 8 nm PAA. Results of the partition coefficient calculations are presented in **Table 5.2**. The experimentally determined K for hexane and methanol is in fair agreement with the predicted value. The difference between the calculated and experimental K for acetone, however, is significant. The experimental value for the partition coefficient is about seven times lower than the predicted value. Therefore, for this PAA film χ obtained from the Flory-Rehner equation has limited applicability to predict the partition coefficient.

Table 5.2. Calculated partition coefficients and experimental partition coefficients for 8 nm PAA film

	K_{calc}	K_{exp}
MeOH	3506	2402
Acetone	1974	278
Hexane	632	197

5.3.2. PGMA-PAA six-layer EPLS

5.3.2.1. Characterization

There are three distinct carbonyl functional groups in the layered PGMA-PAA grafted system: the PGMA ester carbonyl, the carboxylic acid in PAA, and the carbonyl ester when PAA bonds with the epoxy group in PGMA. These three carbonyls have similar absorbance coefficients which cause the absorbance in the 1700 cm^{-1} region to broaden when layers are added. Presented in **Figure 5.2** is the carbonyl IR absorbance curve for PGMA, PAA, and the two-layer grafted combination. PAA has a prominent peak at 1710 cm^{-1} and a large shoulder around 1740 cm^{-1}, which corresponds to free acid groups in the layer that are not bound by hydrogen bonding. The PGMA ester carbonyl has a single broad peak at 1735 cm^{-1}. The carbonyl peak of the two polymers combined in a layered system shows that the interactions and bonding between the two polymers broaden this region. Therefore, deconvolution of any free groups in either polymer layer might be challenging.

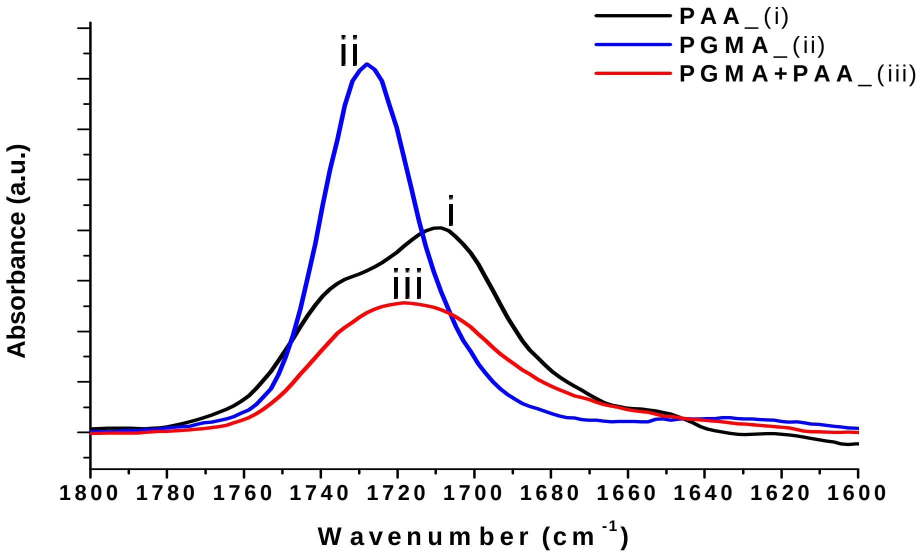

Figure 5.2. Comparison of carbonyl absorbance regions of PAA and PGMA.

Table 5.3 has the surface density and chain coverage for each layer in the six-layer EPLS calculated from Equations 3.1 and 3.2.

Table 5.3. Six-layer system layer characteristics

Six-layer system			
Layer	**Thickness [nm]**	**Surface coverage [mg/m^2]**	**Chain density [chains/nm^2]**
PGMA L1	3	3.24	1.45E-02
PAA L2	8	8.72	5.25E-02
PGMA L3	5.5	5.94	2.65E-02
PAA L4	5.5	6	3.61E-02
PGMA L5	3	3.24	1.45E-02
PAA L6	7	7.63	4.60E-02
PGMA fraction*	0.36		
PAA fraction*	0.64		

*Fractions are of total thickness contributions of each polymer.

As the PGMA-PAA enrichment polymer layer was synthesized, the thickness of the system and the overall carbonyl area were monitored (**Figure 5.3**). The total thickness of the EPLS was kept to ~30 nm, which ensured that the absorbed analyte was within the evanescent wave field for detection.[2] IR absorbance spectra were taken as layers were added to confirm the additions of polymer layers. Furthermore, each layer, after grafting, was rinsed with a good solvent to assess the grafting strength and confirm that the layers were not rinsed off. Chloroform was used for rinsing PGMA. De-ionized water was used for rinsing PAA.

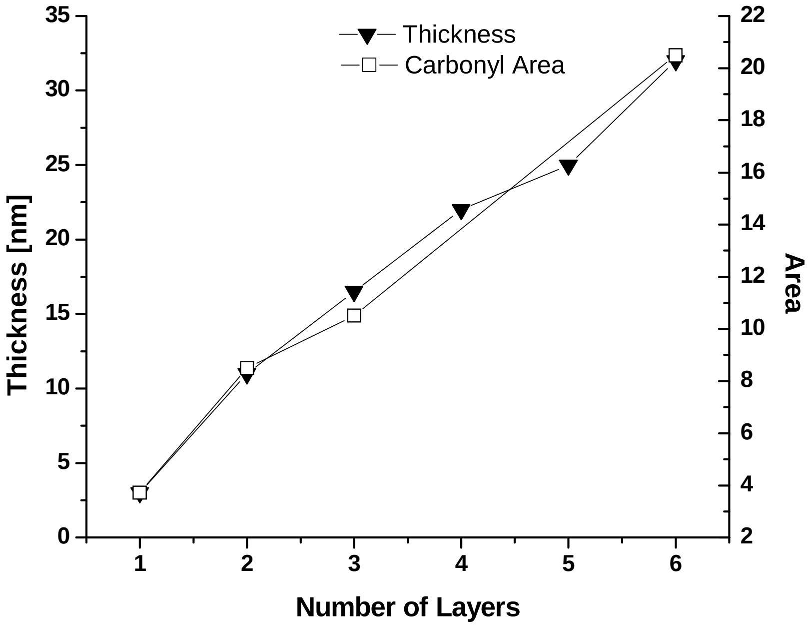

Figure 5.3. Thickness and carbonyl total area change with number of layers.

The full spectrum of the six-layer system when first made and after four months of testing is presented in **Figure 5.4**. The free acid groups from the PAA make the layered film highly hygroscopic. The proof of this is the strong and broad O-H region between 3000 cm^{-1} and 3500 cm^{-1}. After four months of testing, it can be seen that qualitatively there are no new peaks. However, there is a decrease of about 20% in the carbonyl region calculated by integration over the area between 1608 cm^{-1} and 1774 cm^{-1}. It is unclear if this decrease is the result of humidity, or a slight variation in the measurement. Nevertheless, there are no new peaks formed after four months. Therefore, the stability of the film against multiple VOC exposures and long storage is very good.

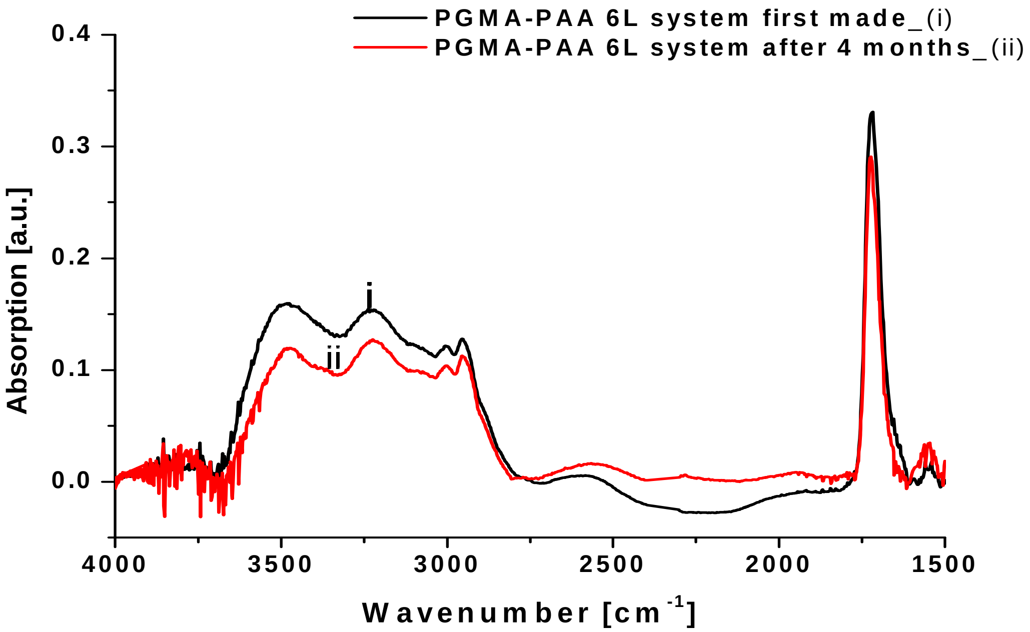

Figure 5.4. IR spectrum of PGMA-PAA six-layer system when first synthesized and after four months of testing.

5.3.2.2. Morphology of polymer layer surfaces

It was important to study the morphology of the layered films because covalent grafting of polymer layers forcibly arranges the polymer chains, which can cause stresses in the layers. Morphology of each of the six layers of the PGMA-PAA system coated onto a silicon waveguide crystal and model silicon wafer is presented in **Figure 5.5**. Most notable are the wrinkles that formed in the PGMA third layer on both the silicon crystal and wafer. The formation of the surface wrinkles in the cross-linked film is a well-known phenomenon. Solvent contributions can destabilize the polymer deposition causing dewetting.[2-5] If the deposition of the polymer is done on an inorganic, non-swellable surface and the deposition is enthalpically favorable, as is the case with PGMA and the hydroxyl groups on the silicon surface, then the polymer layer is grafted uniformly.

When a polymer is deposited onto a polymer, the underlying polymer can swell or contract with solvent addition and evaporation. This can cause the polymer to be deposited as a non-flat layer. When the polymer is grafted, wrinkles can form in these regions.[6] Wrinkles can also form when polymer chains in the grafted layer have a certain amount of cross-linked density that causes instability. When grafting PGMA onto a substrate, stresses are caused when the polymer passes its glass transition temperature but movements of the chains are restricted due to cross-linking and grafting to the PAA layer. It is important to note that other layers were wrinkle free. Reasons for the wrinkles not carrying over in the additional layers can be the multiple annealing cycles that the layers experience and that PAA is not as inhibited in movement as PGMA. Surface roughness from AFM for layers 1, 2, 4, 5, and 6 were between 0.2 nm and 0.5 nm. For layer 3, having the wrinkles, roughness was 0.8 nm.

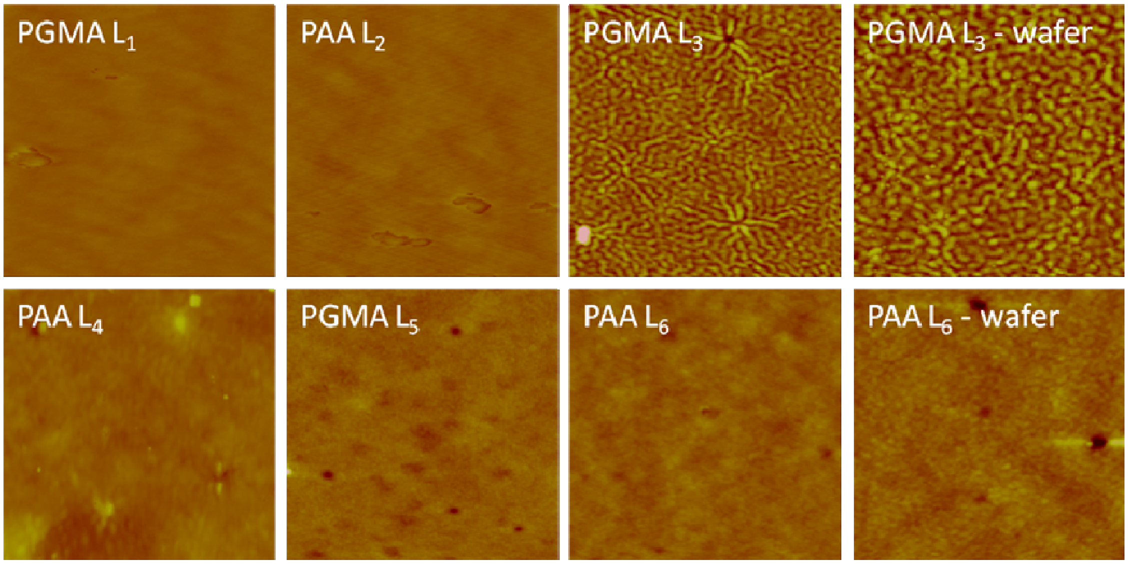

Figure 5.5. AFM images of polymer layers comprising a six-layer system. Unless stated, images are of layers on Si hexagonal crystal. Images of two layers on wafers are presented for comparison. All images have a vertical height of 10 nm and an area of 1×1 um.

5.3.2.3. Swelling with VOCs

PGMA and PAA are relatively polar and hygroscopic polymers. As such, the system was expected to show the strongest non-reactive affinity to polar analytes such as alcohols. The PAA layers are also capable of forming salts with basic VOCs such as ammonia. The average maximum swelling fraction for the layered system during exposure to analyte vapors is presented in **Figure 5.6**. The swelling was monitored by *in-situ* ellipsometry. Compared to the PGMA single-component EPL from the previous chapter (**Figure 4.3**), acetone no longer has the highest swelling fraction. Furthermore, because of the reactivity of PAA, ammonium hydroxide demonstrated a swelling fraction over 1.5 or 150%.

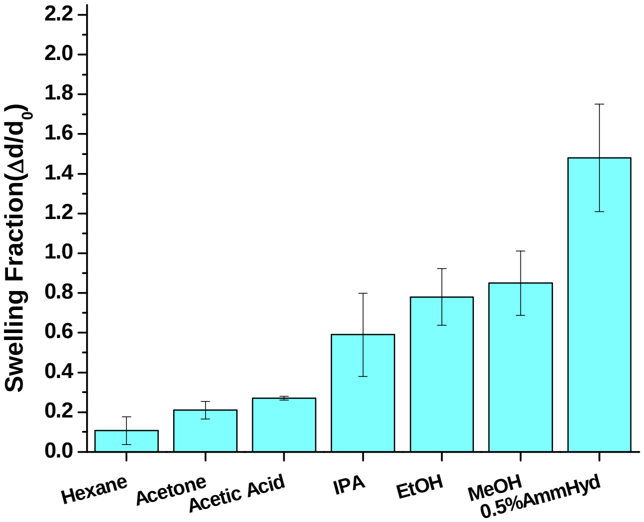

Figure 5.6. Swelling fraction of the six-layer PGMA-PAA polymer system in the presence of various analyte vapors.

The kinetics of the swelling are presented **Figure 5.7**. The average time for each analyte to reach equilibrium is approximately 20 minutes except for ammonium hydroxide which takes well over the 40 minute period. This is because of the formation of ammonium carboxylate salt in the film.[6] To completely remove the absorbed ammonium the film was rinsed with a 0.01M solution of HCl.

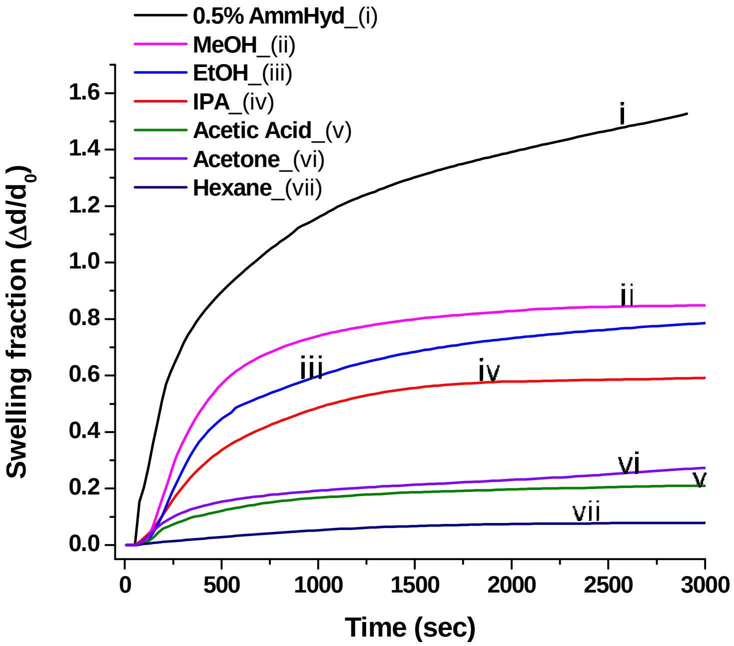

Figure 5.7. Average swelling kinetics of the six-layer PGMA-PAA system with different analyte vapors.

Using swelling fractions from the single 8 nm PAA, υ_{PAA}, and 8 nm PGMA υ_{PGMA}, the swelling of the six-layer system was calculated to determine if the swelling of the layered system can be predicted from the swelling of the single grafted layers. The swelling was predicted by the following equation:

$$\phi_{\mathrm{calc}} = \upsilon_{\mathrm{PAA}}\varphi_{\mathrm{PAA}} + \upsilon_{\mathrm{PGMA}}\varphi_{\mathrm{PGMA}}. \quad (5.1)$$

In the equation above, φ_{PAA} is the volume fraction of PAA in the six-layer EPLS, and φ_{PGMA} is the PGMA volume fraction (given in **Table 5.3**). **Table 5.4** shows the raw data and the experimental level of swelling. The predicted and experimental results are given in **Figure 5.8**. The predicted values do not produce a good correlation with experimental results. This indicates that the interaction of the layered assembly with the solvent significantly differed from the interaction with single-component films.

Table 5.4. Experimental and predicted swelling fractions of the six-layer PGMA-PAA EPLS.

Predicted swelling	Experimental	R^2
0.16	0.07	0.749
0.51	0.21	
0.67	0.85	

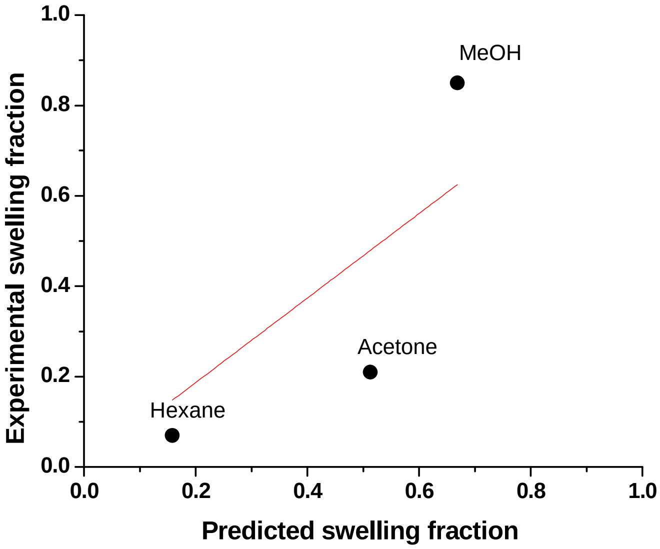

Figure 5.8. Experimental swelling fraction of the six-layer system versus predicted values. R^2 = 0.749

The partition coefficient for the enrichment system is predicted by using the experimental partition coefficients of the individual polymer layers in the following equation:

$$K_{tot} = K_1\varphi_1 + K_2\varphi_2 + \cdots K_n\varphi_n. \tag{5.2}$$

Here φ is the volume fraction of the polymer in the system. The experimental partition coefficient was calculated with **Equation 4.19**. In **Table 5.5**, the partitioning results of methanol, acetone, and hexane into the six-layer PGMA-PAA system are presented.

Table 5.5. Calculated and experimental partition coefficients for the six-layer PGMA-PAA system from single-grafted film data

	K_{Calc}	K_{Exp}	R^2
Acetone	400	233	0.981
Hexane	220	66	
Methanol	2408	3093	

In **Figure 5.9**, there is good correlation between the predicted and experimental partition coefficients.

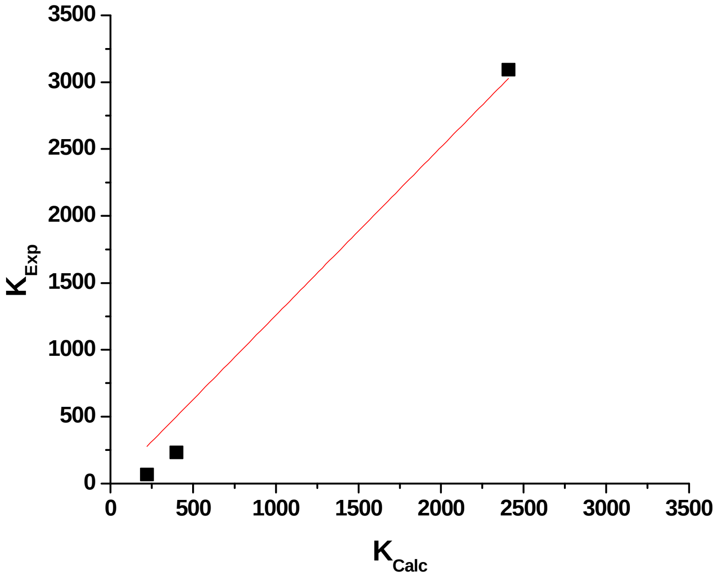

Figure 5.9. The relationship of K_{exp} and K_{calc} for the six-layer PGMA-PAA system. R^2 = 0.981

5.3.3. FT-IR ATR spectra obtained in static conditions

Exposure of the six-layer PGMA-PAA film deposited on a silicon crystal waveguide to various VOCs was performed while monitoring absorbance using an *in-situ* FT-IR ATR setup. Each VOC spectrum was obtained as described in **Chapter 3.3**.

5.3.3.1. Methanol

Presented in **Figure 5.10** is the FT-IR spectrum for methanol vapor absorbed into the 30 nm six-layer PGMA-PAA film. The spectrum of liquid methanol, placed on the uncoated silicon crystal, is also presented for comparison. Methanol as a liquid has a broad and intense band between 3100 cm^{-1} and 3600 cm^{-1} corresponding to the oxygen-hydrogen stretching (O-H). The O-H region of the methanol-EPLS spectrum starts becoming negative around 3500 cm^{-1}. This may be due to strong hydrogen-bonding interactions being disrupted in the combined PGMA and PAA background. However, there is a small positive broad O-H region between 3300 cm^{-1} and 3400 cm^{-1}.

The carbon-hydrogen (C-H) stretching of the methanol absorbed into the EPLS is significantly broader, ranging from 2650 cm^{-1} to 3117 cm^{-1} where the liquid ranged from 2750 cm^{-1} to 3060 cm^{-1}. In addition, C-H absorbance peak intensities appear more defined. Specifically, the three peaks at 2915 cm^{-1}, 2950 cm^{-1}, and 2987 cm^{-1}, while present in the liquid spectra as shoulders, appear more intense.

Changes in the carbonyl region can be observed as well. These are similar to but more pronounced than for the single-component PGMA film. As methanol is absorbed into the layer, the carbonyl region becomes negative. The unique IR signature observed can be used to identify the substance.

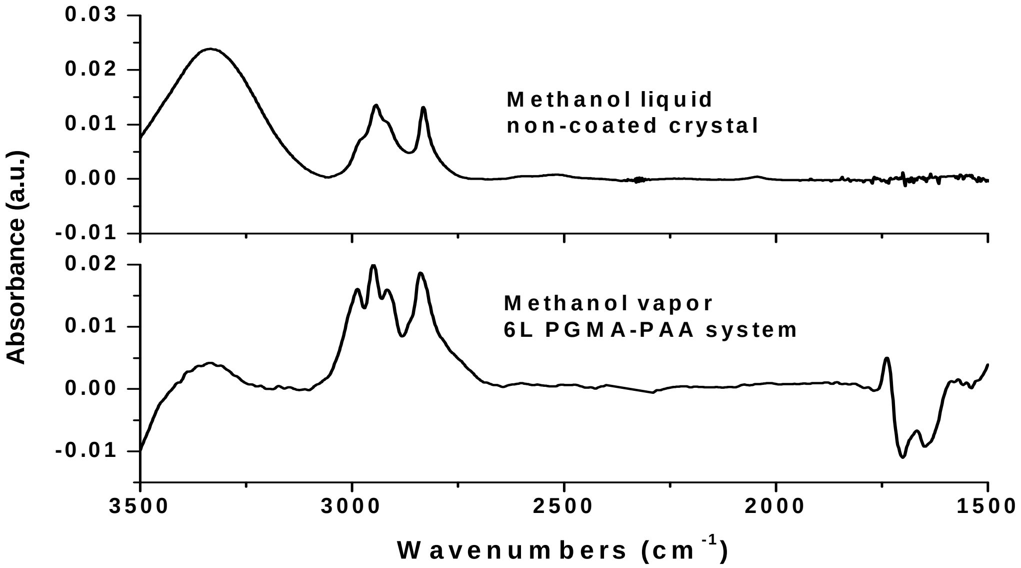

Figure 5.10. IR spectra of methanol vapor absorbed by a 30nm PGMA-PAA EPLS. The IR spectrum of liquid methanol is added for comparison.

5.3.3.2. Ethanol

The IR absorbance spectrum of ethanol absorbed in the 30 nm PGMA-PAA six-layer film and the liquid ethanol spectrum is given in **Figure 5.11**. Ethanol vapor has a similar swelling fraction to methanol vapor as well as IR absorbance regions but significantly different absorbance wavelengths. There are apparent differences in the absorbance of the carbonyl region which is negative. As compared to methanol, a more intense secondary carbonyl peak is present at 1741 cm^{-1}. A broadening of about 10 cm^{-1} is also noted for the C-H stretching region.

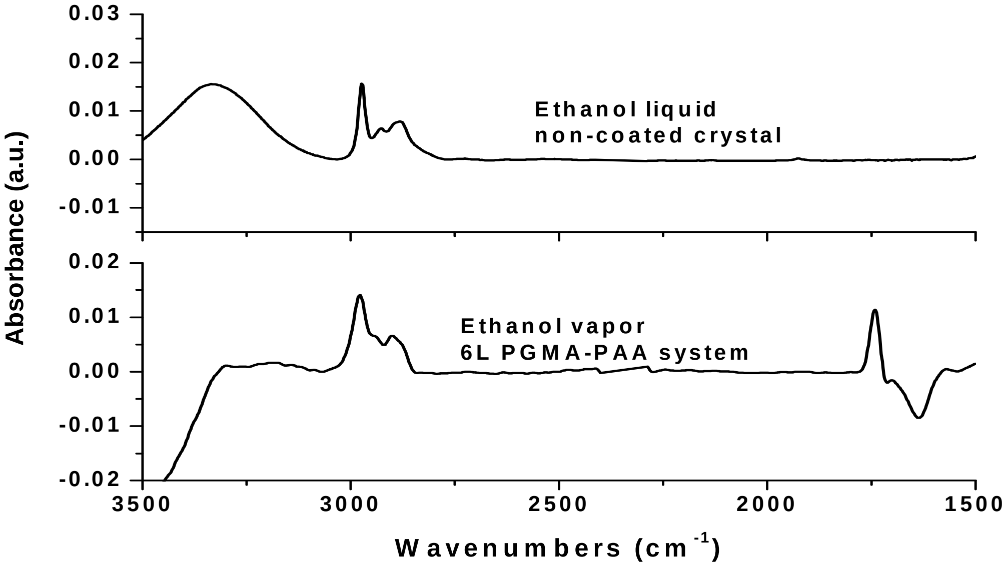

Figure 5.11. IR spectra of ethanol vapor absorbed by a 30nm PGMA-PAA EPLS. The IR spectrum of liquid ethanol is added for comparison.

5.3.3.3. Isopropyl alcohol (IPA)

The IR absorbance spectra of IPA absorbed in the 30 nm PGMA-PAA six-layer film and the liquid IPA spectrum are presented in **Figure 5.12**. The spectroscopic signature of IPA definitely appears when the silicon crystal covered with the enrichment layer is exposed to the solvent vapor. For IPA absorbed in the layer, the negative carbonyl region spans from 1570 cm^{-1} to 1727 cm^{-1}. IPA is the least polar substance among the three alcohols tested. A less intense secondary carbonyl peak at 1743 cm^{-1} is further evidence of reduced polar interactions between IPA and the enrichment layer.

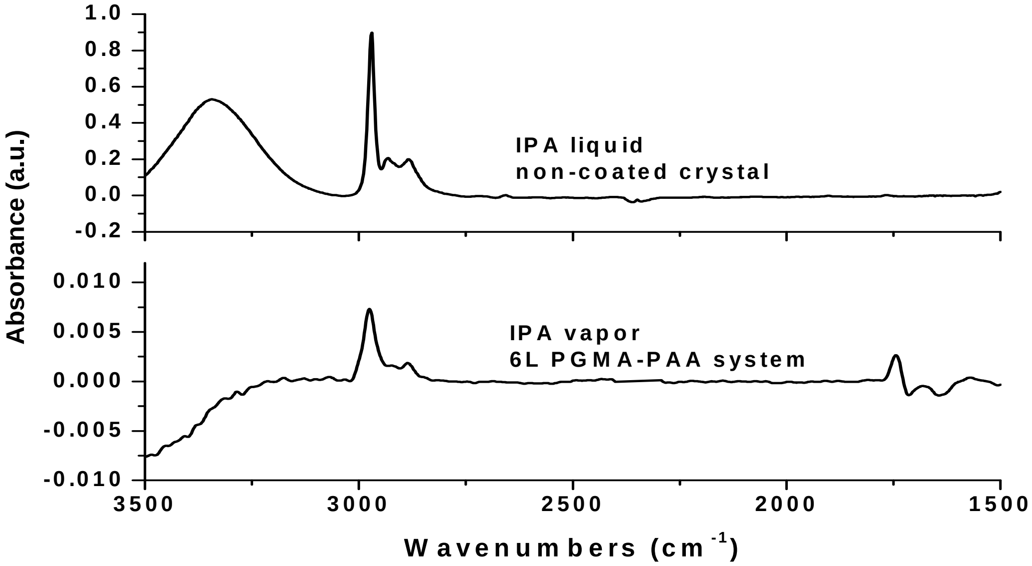

Figure 5.12. IR spectra of IPA vapor absorbed by a 30nm PGMA-PAA EPLS. The IR spectrum of liquid isopropanol is added for comparison.

5.3.3.4. Acetone

The IR absorbance spectrum for acetone vapor incorporated into the 30-nm six-layer PGMA-PAA system, along with the liquid acetone spectrum, is presented in **Figure 5.13**. A broadening of the fundamental carbonyl (C=O) peak of acetone at 1710 cm^{-1} can be observed. Similar spectral changes were found with acetone absorbed in the 130 nm PGMA film (**Figure 4.8**).

The negative region between 3100 cm^{-1} and 3800 cm^{-1} may be indicative of hydrogen bonding of the acetone with hydroxyl groups in the polymer. Similar to the one-component PGMA film, there is very little change in the C-H band observed as acetone is absorbed into the EPLS.

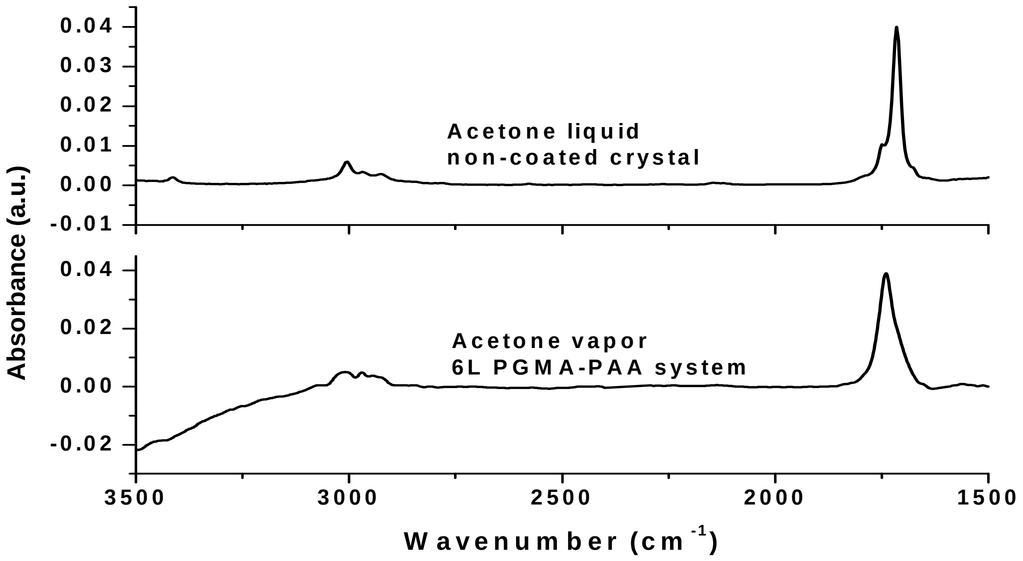

Figure 5.13. IR spectra of acetone vapor absorbed by a 30nm PGMA-PAA EPLS. The IR spectrum of liquid acetone is added for comparison.

5.3.3.5. Acetic Acid

The IR absorbance spectrum for acetic acid vapor absorbed into the six-layer PGMA-PAA system is compared with the liquid acetic acid spectrum and presented in **Figure 5.14**. The carbonyl peak splitting is less pronounced than observed for the 130 nm PGMA film (**Figure 4.9**). The O-H region appears positive and broad. Some negative absorbance is present in the 4000 to 3500 cm^{-1} and 1700 to 1650 cm^{-1} regions. This can be due to pre-sorbed water in the EPLS.

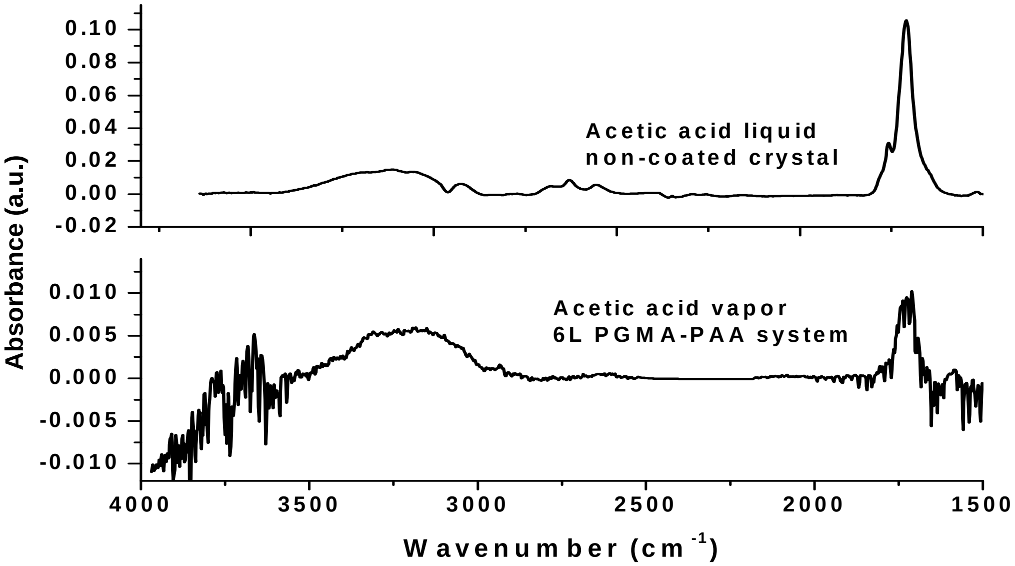

Figure 5.14. IR spectra of acetic acid vapor absorbed by a 30nm PGMA-PAA EPLS. The IR spectrum of liquid acetic acid is added for comparison

5.3.3.6. Hexane

The six-layer system was tested with hexane vapor to determine if an absorbance signature can be observed. It is necessary to note that PAA is likely to collapse due to its low affinity toward the non-polar VOC. In **Figure 5.15**, the IR absorbance spectrum of hexane vapor absorbed in the EPLS is presented. The strong C-H stretching characteristic of hexane indicates that the system can absorb non-polar VOCs well. The stretching region is less defined; peaks have started merging together. Some minor change can also be seen in the O-H region after 3500 cm^{-1}, where the absorbance seems to go negative.

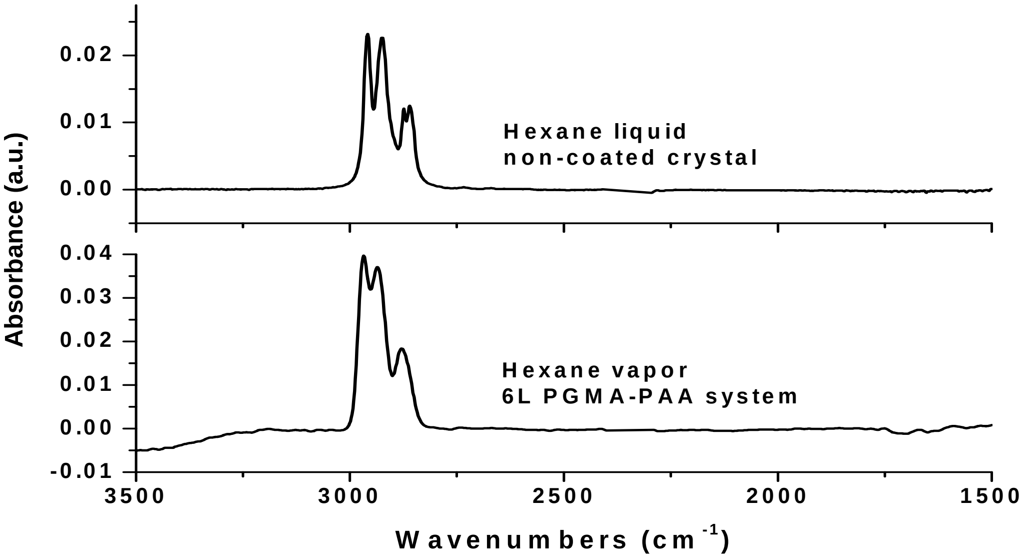

Figure 5.15. IR spectra of hexane vapor absorbed by a 30nm PGMA-PAA EPLS. The IR spectrum of liquid hexane is added for comparison

5.3.3.7. Ammonium hydroxide

The IR spectrum of the six-layer PGMA-PAA EPLS exposed to vapor of a 0.5% ammonium hydroxide solution is presented in **Figure 5.16**. The liquid spectrum is provided for comparison. Ammonia can form a carboxylate salt with PAA, which can make the EPLS extremely sensitive to the analyte. A decrease in absorbance intensity in the region between 1657 cm^{-1} and 1780 cm^{-1} corresponds to the change from the PAA acid carbonyl to the salt formation, and new peak forms at 1550 cm^{-1}. The area of the negative region is half of the secondary absorbance peak. It can be concluded that this EPLS has the highest sensitivity to basic VOCs and can be used to target ammonia that is used in, for example, the manufacturing of nuclear weapons.

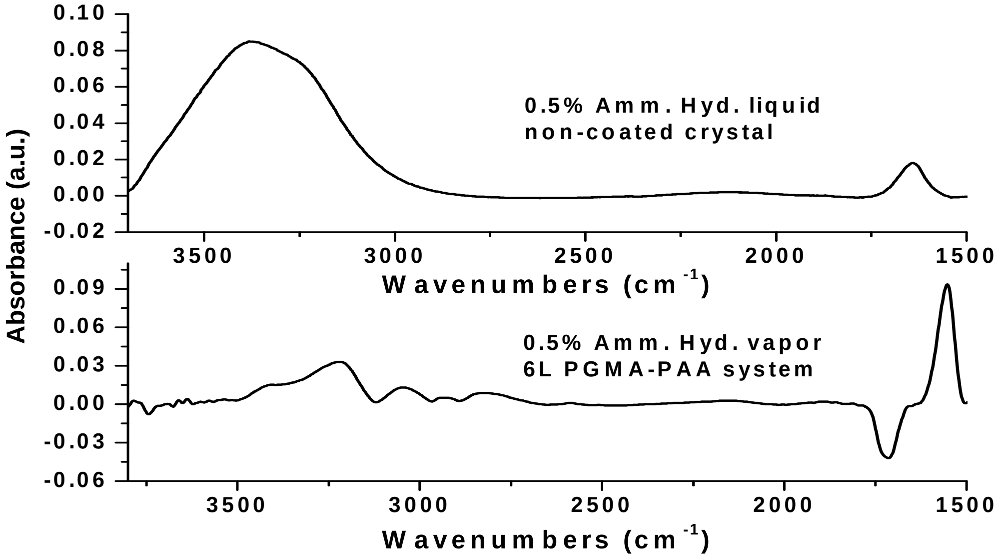

Figure 5.16. IR spectra of ammonium hydroxide absorbed by a 30nm PGMA-PAA EPLS. The IR spectrum of the liquid solution is given for comparison.

5.3.4. Efficiency of PGMA-PAA six-layer system to pick up VOCs

The EPLs are designed to attract and concentrate VOCs in the evanescent wave region to produce a substantial signal. In order to quantify the ability of the six-layer PGMA-PAA EPLS to detect VOCs, the efficiency of the system was determined, as discussed in Chapter 4.

In **Table 5.6**, the C-H and “main” peak absorbance of the VOCs used are presented with their corresponding efficiencies. As with the PGMA film, the C-H absorbance is dominated by hexane and thus gives a higher efficiency. For the “main” peaks, acetone and acetic acid have a greater absorbance per area with their main carbonyl stretch. The alcohols have a lower efficiency despite their hydroxyl region having a positive absorbance. In general, if thickness of the layers is taken into consideration, the efficiencies are on the same level as the ones found for the PGMA films (**Tables 4.9 and 4.10**).

Table 5.6. Efficiency percentages of the six-layer PGMA-PAA system, both C-H and main peak efficiencies

VOC	6L abs C-H	6L CH abs/cm^2	% Efficiency
Acetone	0.0050	0.0009	2.6
MeOH	0.0190	0.0036	4.9
Hexane	0.0389	0.0073	16.8
EtOH	0.0130	0.0024	5.8
IPA	0.0070	0.0013	3.3
Acetic acid	0.0010	0.0002	1.8
	6L Abs main peak	**6L CH abs/cm^2**	**% Efficiency**
Acetone	0.0380	0.0071	9.9
MeOH	0.0004	0.0001	0.04
EtOH	0.0001	0.00002	0.01
IPA	0.0001	0.00002	0.03
Acetic Acid	0.0120	0.0022	1.4

5.4. Conclusions

PGMA and PAA can be grafted together to form an enrichment layer system. The degree of swelling of this six-layer PGMA-PAA enrichment polymer layer system is significantly sensitive to the polarity of VOCs. More polar solvents demonstrate higher degree of swelling. Cross-linking with multiple grafting sites on the PAA backbone reduces loading capabilities; however, it does not seem to inhibit sensing and differentiation between VOCs. The results of IR analysis have a correlation with swelling analysis. There are more intense secondary IR absorbance peaks for strong hydrogen-bonding VOCs that has high swelling fractions with the EPLS. Each analyte gave a unique IR spectrum that can be used to distinguish it from similar VOCs (specifically the alcohols) and from a pure PGMA film as well.

5.5. References

1. Azuma, H.; Hanada, K.; Yoshikawa, Y.; Baba, Y.; Kagemoto, A., Heats of Disolution of Water Soluble Polymer Solutions. *Thermochimica Acta* **1988,** *123*, 271-283.

2. Hayward, R. C.; Chmelka, B. F.; Kramer, E. J., Template cross-linking effects on morphologies of swellable block copolymer and mesostructured silica thin films. *Macromolecules* **2005,** *38* (18), 7768-7783.

3. Chen, C. M.; Yang, S., Wrinkling instabilities in polymer films and their applications. *Polymer International* **2012,** *61* (7), 1041-1047.

4. Yoo, P. J.; Lee, H. H., Evolution of a stress-driven pattern in thin bilayer films: Spinodal wrinkling. *Phys. Rev. Lett.* **2003,** *91* (15).

5. Zang, J. F.; Zhao, X. H.; Cao, Y. P.; Hutchinson, J. W., Localized ridge wrinkling of stiff films on compliant substrates. *Journal of the Mechanics and Physics of Solids* **2012,** *60* (7), 1265-1279.

6. Hansen, C. M.; Abbott, S.; Yamamoto, H.; Valpey III, R. S. *HSPiP*, 2; 2009.

Chapter 6. Multi-Component EPLS: Toward a "Universal" Enrichment Layer

6.1. Introduction

Previous chapters presented the use of PGMA and a PGMA-PAA combination as an EPL and as an EPLS, respectively. This chapter addresses the idea of targeting multiple types of VOCs with one EPLS. Four polymers in one EPLS (five layers total) were used to broaden the chemical affinity of the enrichment system. The polymers used were PGMA, PAA, epoxidized 60% poly(butadiene) (EPB60), and poly(2-vinyl pyridine) (P2VP).

A five-layer EPLS was synthesized. Polymers were layered in the following order (starting from the substrate surface): PGMA, PAA, EPB60, PGMA, and P2VP. Each of these polymers has a unique chemical composition that carries specific absorption affinities. PGMA's swelling fractions were reported in Chapter 4. PAA has strong hydrogen-bonding capability, which makes the polymer efficient to target basic VOCs (e.g., ammonia), and hydrogen bonding compounds (e.g. alcohols). EPB60 was used because the backbone of the polymer is non-polar compared to PGMA, PAA, and P2VP. Finally, P2VP has the pyridine ring, which can form a salt with acidic VOCs.

6.2. Experimental

For synthesis of the EPLS, a solution of EPB60 in toluene at a concentration 0.5% w/v and a solution of P2VP in methanol at a concentration of 1% w/v were prepared. The EPB60 layer was grafted at 120 °C for 20 min. The P2VP layer was grafted for 15 hrs at 150 °C to reach the necessary grating density.

Using equations 3.1 and 3.2, the surface coverage and chain density were calculated for each layer of the EPLS. **Table 6.1** presents the results obtained. In the calculations, the density of EPB60[1] was taken to be 0.9 g/cm^3, and the density of P2VP[2] was taken to be 1.114 g/cm^3.

Table 6.1. Multi-polymer system layer characteristics

Polymer Layer	Layer Thickness (nm)	Surface Coverage [mg/m^2]	Chain Density [chains/nm^2]	Polymer Volume Fraction
PGMA	2	2.16	0.01	0.34*
PAA	8	9.76	0.06	0.34
EPB60	8	7.20	0.01	0.25
PGMA	7	7.56	0.03	0.34*
P2VP	2	2.23	0.03	0.07

*This is the total volume fraction that PGMA has in the system combining two layers.

6.3. Results and Discussion

6.3.1. Characterization of the five-layer EPLS

The multi-polymer EPLS, with a total thickness of ~27 nm, consisted of five polymer layers possessing different chemical natures, was obtained by the "grafting to" technique.[3] The nanostructured coating was firmly anchored to the surface of Si ATR crystals via the first PGMA layer.[4] The stability of each layer was confirmed by rinsing the grafted film multiple times in different solvents (see Chapter 4 for duration and number of rinses).

The increase in thickness of the system as well as the change in the carbonyl area of the IR spectra of the EPLS after each layer was added is presented in **Figure 6.1**. The total area in the carbonyl region, spanning 1640–1780 cm^{-1}, was used to gauge the influence of each additional layer on the IR signature in this absorbance region. The samples were positioned in the spectrometer in such a way that the IR spectra were obtained practically from the same spot. PGMA and PAA were expected to contribute the total carbonyl absorbance. In contrast, EPB60 and P2VP were expected to contribute no carbonyl groups. However, as can be seen from the inset in **Figure 6.1**, carbonyl absorbance did increase after addition of EPB60 to the EPLS, suggesting that deposition of the additional layer gave rise to effective extinction coefficients of the carbonyls in the polymers. This means that the broadening of the area was caused by interactions of the carbonyls in the polymer films because of grafting.

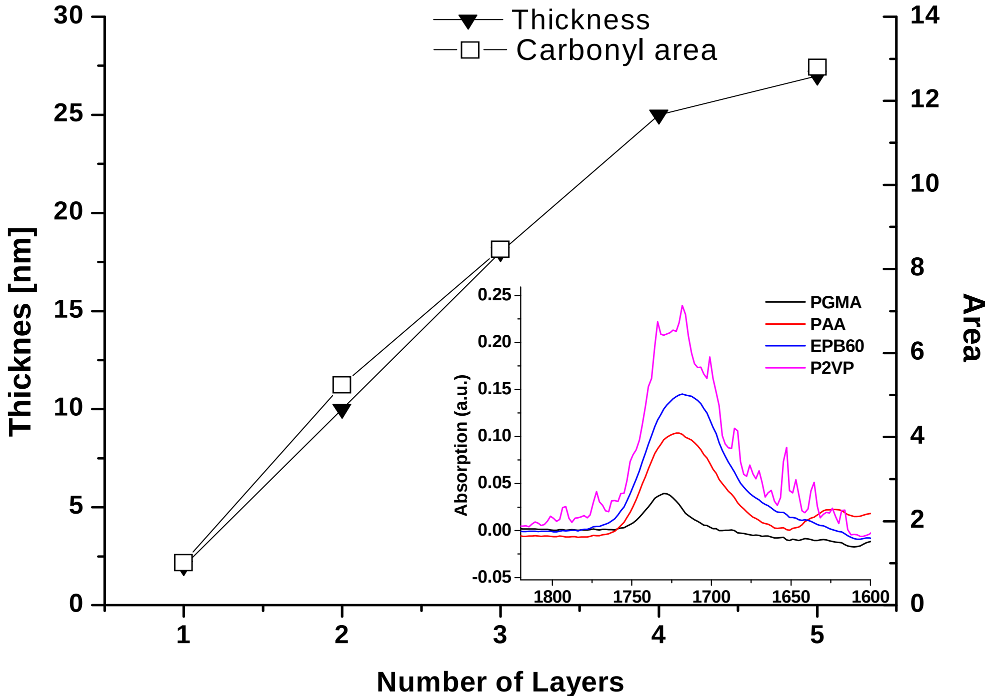

Figure 6.1. Thickness of polymer system and area of carbonyl region versus number of layers in five-layer multi–system.

The full spectrum of the five-layer multi-system when first made and after four months of testing is given in **Figure 6.2**. Spectrum of the silicon crystal, taken before the polymer film deposition, was used as the background. The main regions that show change are the O-H region above 3500 cm^{-1} and the carbonyl region. The O-H and carbonyl regions show a smoother curve and a decrease in absorbance, indicating that the system was somewhat affected during testing. After four months of testing, qualitatively, there are no new peak formations; however, there is a significant decrease of about 42% in the carbonyl area (1619 and 1807 cm^{-1}).

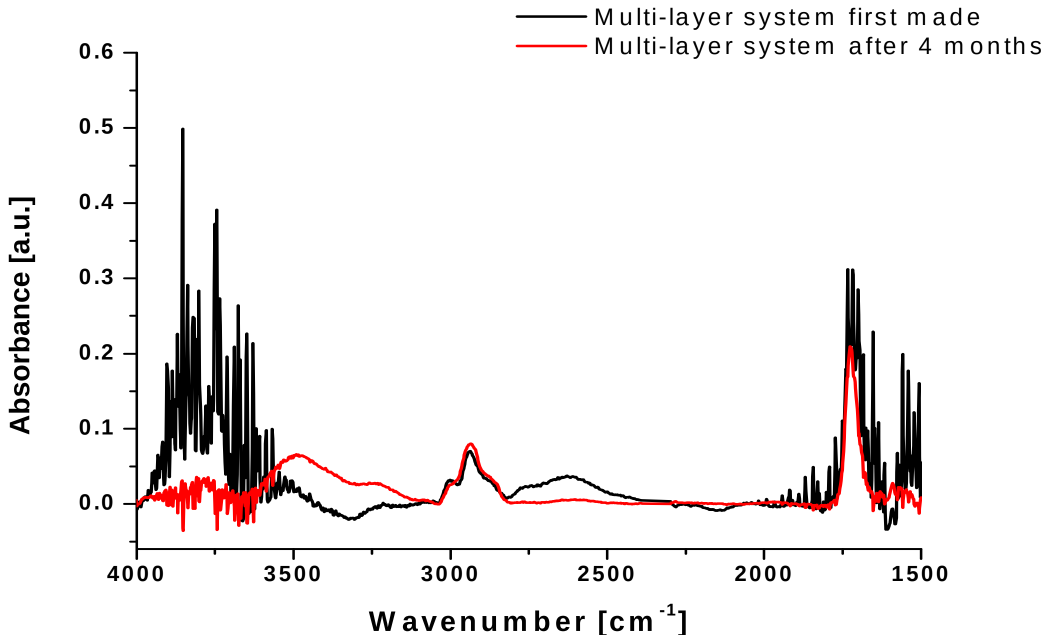

Figure 6.2. IR spectrum of five-layer multi-system when first synthesized and after four months of testing, demonstrating stability.

It was important to study the morphology of the layers because, as previously discussed, solvent evaporation and grafting forcibly arrange the polymer chains, which can cause stresses in the layers. The morphology of the polymer layers in the five-layer system grafted to a silicon wafer were observed by atomic force microscopy and are shown in **Figure 6.3**. The PGMA layer shows even surface coverage. The PAA layer has a smooth surface on top of the PGMA, as does EPB60 on the PAA layer. The fourth PGMA layer is begins to show signs of clustering due to the limited grafting sites on EPB60. Grafting, however, does anchor PGMA to the EPB60 layer. The P2VP layer has a cluster-like formation, as it is the only polymer with end functional groups, which tethers it to the underlying PGMA layer. This causes the P2VP chains to have a thermodynamic affinity to themselves rather than being spread out over the PGMA layer.

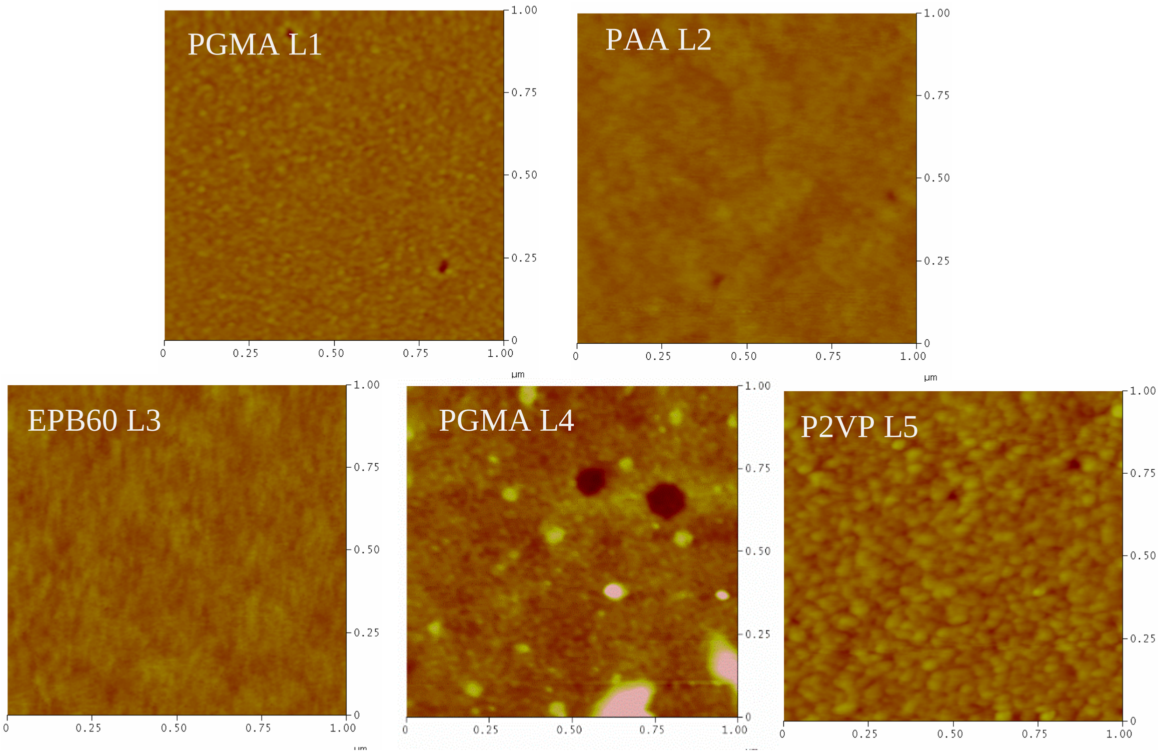

Figure 6.3. AFM images of layers composing multi-system. Images are 1 x 1 um and 10 nm vertical scale. RMS roughness for each layer is PGMA = 0.4, PAA = 0.2, EPB60 = 0.2, PGMA = 1, P2VP = 0.6.

The affinity of the multi-polymer EPLS was expected to be more complex, as each layer possessed its own chemistry. The system is rich with polar functional groups and groups that have strong hydrogen-bonding capabilities. In **Figure 6.4**, the average maximum swelling fraction for the system after exposure to VOC vapors of methanol,

ethanol, isopropanol, acetone, acetic acid, hexane, and ammonium hydroxide is provided. If this EPLS is compared to the six-layer PGMA-PAA EPLS (**Figure 5.6**), acetone and hexane still swell the least. Among the alcohols, ethanol swells the system the least. Methanol and isopropanol have very similar swelling levels and are statistically identical in a Student's T-test with a 95% confidence interval. In addition, the swelling fractions of ammonium hydroxide and acetic acid are not statistically different. All t and p values are given in the appendix for the six layer PGMA-PAA system. The EPLS demonstrates the highest average swelling level with acetic acid which is also statistically the same as ammonium hydroxide. The reason for the strong attraction to acetic acid is the basic nature of P2VP, caused by the pyridine ring. Similar to how PAA forms a salt with ammonium hydroxide, P2VP can form a salt with acetic acid.

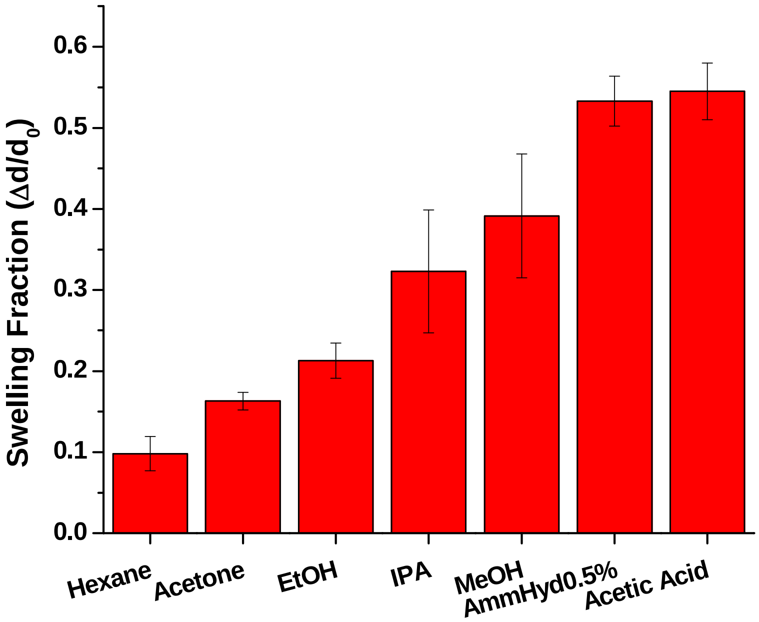

Figure 6.4. Swelling fraction of five-layer multi-polymer system in the presence of various analyte vapors.

The average absorption kinetics are presented in **Figure 6.5**. Ammonium hydroxide and acetic acid take longer time to reach equilibrium most probably due to the nature of the salt formation taking place within the EPLS.

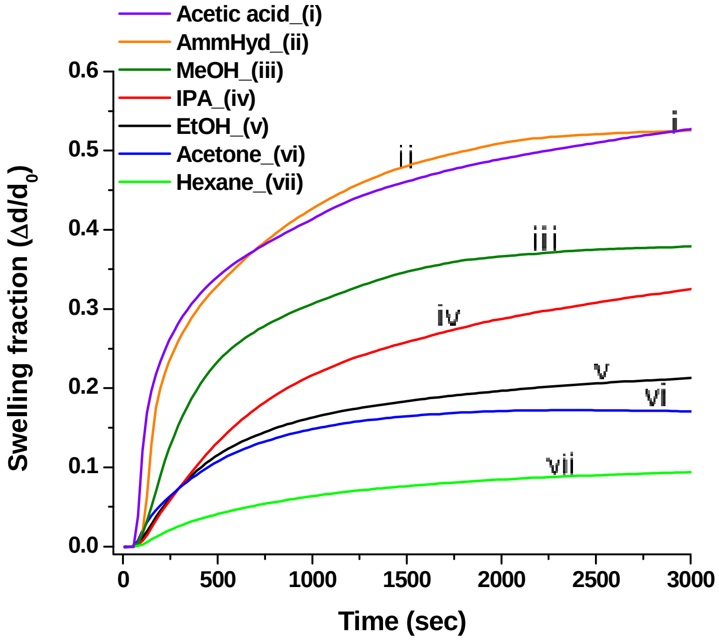

Figure 6.5. Average swelling kinetics of the five-layer multi-system with different analyte vapors.

6.3.3. FT-IR ATR spectra obtained in static conditions

Exposure of the multi-polymer EPLS film, deposited on a silicon crystal waveguide, to various VOCs was performed while monitoring IR absorbance using an FT-IR ATR setup. In addition, a non-modified crystal was exposed to the same VOCs to demonstrate that a polymer coating is necessary to pick up vapor to produce substantial IR signals. Each IR spectrum of the VOC absorbed into the enrichment film was compared to an IR spectrum of the liquid VOC analyte obtained using a non-coated silicon waveguide ATR crystal.

6.3.3.1. Methanol

The FT-IR spectrum for methanol vapor absorbed into the multi-polymer EPLS is given in **Figure 6.6**. The spectrum of liquid methanol is presented for comparison. This enrichment system has fewer hydroxyl groups than the PGMA-PAA system. Therefore, in contrast to the PGMA-PAA layer (Figure 5.10) methanol vapor produces a broad and positive O-H absorbance between 3100 cm^{-1} and 3600 cm^{-1}.

PGMA and PAA should be capable of providing a well-defined secondary absorbance peak in the carbonyl region. However, because of other unique chemistries in the EPLS, the carbonyl absorbance region is not as well defined. The EPLS has its own unique interactions with methanol, which can be used in conjunction with the PGMA-PAA EPLS to identify the VOC.

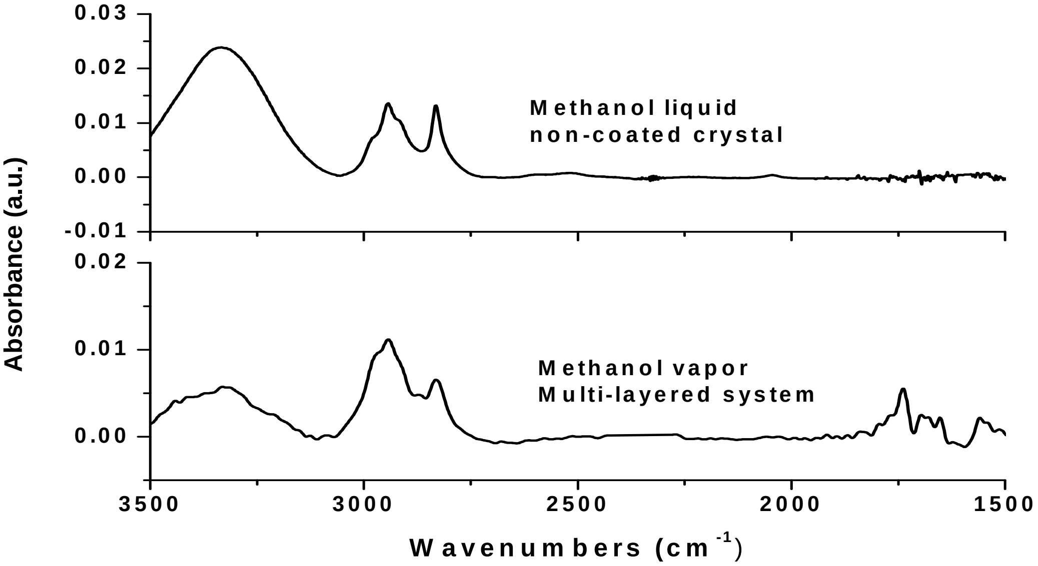

Figure 6.6. IR spectra of methanol vapor absorbed by a 27 nm multi-polymer EPLS. The IR spectrum of liquid methanol is added for comparison.

6.3.3.2. Ethanol

The FT-IR absorbance spectrum of ethanol absorbed by the multi-polymer EPLS is given in **Figure 6.7**. The liquid ethanol spectrum is also given for comparison. Ethanol has a statistically different swelling level than methanol. Specific differences in their IR absorbance spectra are similar to ones that have been observed previously for PGMA-PAA EPLS. In addition, there is a relatively low intensity secondary carbonyl absorbance peak of 1738 cm^{-1}, which suggests that ethanol does not have such intense interactions with this EPLS. It can be said that this layer system produces a signature that can be distinguished from methanol based on the 1500-2000 cm^{-1} region.

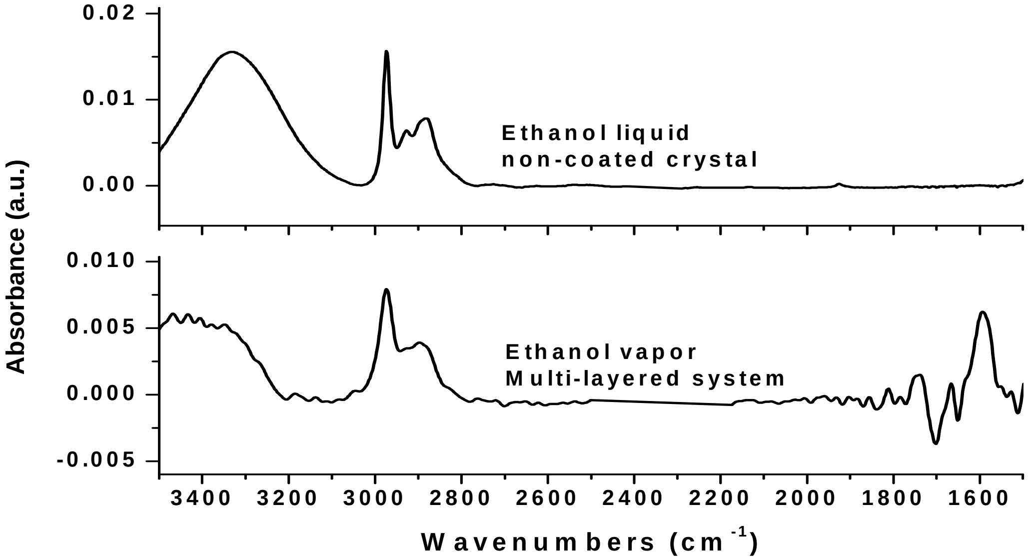

Figure 6.7. IR spectra of ethanol vapor absorbed by a 27 nm multi-polymer EPLS. The IR spectrum of liquid ethanol is added for comparison.

6.3.3.3. Isopropyl alcohol (IPA)

The FT-IR absorbance spectrum of isopropanol absorbed in the multi-polymer EPLS is presented in **Figure 6.8** with the liquid IPA spectrum for comparison. IPA demonstrates a swelling fraction with the EPLS on par to that of methanol. Liquid isopropanol has C-H absorbance peaks of 2979 cm^{-1} and 2890 cm^{-1}. There is a more pronounced secondary peak present for IPA absorbed into the EPLS.

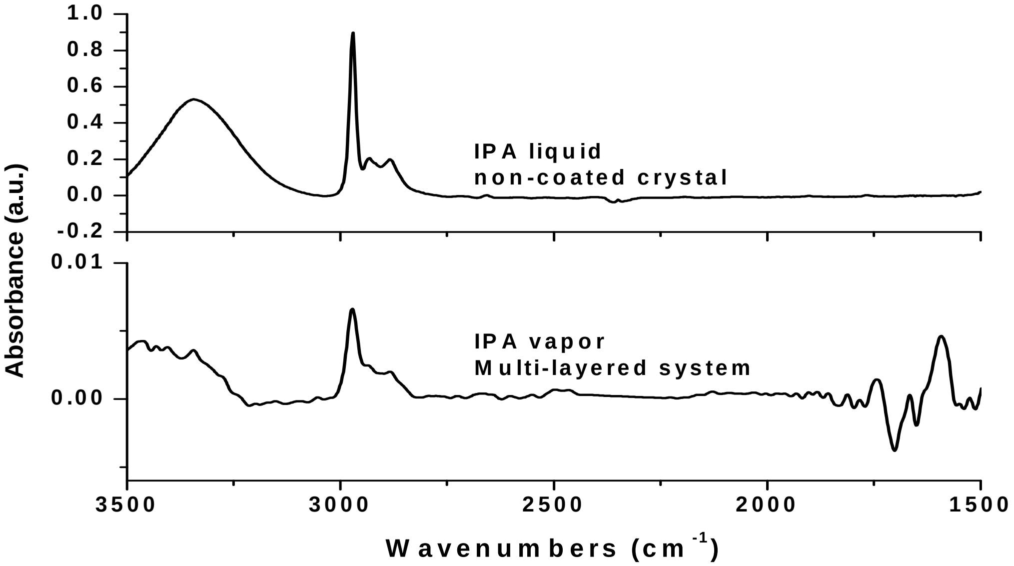

Figure 6.8. IR spectra of IPA vapor absorbed by a 27 nm multi-polymer EPLS. The IR spectrum of liquid IPA is added for comparison.

6.3.3.4. Acetone

The FT-IR spectrum of acetone vapor absorbed into the multi-polymer EPLS is compared to the liquid acetone spectrum in **Figure 6.9**. Acetone does not have a high swelling fraction with the system. The IR spectrum of acetone vapor absorbed into the multi-polymer EPLS shows a broadening of the acetone carbonyl (C = O) peak at 1710 cm^{-1}. This peak combines with the secondary peak at 1737 cm^{-1}.

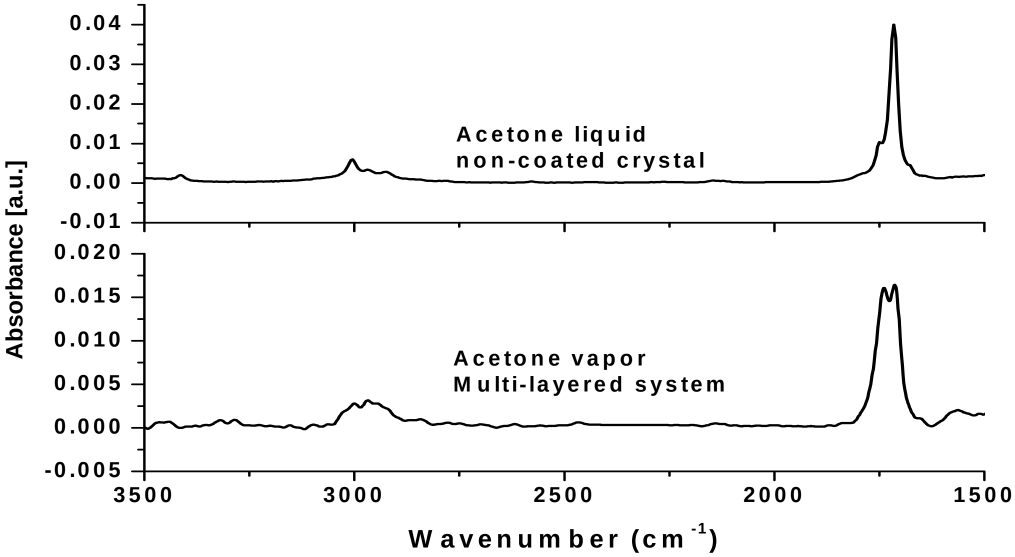

Figure 6.9. IR spectra of acetone vapor absorbed by a 27 nm multi-polymer EPLS. The IR spectrum of liquid acetone is added for comparison.

6.3.3.5. Acetic acid

The FT-IR spectrum for acetic acid vapor absorbed into the multi-polymer EPLS is compared to the liquid acetic acid spectrum in **Figure 6.10**. The carbonyl region does not split as it did with PGMA film. Instead there is a shoulder at 1761 cm^{-1}. This band can be associated with "free" acetic acid molecules that are not readily engaged in hydrogen bonding.[5] The carbonyl peak is also more defined compared to the PGMA-PAA EPLS. While acetic acid is capable of forming a complex with the P2VP top layer, no evidence can be found in the spectra. No change in the C-H region can be determined. The O-H region appears positive and broad from the incorporated acid hydroxyl group. The absorbance intensity of acetic acid is greater than that of acetone, showing that its high swelling fraction can be linked to its IR absorbance intensity. Thus, this five-layer polymer system appears to be very sensitive to acidic VOCs despite having a thin P2VP targeting layer.

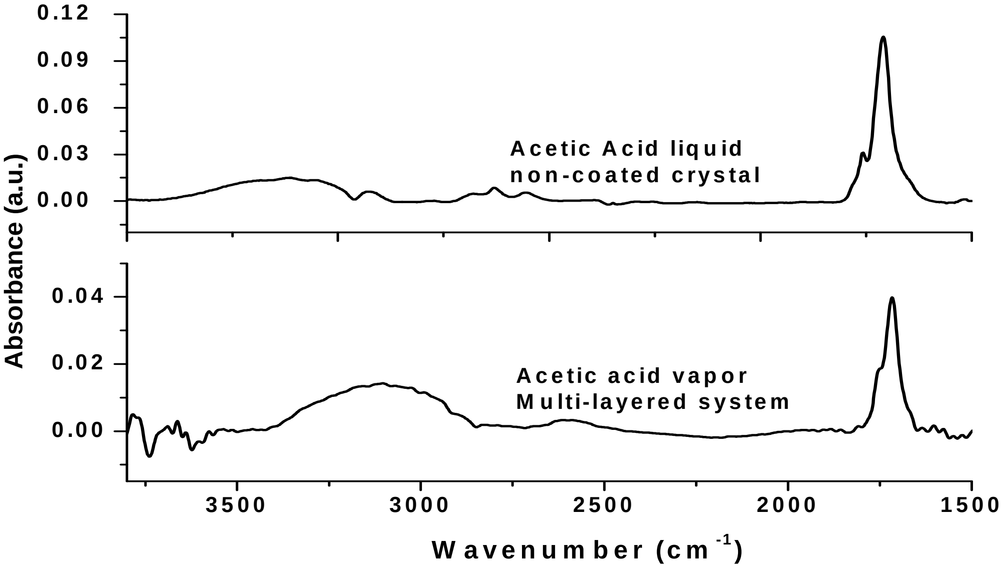

Figure 6.10. IR spectra of acetic acid vapor absorbed by a 27 nm multi-polymer EPLS. The IR spectrum of liquid acetic acid is added for comparison.

6.3.3.6. Hexane

The IR absorbance spectrum of hexane vapor absorbed to the multi-polymer EPLS is compared with the liquid spectra in **Figure 6.11**. The strong C-H stretching characteristic of hexane shows up in the IR spectrum. The 1500 to 1700 cm^{-1} region is rather noisy but changes from the baseline indicate interactions taking place with the carbonyls in the EPLS as hexane is absorbed. Non-polar VOCs can be absorbed and detected by this and other enrichment polymer layers studied in this work.

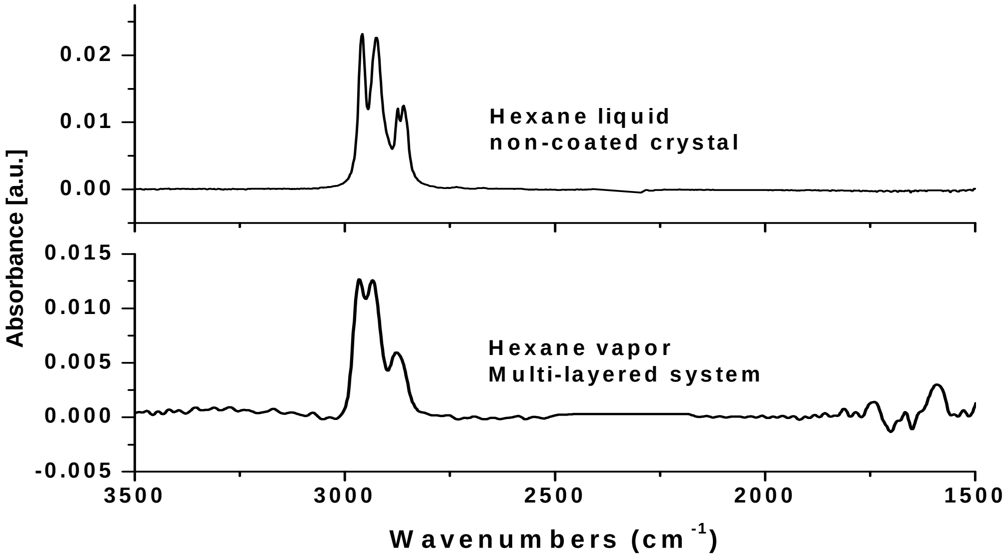

Figure 6.11. IR spectra of hexane vapor absorbed by a 27 nm multi-polymer EPLS. The IR spectrum of liquid hexane is added for comparison.

6.3.3.7. Ammonium hydroxide

The IR absorbance spectrum for vapor of a 0.5% ammonium hydroxide solution absorbed into the multi-polymer EPLS is presented in **Figure 6.12**. The corresponding liquid spectrum is provided for comparison. The PGMA-PAA six-layer EPLS has been shown to be a strong targeting system for basic analytes, such as ammonia. The multi-polymer EPLS has a layer of PAA, which can target basic analytes. A decrease in absorbance intensity around 1740 cm^{-1} corresponds to the change from acid carbonyl in the background forming a salt with the ammonia. While other polymers provide specific targeting sensitivity, the multi-polymer EPLS allows enrichment of many types of VOCs: acidic, basic, polar, and non-polar. In addition, it can be used in parallel with another EPLS if needed for differentiating analysis.

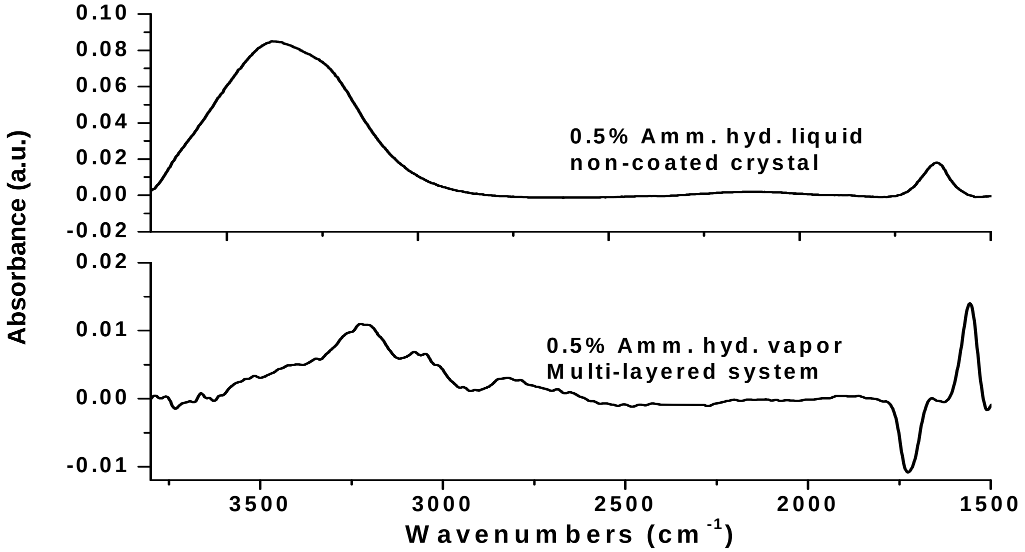

Figure 6.12. IR spectra of ammonium hydroxide vapor absorbed by a 27 nm multi-polymer EPLS. The IR spectrum of liquid ammonia solution is added for comparison.

6.3.4. Efficiency of the multi-polymer EPLS

The efficiency of the EPLS was calculated to quantify their ability detect a VOC by IR absorbance. The C-H stretching and “main” peak absorbance of VOCs in the multi-polymer EPLS, along with their efficiencies (as defined in Chapter 4 page109) are listed in **Table 6.2**. As previously seen in the PGMA film and the PGMA-PAA EPLS, hexane has substantial efficiency when calculated using its C-H stretching. Methanol and isopropanol have similar efficiencies, but ethanol has greater efficiency for the multi-polymer EPLS. Acetic acid has the highest efficiency when calculated using its C-H stretching. Main peak efficiencies for the alcohols show a different trend. Efficiencies of the alcohols go up with increasing hydrocarbon length. Using the carbonyl absorbance, acetone and acetic acid have comparable efficiencies. Despite differences in swelling levels, each of these VOCs has a substantial affinity with the multi-polymer EPLS.

Table 6.2. Efficiency percentages of the five-layer multi-polymer EPLS, both C-H and main peak efficiencies.

VOC	5L - CH Abs	5L Abs/cm2	Efficiency %
Acetone	0.004	0.001	1.84
MeOH	0.011	0.002	2.91
Hexane	0.014	0.003	5.84
EtOH	0.010	0.002	4.24
IPA	0.005	0.001	2.24
Acetic	0.005	0.001	8.95
	5L - Main Peak Abs	**5L Abs/cm2**	**Efficiency %**
Acetone, carbonyl	0.018	0.003	4.67
Acetic acid, carbonyl	0.042	0.008	5.00
Methanol, hydroxyl	0.006	0.001	0.58
Ethanol, hydroxyl	0.006	0.001	0.79
IPA, hydroxyl	0.004	0.001	1.16

6.3.5. FT-IR ATR spectra obtained in dynamic conditions

6.3.5.1. Signal dependence on concentration of VOCs

The sensitivity of the multi-polymer EPLS to low concentrations of acetone is assessed under dynamic conditions using a flow rate of 100 mL/min. The absorbance of the 1710 cm^{-1} peak with different concentrations of acetone delivered at flow rates of 100, 70, 50, and 20 mL/min with the total flow remaining at 100 mL/min is presented in **Figure 6.13**. Flow rates lower than 20 mL/min. demonstrated high deviations and are not shown. The intensity of the acetone carbonyl peak obtained in this experiment is in good agreement with static measurement. When acetone flow is stopped completely, the signal eventually comes back to the baseline with nitrogen purge for flows lower than 70mL/min.

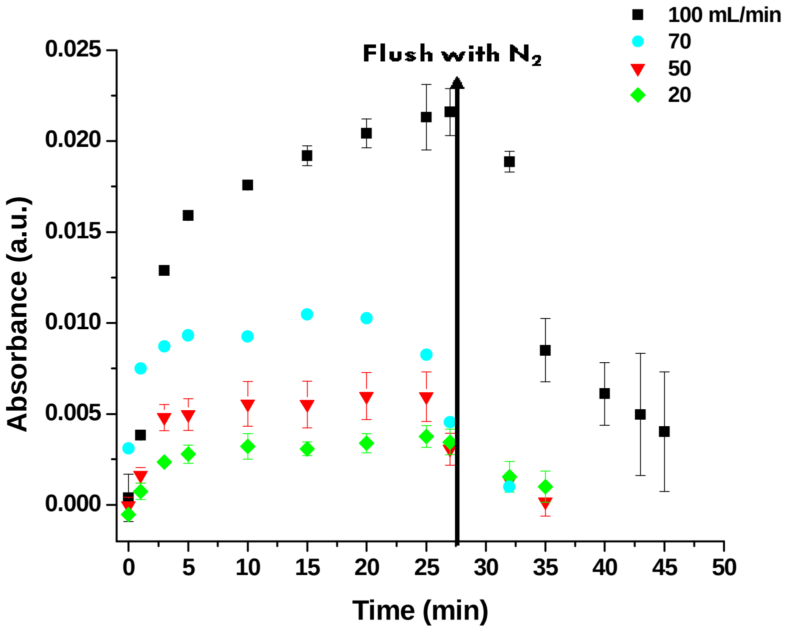

Figure 6.13. Five-layer system loaded with different concentrations of acetone delivered in dynamic conditions. Absorbance is of the 1710 cm^{-1} wavenumber.

6.4. Conclusions

The EPLS synthesized and studied in this chapter contained polymer layers that added unique functionality and targeting ability. The swelling level of the multi-polymer EPLS was, on average, lower for the tested VOCs than for the previous six-layer PGMA-PAA EPLS. However, the EPLS was able to incorporate each analyte. Therefore, the system can act as a “universal” enrichment system.

IR analysis demonstrated that each analyte gave a unique IR spectrum that could be used to distinguish substances. Additionally, the spectra observed with this EPLS were significantly different from a pure PGMA film and from the PGMA-PAA EPLS. Furthermore, analyte VOCs that have higher swelling with the multi-polymer system (e.g., acetic acid) had stronger IR absorbance than they had with the PGMA-PAA EPLS. Analytes that have affinity with both, such as ammonium hydroxide, gave IR signatures that were differentiable by intensity. However, those signatures were slightly weaker due to the broader scope of chemical attraction with the multi-polymer system.

6.5. References

1. Zdyrko, B.; Iyer, K. S.; Luzinov, I., Macromolecular anchoring layers for polymer grafting: comparative study. *Polymer* **2006,** *47* (1), 272-279.

2. Brandrup, J.; Immerqut, E. H.; Grulke, E. A., *Polymer Handbook*. John Wiley & Sons Incorporated: New York, 1998.

3. Hoy, O.; Zdyrko, B.; Minko, S.; Luzinov, I., Protein adsorption on hydrophobic regions imbedded in a hydrophilic grafted polymer layer. *Abstracts of Papers of the American Chemical Society* **2006,** *231*.

4. Iyer, K. S.; Luzinov, I., Effect of macromolecular anchoring layer thickness and molecular weight on polymer grafting. *Macromolecules* **2004,** *37* (25), 9538-9545.

5. Silverstein, R. M.; Webster, F. X.; Kiemle, D. J., *Spectrometric Identification of Organic Compounds*. Seventh ed.; John Wiley & Sons, Inc.: New York, 2005.

Chapter 7. Detection of Mixtures with EPLS

7.1. Introduction

The swelling fractions of the EPLS demonstrate that they will have a high or low affinity with VOCs. A preliminary study of the sensitivity of the EPLS towards mixtures of VOC vapors was conducted. The purpose was to identify changes between the IR absorbance of specific peaks with concentration of analytes. Mixtures that were chosen for this were acetone and methanol, acetone and hexane, and methanol and ethanol.

7.2. Experimental

Conditions for ATR FT-IR static measurements, and the processing of the spectra is the same as described in Chapter 3. Liquid mixtures of analytes were made at mole ratios which were used for FT-IR absorption experiments. To estimate the ratio of components in the gas phase, Raoult's law was used.[1] Estimated mole fractions of the methanol vapor in the acetone-methanol mixtures were: 0.08, 0.12, 0.25, 0.5, 0.69, and 0.76. Mole fractions of the hexane vapor in the acetone-hexane mixtures were: 0.1, 0.28, 0.41, 0.72, and 0.79. For dynamic experiments, ratios were of flow rates. Likewise, the procedure for ATR FT-IR static and dynamic measurements is given in Chapter 3. Liquid mixtures were not used for dynamic experiments. Flow rates of individual VOCs used in dynamic experiments were conducted at 25mL/min each, producing a total flow of 50mL/min. For all dynamic experiments, a nitrogen purge was used as stated in Chapter 3.

7.3. Results and Discussion

7.3.1. ATR FT-IR static absorption:

7.3.1.1. PGMA single component film

7.3.1.1.1. Acetone-Methanol

A 130nm PGMA film was exposed to the vapors of mixtures of acetone and methanol. The IR absorbance spectra of the corresponding absorption are presented in **Figure 7.1**. Acetone swells the 90 nm PGMA film to a high extent. It was anticipated that the two component mixture would have an additive effect on the absorbance spectrum. The absorbance region presented in **Figure 7.1** is the 1800 to 1700 cm^{-1}. The changes of the carbonyl absorbance associated with acetone, 1710 cm^{-1}, and the carbonyl associated with the PGMA film, 1738 cm^{-1} are important to mention. This is because all IR absorbances in this region associated with methanol are directly connected to interactions with the polymer film. The shape of the secondary carbonyl absorbance peaks for methanol have a much different intensity and shape than that formed with acetone. In addition, the absorbance of the acetone carbonyl peak decreases in intensity with the increase of methanol.

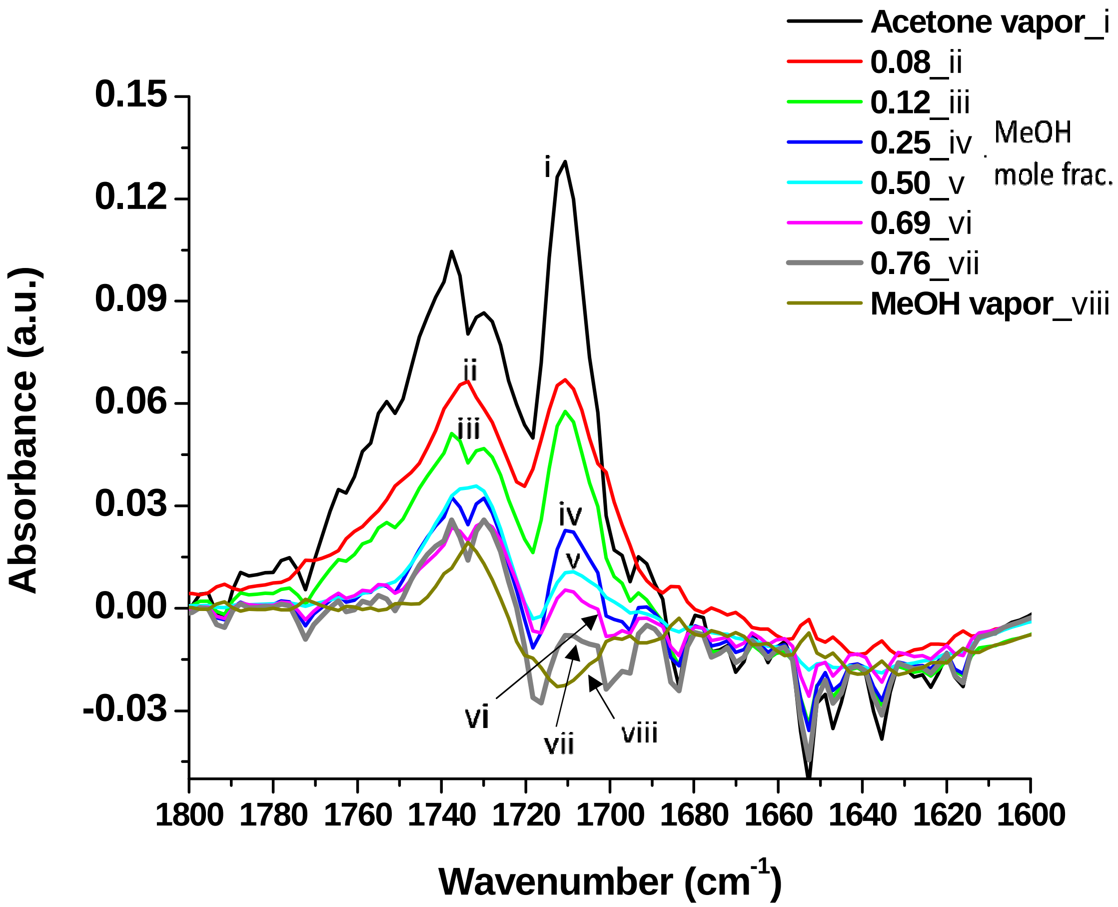

Figure 7.1. The IR absorbance of acetone/methanol mixtures along with pure acetone and methanol absorbed into a 130nm PGMA.

The absorbance trend of the 1710 cm^{-1} peak and the 1738 cm^{-1} peak for the acetone-methanol mixtures is presented in **Figure 7.2**. The trend shows that there is a sharp drop in the 1710 cm^{-1} carbonyl absorbance with very little methanol added. A mixture with 0.08 mole fraction of methanol in the vapor phase changes the acetone carbonyl absorbance from 0.13 for concentrated acetone to 0.06. A 0.25 mole fraction of methanol brings the absorbance down to 0.02. Above a 0.25 mole fraction of methanol, the slope of both absorbance peaks continue to decrease but with a different dependence.

There is not a linear relationship over the entire methanol concentration range. This can be interpreted as a non-ideal behavior of the acetone-methanol vapor and their absorption into the PGMA film. Regardless, it is clear that the layer is sensitive to varying concentrations of VOCs. For further study, there appears to be high sensitivity to small amounts of VOCs for which the polymer has lower affinity.

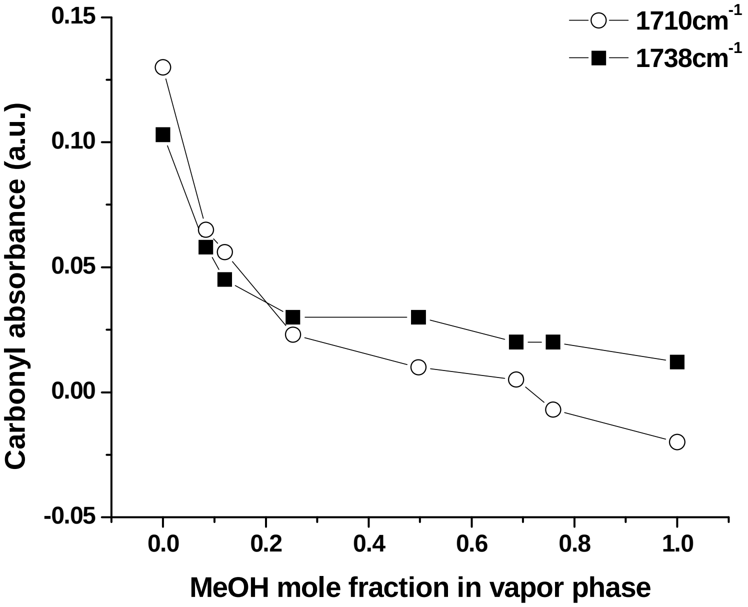

Figure 7.2. Change of absorbance in 1710 cm^{-1} and 1738 cm^{-1} spectral regions as a function of methanol mole fraction in the vapor phase for acetone-methanol mixtures. Lines are guides for eyes only.

The O-H absorbance region of the spectra is heavily influenced by the ambient humidity, which resulted in non-conclusive trends. The absorbance of the C-H groups is presented in **Figure 7.3**. As more methanol is added, the C-H stretching region between 3100 to 2700 cm^{-1} changes in concurrence. What is unexpected is that there are three mixtures where the C-H stretching favors an absorbance closer to that of the acetone vapor. These mixtures contain 0.76, 0.5, and 0.25 mole fraction of methanol.

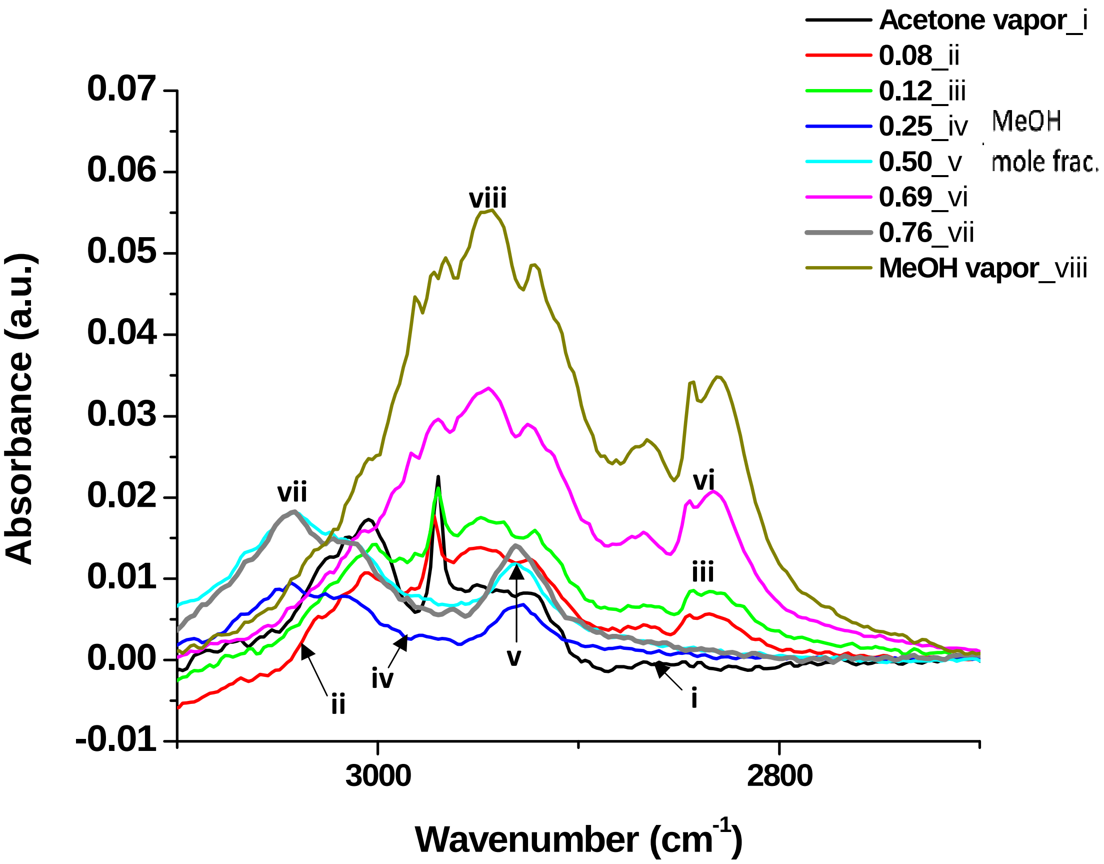

Figure 7.3. The IR absorbance of acetone/methanol mixtures absorbed into a 130nm PGMA.

7.3.1.1.2. Acetone-Hexane

A 130nm PGMA film was exposed to the vapors of acetone-hexane mixtures. The IR absorbance spectra of the corresponding absorption are presented in **Figure 7.4**. The 1800 to 1600 cm^{-1}region is used to monitor changes of the carbonyl absorbance. The peaks decrease in intensity with increasing the concentration of hexane. There is very little absorbance peak for pure hexane vapor in this region but it is clearly non-zero.

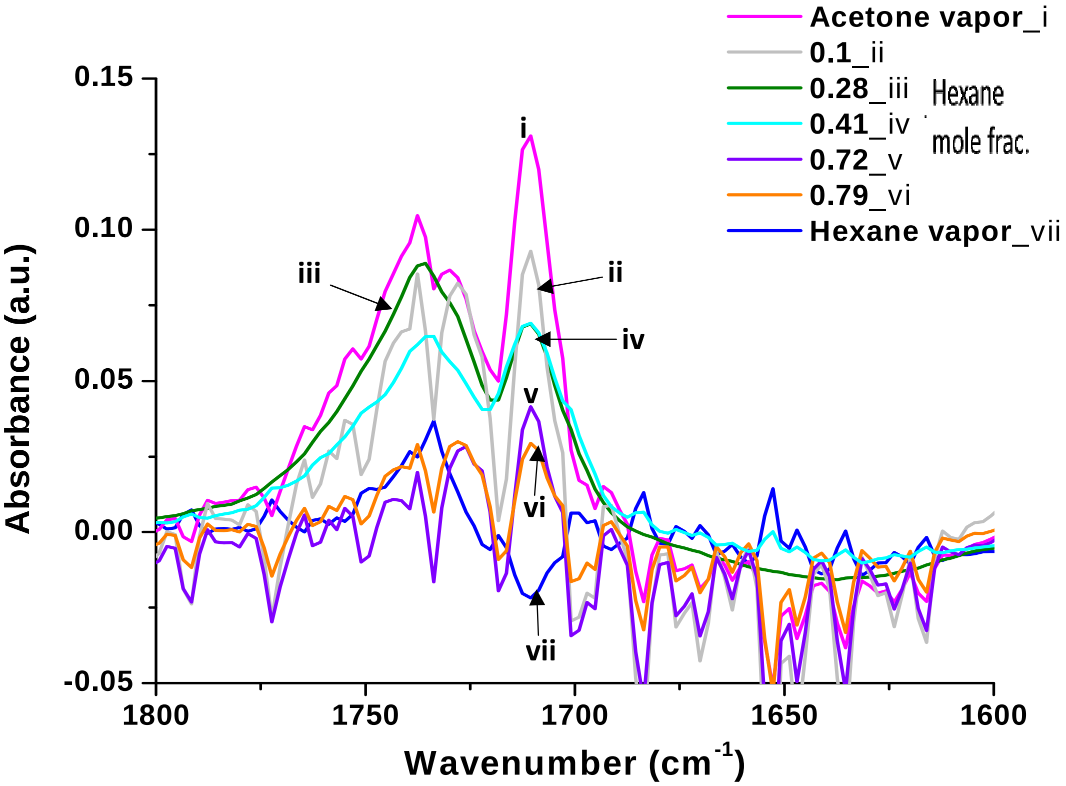

Figure 7.4. The IR absorbance of acetone/hexane mixtures absorbed into a 130nm PGMA.

The trend for the 1710 cm^{-1} carbonyl absorbance is presented in **Figure 7.5**. It is linear over the hexane concentration range (R-squared is 0.91). The secondary carbonyl absorbance, 1738 cm^{-1}, has more deviation from linearity (R-squared is 0.73).

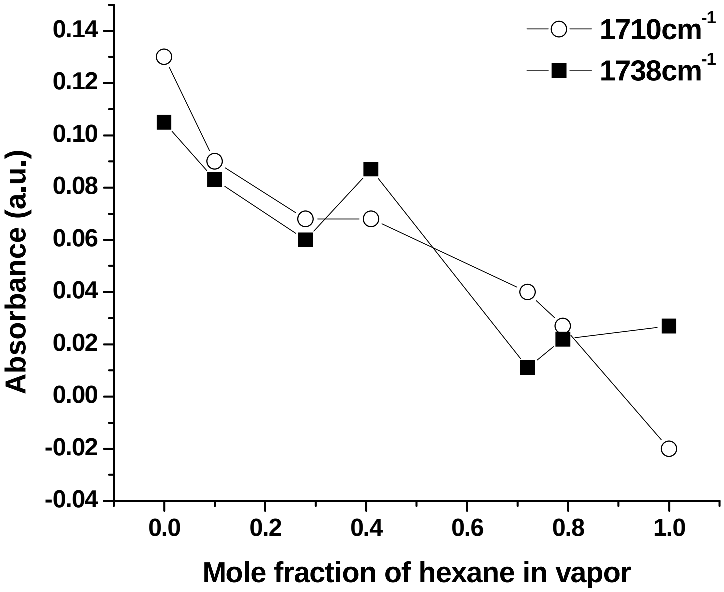

Figure 7.5. Change of absorbance 1710 cm^{-1} and 1738 cm^{-1} spectral regions as a function of hexane mole fraction in the vapor phase for acetone-hexane mixtures. Lines are a guide for eyes only.

In addition to the carbonyl region, the C-H stretching region between 3100 cm^{-1} and 2800 cm^{-1} can also be used to analyze changes of IR absorbance. The absorbance of the C-H groups is presented in **Figure 7.6**. It is necessary to note that there is a shifting of fundamental absorbance bands for hexane vapor absorbed into the polymer film. In addition, hexane absorbance in this region obscures any contributions from acetone's methyl groups.

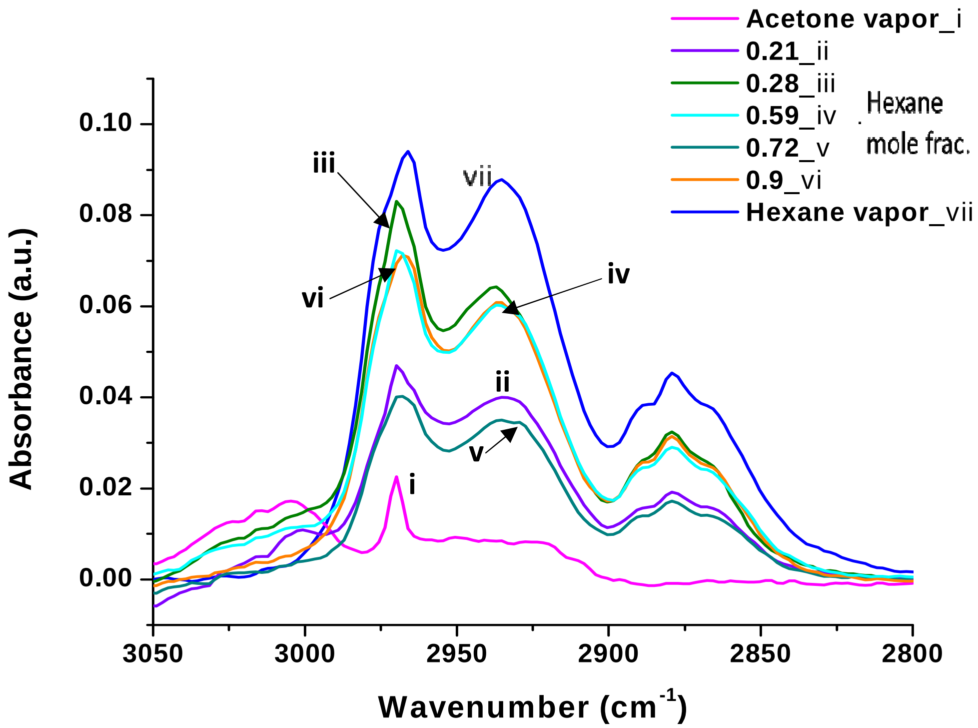

Figure 7.6. The IR absorbance of acetone/hexane mixtures absorbed into a 130nm PGMA.

7.3.2. ATR FT-IR Dynamic absorption: Simultaneous delivery

7.3.2.1. PGMA single component film

7.3.2.1.1. Acetone-Methanol

In the spectra, 1710 cm^{-1} represents the acetone carbonyl peak while 2831 cm^{-1} represents the methanol C-H peak. 1722 cm^{-1} is a carbonyl secondary peak that originates from interactions with the PGMA film. The IR absorbance spectrum of the individual VOCs and the mixture are presented in **Figure 7.7a**. In **Figure 7.7b**, the carbonyl region is expanded. There are significant differences of absorbance of each single analyte and the 1-to-1 mixture. A reference absorbance spectrum (with no analyte present) is provided. Observation shows that the mixture causes a greater absorbance in the PGMA film at the 1710 cm^{-1} peak and with the secondary absorbance peak. When the mixture is removed from the polymer film, nitrogen passes over the film for a period of approximately 10 minutes. The absorbance does not come completely back to the baseline.

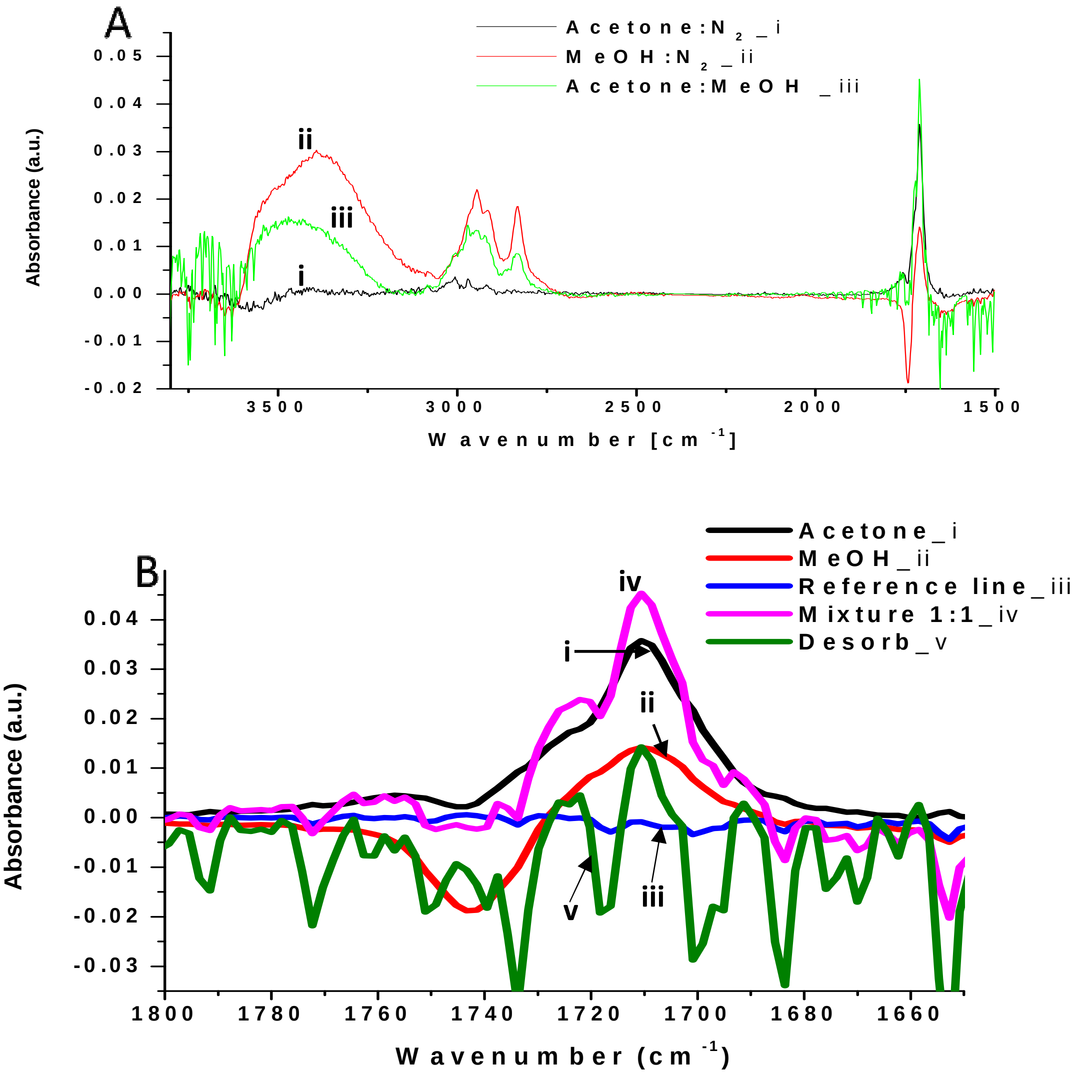

Figure 7.7. 130nm PGMA film exposed to a mixture of acetone and methanol delivered in dynamic conditions. a) Full spectra of individual components and mixture; b) The absorbance of the carbonyl region.

7.3.2.1.2. Methanol-Ethanol

Methanol and ethanol were chosen as a mixture for analysis because they have strong hydrogen bonding characteristics and are similar in chemical nature. The flow rates used remain as with the previous experiment. Each analyte was introduced separately to obtain a clean spectrum for comparison. The IR absorbance spectra of the individual VOCs loaded into the PGMA film with their mixture spectrum are provided in **Figure 7.8a**. These two VOCs are difficult to deconvolute to obtain quantitative results, because there are overlapping peaks. As can be seen, the spectrum of methanol has a distinctive peak at 2831cm^{-1}. However, in the ethanol spectrum, 2971cm^{-1} overlaps with the methanol spectrum. Performing a subtraction of the methanol spectrum from the mixture spectrum does yield a spectrum that is qualitatively close to that of the individual ethanol spectrum (also in **Figure 7.8a**). The intensity is also close to the individual ethanol. The secondary absorbance in the carbonyl region is provided in **Figure 7.8b**. The subtraction of the secondary interaction peak for methanol and the mixture is produces a peak with a lower intensity than the individual ethanol spectrum. This shows that the combination absorbance of these analytes is complex. After the removal of the mixture is conducted, the IR absorbance does not return completely to the baseline.

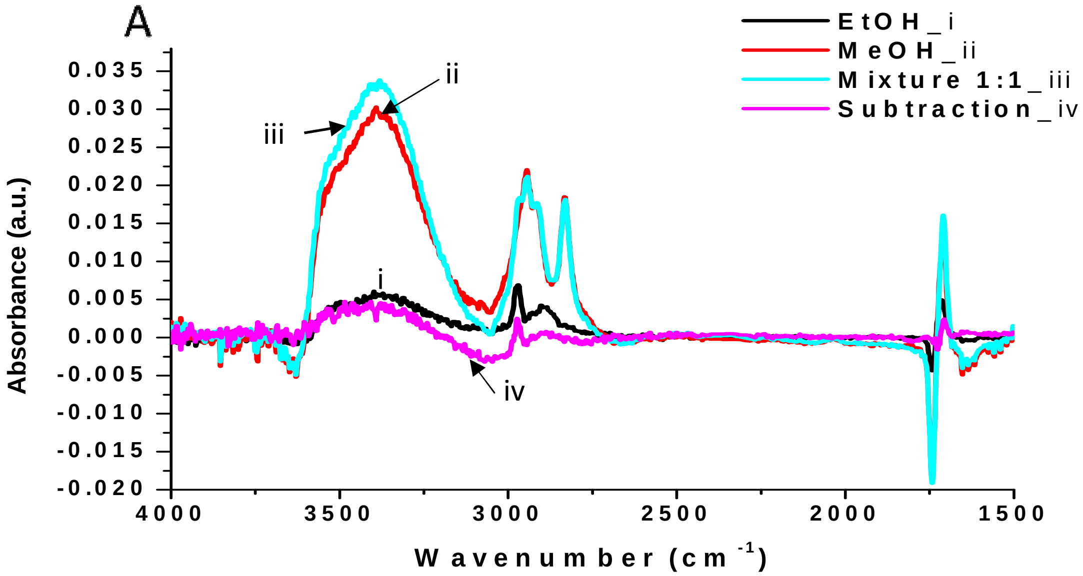

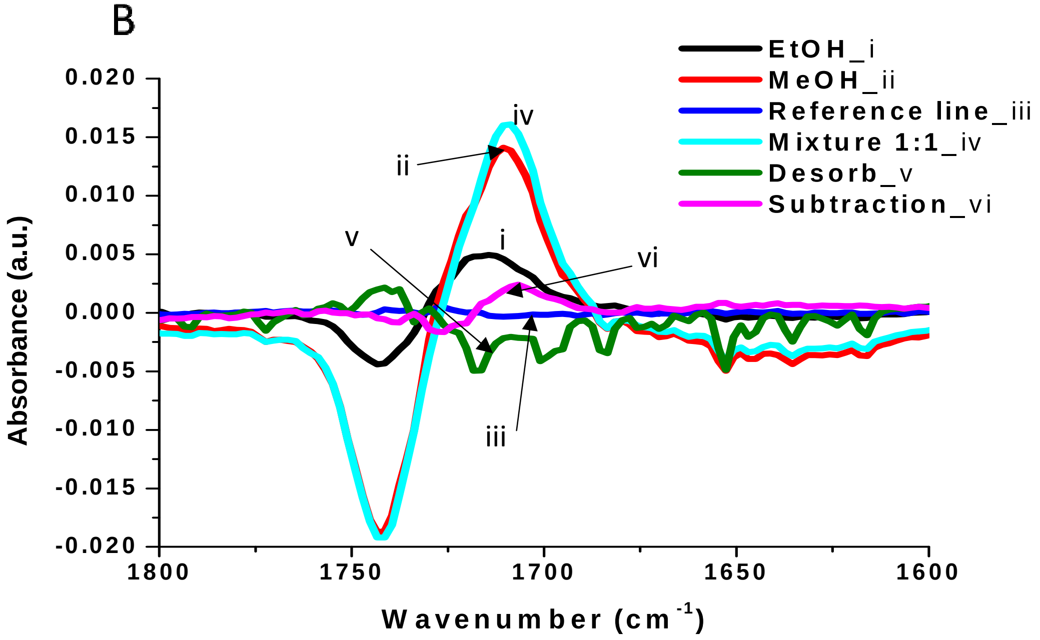

Figure 7.8. IR spectra of a) the spectra of the ethanol, methanol, a 1:1 mixture, and the resulting spectrum after performing a subtraction on the mixture of methanol b) The secondary absorbance region. All were delivered in dynamic conditions to a 130nm PGMA film.

7.3.2.2. Six-layer PGMA-PAA

7.3.2.2.1. Acetone-Methanol

The six-layer PGMA-PAA system was also tested for its sensitivity to VOC mixtures. The VOCs were delivered simultaneously in dynamic conditions. Flow rates are the same as previously given. In **Figure 7.9a,** the full spectra of acetone, methanol and the 1:1 mixture absorbed into the six-layer EPLS is presented. There is a negative IR absorbance in the region between 3000 cm^{-1} and 3500 cm^{-1}. This gives evidence that the analytes are interacting with the hydroxyl groups in the EPLS. In addition, the mixture has an absorbance intensity in the C-H region of 2700 to 3000 cm^{-1} that is greater than either component combined. This does not allow for any determination of concentration by subtraction. In **Figure 7.9b**, the carbonyl region is expanded to show changes in the 1710 cm^{-1} peak and the secondary absorbance peak after desorption. A reference absorbance spectrum is also shown for comparison. A final observation is that the carbonyl absorbance is significantly less in the mixture than the acetone or methanol spectra.

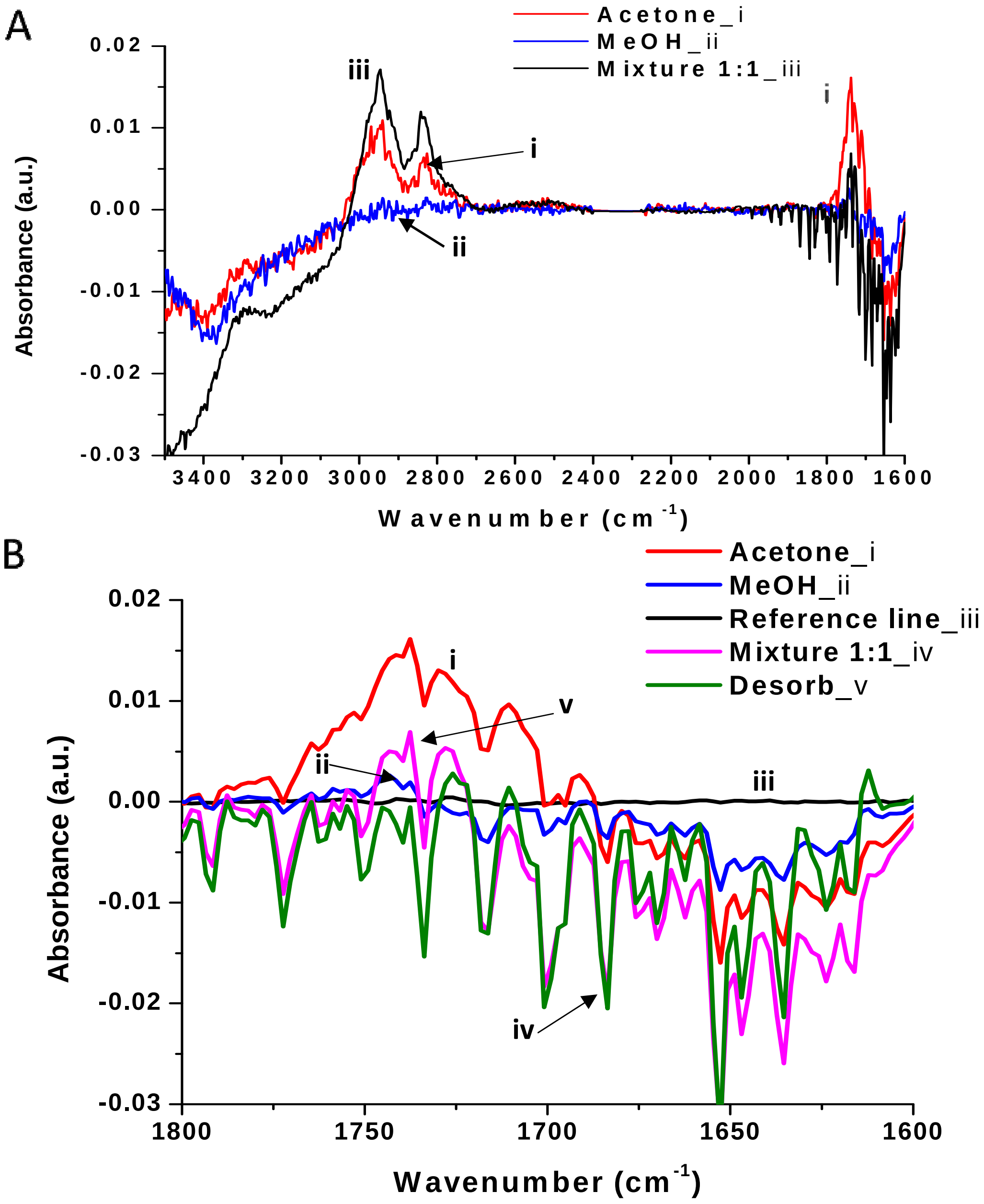

Figure 7.9. IR spectra for six-layer PGMA-PAA EPLS exposed to a mixture of acetone and methanol delivered in dynamic conditions a) Full spectra of individual components, and mixture b) The absorbance of the carbonyl region.

7.3.3. ATR FT-IR Dynamic absorption: Sequential delivery

7.3.3.1. PGMA single component

7.3.3.1.1. Acetone-Methanol

The sequential delivery of VOCs to the EPLS was conducted to identify changes in IR absorbance associated with the addition and/or subtraction of an analyte to the EPL. Flow rates remain constant. The total flow remained the same throughout the experiment. The IR absorbance of each step is presented in **Figure 7.10** (a reference line is given for the eye). After the acetone reached a steady state (**1**), methanol delivered to the EPL. There is an increase in the absorbance of the O-H region (**2**). Both VOCs are then removed using nitrogen (**3**). After 10 minutes of purging with nitrogen, acetone is clearly removed from the layer. Methanol is also presumed to leave the film as well, but the film is slightly altered as a small positive hydroxyl absorbance can be seen.

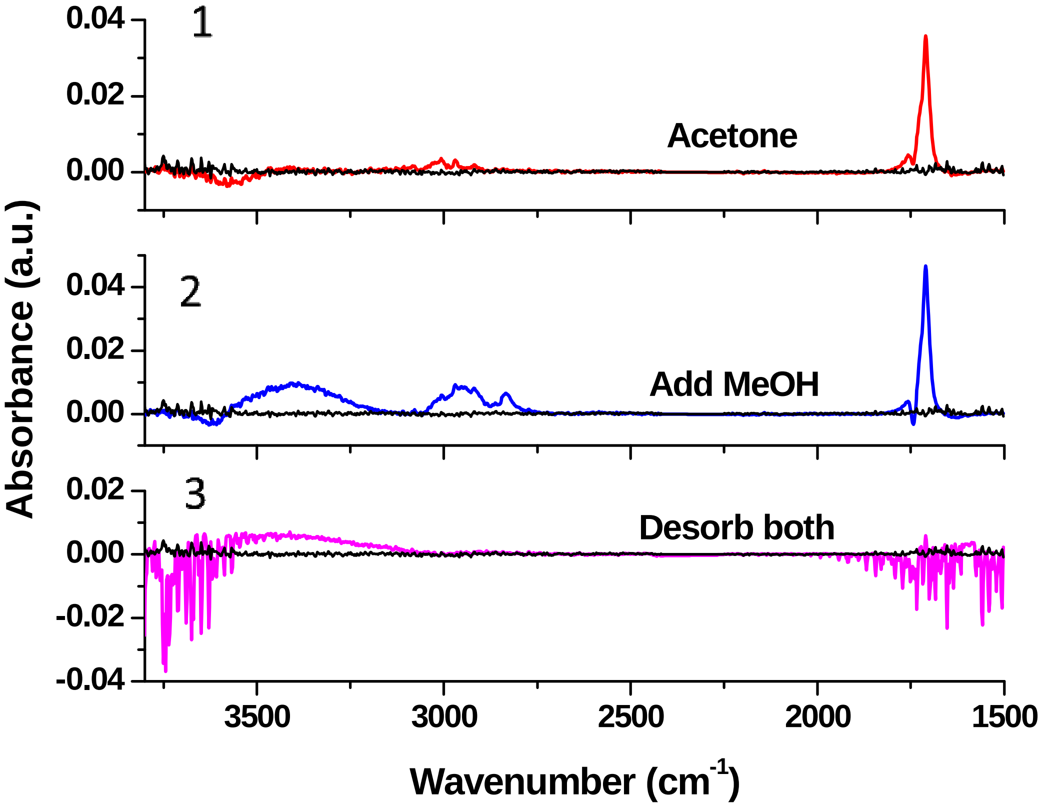

Figure 7.10. IR spectra for 130nm PGMA film exposed to a mixture of acetone and methanol delivered in dynamic conditions in sequence.

7.3.3.1.2. Methanol-Ethanol

The second mixture was methanol and ethanol. IR absorbances of the analytes with the EPLS are provided in **Figure 7.11**. After a steady absorbance is reached (**1**), ethanol has a clear absorbance that is characteristic of what was observed in previous experiments. When methanol is added to the film (**2**), there is an increase in the hydroxyl absorbance region between 3000 cm^{-1} and 3500 cm^{-1}. In addition, the secondary absorbance peak increases as well. This lends more evidence to the hypothesis that the secondary interactions can be advantageous for identification analysis. When ethanol is removed (**3**), the intensity decreases semi-proportionally to the original amount of ethanol. After methanol is removed from the system (**4**), and there is a non-zero spectrum after 10 minutes of nitrogen purge.

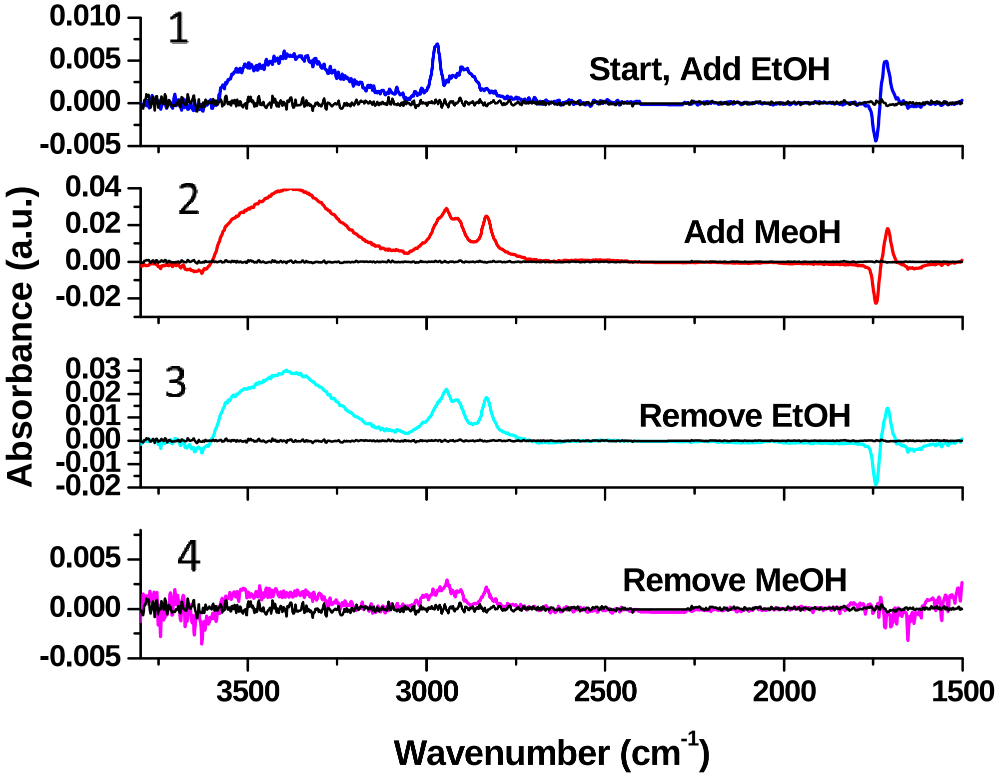

Figure 7.11. IR spectra for 130nm PGMA film exposed to a mixture of ethanol and methanol delivered in dynamic conditions at 25mL/min (each) in sequence. A reference zero-line is given for the eye.

7.3.3.2. 6L PGMA-PAA EPLS

7.3.3.2.1. Acetone-Methanol

The sequential delivery of VOCs to the six-layer PGMA-PAA EPLS was also performed. The flow rates remain the same as with the previous experiments. The absorbance spectrum of the VOC as one is added and removed is given in **Figure 7.12**.

The saturated acetone vapor was delivered to the EPLS (**1**). The spectrum is the same as with previous experiments. When methanol is added (**2**), there is a decrease in the absorbance of the O-H region. This is accompanied by an increase in intensity and broadening of the C-H absorbance. When methanol is removed (**3**), the spectrum goes back to that of acetone. Next, acetone is removed last from the layer (**4**). After 10 minutes of a nitrogen purge, it is clear that there are still some changes with the layer. From this and the past results, it is presumed that the dynamic purge does not allow all VOC to leave the film.

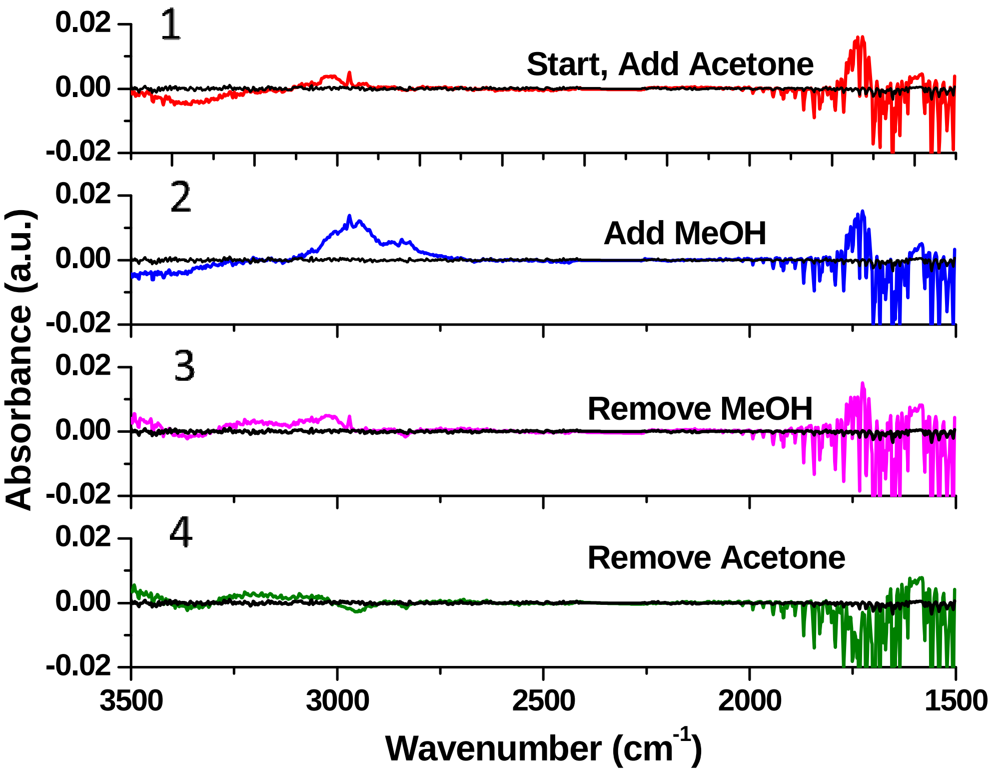

Figure 7.12. IR spectra for six-layer PGMA-PAA EPLS exposed to a mixture of acetone and methanol delivered in dynamic conditions at 25mL/min (each) in sequence. A reference zero-line is given for the eye.

7.3.3.2.2. Methanol and Ethanol

The final sequential mixture conducted was with methanol and ethanol. The absorbance spectra are given in **Figure 7.13**. When ethanol is delivered (**1**), C-H absorbance is observed coinciding with an absorbance in the O-H region. Very little change is observed in the carbonyl region. When methanol is added (**2**), there is a strong spike in the C-H absorbance intensity accompanied by broadening. In addition, there is a strong decrease in the hydroxyl absorbance region between 3000 cm^{-1} and 3500 cm^{-1}. When ethanol is then removed (**3**), the intensity of these regions decreases proportionally to the original amount of ethanol that was added. Methanol is then removed from the system (**4**). The removal of methanol leave a non-zero absorbance in the carbonyl region after a purge; however, the hydroxyl region is very close to the original baseline. Ethanol is added back to the EPLS one last time to demonstrate repeatability (**5**). The absorbance intensity appears to be sharper.

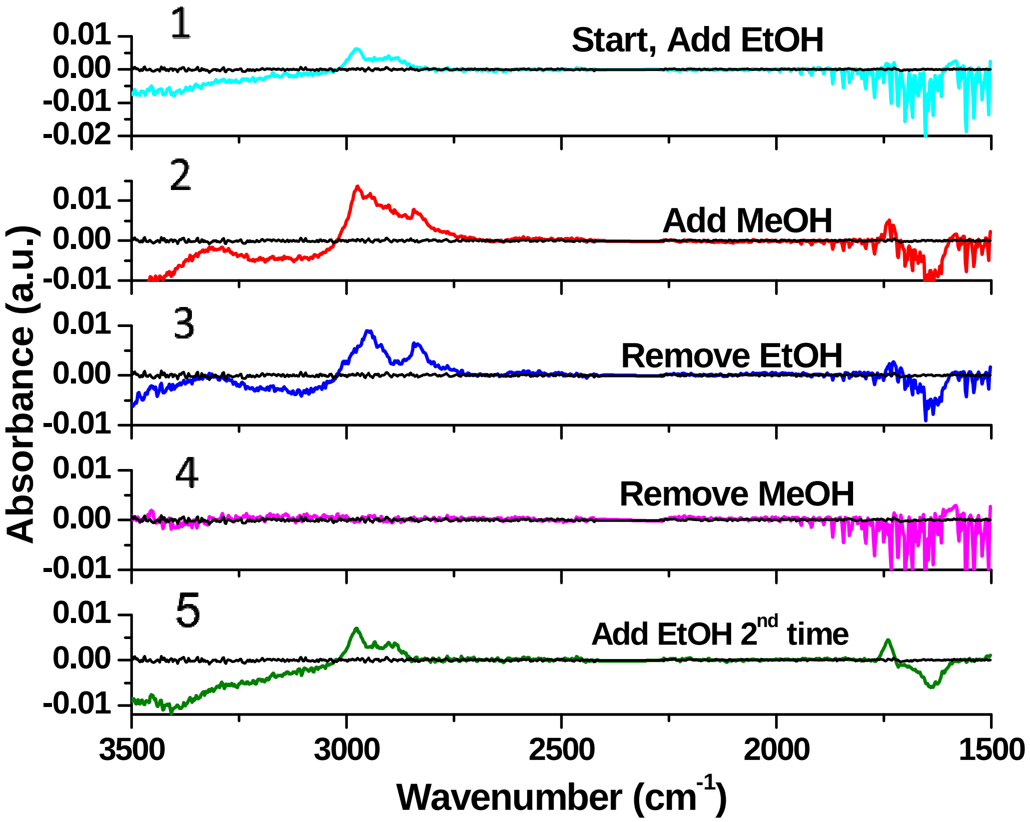

Figure 7.13. IR spectra for six-layer PGMA-PAA EPLS exposed to a mixture of methanol and ethanol delivered in dynamic conditions at 25mL/min (each) in sequence. A reference zero-line is given for the eye.

7.4. Conclusions

For both the PGMA EPL and the six-layer PGMA-PAA EPLS, absorption of analytes mixtures is possible. Detection can be done easily when specific and separate absorbance peaks are known and present. Secondary absorbance peaks can also be used to distinguish certain analytes due to their position, intensity, and shape. Deconvolution of similar analytes that have overlapping absorbance bands requires more study. There is an apparent high sensitivity to low amounts of a poor VOC. Further studies warrant what the cause of this might be and how it may be used in favor of chemical detection.

Sequential addition of the alcohols shows that there is an additive affect that, with more experimentation, can be used for concentration analysis. IR absorbance spectra of various concentrations of acetone and methanol, as well as acetone and hexane, show signal intensities that decrease with a decreasing component in the mixtures. These decreases are mostly, but not always, linear over the entire range of concentrations made.

Mixtures delivered with a nitrogen stream generally have lower overall absorbances. This is partially due to dilution with the nitrogen carrier gas. Simultaneous addition of two analytes was done and spectra match well with sequential addition of two VOCs.

7.5. References

1. Atkins, P. W. D. P. J., *Physical chemistry*. Freeman: Oxford [u.a., 2010.

Chapter 8. Enrichment layers coated on Micro-disk Resonators

8.1. Introduction

The work presented in this chapter probes the response of IR resonant devices coated with the multi-polymer and six layer PGMA-PAA enrichments systems. The sensitivity of the signal to VOCs has been tested and compared to non-coated devices. The devices act as micro- ATR crystals whereby evanescent waves are generated at the surface of the device. Due to their geometry and dimensions, the light is retained in the device long enough to produce 1000 evanescent waves which gives them high sensitivity to their environments.

A micro-fluidic flow system for analyte transport and an optical sensing unit for generating signals modulated by the presence of targeted chemical species (**Figure 8.1**) was fabricated by employing photolithography and thermal vapor deposition for use in this work. At the core of the device, the optical sensing unit consists of several sequential components: an off-chip laser source to emit the probing light, planar waveguides to couple the light into the resonator, the on-chip chalcogenide [ChG] glass or amorphous silicon optical resonator, and finally fiber-coupled photo-detectors to receive the signal through waveguides that couple the light out of the sensor module.

Measurements of resonance wavelength shits were performed at the Massachusetts Institute of Technology (MIT) by Vivek Singh or Dr. JJ Hu under the guidance of Dr.L. Kimerling and Dr. A. Agarwal.

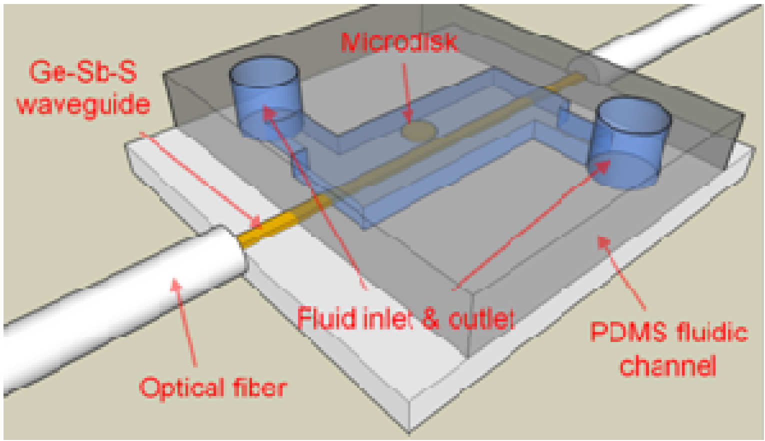

Figure 8.1 Proposed design for micro fluidic cell for exposing polymer coated resonators to VOCs.

8.2. Experimental

8.1.1. Fabrication of Amorphous Silicon(Am-Si) devices

The fabrication of the Am-Si devices (SEM image presented in **Figure 8.2a**) was done at MIT, by Vivek Raghunathan, and utilizes an etching process to remove contamination on the surface. Chemical vapor deposition (CVD) is used to grow a layer of amorphous Si on a silicon wafer coated with thermal oxide. UV lithography is carried out after coating the wafer with a positive photoresist followed by etching which removes the amorphous Si in areas not protected by the resist. This results in Am-Si devices on the silicon dioxide.

8.2.1. Fabrication of ChG micro-disc resonators

Bulk $Ge_{23}Sb_7S_{70}$ glass for film deposition was prepared from high purity elements using a traditional melt-quenching technique by students under the supervisor of Dr. Kathleen Richardson. The synthesis procedures of the bulk As and Ge based glasses used in this study are explained in detail, elsewhere.[1-2] All glasses are prepared from high purity elements (As, Alfa Aesar 99.999%; Ge, Alfa Aesar 99.999%; Sb, Sigma Aldrich 99.9%; S, Sigma Aldrich 99.999%) with no further purification. Thus starting bulk glasses used for target materials for film deposition have measurable loss in the near and mid-IR region of the spectrum due to quantities of adsorbed oxide and hydride. $Ge_{23}Sb_7S_{70}$ glass films are thermally deposited from targets of bulk glass pieces onto substrates in an Edwards E306A single-source evaporator using an optimized procedure described elsewhere.[3] The substrates for thin film deposition were 6 inch Si wafers pre-coated with a 3μm-thick thermal oxide (Silicon Quest International Inc.). Waveguides and micro-ring resonators were fabricated by a lift-off process: reverse photoresist patterns of the device were formed on the substrates prior to chalcogenide glass deposition (SEM image presented in **Figure 8.2b**). Details of the lithographic device fabrication can be found elsewhere.[4] Detection mechanisms for ring and disk devices are based on shifting of light wavelength based on changes local refractive indices caused by analyte incorporation into the polymer film or absorption of the light by the penetrating chemical (image of concept provided in **Figure 8.3**).

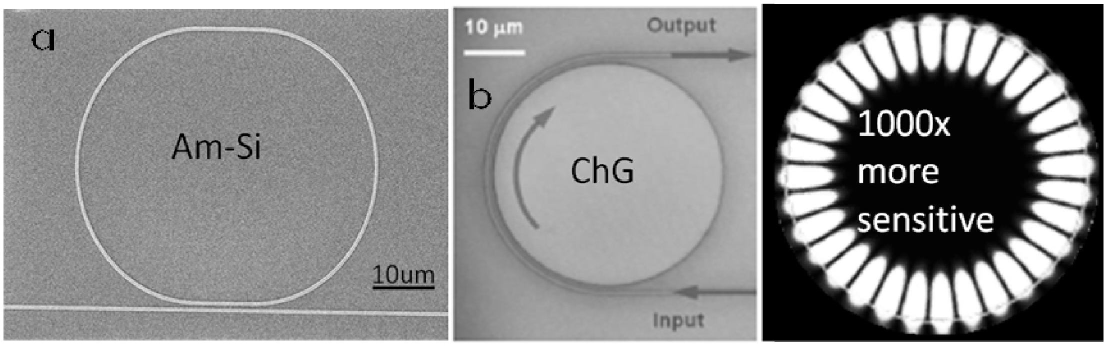

Figure 8.2 SEM images of resonator structures a) Am-Si and b) ChG. Image on right is depiction of evanescent wave propagation in a micro-disk resonator.

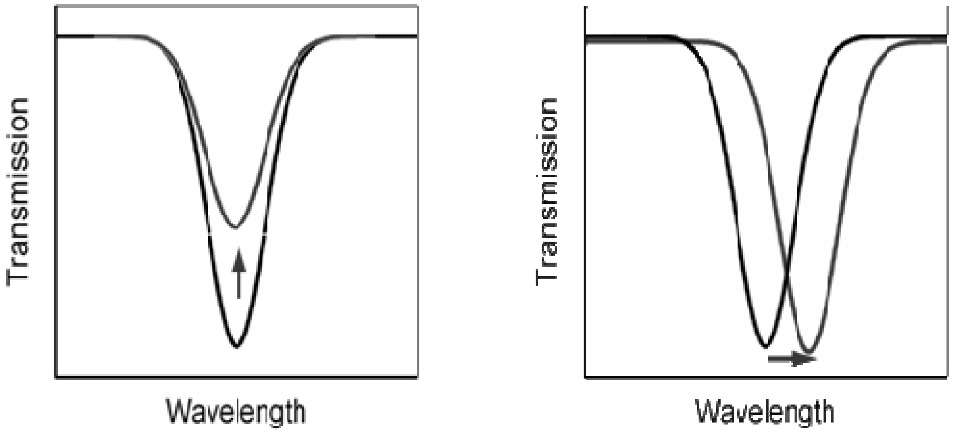

Figure 8.3 Possible mechanisms of detection when using polymer coated IR transparent resonators.

8.2.2. Coating of Am-Si and ChG resonators

The resonators were rinsed with MEK prior to the grafting instead of the piranha solution. The same grafting procedure was used for the ChG micro-disc resonators, though drop casting was used for the Am-Si resonators (performed by the author). The polymers were deposited and grafted consecutively in the following order for 6 layer system: PGMA-PAA-PGMA-PAA-PGMA-PAA, and the multi five layer system: PGMA-PAA-EPB60-PGMA-P2VP. The single layers have a PGMA layer with a thickness determined to be between 1-2 nm.

8.2.3. Analyte detection with ChG micro-disc resonators

The following experiments were conducted by Dr. Bogdan Zdyrko and Dr. J.J. Hu. Transmission spectra of the fabricated device have been measured on a Newport AutoAlign workstation in combination with a tunable laser (optical vector analyzer external laser, LUNA Technologies, Inc.). Lens-tip fibers were used to couple light from the laser into and out of the devices. Reproducible coupling was achieved via an automatic alignment system with a spatial resolution of 50 nm. The sample was mounted on a thermostat stage and kept at 25 ˚C for all measurements. Analyte was delivered in a small Al bucket placed near micro-ring resonator and enclosed with PDMS chamber. A series of transmission spectra were recorded until shift in the micro-ring resonance reached it maximum.

8.2.4. Analyte detection with Am-Si microring resonators

All resonator transmission measurements were made on a LUNA Optical Vector Analyzer (OVA). Experiments were conducted by Vivek Singh with the author. The resonator samples were placed on a static stage while the input and output fibers are aligned using precise software controlled, and motorized three-axis stages that allow movements as small as 10 nm. A reference exposure was done with acetone before polymer modification. Transmission spectra were recorded as polymers were deposited onto the devices by a drop casting technique. Devices were annealed under vacuum to graft polymer layers and exposed to organic solvents to rinse away ungrafted polymer. A reference measurement was made before exposing the resonator devices to any analyte, and compared to the measurements taken after analyte exposure, to calculate observed resonator peak shifts. For analyte exposure, an in house made glass cell was used, which consisted of a reservoir filled with the liquid analyte placed next to the sample. Aluminum foil was used to drape the sides of the cell to maintain a minimal exposure of analyte vapor over the coated devices however the necessity to align the fibers prompted the need for slit-like openings on the sides of the cell making it open to the environment on both sides. Transmission measurements were systematically made at 1, 2, 4, 8, 16, and

32 minutes. Between analytes, the sample was allowed to recover for a few minutes in open air.

8.3. Results and Discussion

8.3.1. Am-Si Resonators with EPLS

8.3.1.1. PGMA-PAA six layer system

The designed enrichment polymer nanocoatings can be applied not only to macroscopic waveguides such as silicon crystals but also to miniaturized IR sensing devices such as micro-disc resonators.[3, 5] In an optical resonator, working on evanescent field principles, circulating light is confined within a small volume. When the resonant condition is met, the optical power becomes resonantly enhanced up to a factor approximating cavity finesse. This increases their sensitivity to environmental stimuli.

Micro-ring resonators were modified with the six layer PGMA-PAA polymer enrichment system. Optical imaging revealed that the devices were not destroyed during the polymer layer deposition procedure. AFM images taken of the top of the PAA layer (**Figure 8.4**) shows that around the micro-ring, the polymer coating has wrinkles from variable vaporization of the solvent after applied by drop casting. Images of a 1x1um area has less wrinkle formation.

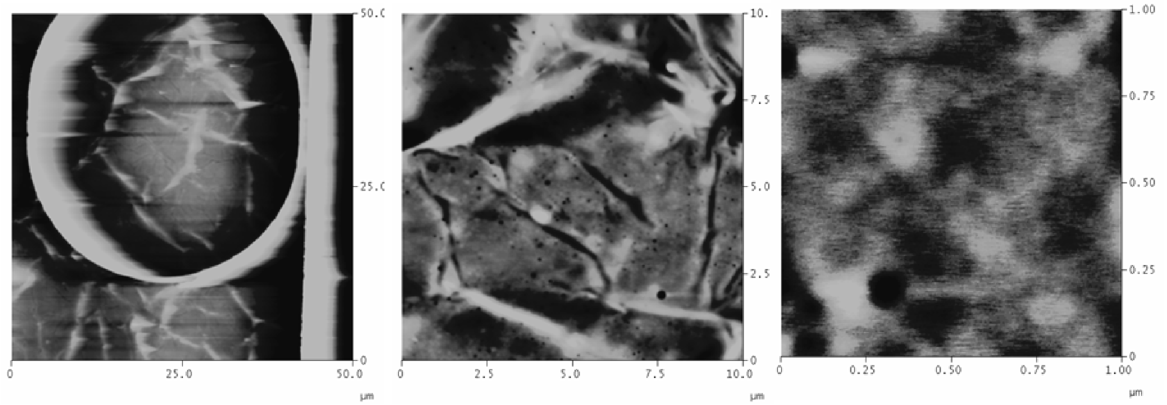

Figure 8.4 AFM topography of the top PAA layer of the enrichment system coated onto a Am-SI micro-ring resonator. Images sizes are 30x30um, 10x10um, and 1x1um left to right respectively. Height values are 250, 40 and 5 nm left to right respectively. RMS of the 1x1um image is 0.5nm

In **Figure 8.5** the deposition and grafting of the polymer layer permanently changes the baseline intensity of the resonator along with the resonant coupling and continues to change for subsequent layer depositions. It can be seen that intensity of the coupling remains significant showing that the polymer film does not hinder the use of the device as an environment response sensor.

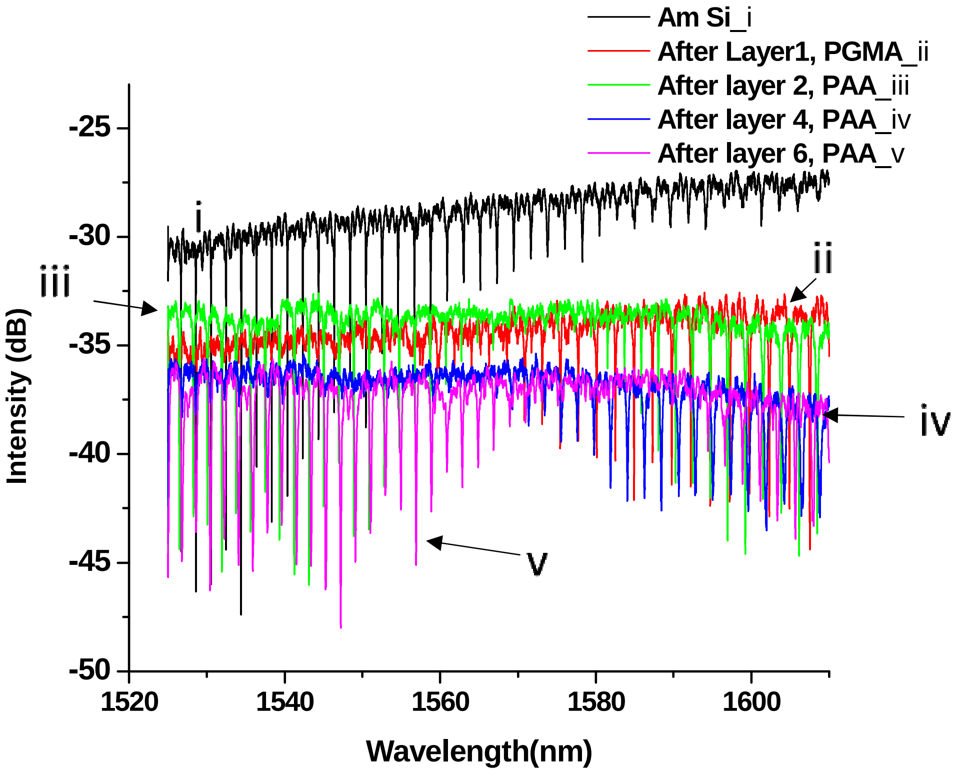

Figure 8.5. Baseline intensity change of an Am-Si ring resonator coupling upon coating with polymer layers.

Proof that the polymer film is necessary for detection of gas phase VOCs is given in **Figure 8.6a.** A non-coated Am-Si micro-ring resonator was exposed to acetone vapor for 32 minutes with no resulting significant shift (resolution is 1.5pm, spectra were taken in periods of 2, 4, 8, 16, and 32 minutes). In **Figure 8.6b,** after coating with the six layers, a 1551 nm wavelength is used to show that upon exposure to acetone vapor there is not only a shift but a decrease in intensity of the coupling. Acetone has only minor absorption in this near IR region so the majority of the change in intensity of the coupling peak is thought to be due to the swelling of the polymer film.

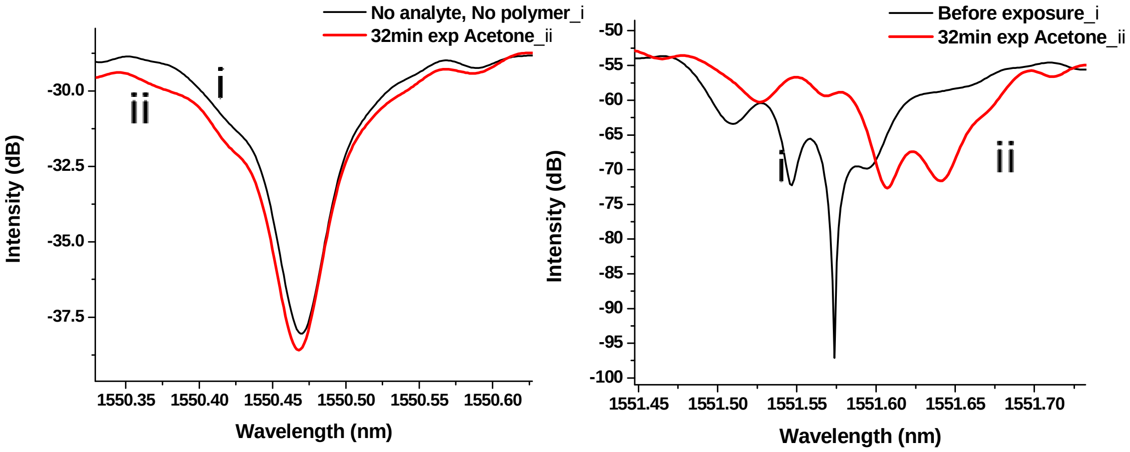

Figure 8.6 Am-Si ring resonator coupling shift after 32 minutes in the presence of acetone vapor a) before coating with 6L PGMA-PAA coating, b) after application and grafting of 6L PGMA-PAA system.

The maximum shifts of the 1551 nm wavelength when exposed to acetone, methanol, ethanol and water were recorded and are presented in **Figure 8.7**. All of the analytes used demonstrated a unique peak shift upon exposure to the chemicals with different magnitudes.

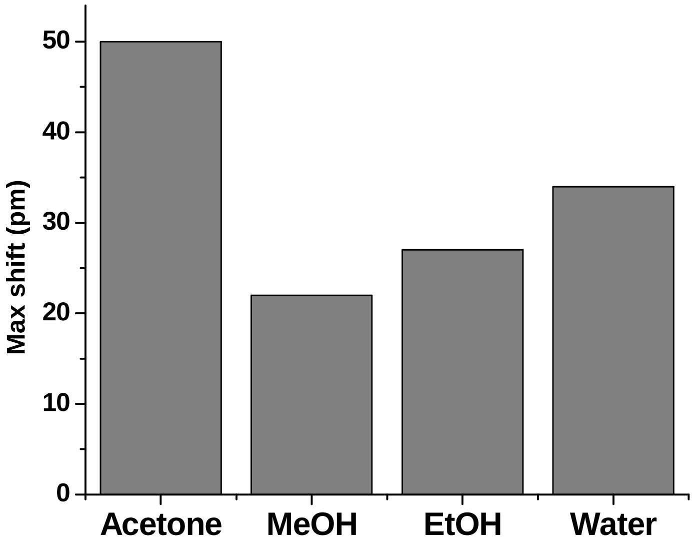

Figure 8.7 Differences in the maximum shift observed for the Am-Si ring resonator in the present of analyte vapors 6L PGMA-PAA.

8.3.2. ChG Resonators with EPLS

8.3.2.1. Six Layer PGMA-PAA

Microdisk resonators made of chalcogenide glass were modified with the six layer PGMA-PAA polymer enrichment system. Optical analysis demonstrated that the devices were not destroyed during the polymer layer deposition procedure. Modified ChG resonators were exposed to the vapors of the water, methanol, ethanol, isopropanol, acetone, hexane and aqueous ammonia solution (0.027%). Resonant peak shift of 1550 nm wavelength was monitored as device output. All of the analytes used demonstrated peak shift upon exposure to the chemicals. Unique shifts of the resonant wavelength for each analyte vapor for this system are given in **Figure 8.8**. As with the coated Am-Si resonator devices, the polymer coatings demonstrated different resonance peak shift magnitudes when exposed to different analytes.

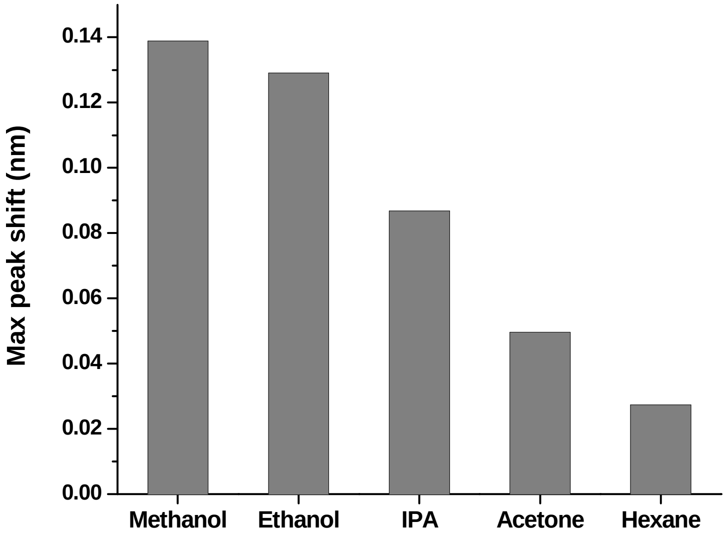

Figure 8.8 Resonator resonance maximum shift observed for the ChG disk coated with 6L PGMA-PAA in the present of analyte vapors.

8.3.2.2. Multi-polymer system

Modification of the micro-disc resonators was conducted with the multilayered coating according to the procedure designed for the Si crystals. Optical testing demonstrated that the devices were not destroyed during the modification (polymer layer deposition) procedure. In fact, the polymer film evenly covered the devices on both the micro and nano-levels (**Figure 8.9**) and increased the measured cavity quality factor (Q-factor) on average by ~ 15% compared to uncoated resonators, which can be attributed to the sidewall roughness smoothing effect and consequent scattering loss reduction.[6]

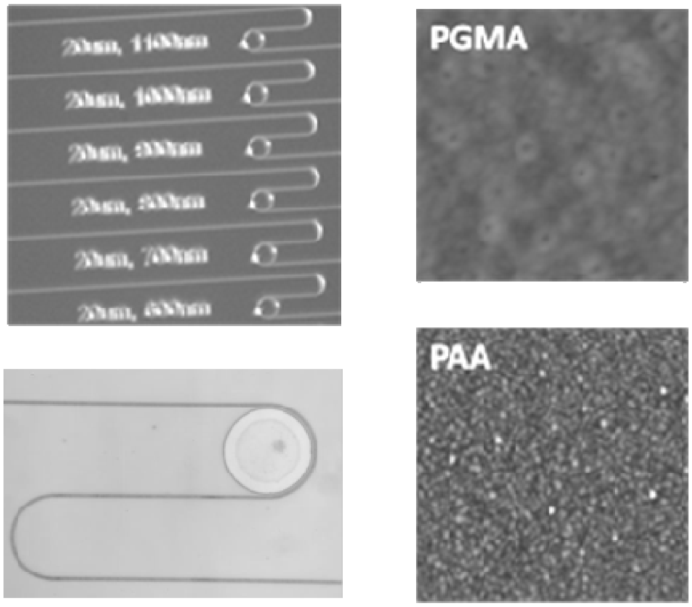

Figure 8.9 Top left: The IR sensor device (made of IR transparent chalcogenide [ChG] glass). Bottom left: Close up optical image of ChG pully design used. Top right: AFM morphology image of the PGMA coating surface. Bottom right: AFM morphology image of the PAA coating surface. Image size: 1x1 μm, vertical scale: 10 nm.

To monitor interaction of the analyte with the coating, shift of the resonance peak near 1550 nm wavelength was used (**Figure 8.10 insert**). Modified ChG resonators were exposed to the vapors of the water, methanol, ethanol, isopropanol, acetone, hexane and aqueous ammonia solution (0.027%).

Resonant peak shift of micro-disc resonators was monitored as device output (**Figure 8.10**). All of the analytes used demonstrated peak shift upon exposure to the chemicals. In addition, polymer coatings demonstrated different resonance peak shift when exposed to different analytes. This setup, in principle, can be used as micro on-chip IR sensor provided that the ChG bus waveguides are coupled to an IR source and detector. Analysis of scientific literature shows that all components of the sensor (IR source, sensing element and detector)[5-10] can be integrated into one chip yielding a miniature, low power consumption and low cost sensor preserving all advantages of sensing in mid-IR.

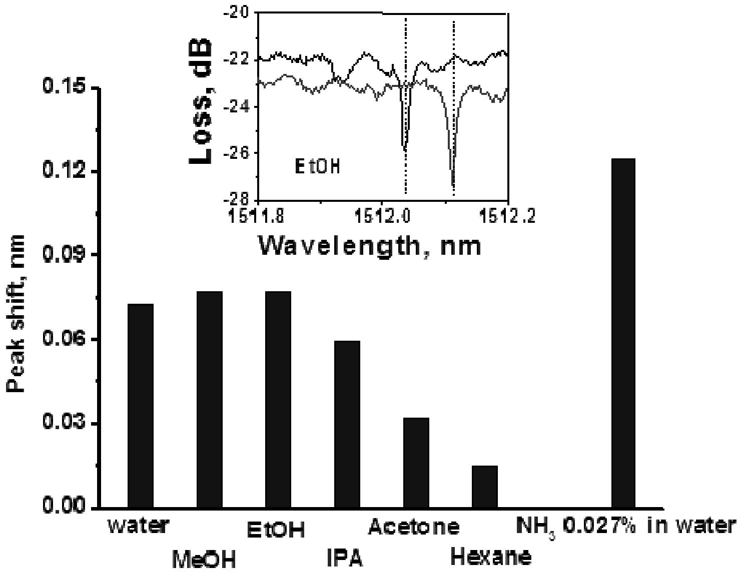

Figure 8.10 Resonator resonance maximum shift observed for the ChG disk coated with 6L PGMA-PAA in the present of analyte vapors. Insert: shift of resonance peak near 1550 nm wavelength.

8.4. Conclusions

All polymer layers can be used to modify the micro-ring and micro-disk devices. Resonance coupling of the near IR light with the amorphous silicon devices were monitored as the polymer layers were applied and grafted. As the coupling intensities remain significantly strong, it can be concluded that applying polymers does not damage the devices and the unique couplings can be used to monitor absorption of VOCs. Both chalcogenide and amorphous silicon are good optical materials to use of mid-IR transparent chemical vapor sensors. Each analyte exposure to the coated devices produced a significant resonance shift and returned to baseline after VOCs were removed from the resonator environment.

8.5. References

1. Anderson, T. Fabrication of integrated optofluidic circuits in chalcogenide glass using femtosecond laser direct writing. PhD Thesis, University of Central Florida, 2009.

2. Lopez, C. Evaluation of the photo-induced structural mechanisms in chalcogenide glass. PhD Thesis, University of Central Florida, 2004.

3. Richardson, K.; Petit, L.; Carlie, N.; Zdyrko, B.; Luzinov, I.; Hu, J.; Agarwal, A.; Kimerling, L.; Anderson, T.; Richardson, M., Progress on the fabrication of on-chip, integrated chalcogenide glass (chg)-based sensors. *Journal of Nonlinear Optical Physics & Materials* **2010,** *19* (1), 75-99.

4. Hu, J. J.; Tarasov, V.; Carlie, N.; Petit, L.; Agarwal, A.; Richardson, K.; Kimerling, L., Exploration of waveguide fabrication from thermally evaporated Ge-Sb-S glass films. *Optical Materials* **2008,** *30* (10), 1560-1566.

5. Hu, J. J.; Carlie, N.; Petit, L.; Agarwal, A.; Richardson, K.; Kimerling, L., Demonstration of chalcogenide glass racetrack microresonators. *Optics Letters* **2008,** *33* (8), 761-763.

6. Hu, J. J.; Feng, N. N.; Carlie, N.; Petit, L.; Wang, J. F.; Agarwal, A.; Richardson, K.; Kimerling, L., Low-loss high-index-contrast planar waveguides with graded-index cladding layers. *Optics Express* **2007,** *15* (22), 14566-14572.

7. Petit, L.; Carlie, N.; Zdyrko, B.; Luzinov, I.; Richardson, K.; Hu, J. J.; Agarwal, A.; Kimerling, L.; Anderson, T.; Richardson, M., Development of novel integrated bio/chemical sensor systems using chalcogenide glass materials. *International Journal of Nanotechnology* **2009,** *6* (9), 799-815.

8. Wang, J. F.; Hu, J.; Becla, P.; Agarwal, A. M.; Kimerling, L. C., Resonant-cavity-enhanced mid-infrared photodetector on a silicon platform. *Optics Express 18* (12), 12890-12896.

9. Wang, J. F.; Hu, J. J.; Sun, X. C.; Agarwal, A. M.; Kimerling, L. C.; Lim, D. R.; Synowicki, R. A., Structural, electrical, and optical properties of thermally evaporated nanocrystalline PbTe films. *Journal of Applied Physics* **2008,** *104* (5).

10. Gmachl, C.; Capasso, F.; Sivco, D. L.; Cho, A. Y., Recent progress in quantum cascade lasers and applications. *Reports on Progress in Physics* **2001,** *64* (11), 1533-1601.

Chapter 9. Summary and Future work

9.1. Summary

9.1.1. PGMA as a single component enrichment layer

PGMA can be utilized as a single component EPL. Exposure to VOCs with *in-situ* ellipsometry showed a swelling trend for PGMA. *In-situ* FT-IR showed new peak formations that were not present in the VOC. This can provide clearer of identification of VOCs. The strongest IR signals for VOCs were obtained with the thicker 130 nm film However, even 15 nm of PGMA is sufficient to trap VOC molecules to obtain spectra. The time that is needed to confirm VOC absorption is less than 30 seconds under static conditions and identification can be accomplished in less than a minute. Equilibrium time can be up to 20 minutes for high vapor pressure VOCs. A minimum of 40 minutes is required for low vapor pressure VOCs to reach equilibrium in static conditions. Dynamic conditions decrease these times.

9.1.2. PGMA and PAA built into one enrichment system

PGMA and PAA can be grafted together to form an enrichment layer system. The swelling fractions of this six-layer PGMA-PAA enrichment polymer layer system is sensitive to VOCs with strong hydrogen-bonding characteristics. The system has affinities that are more similar to PAA than to PGMA. Cross-linking with multiple grafting sites on the PAA backbone reduces loading capabilities; however, it does not seem to inhibit sensing and differentiation between VOCs.

The results of IR analysis have a correlation with swelling analysis. There are more intense secondary IR absorbance peaks for strong hydrogen-bonding VOCs that has high swelling fractions with the EPLS. Each analyte gave a unique IR spectrum that can be used to distinguish it from similar VOCs (specifically the alcohols) and from a pure PGMA film as well.

9.1.3. Multi-polymer enrichment system

The main implication of IR absorbance studies with two-layer systems is that addition of various polymers in one system can promote an absorbance spectrum when a VOC is incorporated into the system that is unique from the previous six-layer PGMA-PAA system and PGMA film. This function works best when an array of enrichment systems is used to identify unique points for VOC identification.

The EPLS synthesized and studied in this chapter contained polymer layers that added unique functionality and targeting ability. The swelling level of the multi-polymer EPLS was, on average, lower for the tested VOCs than for the previous six-layer PGMA-PAA EPLS. However, the EPLS was able to incorporate each analyte. Therefore, the system can act as a "universal" enrichment system.

IR analysis demonstrated that each analyte gave a unique IR spectrum that could be used to distinguish substances. Additionally, the spectra observed with this EPLS were significantly different from a pure PGMA film and from the PGMA-PAA EPLS. Furthermore, analyte VOCs that have higher swelling with the multi-polymer system (e.g., acetic acid) had stronger IR absorbance than they had with the PGMA-PAA EPLS. Analytes that have affinity with both, such as ammonium hydroxide, gave IR signatures that were differentiable by intensity. However, those signatures were slightly weaker due to the broader scope of chemical attraction with the multi-polymer system.

9.1.4. Mixture absorption analysis by ATR FT-IR

For both the PGMA EPL and the six-layer PGMA-PAA EPLS, absorption of analytes mixtures is possible. Detection can be done easily when specific and separate absorbance peaks are known and present. Secondary absorbance peaks can also be used to distinguish certain analytes due to their position, intensity, and shape. Deconvolution of similar analytes that have overlapping absorbance bands requires more study. There is an apparent high sensitivity to low amounts of a poor VOC. Further studies warrant what the cause of this might be and how it may be used in favor of chemical detection.

Sequential addition of the alcohols shows that there is an additive affect that, with more experimentation, can be used for concentration analysis. IR absorbance spectra of various concentrations of acetone and methanol, as well as acetone and hexane, show signal intensities that decrease with a decreasing component in the mixtures. These decreases are mostly, but not always, linear over the entire range of concentrations made.

Mixtures delivered with a nitrogen stream generally have lower overall absorbances. This is partially due to dilution with the nitrogen carrier gas. Simultaneous addition of two analytes was done and spectra match well with sequential addition of two VOCs.

9.1.5. Polymer coated evanescent waveguide resonator devices

All polymer layers can be used to modify the micro-ring and micro-disk devices. Resonance coupling of the near IR light with the amorphous silicon devices were monitored as the polymer layers were applied and grafted. As the coupling intensities remain significantly strong, it can be concluded that applying polymers does not damage the devices and the unique couplings can be used to monitor absorption of VOCs. Both chalcogenide and amorphous silicon are good optical materials to use of mid-IR transparent chemical vapor sensors. Each analyte exposure to the coated devices produced a significant resonance shift and returned to baseline after VOCs were removed from the resonator environment.

9.2. Future work

This work has been geared to develop multi-polymer layers that can be used for enrichment of chemical sensors. This has led to develop an understanding some trends involved with thin polymer layer affinity towards VOCs that has not been studied previously. More to the point, this work has delved into the fundamental relationships between intermolecular interactions between polymers and VOCs that can be observed by changes in mid-IR spectroscopy. To elucidate some points that are not fully investigated in this work, it is important to perform the following tasks.

- *In-situ* 2D IR spectroscopy can provide the capabilities needed to deconvolute which chemical functional groups are interacting with absorbing VOCs. Fundamental vibrations are correlated with each other generating a unique map with changes of frequencies are aligned with other corresponding changes in the spectrum.
- Determine experimentally (for PGMA and other polymers involved) the interaction parameter χ via osmotic measurements or dissolution calorimetry.
- Mathematical or experimental determination of the cross linking density of PGMA films of different thicknesses and different annealing times.

- IR ellipsometry can be used on the swelling systems to determine, by modelling, the real change in refractive index as the film is swollen and its effect on IR absorbance. In addition, multi-angle, and multi-wavelength ellipsometry should be used for layer swelling fraction calculation. This will require better and more sophisticated modelling than what is available.

- This work has not presented an in-depth analysis of the limit of detection for the evanescent waveguide chemical sensors with and without polymer films. In order to show that these devices are truly on the cutting edge of sensor development, such experiments to accurately assess the concentration of the delivered VOC to the sensor device will need to be done.

9.3. Publications and Presentations

This is a list of publications and presentations that have been made because of this work.

9.3.1. Papers

9.3.1.1. In Progress

- **J. Giammarco**, B. Zdyrko, J.D.Musgraves, J.J. Hu, V. Singh, A. Agarwal, L. Kimerling, K. Richardson, I. Luzinov, Multi-layered polymer system for detection of ammonia hydroxide and other VOCs(working title).

- Y. Galabora, AnnaPaola Soliani, **J. Giammarco**, B. Zdyrko, I. Luzinov, Actuation potential of grafted nanofoams. Soft Matter (waiting for review).

- Vivek Singh, Pao-Tai Lin, Neil Patel, Hongtao Lin, Lan Li, Yi Zou, Fei Deng, Chaoying Ni, Juejun Hu, **James Giammarco,** Anna Paola Soliani, Bogdan Zdyrko, Igor Luzinov, Spencer Novak[3], Jackie Novak, Peter Wachtel, Sylvain Danto, J. David Musgraves, Kathleen Richardson, Lionel C Kimerling, and Anuradha M Agarwal, Mid-IR devices on Si for optical sensing, *Sci. Tech. Adv. Mater.* (waiting for acceptance)

9.3.1.2. Published

- **Giammarco, J**.; Zdyrko, B.; Petit, L.; Musgraves, J. D.; Hu, J.; Agarwal, A.; Kimerling, L.; Richardson, K.; Luzinov, I., Towards universal enrichment nanocoating for IR-ATR waveguides. *Chem Commun* **2011,** *47*, 9104-9106.

9.3.2. Oral Presentations

- **Giammarco, James.** Bogdan Zdyrko, Jackie Wilkinson, J. David Musgraves, Kathleen Richardson, Anu Agarwal, Lionel Kimerling, Juejun Hu, Igor Luzinov **Enrichment polymer systems for FT-IR detection of chemical vapors** 244st ACS National Meeting, Philadelphia, PA United States, August 2012
- **Giammarco, James**; Bogdan Zdyrko, Juejun Hu, Anu Agarwal, Lionel Kimerling, Nathan Carlie, Laeticia Petit, Kathleen Richardson, and Igor Luzinov **Enrichment polymer layers for detection of volatile vapors by ATR FT-IR** 241st ACS National Meeting, Anaheim, CA, United States, March 2011

9.3.3. Poster Presentations

- **Giammarco, James**; Bogdan Zdyrko, Juejun Hu, Anu Agarwal, Lionel Kimerling, Nathan Carlie, Laeticia Petit, Kathleen Richardson, and Igor Luzinov; **Detection of volatile vapors by FT-IR spectroscopy with the aid of enrichment polymer nano-layers**, 3rd International Conference from Nanoparticles and Nanomaterials to Nanodevices and Nanosystems (IC4N); Crete, Greece, June 29 2011
- **Giammarco, James**; Bogdan Zdyrko, Juejun Hu, Anu Agarwal, Lionel Kimerling, Nathan Carlie, Laeticia Petit, Kathleen Richardson, and Igor Luzinov CCOMC, Clemson, SC, United States November 2010
- **Giammarco, James**; Bogdan Zdyrko, Juejun Hu, Anu Agarwal, Lionel Kimerling, Nathan Carlie, Laeticia Petit, Kathleen Richardson, and Igor Luzinov **Design and application of multiple polymer layered systems to facilitate waveguide sensor detection** Abstracts of Papers, 240th ACS National Meeting, Boston, MA, United States, August 2010
- **Giammarco, James**; Bogdan Zdyrko, Juejun Hu, Anu Agarwal, Lionel Kimerling, Nathan Carlie, Laeticia Petit, Kathleen Richardson, and Igor Luzinov **Grafted enrichment polymer layer system for waveguide sensor** Abstracts of Papers, 240th ACS National Meeting, Boston, MA, United States, August 2010
- **Giammarco, James**; Bogdan Zdyrko, Juejun Hu, Anu Agarwal, Lionel Kimerling, Nathan Carlie, Laeticia Petit, Kathleen Richardson, and Igor Luzinov **Fabrication and Characterization of Grafted Enrichment Layers for Evanescent Wave Sensors** 5th Annual Materials and Optics Poster Competition, Mar 2010
- **Giammarco, James**; Bogdan Zdyrko, Juejun Hu, Anu Agarwal, Lionel Kimerling, Nathan Carlie, Laeticia Petit, Kathleen Richardson, and Igor Luzinov Abstracts of Papers, 238th ACS National Meeting, Washington, DC, United States, August, 2009

Appendix

1. Ellipsometry

For purely comparative purposes, a refractive index of 1.5 was used for the results presented in this dissertation. The swelling fraction data using two different refractive indices (1.5 for the polymer and 1.3 for the liquid solvent) is presented in **Figure A1**. Results show that for the single films, there is a small difference in fractional swelling values. For the multi films there is a larger difference due to the EPLS absorbing more VOC vapor. The differences seen in these results demonstrate that the software modelling available is not extremely sensitive. The low swelling fraction was taken to identify trends of the layers. This is because the polymer films are not saturated with VOC liquid. Future work identifies that more robust modelling is needed.

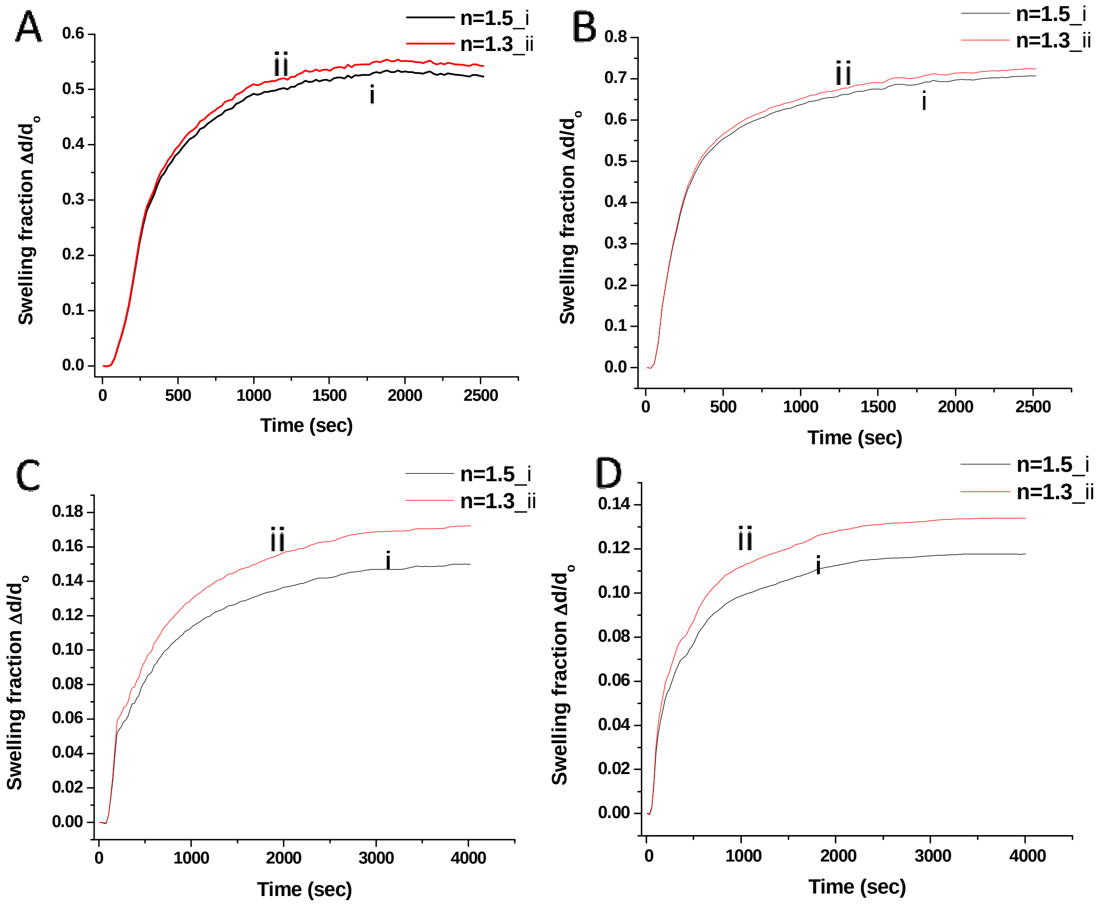

Figure A9.1. Swelling fractions of acetone vapor in: A) PAA 8nm film, B) PGMA 8nm film, C) six layer PGMA-PAA system, D) five layer Multi-polymer system

The polymer films will never reach the volume fraction needed to bring the refractive index to that of the liquid solvent. Therefore, the trends shown with the polymer layers are real (e.g. for a 90nm PGMA film, acetone will always be greater than hexane). The refractive indices of five of the major VOCs are presented in **Table A1**. These were obtained using a Spectronic Unicam visible light reflectrometer Model 334610 at a temperature of 25°C.

Table A1. Refractive indices for major VOC liquids used in this work.

VOC	Refract Index
Acetone	**1.358**
Methanol	**1.329**
Acetic acid	**1.372**
Hexane	**1.374**
Isopropanol	**1.377**

2. Depth of penetration

The depth of penetration of the evanescent wave was calculated for a waveguide made of silicon (refractive index is 3.4)[1], amorphous silicon (refractive index 4.66)[2] and chalcogenide (refractive index 2.5)[3]. The results over a range of wavelengths is presented in **Figure A2**. A refractive index of 1.5 was used for the polymer materials used in this work. A refractive index of 1.3 represents the lowest index of refraction for the liquid VOC analytes used in this work.

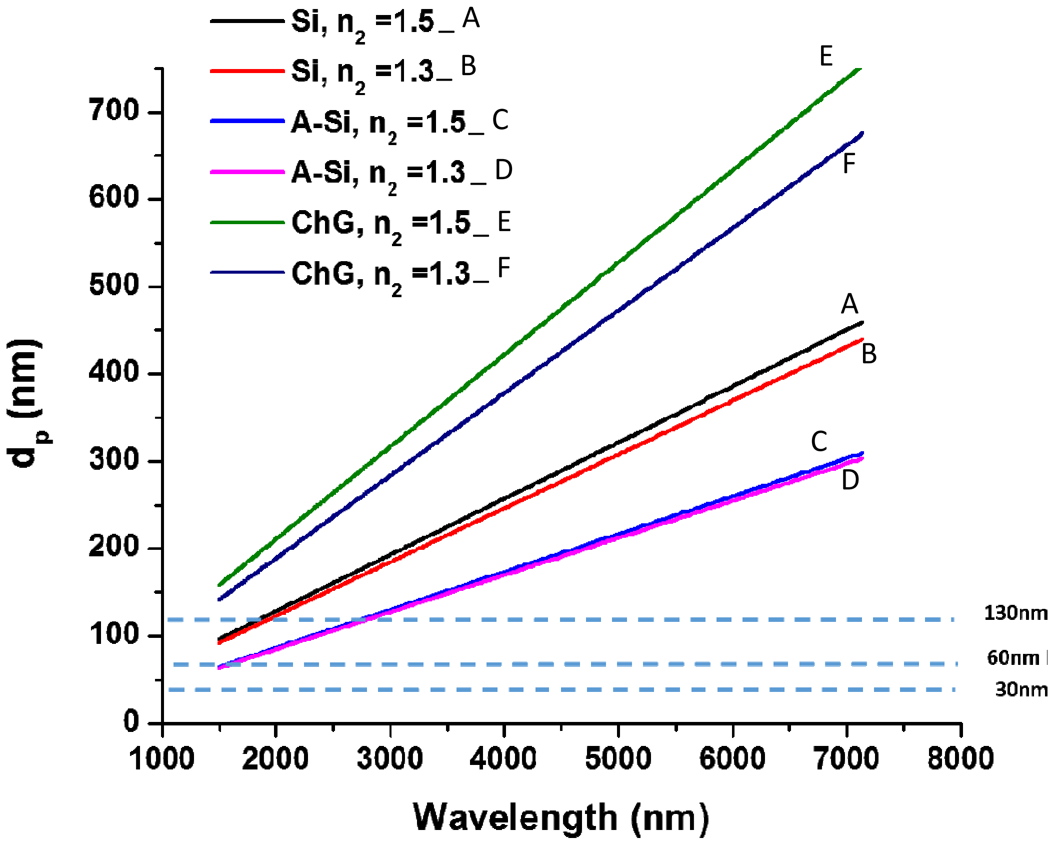

Figure A9.2. Depth of penetration calculated for near IR through mid-IR using waveguide materials used in this work and a standard refractive index for the polymers and liquid VOC for comparison. Dashed lines are thicknesses of polymer layers that have been used in this work.

The dashed lines represent the thickness of the polymer films and EPLS made and the graph clearly shows that the thicknesses of the systems falls well below the maximum evanescent wave depth for mid-IR and is also below the ChG resonator depth as well.

3. Statistical Analysis

Statistical analysis was done using a single tail standard student's T-test with a 95% confidence interval. T values presented in Table A2, Table A3, Table A4, and Table A5 are for the 90 nm PGMA film, the six layer PGMA-PAA EPLS, the five layer multi-polymer EPLS.

Table A2. Student T-test t and p values for the swelling fractions of the 90 nm PGMA layer with various analyte vapors. Degrees of freedom = 2

T-test values \ p values

PGMA 90 nm	**Hexane**	**MeOH**	**Acetone**	**IPA**	**EtOH**	**Acetic Acid**
Hexane		0.001	0.00001	0.002	0.0001	0.002
MeOH	**7.58**		0.0006	0.27	0.15	0.04
Acetone	**14.52**	**8.19**		0.001	0.001	0.04
IPA	**5.87**	**0.69***	**7.06**		0.45	0.05
EtOH	**12.65**	**1.24***	**7.71**	**0.13***		0.05
Acetic Acid	**5.7**	**2.67**	**2.31**	**2.23**	**2.31**	

* **Are not statistically different**

Table A3. Swelling mean and standard deviation values for the 90nm PGMA film

PGMA 90 nm	**Hexane**	**MeOH**	**Acetone**	**IPA**	**EtOH**	**Acetic Acid**
Mean	0.024	0.114	0.41	0.135	0.138	0.28
STDEV	0.004	0.022	0.046	0.035	0.016	0.08

Table A4. Student T-test t and p values for the swelling fractions of the six layer PGMA-PAA EPLS and various analyte vapors. Degrees of freedom =4

T-test values\p values

6L PGMA-PAA	**Hexane**	**MeOH**	**Acetone**	**IPA**	**EtOH**	**Acetic Acid**	**AmmHyd**
Hexane		0.001	0.085	0.007	0.001	0.003	0.007
MeOH	7.53		0.0004	0.08	0.388	0.0009	0.013
Acetone	2.18	7.2		0.007	0.0003	0.0004	0.007
IPA	4.21	1.63	3.65		0.1	0.02	0.006
EtOH	8.03	0.3	7.82	1.46		0.0006	0.01
Acetic Acid	4.63	6.06	7.12	2.74	6.51		0.009
AmmHyd	8.45	3.47	8.14	4.47	3.79	7.49	

* **Are not statistically different**

Table A5. Swelling mean and standard deviation values for the six layer PGMA-PAA EPLS

6L PGMA-PAA	**Hexane**	**MeOH**	**Acetone**	**IPA**	**EtOH**	**Acetic Acid**	**AmmHyd**
Mean	0.107	0.814	0.198	0.61	0.81	0.3	1.48
STDEV	0.07	0.135	0.017	0.19	0.13	0.017	0.27

Table A6. Student T-test t and p values for the swelling fractions of the five layer multi-polymer EPLS and various analyte vapors. Degrees of freedom = 4

T-test values\p values

5L Multi-system	**Hexane**	**MeOH**	**Acetone**	**IPA**	**EtOH**	**Acetic Acid**	**AmmHyd**
Hexane		0.001	0.002	0.008	0.0004	0.00002	0.000002
MeOH	**6.08**		0.002	0.16	0.007	0.03	0.02
Acetone	**5.09**	**4.73**		0.01	0.01	0.00002	0.000003
IPA	**3.62**	**1.12***	**3.62**		0.07	0.008	0.003
EtOH	**7**	**3.67**	**3.5**	**1.71***		0.0001	0.00001
Acetic Acid	**18.62**	**2.5**	**18.59**	**4**	**14.03**		0.32
AmmHyd	**20.71**	**2.87**	**19.75**	**4.72**	**15.37**	**0.51***	

* **Are not statistically different**

Table A7. Swelling mean and standard deviation values for the five layer multi-polymer EPLS

5L Multi-system	**Hexane**	**MeOH**	**Acetone**	**IPA**	**EtOH**	**Acetic Acid**	**AmmHyd**
Mean	0.09	0.386	0.16	0.31	0.21	0.545	0.53
STDEV	0.021	0.081	0.01	0.07	0.02	0.035	0.03

Table A8. Student T-test. t and p values for the swelling fractions of the five layer multi-polymer EPLS compared with the 6L PGMA-PAA EPLS. Only same analytes are compared. Degrees of freedom = 4

5L system vs 6L system

	Hexane	**MeOH**	**Acetone**	**IPA**	**EtOH**	**Acetic Acid**	**AmmHyd**
T value	0.32*	4.57	2.88	2.45	7.64	10.65	9.41
p value	0.38	0.003	0.017	0.029	0.0003	0.0002	0.0001

* **Are not statistically different**

4. References

1. Kaye and Laby online. http://www.intute.ac.uk/sciences/cgi-bin/fullrecord.pl?handle=20070206-164427.

2. Polyanskiy, M. Refractive Index Database. http://refractiveindex.info/?group=PLASTICS&material=PMMA (accessed June 2010).

3. Laniel, J. M.; Ménard, J.-M.; Turcotte, K.; Villeneuve, A.; Vallée, R.; Lopez, C.; Richardson, K. A., Refractive index measurements of planar chalcogenide thin film. *Journal of Non-Crystalline Solids* **2003,** *328* (1–3), 183-191.